DESIGN DEVELOPMENT AND CHARACTERIZATION OF A SINGLE LONGITUDINAL MODE (SLM) PULSED DYE LASER

By

VINOD SINGH RAWAT

Enrollment No: PHYS01200704006

Bhabha Atomic Research Center, Mumbai

A thesis submitted to the

Board of Studies in Physical Sciences

In partial fulfillment of requirements

For the Degree of

DOCTOR OF PHILOSOPHY

of

HOMI BHABHA NATIONAL INSTITUTE

November 2014

Homi Bhabha National Institute

Homi Bhabha National Institute

Recommendation of the Viva Voce Board

As members of the Viva Voce Committee, we certify that we have read the dissertation prepared by Vinod Singh Rawat entitled "**Design, Development and Characterization of a Single Longitudinal Mode (SLM) Pulsed Dye Laser**" and recommend that it may be accepted as fulfilling the thesis requirement for the Degree of Doctor of Philosophy.

Chairman: Dr S C Gupta **Date:** 28.05.2015

Satish C Gupta

Guide / Convener: Dr L M Gantayet **Date:** 21.5.2015

Lalit Mohan Gant

Dr A K Mohanty, **Date:** 21-5-2015

Dean Academic, Physical Sciences

Member 1: Dr D J Biswas **Date:** 21-5-2015

Member 2: Dr S G Nakhate **Date:** 21.5.2015

External Examiner: Prof Prem B Bisht, **Date:** 21.5.2015

IIT Madras

Final approval and acceptance of this dissertation is contingent upon the candidate's submission of the final copies of the dissertation to HBNI.

I hereby certify that I have read this dissertation prepared under my direction and recommend that it may be accepted as fulfilling the dissertation requirement.

Date: 21.5.2015

Place: Mumbai

Lalit Mohan Gant

Guide:

Prof. L M Gantayet

Date:

STATEMENT BY AUTHOR

This dissertation has been submitted in partial fulfillment of requirement for an advance degree at Homi Bhabha National Institute (HBNI) and is deposited in the Library to be made available to borrowers under rules of the HBNI.

Brief quotations from the dissertation are allowable without special permission, provided that accurate acknowledgement of source is made. Requests for permission for extended quotation from or reproduction of this manuscript in whole or in part may be granted by the Competent Authority of HBNI when in his or her judgment the proposed use of the material is in the interests of scholarship. In all other instances, however, permission must be obtained from the author.

(VINOD SINGH RAWAT)

DECLARATION

I hereby declare that the investigation presented in the thesis has been carried out by me. The work is original and has not been submitted earlier as a whole or in part for a degree / diploma at this or any other Institution / University.

(VINOD SINGH RAWAT)

List of Publications arising from the thesis

In Journal

1. “Computational model for transient temperature rise in a dye laser gain medium pumped by a copper vapor laser”, **V S Rawat**, L M Gantayet, G Sridhar, S Singh, **Laser Phys**, 24, 025005, 2014.
2. “Measurement of flow fluctuations in Single Longitudinal Mode Pulsed Dye Laser”, **V.S.Rawat**, N Kawade, G.Sridhar, S.Singh, L.M.Gantayet, **Pramana – J. Phys**., Vol. 82, No. 2, 203 – 210, 2014.
3. “A design of the dye cell of a dye laser to facilitate its repetitive operation in the Single Longitudinal Mode”, **V S Rawat**, L M Gantayet, G Sridhar, S Singh, **Laser Phys**, 23, 0350001, 2013.
4. "Study of Solvent Temperature Effects in Single Longitudinal Mode Pulsed Dye Laser" ,**V.S.Rawat**, G.Sridhar, N.Kawade, S.Singh L.M.Gantayet **Laser Phys**, 23, 0350002, 2013
5. “Operation of a CVL pumped Dye Laser in the Single Longitudinal Mode and its Parametric Characterization”, **V S Rawat**, G Sridhar, S Singh, L M Gantayet, **Optik –** Int. J. Light Electron Opt, 124, 2837 – 2843, 2013.
6. “Temporal dynamics of high repetition rate pulsed single longitudinal mode dye laser”, G.Sridhar, **V.S.Rawat**, Sunita Singh, L.M.Gantayet, **Pramana – J. Phys** Vol. 81, 295 – 308 2013.
7. **“**Spectral studies of single mode dye oscillator and preamplifier system”, G.Sridhar, **V.S.Rawat**, Sunita Singh, L.M.Gantayet, **J. Opt**., 42, 239 – 246, 2013.
8. “Physics and technology of tunable pulsed single longitudinal mode dye laser”, G Sridhar, **V S Rawat**, Nitin Kawade, Sunita Singh and L M Gantayet, **Pramana J Phys**, Vol. 75, No. 5, 807 – 816, 2010.
9. “Design aspect of the control system of single longitudinal mode pulsed dye laser”, N Kawade, **V S Rawat**, G Sridhar, L M Gantayet, **Communicated under review with Laser Physics.**

In Newsletters

1. “Experimental and Theoretical Studies of high repetition rate SLM dye oscillator-pre amplifier pumped by CVL”, G.Sridhar, **V.S.Rawat**, Sunita

Singh, **BARC News Letters** founder's day special Issue No. 297, 180 – 184 October 2010.

2. "Performance characteristics of remotely tunable high repetition rate copper vapour laser pumped single longitudinal mode dye laser", Sunita Singh, G Sridhar, **V S Rawat**, N Kawade, A S Rawat, S K Mishra, L M Gantayet, **KIRAN**, A bulletin of the Indian Laser Association Vol 19 No. 1, 35 – 37, April 2008.
3. "Performance characteristics of remotely tunable high repetition rate copper vapour laser pumped single longitudinal mode dye laser", Sunita Singh, G Sridhar, **V S Rawat**, N Kawade, A S Rawat, S K Mishra, L M Gantayet, **BARC News Letters** founder's day special Issue No. 297, October 2008.
4. "Automated wavelength control system for single longitudinal mode dye laser", N O Kawade, **V S Rawat**, G Sridhar, **KIRAN**, A bulletin of the Indian Laser Association Vol. 24, No. 3, 77 – 81, December 2013.

In Conferences

1. "Computational model for transient temperature rise in Single Longitudinal Mode dye laser gain medium", **V S Rawat**, L M Gantayet, 22nd DAE-BRNS National Laser Symposium (NLS-22), Manipal University, Manipal, January 8 – 11, 2014.
2. "Operation and spectral studies of Nd:YAG pumped single longitudinal mode DCM dye laser oscillator and amplifier system", Rushal Shah, G Sridhar, S P Sahoo, Nitin Kawade, **V S Rawat,** Mukesh Shah, Jaya Mukherjee. 22nd DAE-BRNS National Laser Symposium (NLS-22), Manipal University, Manipal, January 8 – 11, 2014.
3. "Automated wavelength control system for single longitudinal mode dye laser", Nitin Kawade, **V S Rawat**, G Sridhar, 22nd DAE-BRNS National Laser Symposium (NLS-22), Manipal University, Manipal, January 8 – 11, 2014.
4. "Measurement of flow fluctuations in Single Longitudinal Mode Pulsed Dye Laser" **V.S.Rawat**, N Kawade, G.Sridhar, S.Singh, L.M.Gantayet, 21st DAE-BRNS National Laser Symposium (NLS-21), BARC, Mumbai, February 6-9, 2013.
5. "Experimental and Theoretical Studies on Temporal Pulse stretching of High Repetition Rate Pulsed Single Longitudinal Mode Dye Laser" G.Sridhar,

V.S.Rawat, S.Singh, L.M.Gantayet, 21st DAE-BRNS National Laser Symposium (NLS-21), BARC, Mumbai, February 6-9, 2013.

6. “Study of build up time in Single Longitudinal Mode Pulsed Dye Laser ” **V S Rawat**, G Sridhar, Sunita Singh, L M Gantayet National Laser Symposium (NLS-20) held at Anna University, Chennai, 2012.
7. “ASE measurement and gain spectrum matching of single mode dye oscillator and pre-amplifier system”, G Sridhar, **V S Rawat**, Sunita Singh, L M Gantayet National Laser Symposium (NLS-20) held at Anna University, Chennai, 2012.
8. “Temperature effects on Single Longitudinal Mode Dye Laser Spectrum”, **V S Rawat,** G Sridhar, N O Kawade and Sunita Singh National Laser Symposium (NLS-08) held at LASTEC Delhi, 6-10th January 2009.
9. “VME based automated wavelength control system for Single Longitudinal Mode Dye Laser”, N O Kawade, **V S Rawat**, G Sridhar, Sunita Singh L M Gantayet National Laser Symposium (NLS-08) held at LASTEC Delhi, 6-10th January 2009.
10. “Narrow band tunable laser for Uranium – 233 Cleanup process”, S Singh, G Sridhar, **V S Rawat,** Nitin Kawade, A K Sinha, Samir Bhatt, L M Gantayet International conference on Peaceful Uses of Atomic Energy 2009, New Delhi September 29 – October 1st 2009.

(VINOD SINGH RAWAT)

Dedicated to

My Parents

Shri Pooran Singh Rawat

Smt. Nandi Rawat

My Wife

Smt. Renu Rawat

My Daughter

Siddhi

ACKNOWLEDGEMENTS

I would like to extend my humble gratitude to my mentor Dr L M Gantayet, Distinguished Scientist, Director, Beam Technology Development Group, BARC for his generous support, guidance and for his constant encouragement to pursue computational fluid dynamic studies, the latitude granted to me and trust shown in me were truly invaluable. He is an excellent teacher, a very good mentor; logical and very amicable person. He helped me with his invaluable advices and critically reviewed my work. I have learnt so much from him, even while I know that I still have to learn a lot more. I would never have been able to finish my thesis without his generous help.

I would like to extend my gratitude to Dr K Dasgupta, Associate Director, BTDG and Head, L&PTD, for his unconditional support.

I am indebted to Dr D J Biswas for critically reviewing my manuscripts. He is a great physicist and a very good person.

I would like to thank Dr Jaya Mukherjee, Head, ICPES, for her support to me during entire course of this work.

I would like to express my humble thanks to Dr S C Gupta, Distinguished Scientist Chairman Doctoral Committee HBNI, Dr S G Nakhate, member doctoral committee for reviewing my work, necessary guidance, time, interest and helpful comments.

I would be grateful to Dr K G Manohar, for introducing me to the single longitudinal mode dye lasers and sharing his immeasurable experience.

I would like to express my humble gratitude to Dr Alok K Ray, for his unconditional support and encouragement.

I would like thank Dr A K Mohanty, Dean Academic, Physical Sciences, HBNI, for his support and encouragement.

I would like to acknowledge, Dr Sunita Singh, Dr G Sridhar, Shri Paramjit and Shri S K Mishra from whom I got lot of help during experiments. I would like to thank Shri A K Sinha and Shri Sameer Bhatt for their help in designing and fabrication of dye laser at CDM, BARC, Mumbai.

I would like to expresses my thanks to Dr S Pradhan and Shri Nitin Kawade, from whom I learn lot. They shared their intelligence and knowledge specially for understanding the wavelength locking concepts in dye lasers. The discussions with them have been interesting and exciting.

I would like to thank my friends Dr Manoj Kumar, Dr Ashok Verma, Shri M L Shah, Shri S P Dey, Smt Anupama for their moral support and help during this course.

I owe my gratitude to my parents, brother and sister for their constant love, concern and prayers. They showed unconditional love, appreciation for my infinitesimal successes, I would achieve, just to keep my moral up and ensure that I work with more enthusiasm.

Finally, I appreciate my wife, Renu. She was always there cheering me up and stood by me through the good times and bad. Special thanks to my little angel Siddhi, for her great patience and for all her sacrifices.

(VINOD SINGH RAWAT)

CONTENTS

ABBREVIATIONS AND NOMENCLATURE

ABBREVIATIONS USED

ASE	- Amplified Spontaneous Emission
AVLIS	- Atomic Vapor Laser Isotope Separation
CCD	- Charge Coupled Device
CFD	- Computational Fluid Dynamics
CVL	- Copper Vapour Laser
CW	- Continuous Wave
DAC	- Digital to Analog Converter
DFB	- Distributed Feed Back
DNS	- Direct Numerical Simulation
EDM	- Electro Discharge Machining
FFT	- Fast Fourier Transformation
FP	- Fabry Perot
FPI	- Fabry Perot Interferometer
FPC	- Fabry Perot Cavity
FPE	- Fabry Perot Etalon
FSR	- Free Spectral Range
FVM	- Finite Volume Method
FWHM	- Full Width Half Maximum
GI	- Grazing Incidence
GIG	- Grazing Incidence Grating
HMI	- Human Machine Interface
HMPGI	- Hybrid Multiple Prism Grazing Incidence
ID	- Internal Diameter
IR	- Infra Red
LES	- Large Eddy Simulation
LIS	- Laser Isotope Separation
lpm	- liters per minutes
MOPA	- Master Oscillator Power Amplifier
MPL	- Multiple Prism Littrow
NBA	- Narrow Band Amplifier

PC	- Personnel Computer
PID	- Proportional Integral and Differential
PZT	- Lead Zirconium Titanate
PRF	- Pulse Repetition Frequency
ppm	- Parts per million
QRC	- Quick Release Connectors
RANS	- Reynolds Averaged Stokes Simulation
rf	- Radio frequency
RMS	-Root Mean Square
RPM	- Revolution per minute
SBC	- Single Board Computer
SCL	- Short Cavity Laser
SFM	- Sum Frequency Mixing
SHG	- Second Harmonic Generation
SLM	- Single Longitudinal Mode
SS	- Stainless Steel
SST	- Shear Stress Transport
UDF	- User Defined Function
USB	- Universal Serial Bus
UV	- Ultra Violet
VFD	- Variable Frequency Derive
VIS	- Visible
VME	- Versa Module Europa
WM	- Wavelength Meter

NOMENCLATURE

a	: Width of Incident Beam (m)
b	: Width of Diffracted Beam (m)
c	: Velocity of Light (ms^{-1})
d	: Groove Density (lines m^{-1})
d_1	: Distance Between Gain Diameters to End Mirror (m)
d_2	: Distance Between Grating and Cell (m)
d_m	: Separation Between the Mirrors (m)
dL	: Change in Cavity Length (m)
$d\nu$	: Change in Frequency (Hz)

$e(t)$	: Error Signal (volt)
h	: Plank's Constant (JHz^{-1})
k	: Thermal Conductivity (W/m-K)
k_1	: Turbulent Kinetic Energy Per Unit Mass (m^2s^{-2})
l_1	: Distance Between Grating and End Mirror (m)
l_2	: Distance Between Grating and Tuning Mirror (m)
l_a	: Cavity Length in Air (m)
l_g	: Glass Window Thickness (m)
l_d	: Dye Cell Width (m)
m	: Order of the Grating
m'	: Order of Grating
n	: Refractive Index
n_i	: Refractive Index of Medium
n_a	: Refractive Index of Air
n_g	: Refractive Index of Glass
n_d	: Refractive Index of Dye Solution
p	:Interference Order of Fringe
q	: Mode Index Number
t_c	: Characteristics Time (s)
t	: Time (s)
u	: Velocity (ms^{-1})
$u(t)$	: PZT Voltage (volt)
u'	: Turbulent Velocity Fluctuations (ms^{-1})
u_g	: Guessed Velocity (ms^{-1})
v	: Average Velocity (ms^{-1})
v_g	: Average Volume Flow (m^3s^{-1})
w	: Grating Length (m)
A_1	: Grating Input Aperture (m)
A'	: Absorption Losses (m^{-1})
B	: Measurement Bandwidth (Hz)
C_p	: Specific Heat at Constant Pressure (J/kg-K)
C_μ, $C_{\varepsilon 1}$, $C_{\varepsilon 2}$	: Equation Constants
D	: Hydraulic Diameter (m)

D_T : Thermal Diffusivity (m^2s^{-1})

E : Young's Modulus (Nm^{-2})

F : Finesse of Etalon

F' : Coefficient of Finesse

F(t) : Feed Back Signal (volts)

H_{abs} : Rate of Absorbed Energy per Unit Volume ($J\ m^{-3}$)

I : Pump Intensity (Wm^{-2})

I_T : Transmitted Intensity (Wm^{-2})

I : Intensity (Wm^{-2})

I_0 : Initial Intensity (Wm^{-2})

K : Cavitation Parameter

K_p : Proportionality Constant

K_c : Conversion Factor (Wavelength to voltage)

K_A : Amplifier Gain

K_D : PZT Conversion Factor

K_I : Laser Transfer Function

L : Resonator Length (m)

L_1 : Path Length (m)

L_i : Length of Medium (m)

L_g : Grating Length (m)

L_p : Distance Between Grating Center to Pivot Point (m)

L_D : Diffusion Length (m)

L_R : Rayleigh Range (m)

M : Magnification

N : Number of Illuminated Lines in Grating

N' : Number of Molecule (m^{-3})

N_1 : Number of Grid Points

N_F : Fresnel Number

P : Proportional Gain

P_d : Pressure (Nm^{-2})

ΔP : Change in Pressure (Nm^{-2})

P_k : Turbulence Production

P_v : Vapor Pressure (Nm^{-2})

P_o : Laser Input Power (W)

R	: Resolving Power of Grating
R_e	: Reynold's Number
R_1	: Residual Value
R'	: Reflectance
S'	: Scattering Losses
S(t)	: Set point Signal (volt)
T_1	: Repetition Period (s^{-1})
T	: Temperature (K)
T'	: Transmittance
ΔT	: Change in Temperature (K)
T_e	: Transmission Efficiency
T_d	: Derivative Time (s)
T_i	: Integration Time (s)
T_o	: Initial Dye Temperature (K)
T_m	: Temperature Rise at Pump Beam Surface (K)
U_∞	: Free Stream Velocity (ms^{-1})
V	: Cell Volume (m^3)
W	: Total Illuminated Width of Grating (m)
α	: Thermal Expansion Coefficient (K^{-1})
α_1	: Absorption Coefficient (m^{-1})
ω_o	: Beam Waist (m)
λ	: Wavelength (nm)
λ_G	: Grating Wavelength (nm)
λ_L	: Cavity Wavelength (nm)
$\Delta\lambda_{laser}$	: Laser Bandwidth (nm)
$\Delta\lambda_{FSR}$	: FSR of etalon (nm)
$\Delta\lambda$	: Longitudinal Mode Spacing in Wavelength (nm)
$\Delta\lambda_G$	: Grating Pass Band (nm)
$\Delta\lambda_O$	: Passive Band Width (nm)
$\Delta\nu_{etalon}$	: Free Spectral Range of Etalon (GHz)
$\Delta\nu_{cavity}$	: Longitudinal Mode Spacing in Frequency (GHz)
$\Delta\nu_{single}$	: Single Pass Linewidth (GHz)
$\Delta\nu$	: Linewidth (GHz)

$\delta\nu_{cavity}$	: Axial Mode Separation (GHz)
$\delta\nu_{c}$	: Reference cavity FWHM (GHz)
$\delta\nu(\tau)$	: Frequency fluctuations (Hz)
σ	: Absorption Cross Section (m^{-1})
σ_k, σ_ε	: Equation Constants
ρ	: Density of Liquid ($N\ s^2 m^{-4}$)
μ	: Viscosity of Liquid ($N\ s/m^2$)
μ_t	: Eddy Viscosity (Pa s)
Φ	: Quantum Yield
η	: Quantum Efficiency
θ	: Incidence Angle (degree)
θ_1, θ_3	: Incidence Angle (degree)
θ_2 θ_4	: Diffraction Angle (degree)
φ	: Diffraction Angle (degree)
Θ	: Beam Divergence (mrad)
ν	: Frequency (Hz)
ν_{ab}	: Absorbed Frequency (Hz)
ν_{em}	: Emission Frequency (Hz)
ω	: Turbulent Kinetic Frequency (s^{-1})
ε	: Turbulent Kinetic Energy Dissipation ($m^2 s^{-3}$)
ξ	: Conversion Factor for Absorbed Energy to Heat
δ_r	: Surface Roughness (µm)
τ	: PZT Response (s)
γ	: Perturbing Acceleration (ms^{-2})
$\frac{\delta}{x}$	: Ratio of Boundary Layer to Distance
$\frac{\partial\theta}{\partial\lambda}$	: Angular Dispersion
$\frac{\partial\varphi}{\partial\lambda}$	: Overall Intra Cavity Dispersion (nm^{-1})
$\frac{\partial\nu}{\partial\varphi}$	: Rate of Change of Frequency with Diffraction Angle ($MHz\ rad^{-1}$)
$\frac{d\theta_i}{d\lambda}$	: Spectral Selectivity (nm^{-1})
$\frac{dn}{dT}$	: Temperature Dependent Refractive Index (K^{-1})

$\frac{dT}{dx}$: Temperature Gradient Along Pump Beam (Km^{-1})

$\frac{dn_d}{dT}$: Temperature Dependent Refractive Index for Ethanol (K^{-1})

$\frac{dn_g}{dT}$: Temperature Dependent Refractive Index for Glass (K^{-1})

$\frac{dn_a}{dT}$: Temperature Dependent Refractive Index for Air (K^{-1})

$\frac{dn}{dx}$: Refractive Index Gradient Along Pump Direction (m^{-1})

LIST OF FIGURES

LIST OF TABLES

Chapter – I

INTRODUCTION

1.1 Introduction

Dye laser is a powerful tunable source of radiation, which can generate light in visible (VIS), near ultraviolet (UV) and near infrared (IR) region of the wavelength. The dye lasers can emit the laser radiation either in pulse regimes (a few tens of femtosecond) or continuous wave (CW) mode. The dye laser technology has seen very significant progress over the last 45 years since its first demonstration by Sorokin and Lankard in 1966 [1.1] and independently by Schafer et al., [1.2] Spaethn, Bortfield and Stepanov et al., [1.3]. Soffer and McFarland then demonstrated for the first time efficient spectral narrowing and continuous tunability in the xanthenes and carbocyanine dye families using diffraction grating as cavity reflectors in Littrow configuration [1.4]. Among various tunable sources developed till today, the dye laser continues to be the best choice for many applications, where the wavelength is in the visible range and high average powers as well as high pulse energies are required.

The visible region 400 – 800 nm of the electromagnetic spectrum is of great importance to study many chemical, physical and biological processes based on spectroscopy, where the resolution depends on the narrow spectral linewidth from tunable laser sources. For numerous applications a combination of narrow linewidth and high pulse power as well as high average power is obligatory; they include areas of medicine, laser isotope separation, LIDAR and coherent control [1.5]. In the industry, these lasers have been used in semiconductor fabrication, chemical purification, catalyst production, curing of pigment coatings and combustion diagnostics [1.6]. The major advantages of the dye lasers are wavelength diversity, wavelength tunability, scalable technology and high average power of the device.

Dye lasers employ highly fluorescent organic compounds, possessing some specific spectroscopic properties, dissolved in organic solvents, they have a high quantum yield. A brief discussion on the importance of the characteristics of the laser gain medium to the performance, dye lasers are presented here. Organic laser dyes are compounds having conjugate double bonds that absorb light at wavelengths more than

200 nm. There are several classes of laser dyes, including polymethines (750 – 1200 nm), xanthenes (500 – 700 nm), coumarines (400 – 500 nm) and scintillators (320 – 430 nm). The photochemical and thermal stability of the laser dye are major parameters for selection of a dye. It has been seen that the problem of thermal stability and photochemical decomposition is relatively less severe for laser dyes, having absorption bands in the visible region of the spectrum. The dye molecule should also never react with the solvent molecules and nor should have any absorption in the emission band of the dye molecule.

The organic dye molecule emits the Stokes shifted broadband emission on excitation by a suitable wavelength, which lies in the absorption band of the dye molecule. This broadband absorption and emission for the laser dyes are due to the large number of atoms contributing to the spectroscopic properties of a dye molecule. The electronic levels of the organic dye molecules are composed of a quasi continuum of vibrational and rotational sublevels. The overlapping of the emission and absorption spectrum in a laser dye, as shown in figure 1.1 can inhibit the laser action as the emitted photon will be subsequently absorbed by the dye molecules. Thus, a dye is selected where the Stokes shift is large, so that the degree of overlap is the least [1.7].

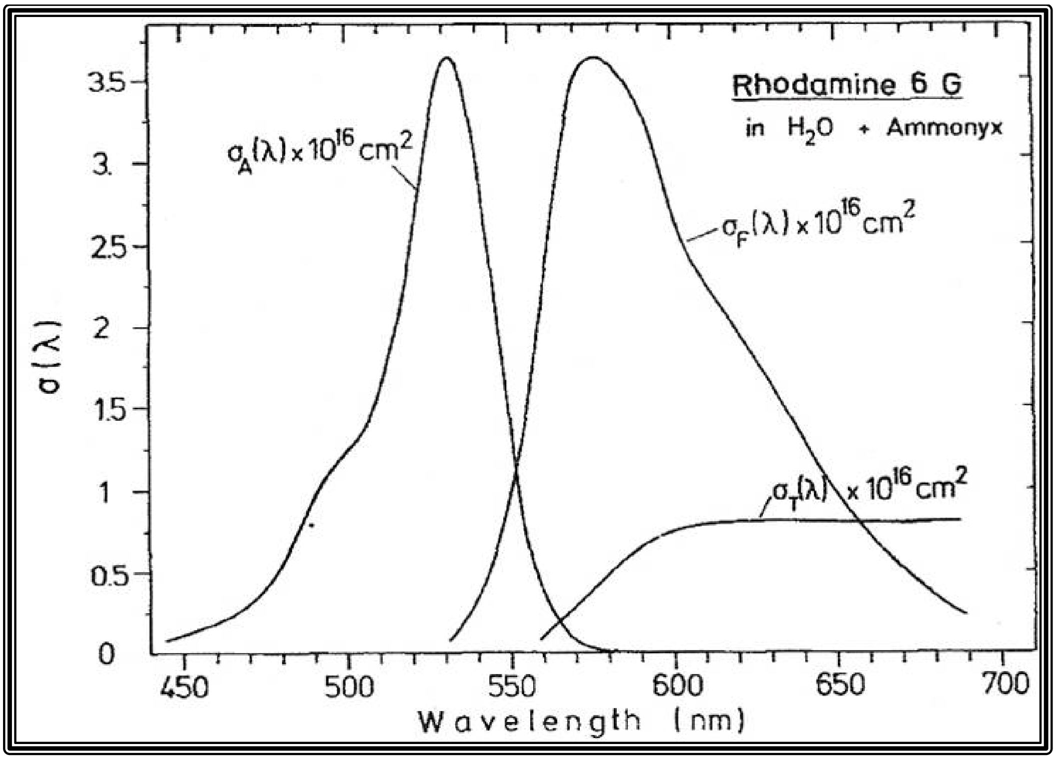

Fig 1.1 Typical spectrum of absorption, fluorescence and triplet absorption for rhodamine – 6G [Ref 1.7]

The absorption band for the popular Rhodamine – 6G dye is about ~ 100 nm at full width half maximum (FWHM) wide and the fluorescent emission band is about ~ 150 nm wide around the central wavelength, which shows nearly 50 nm Stokes shift.

Rhodamine – 6G exhibits a near unity quantum efficiency and may lose its efficiency, if the dye concentration is too high, due to interaction between the dye molecules. The efficiency of Rhodamine – 6G is significantly reduced when highly polar solvents such as water, ethanol, methanol and ethylene glycol are used. The absorption (σ_A) of pump light from the singlet electronic ground state S_0 to the first excited singlet state S_1 is followed by a rapid thermalization in the excited vibronic manifold in S_1. The thermalization takes place within a few picoseconds, whereas the radiative decay time of the vibronic state S_1 is typically in the order of a few nanoseconds.

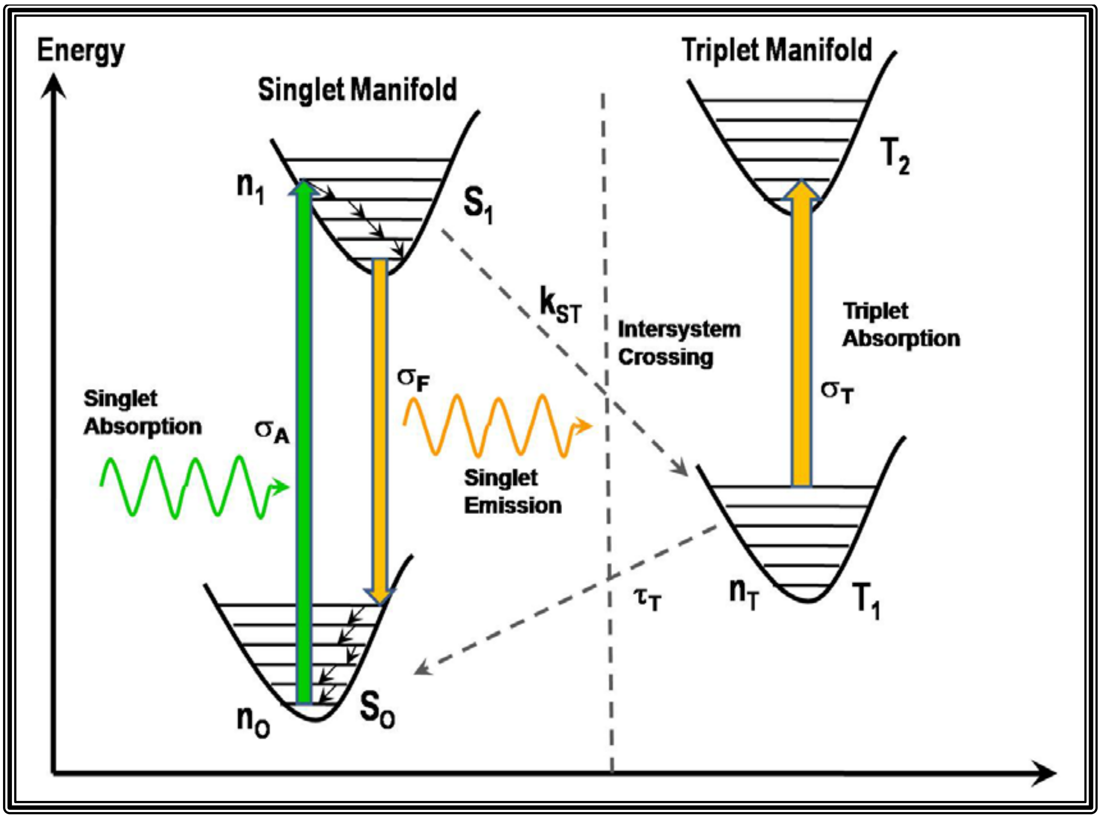

Fig1.2: Schematic of energy level diagram for typical organic dye molecule

As the fluorescence decay time for the dye molecule is a few nanoseconds, an intense pumping source is required to achieve significant population inversion in a fairly short time. The inversion must be sufficient to produce a net gain in the laser to overcome the absorption losses. The intensities required for a typical dye laser are of the order of 1 MW/cm^2. The excited molecule can lose its energy by emission of a photon (σ_F), undergo a non-radiative transition to the ground state or can populate the triplet state via inter system crossing (k_{ST}). An energy level diagram of a typical organic dye is shown in figure 1.2, which shows that there are two energy manifolds in dye molecules: the singlet (S_n) and triplet (T_n) states. The excited triplet states are long lived in comparison with the excited singlet states. The internal conversion (transitions in between states of the same multiplicity) and inter system crossing (k_{ST}) reduce the quantum efficiency for fluorescence. Once the triplet state is populated, this may lead to further losses of dye molecules by internal triplet absorption as shown in figure 1.2. The triplet absorption cross section σ_T can overlap with the emission band. The population, which has accumulated in the triplet state has a decay time (τ_T), several times slower than the singlet state. For example, the triplet state T_1 lifetime is quite long about 2 μs for Rhodamine – 6G. It is obvious that by pumping an ensemble of Rhodamine – 6G molecules continuously nearly all will quickly end up in the T_1 state. Due to the tendency to accumulate in the triplet state, the dye must be optically pumped in the pulsed mode. The optical excitation can render the molecule optically inactive either by decomposition of the dye molecule with single or two photon absorption processes or by local heating of the dye molecule. The local heating occurs by non-radiative transitions in the dye molecule by dissipating excess energy as heat. The combined effect of these processes is known as the photo-bleaching, which renders the dye molecule optically inactive.

The photochemical processes are important in the high repetition pumping of the dye laser. The narrow linewidth is achieved by generally operating the dye laser in single longitudinal mode. High power is obtained by pulsed operation usually by optical pumping with a high power fixed frequency laser. Unfortunately, for pulsed lasers, having pulse duration of a few nanoseconds the number of cavity round trips of laser through frequency selective elements is limited. Shorter cavity laser increases the number of round trips for obtaining the single mode operation. For most tunable organic lasers efficient spectral narrowing in the dye oscillator occurs when a frequency selective element is inserted into the optical cavity. Since the laser transition of organic dye laser is homogeneously broadened, it is possible, in principle, to channel all the stored energy into a small oscillating bandwidth. A dye laser oscillates usually in broad bandwidth of 0.5 – 1 nm with broadband cavity. With insertion of frequency selective elements into the optical cavity, the bandwidth reduces to a small fraction of an Angstrom without appreciable loss in optical power [1.3]. Mostly wavelength tuning mechanisms for dye laser use the inherent angular dispersive elements such as prisms, etalons and gratings to vary the resonant wavelength. A plane diffraction grating has also been used in place of one cavity mirror in Littrow mode for their dye laser. Rotation of the diffraction grating resulted in tuning of the dye laser wavelength [1.4]. The plane diffraction grating provides frequency selective feedback to the resonator cavity. Hence, only the desired frequency of oscillation is returned to the cavity with lower losses. The cavity Q (quality factor) is high only in a narrow region of the spectrum where the laser oscillates.

The LIS process places a strict requirement on the nature of the laser emission in terms of spectral purity and frequency stability. Laser specifications are mainly governed by the spectroscopy parameters of the isotopic species of the element. For example, the heavy elements have isotope shifts typically in the range of 1 – 10 GHz and hyperfine structure splitting in the range of 100 MHz to a few GHz. Hence several isotope separation processes require single mode laser, which is coarsely tunable in the GHz and finely tunable in the MHz range.

The narrow band, Single Longitudinal Mode (SLM) pulsed dye laser has to match the stringent requirement in the isotope selective multistep excitation/photo ionization of atoms where the spectral lines at all the steps are very close to each other. Various methods had been used for narrow band operation of tunable lasers such as single mode CW and pulsed dye laser oscillators, externally filtered multimode laser, pulsed amplification of CW single mode laser, single mode seeded power oscillator [1.8 – 1.11]. For obtaining the single mode laser various cavity configurations have been reported in the literature such as hybrid multiple prism-grazing incidences (HMPGI) [1.12, 1.13], grazing incidence (GI) [1.14 – 1.19], multiple prism Littrow (MPL) [1.20] and Littrow cavity [1.21]. In the Hansch type cavity single mode is achieved by using a prism beam expander instead of a telescopic arrangement [1.13, 1.22 – 1.24]. A pulsed single mode laser was developed by Littman using grazing incidence type cavity. Although the combination of beam expander and diffraction grating reduces the bandwidth of the dye laser, it introduces more losses in the cavity causing reduction in overall conversion efficiency [1.22 – 1.25]. The short Grazing Incidence Grating (GIG) Littman cavity has provided the narrowest linewidth, less than 150

MHz by increasing the round trip time and the longitudinal mode separation [1.15, 1.19]. The GIG cavity has been used to secure single mode operation for the pulsed dye laser.

1.2 Dye Laser Pumping Sources

For obtaining high pulse energy, high average power, several excitation sources have been used for pumping the organic dye lasers. The laser operating in single longitudinal mode and emitting narrower linewidth is generally known as a master oscillator. The oscillators are operated in a smaller power of a few tens of mW while higher power can be obtained by amplifying the narrow linewidth oscillator signal in several amplifying stages. This combination of oscillator and amplifying stages are known as master oscillator and power amplifiers (MOPA) configuration for obtaining higher powers from any laser system. The commonly used pumping sources for dye lasers are nitrogen laser, excimer laser, copper vapor laser, ruby laser, argon ion laser, flash lamp and the second harmonic of Nd:YAG laser [1.6, 1.32 – 1.36]. Pump sources that emit short rise time pulses are needed to overcome excessive triplet state losses present in the organic dyes. The flash lamp pumped dye lasers yield high energy pulses in microseconds with lower pulsed repetition rate. The flash lamp pumped dye laser has been operated at a pulse repletion rate of 850 Hz with average power of 1.2 kW in burst mode [1.23]. Excimer pumped Coumarin dye laser had delivered 800 J per pulse with 500 ns pulse duration in blue green region of the visible spectrum [1.5]. An Excimer pumped dye laser developed by Los Alamos National Laboratory had delivered 50 W with a pulse repletion rate of 250 Hz at 400 nm [1.22]. A 2.5 kW pulsed dye laser pumped by copper vapor laser operating at 13.2 kHz pulse repetition rate has been demonstrated by Lawrence Livermore National Laboratory. This dye laser emission had narrow linewidth and tunability over the spectral range of 550 – 650 nm region developed for atomic vapor laser isotope separation (AVLIS) program [1.38].

Dye lasers can be broadly classified in terms of excitation sources, namely, incoherent pumping and coherent pumping. Many different techniques have been used to excite the gain medium, which leads to generation of laser output of ultra short pulses in femtosecond to continuous wave output from similar dye lasers [1.39, 1.23]. The summary of dye laser excitation techniques is listed in table 1.1 and table 1.2.

Incoherent	Wavelength λ (nm)	τ (μs)	PRF (kHz)	Remarks
Flashlamp Linear	UV to IR	~ 5 to 10^4	~ 1	Limited PRF, life time 10^6 pulses
Flashlamp Coaxial	UV to IR	~ 0.5 to 5	~ 0.001	Limited PRF, life time 10^4 pulses
Surface Discharge	UV to IR	~ 0.15	~ 1	Discrete lines, High PRF, non thermal

Table 1.1: Incoherent Pump Source Characteristics [Henry R Aldag [1.39]]

Coherent	Wavelength λ (nm)	τ (ns)	PRF (kHz)	Remarks
CVL	511 & 578	~ 10 – 60	> 20	High PRF, High average power
Nd:YAG (2ω)	532	~ 5	CW	Variable PRF to CW, Short pulse operation
Nd:YAG (3ω)	355	~ 5	CW	Variable PRF to CW, Short pulse operation
Ion (Ar, Kr...)	UV to Green & Red	~ 0.18 (Mode locked)	CW	Various lines, High PRF to CW, low average power, low efficiency
Nitrogen	337	2 – 10	.01 – 0.3	Low average power, low efficiency, short pulse duration
Excimer	UV	10 – 200	0.5 – 3	Various lines in UV, High PRF, High average power, short pulse
Diode	Red to IR	Long	To CW	Long Wavelength pump, high PRF to CW

Table 1.2: Coherent Pump Source Characteristics [Henry R Aldag [1.39]]

Note: where τ is pulse duration, PRF: pulse repetition frequency, 2ω: second harmonic, 3ω: third harmonic frequency. Hence the anticipated application of dye laser determines the pumping source and class of the laser.

1.3 Motivation

For process applications, high repetition rate high power tunable laser systems are required, which pose a challenge for attainment of narrow band operation with additional factors, namely flow dynamics, mechanical disturbances and pump beam parameters [1.26 – 1.31]. Typically the linewidth of high power pulsed dye laser is in the range of a few hundreds of MHz and frequency stabilized continuous wave dye laser can have linewidth of a few tens of kHz. These parameters are strongly dependent on the quality of the pump beam, flow characteristics inside the dye cell, angle of incidence and rigidity and stability of the cavity components. These essential features are seldom reported; this formed the main motivation for the PhD research work.

The dye laser uses a dye cell to contain the dye solution and for sustained laser operation the dye solution needs to flow through the dye cell. For a sustained laser operation in pulsed mode, the rule of thumb is that every laser pump pulse must see the fresh dye volume. This is ensured by removal of twice the volume of dye solution between excitations. The circulating dye solution removes heat; it takes away the molecules in the triplet state and also the degraded dye molecules from the gain volume. Dye flow along the pumping direction (longitudinal) limits the volume that can be moved through, in a given period, consequently limiting the pulse repletion frequency (PRF). Whereas, transverse flow (perpendicular to pump beam) allows a more rapid removal of the excited molecules and hence provides higher PRF. Design of the dye cell is crucial for achieving optimized performance for a dye laser and the dimensions (active volume) of the dye cell is a key parameter in determining the output characteristics. However, not much work has been reported in the flow dynamics and its effects on the behavior of the SLM laser. The environment related drift for long term operation has not also been adequately addressed in the literature. Practical applications require a thorough understanding of this behavior of the high power SLM dye laser.

The focus of this thesis is on the design, development and characterization of the computer controlled short cavity SLM pulsed dye laser pumped by high repetition rate (~ 9 kHz) copper vapour lasers (CVL). This dye laser should be able to produce single mode oscillation tunable over 100 nm with grating tuning angle and the tunability being limited only by the emission spectrum of the laser medium employed. The computational fluid dynamics (CFD) studies are necessary to understand the flow and heat transfer behavior of the system and for finalizing the dye cell design. The single mode wavelength has to be stabilized by using a feedback controller appropriate to correct the dynamic disturbances. These new effects have to be systematically investigated and addressed in the development of the high repetition rate SLM pulsed tunable dye laser.

1.4 Organization of the Thesis

The outline structure of this thesis is as follows. Chapter – I provides a brief introduction to the main features of the tunable dye laser and high repetition rate tunable dye laser systems, the main motivation towards this research and the organization of the thesis. In Chapter – II, the literature survey and the selection of cavity type of the SLM dye laser for the research work have been presented. The design concepts, selection of optical components, design architecture, geometric configuration of mode hop free tuning are presented in Chapter – III. Chapter – IV describes, the design details of judiciously designed dye cell for SLM dye laser and flow visualization using commercial computational fluid dynamics (CFD) software. Selection of the dye cell for stable SLM operation is also discussed in detail. Chapter – V provides the characterization and optimization studies carried out for the SLM dye laser parameters pumped by high repetition rate CVL. The dye laser parameters such as bandwidth, single pulse bandwidth, tunability, beam divergence, pulse duration, amplified spontaneous emission (ASE) and build up time are discussed in detail. The effect of temperature on the SLM wavelength has been experimentally determined and presented in Chapter – VI. A CFD model has been developed and validated with the published experimental results and with the SLM dye laser made for the research work in this thesis. This model has a capability to estimate the frictional temperature rise in the dye cell and transient temperature rise due to absorption of the pump pulse in the dye gain medium; these have been studied in detail. Chapter – VII discusses the concept of wavelength locking and operation of wavelength stabilized SLM for long hours. This chapter also discusses various types of disturbances and their response time to the wavelength locking loop. Conclusions, summary and the significant contributions are presented in Chapter – VIII of this thesis.

References

[1.1] P P Sorokin, J R Lankard, "Stimulated emission observed from an organic dye, choro-aluminum phthalocyanine", IBM J of Res. and Dev., 10,162 – 163, 1966.

[1.2] F P Schafer, W Schmidt, J Volze, "Organic Dye Solution Laser", App., Phys., Lett., 9, 306 – 309, 1966.

[1.3] C V Shank, "Physics of dye lasers", Rev., of Mod., Phys., 47, (1975), 649 – 657.

[1.4] B H Soffer, B B McFarland, "Continuously tunable narrow band organic dye lasers", App., Phys., Lett,. 10, 266 – 267, 1967.

[1.5] F J Duarte, "Organic dye lasers: Brief history and recent developments" Opt., & Photonics News, October, 20 – 25, 2003.

[1.6] F J Duarte, L W Hillman, "Dye Laser Principles", Academic Press Inc., San Diego, CA, 1990.

[1.7] G Marowsky, "Principles of dye laser operation and dye laser tuning methods", Optica Acta, 23, 855 – 872, 1976.

[1.8] M Hercher, H A Pike, "Single Mode operation of a continuous tunable dye laser", Optics Comm. 3, 346 – 348, 1971.

[1.9] H W Schroder, L Stein, B Fugger, H Welling, "A High Power single mode CW dye Ring laser", Appl. Phys. 14, 377 – 380, 1977.

[1.10] C K Ni, A H Kung, "Pulsed amplification of cw dye laser with undetectable amplified spontaneous emission", Rev., Sci., Instrum., 71, 3309 – 3312, 2000.

[1.11] U Ganiel, A Hardy, D Treves, "Analysis of injection locking in pulsed dye laser system", IEEE J. Quantum Electron, QE – 12, 704 – 716, 1976.

[1.12] C S Zhou, "Design of a pulsed single mode dye laser", Appl., Opt., 23, 2879 – 2885,1984.

[1.13] I. Shoshan, U P Oppenheim, "The use of diffraction grating as a beam expander in a dye laser cavity", Opt. Comm. 25 375 – 378, 1978.

[1.14] M. G. Littman, "Single mode operation of grazing incidence pulsed dye laser", Opt. Lett. 3 138 – 140, 1978.

[1.15] M. G. Littman, H. J. Metcalf, "Spectrally narrow pulsed dye laser without beam expander", Appl. Opt. 17 2224 – 2227, 1978.

[1.16] K. Liu, M. G. Littman, "Novel geometry for single mode scanning of tunable lasers", Opt. Lett. 6, 117 – 118, 1981.

[1.17] M. G. Littman, "Single mode pulsed tunable dye laser", Appl. Opt. 23, 4465 – 4468, 1984.

[1.18] J. D. Corless, J. A. West, J. Bromage and C. R. Stroud Jr, "Pulsed single mode laser for coherent control experiment", J., Rev. Sci. Instrum. 68, 2259 – 2264, 1997.

[1.19] I. T. McKinnie, A. J. Berry and T. A. King, "Stable, efficient, single mode operation of a high repetition rate grazing incidence dye laser", J. Mod. Phys. 38, 1691 – 1701, 1991.

[1.20] A F Bernhardt, P Rasmussen, "Design criteria and operating characteristics of a single mode pulsed dye laser", Appl. Phys. B 26, 141 – 146, 1981.

[1.21] V S Rawat, K G Manohar, "Development of narrow band pulsed SLM dye laser", National Laser Symposium NLS - 2000, LASTEC, Delhi, Allied Publisher New Delhi, 67 – 69, 2000.

[1.22] C Tallman, R Tennant, "Large scale excimer laser pumped dye lasers", in High power dye laser, F J Duarte ed., Springer Verlag, Berlin, 93 – 142,1991.

[1.23]. F J Duarte, "Tunable Laser Optics" Academic Press Inc., San Diego, CA, 2003.

[1.24] T. V. Plakhotnik, A. M. Pyndyk, "Pulsed tunable dye laser with a low level of wide band background", Sov. J Quantum Electron 1, 1267 – 1268, 1987.

[1.25] T. D. Raymond, P. Esherick, A. V. Smith, "Widely tunable single longitudinal mode pulsed dye laser", Opt. Lett. 14 1116 – 1118, 1989.

[1.26] M Amit, G Bialolenker, D Levron, Z Burshtein, "Refractive index gradients and dye solution flow characteristics in pulsed copper vapor laser pumped dye cells", J Appl. Phys 63, 1293 – 1298, 1988.

[1.27] N Singh, H S Vora, "On the stability of the output characteristics of grazing incidence grating dye laser transversely pumped by copper vapor laser, Appl. Phys B 82, 71 – 74, 2006.

[1.28] H W Schroder, H Welling, B Wellegehausen, "A Narrowband single mode dye laser", Appl. Phys. 1, 343 – 348, 1973.

[1.29] F J Duarte, J A Piper, "Narrow linewidth, high prf copper vapor laser pumped dye laser oscillators", Appl. Opt. 23, 1391 – 1394, 1984.

[1.30] Y Maruyama, M Kato, A Sugiyama, T Arisawa, “Narrow linewidth dye laser with double prism beam expander”, Opt Comm., 81, 67 – 70, 1991.

[1.31] A J S McGonigle, A J Andrews, G P Hogan, D W Coutts, C E Webb, “A compact frequency doubled 10 kHz PRF copper vapour laser pumped dye laser”, App Phy B 76, 307 – 311, 2003.

[1.32] B B McFarland, “Laser second harmonic induced stimulated emission of organic dyes” “Appl., Phys., Lett., 10, 208 – 209, 1967.

[1.33] J Lankard, R V Gutfeld, “Organic lasers excited by a pulsed N_2 Laser”, IEEE J Quantum Electron QE – 5, 625, 1969.

[1.34] D G Sutton, G A Capelle, “KrF laser pumped tunable dye laser in the ultraviolet”, Appl., Phys., Lett., 29, 563 – 564, 1976.

[1.35] A A Pease, W M Pearson, “Axial mode structure of a copper vapor pumped dye laser” Appl., Opt., 16, 57 – 60, 1977.

[1.36] J Fort C Moulin, “High power high energy linear flashlamp pumped dye laser”, Appl. Opt., 26, 1246 – 1249, 1987.

[1.37] R G Morton, V G Draggoo, “Reliable high average power high pulse energy dye laser”, IEEE Quantum Electron, QE – 17, 222, 1981.

[1.38] I L Bass, R E Bonanno, R P Hackel, P R Hammond, “High average power dye laser at Lawrence Livermore National Laboratory ” Appl., Opt., 31, 6993 – 7006, 1992.

[1.39] H R Aldag, D H Titterton, “From flashlamp pumped liquid dye lasers to diode pumped solid state dye lasers”, SPIE Photonics West (San Jose, CA) 22 – 27 January 2005.

Chapter – II

LITERATURE SURVEY

2.1 Introduction

This chapter presents a literature review on single mode dye lasers, which are an important source of tunable radiation in the visible and near visible region of the electromagnetic spectrum.

This class of laser has excellent properties, such as broad tunability, high peak power and potential for obtaining extremely low bandwidths. Broad electronic levels characteristic of the organic dyes provide wide tunability to the organic dye lasers. The dye laser can be operated in the single longitudinal mode (SLM) with linewidth in the range of a few MHz and can be tuned essentially to any wavelength in the visible (VIS) and near invisible range (IR). It is possible to extend the tunability of a single mode dye laser using non-linear processes such as second harmonic generation (SHG) and sum frequency mixing (SFM). The power levels available from the single mode dye laser are a few watts to a few hundreds of watts. Higher powers are generated using master oscillator and power amplifier (MOPA) configurations. The broad tuning range and narrower linewidth of the single mode dye laser provide higher resolutions; for example, a single mode dye laser operating with a linewidth of a few MHz, having a tuning range in nanometers is capable of spectral resolution of ~ 10^8 across its tuning range.

Dye lasers can be operated either in pulsed mode or continuous wave (CW) mode; accordingly, the pump source would be pulsed or CW. The CW single mode dye lasers are capable of providing the narrowest line width in the range of a few kHz. The most common and commercially available CW single mode dye laser system is Rhodamine 6G dye laser pumped by the argon ion laser in a ring cavity configuration. In recent times the pump source of CW dye laser has been replaced with second harmonic of Nd:YAG laser pumped by semiconductor diode lasers. The unidirectional ring cavity avoids the spatial hole burning effect, which is responsible for the undesirable multimode oscillations in the homogeneously broadened dye laser gain medium. The CW single mode dye laser has the capability of generating an output power of a few mW to tens of watts. The CW dye laser systems pumped by argon ion laser have lower conversion efficiencies.

Pulsed dye laser systems pumped by Nd:YAG, Excimer, nitrogen or even flash lamp can generate output pulse energies from a few micro joules to more than tens of joules. The duty cycle (~ 10 – 100 Hz) for these lasers is relatively low. A Copper Vapor Laser (CVL) pumped dye laser operates at relatively higher pulse repetition rates (~ kHz) and relatively smaller pulse energies. Its higher conversion efficiency makes it quite an attractive tool for many applications. The CVL has inimitable advantages for pumping dye lasers, as it can operate simultaneously in two wavelengths 510.554 nm (green) and 578.213 nm (yellow). The CVL can operate at higher pulse repetition frequency (PRF) of around ten kHz with pulse durations of 50 – 60 ns. It can be operated with pulse energies of several mJ per pulse. The pulse energies further can be increased by operating CVL in MOPA configuration [2.1]. The CVL due to its lower photon energies is a better pump for a dye laser, as it will have lower photo degradation than a dye laser pumped by ultraviolet lasers such as nitrogen and excimer lasers.

2.2 Single Longitudinal Mode Operation

The SLM operation of homogeneously broadened dye laser system should occur naturally as the strongest mode suppresses all the other neighborhood cavity modes. Unlike, in a ring cavity a standing wave cavity for a homogeneously broadened gain medium supports more than one mode due to spatial hole burning phenomenon. Several methods have been reported by several groups around the globe for achieving single mode operation [1.6, 1.23].

I. The simplest technique is using a very short cavity laser, so only one cavity mode is able to oscillate in the resonator. The SLM is defined by $\Delta\lambda = \lambda^2/2L$, where λ is the laser wavelength and L is the cavity length. A single longitudinal mode is observed if L is made sufficiently short, so that the longitudinal mode spacing $\Delta\lambda$ exceeds the entire wavelength range over which laser oscillations are possible.

II. Internal mode selection techniques have been used in which intracavity etalons are introduced. The etalons are generally tilted to prevent the oscillation in between the cavity mirrors and etalon faces. The free spectral range (FSR) of the etalon is relatively larger than the cavity FSR of the resonator cavity ($\Delta \nu_{etalon} \gg \Delta \nu_{cavity}$).

III. Placing a thin absorbing film of thickness ~ $\lambda/100$ inside the resonator cavity also generates single mode oscillation. A thin metallic coating on a glass substrate is placed in such a manner that a node of the intracavity standing wave is on the metallic coating layer. The other modes of the cavity suffer losses at the film and get suppressed. The placement of the film is essential to the selection of an axial mode. However, the heating of the thin film limits the available power from the laser system.

IV. The single mode selection by a Fox – Smith interferometer works as follows: beam splitter is used for splitting the resonator beam. It splits in two arms like a Michelson interferometer. Thus, the longitudinal mode is divided into two parts by the beam splitter inside the resonator cavity. Amplification in the gain medium takes place in a longitudinal mode when both parts constructively interfere. Spectral narrowing of a dye laser by grating, interferometric devices or a combination of both can attain the compression factor of nearly 1000. Fox – Smith reflectors are superior to other interferometric devices as they incur lower losses in the optical resonators.

V. A mirror inserted in the resonator, which forms the Fabry Perot (F P) etalon with one of the main mirrors of the cavity, is able to discriminate between the longitudinal modes of the resonator. This pair of mirror acts like a frequency selective element for SLM.

VI. In CW, for SLM a travelling wave cavity is formed by three mirrors, where the wave travelling in one direction is suppressed by a Faraday isolator. This prevents spatial hole burning and SLM operation is achieved.

2.3 Single Mode Selection Techniques in Dye Lasers

Various researchers have worked on SLM dye lasers pumped by CW, low repetition rate pulsed and high repetition rate lasers. Given below is a brief summary of the work indicated in the literature.

Peterson et al. had demonstrated CW operation of dye laser using Rhodamine 6G dissolved in water pumped by argon ion laser in 1970 [1.5]. Herscher and Pike had reported several configurations as shown in figure 2.1 a, b and c for tuning their CW dye laser systems [2.2]. They had optically pumped the aqueous solution of Rhodamine 6G with ~1.5 % surfactant by argon ion laser and obtained about 100 mW of tunable output power utilizing 1.5 Watts of pump power. The assumptions in their approach for the standing wave cavity are: (a) confocal parameter is equal to the dye cell length, (b) most of the pump beam is absorbed within the dye cell and (c) the dye laser beam lies within the pumping volume of the dye laser. The dye cell was kept at an angle with respect to the optic axis to avoid the parasitic oscillation within the dye cell windows. The dye cell was made of fused quartz and was antireflection (AR) coated at the air interface.

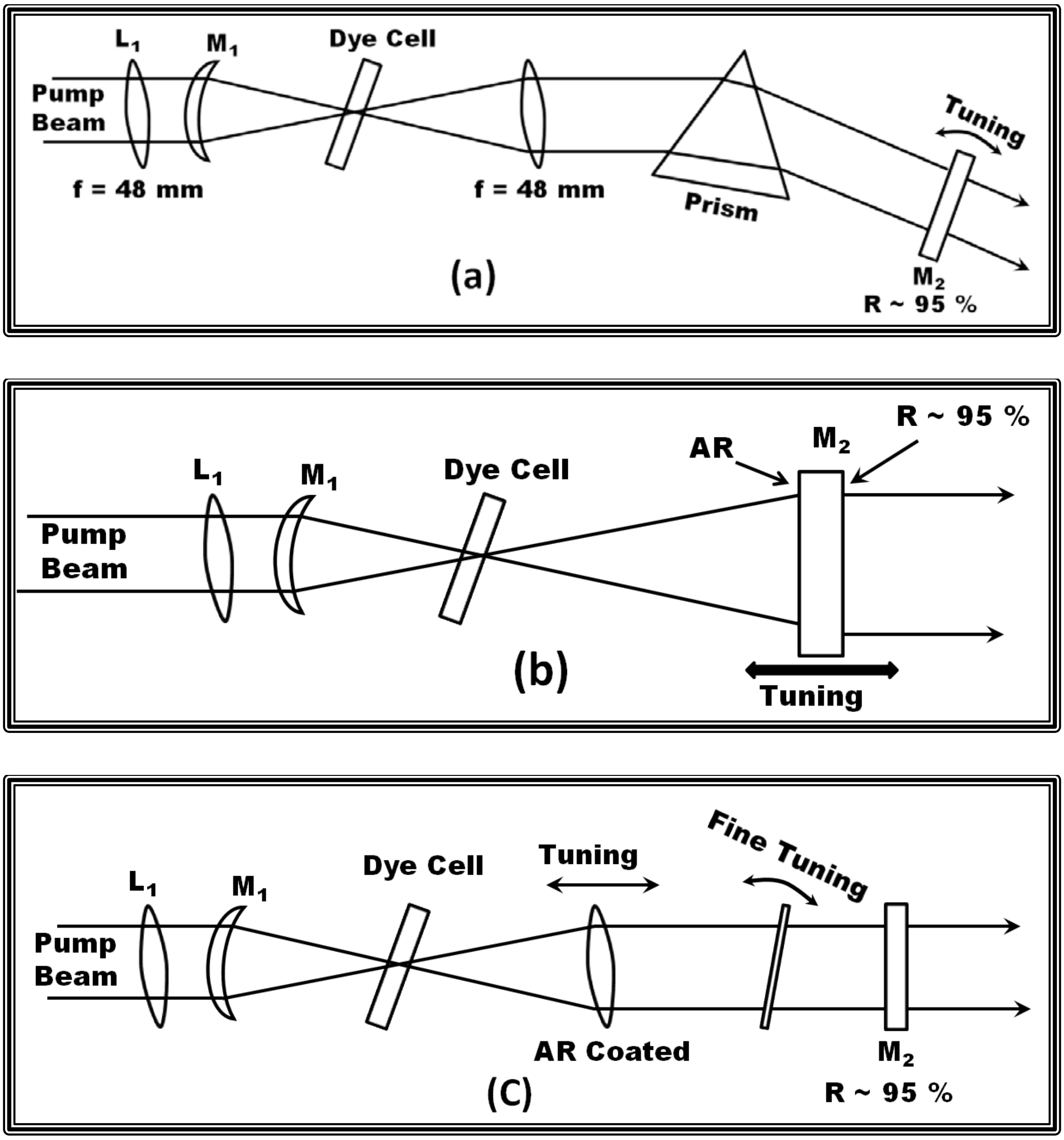

Fig 2.1: Various configurations of CW tunable oscillators: (a) wavelength tuning with prism, (b) tuning with cavity length and (c) tuning with intracavity etalon [Ref 2.2]

All these above configurations had produced dye laser output in TEM_{OO} mode with a bandwidth less than 4 x 10^{-5} nm (~35 MHz) and tuning range greater than 50 nm with a single prism dispersive element inside the resonator cavity [1.8]. In another experiment 0.3 mM Rhodamine 6G solution in water with 1.5% Ammonyx LO was flowing at 10 m/s through a 1x10^{-3} m dye cell with antireflection coated sapphire windows. They had obtained 40 mW single mode power, when the dye laser was pumped by a 1.3 Watt argon ion laser at the peak of the tuning range. Fused quartz windows were changed to sapphire windows in their dye cell to minimize the thermal lensing effect in the single mode laser system. The thermal distortion and shock waves in the dye gain medium limits the minimum achievable bandwidth from the single mode dye laser. Although the resonator configurations described above were used for CW dye lasers, they were also used for pulsed dye laser operation by replacing the pump laser with a flash lamp. The bandwidth of the pulsed system was limited by the angular dispersive power of the prism used in the cavity. A typical bandwidth of flash lamp pumped dye laser without any dispersive element was 7 nm achieved by gain narrowing, which was further reduced to 0.2 – 0.3 nm by insertion of four Brewster angle prisms providing total dispersion of 10^3 nm/radian.

The CW single mode dye laser power is limited to 200 – 300 mW, when they are operated as standing wave lasers; to suppress the oscillation in the other modes a dispersive element such as a prism or F P etalon is inserted into the cavity. This occurs at the cost of single mode efficiency because the dispersive components introduce losses not only for the undesired modes but for the main mode too. For CW single mode lasers prisms are preferred over the grating as dispersive element because the losses associated with prisms are lower than those of a grating, although the linewidth associated with grating cavities is much narrower than that of single prism cavities. The gratings are more commonly used with more efficient pulsed single mode dye laser systems.

2.3.1 Travelling Wave Ring Laser

Higher efficiencies for single mode dye laser are reported for travelling wave cavities because here the spatial hole burning does not exist and therefore a dispersive element is not necessary for introducing selective losses inside the resonator cavity. One of the methods to obtain the travelling wave ring laser is the unidirectional operation by Faraday isolators. The opening angles of the ring cavity should be chosen between

10^{O} and 15^{O} to reduce the effect of coma and astigmatism introduced by the optical components. For unidirectional operation, it is necessary that the lasing in one direction (say clockwise) should suffer huge losses to reduce the gain below the threshold and for laser intensity travelling in the other direction (anti clockwise) should be essentially lossless. Such elements are known as optical diodes, which are made by using a Faraday rotator with optically active quartz crystal. Typical ring cavity used for travelling wave dye laser is illustrated in figure 2.2. It is important that the focused pump beam and cavity beam waist should coincide in the gain medium and both the spots should be approximately equal. The focused pump beam size is defined by the pump beam divergence and focusing mirror parameters such as focal length and astigmatism, while the beam waist is a cavity parameter. The smaller size pump beam can result in power losses due to diffraction, while larger beam waist allows higher order modes to oscillate. The birefringent plates are used to tune the laser to the required wavelength in a single mode. To ensure a single mode oscillation a combination of thin and thick FP etalons is also utilized in the ring cavity. The combination of etalons makes sure a selection of single mode across the entire tuning range of the dye laser. For high power operation of the single mode dye laser Faraday isolator was not utilized by Schroder et.al, [1.9] as it usually produces strong thermal lensing due to absorption. The mode selection takes place by coupling of clockwise and counterclockwise running modes in a ring cavity. The Bragg reflection due to inversion grating generated within the gain medium supports the stronger mode suppressing the weaker modes.

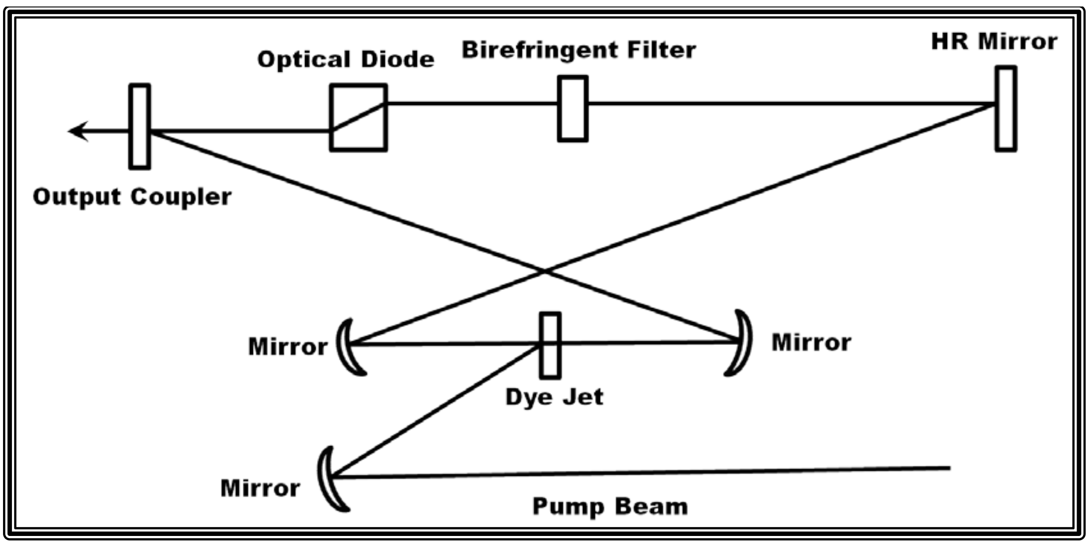

Fig 2.2: Typical travelling wave cavity used for single mode dye lasers

The direction of the laser can be determined by placing a retro reflecting mirror outside the ring cavity. In high power operation, thermal lensing in the dye gain medium also plays an important role, which depends on the type of dye solvent as well as on the flow rates. The heating effects are suppressed by circulating the dye at higher flow velocities in the dye cell. Schroder et al. have studied the effect of microscopic velocity fluctuations due to turbulent flow within the dye cell on the linewidth [1.28]. They have further found that the linewidth of the single mode dye laser depends on the mechanical disturbances and temperature fluctuations in the dye solvent. Nearly 2 MHz linewidth was achieved in the free running a single mode dye laser. It was observed that the intensity of fluctuations decrease and the output power increases with increasing flow velocity inside the dye cell. The maximum flow velocity inside the dye cell is limited by the onset of cavitation in the dye cell. In addition to possible mechanical damage to the dye cell, the cavitations severely degrade the optical homogeneity of the flowing medium. The variation in the excitation power also increases the linewidth of the single mode laser. The change in the excitation power leads to a temperature change in the gain medium which, in turn, causes wavelength variation in the dye laser output.

The window heating problem was removed by using dye free flowing jet instead of dye cells. The free stream jet puts some restriction on the dye solvents such as water and alcohols. In general, ethylene glycol or glycerol based solvents is used in the free stream jets due to their higher viscosities. High efficiency single frequency CW dye laser has been demonstrated by Jarrett and Young [2.3]; they have obtained 0.9 Watt at 580 nm from Rhodamine 6G laser dye, pumped by 4 Watt argon ion laser. Johnston et al. [2.4] had demonstrated high power CW single frequency dye laser with an improved water based dye solvent pumped by all the lines of an argon ion laser. They have generated 5.6 Watt of frequency stabilized single mode dye laser from their ring cavity with Rhodamine 6G pumped by 24 Watt argon laser. They have eliminated thermal effects in the dye jet of water based solvent, a mixture of Ammonyx LO and ethylene glycol by cooling to 10^{O} C. This CW single mode dye laser was tuned over the entire visible spectrum from 407 nm – 887 nm.

2.3.2 CW Dye Laser with Michelson Filter

Liberman and Pinard had used a Michelson type interferometer as one of the cavity mirrors for selecting the single mode in their CW dye laser [2.5] as mentioned earlier.

They had obtained a single mode at relatively low powers of a few milliwatts due to poor selectivity of their Michelson based reflector. The principal advantage of this technique is that all the mirrors are used at normal incidence, which eliminates spurious spots arising due to multiple reflections. Later on Pinard et al. had improved the frequency selectivity of the Michelson type reflector by using the double Michelson device, which uses the properties of the Michelson interferometer twice [2.6]. One of the cavity mirrors of the dye laser was replaced by a three wave interferometer of the Michelson type as shown in figure 2.3. This simple technique provides higher single mode power of 250 mW, a lower threshold and a good geometrical beam quality of the single mode dye laser.

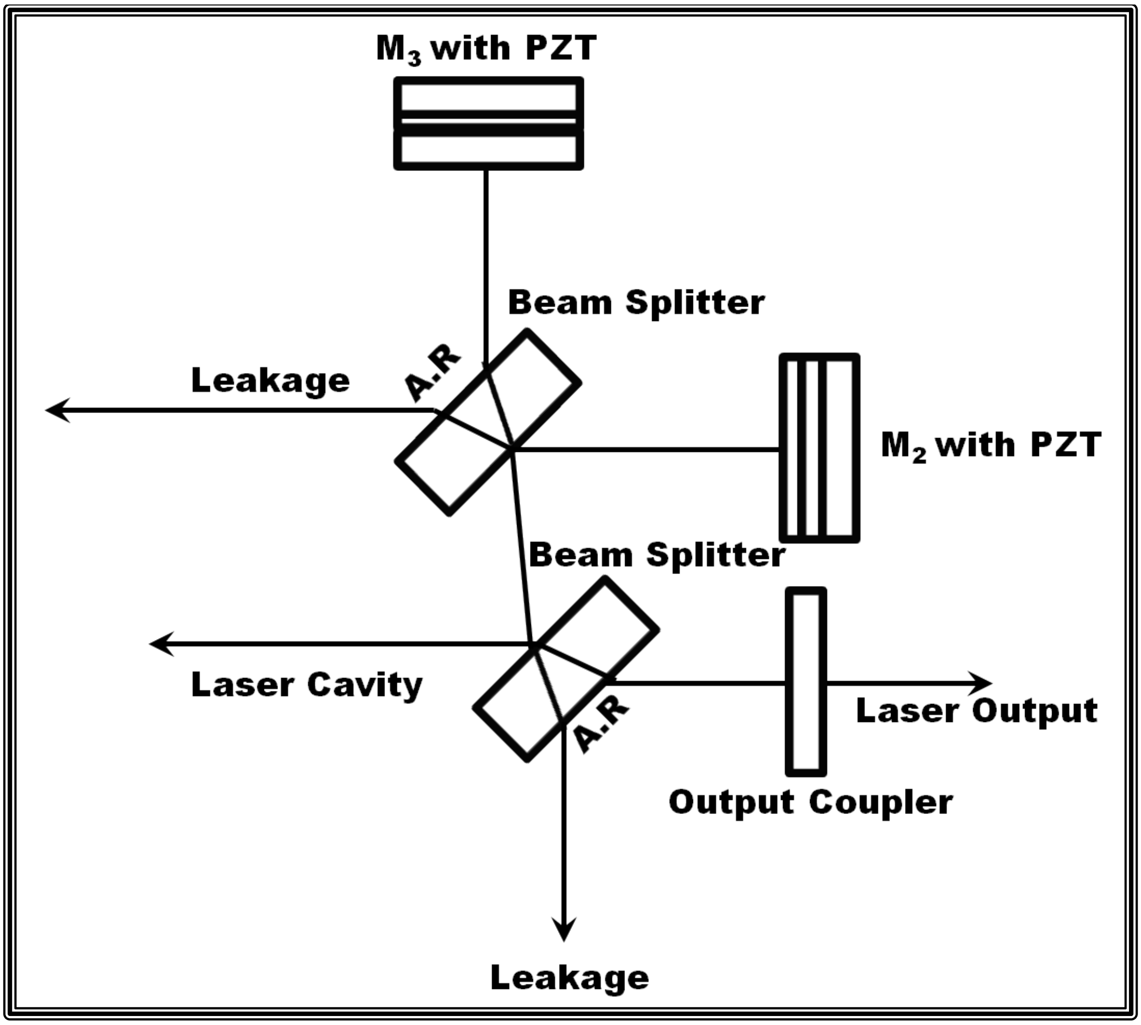

Fig 2.3: Double Michelson interferometer used for obtaining single mode dye laser

The salient features of the CW single mode dye laser reviewed here are summarized in the table 2.1.

Table-2.1: Continuous Wave Single Mode Dye Lasers Pumped by Argon Ion Lasers

S. No.	Gain Medium	Cavity Type for Single Mode	Flow cell /Jet	Wavelength/ Tuning Range	Bandwidth	Output Power/ Conversion efficiency	Authors
1.	0.27 mM Rh6G with 3% Ammonyx LO	Linear Cavity	Dye Cell 1x 4 mm flow channel	*Not Reported*	2 – 15 MHz	10 mW / 0.66 %	Schroder et al., (1973)
2.	Rh6G in Ethanol	Double Michelson Mode selector	Dye jet	40 GHz with pressure scanning	*Not Reported*	250 mW / 5 %	Pinard et al., (1979)
3.	*Not Reported*	Travelling Wave Cavity	Dye jet	595 nm	20 MHz	1.2 W / 19 %	Schroder et al., (1977)
4.	Rh6G , DCM	Ring Cavity	Dye jet with 15 m/s velocity	545 – 770 nm	500 kHz	1.5 W / 15 %	Kobtsev et al., (2006)
5.	0.27 mM Rh6G dye solution with 3% Ammonyx LO	Standing wave Cavity	Dye Cell with quartz windows	*Not Reported*	2 MHz	10 mW / 0.67 %	Schroder et al. (1973)
6.	o.3 mM Rh6G in Water and 1.5% Ammonyx LO	Standing Wave Cavity	Dye Cell 1 mm	570 – 620 nm	35 MHz	40 mW / 3 %	Hercher and Pike (1971)
7.	Rh6G in Ethylene Glycol	Unidirectional Ring cavity	Dye jet	580 nm , 570 – 635 nm	*Not Reported*	1.3 W/ 28 %	Myslinski (1986)

2.3 Pulsed Single Mode Dye Lasers

Compared to conversion efficiencies of ~ 10^{-4} of CW dye lasers, pulsed dye lasers provide conversion efficiencies of ~10^{-2} to 10^{-3} and can generate peak power levels in Mega Watt range. The first pulsed dye laser was demonstrated by Sorokin and Lankard [1.1]; they had observed stimulated emission of spectral width of 5 cm^{-1} at 755 nm from solutions of an organic dye, chloro-aluminum phthalocyanine, while pumping by a ruby laser. Schafer et al., had independently observed stimulated emission while studying saturation and hole burning in organic dyes of the cyanine type by absolute intensity measurement of the ruby laser induced fluorescence [1.2]. They also observed the organic dye solution, laser which emits a spectrally broad pulse up to some hundreds of wave numbers, depending upon dye concentration, cavity length and conditions of cavity gain.

The dye laser pumping with shorter wavelengths such as second harmonics of neodymium and ruby has been reported by several groups. The use of a nitrogen laser as a pump source for single mode dye lasers has been reported by numerous authors [2.5, 2.7 – 2.11]. It is reasonably simple to obtain the laser oscillation in the fundamental transverse mode by introducing a suitable aperture near one of the mirrors in the laser cavity, while a selection of SLM entails some difficulty. A flashlamp pumped dye laser with SLM and single transverse mode (TEM_{OO}) has been shown by Gale [2.7]. He had used an aqueous solution of 0.1 mM Rhodamine 6G with 3% by volume Ammonyx LO (surfactant) flowing at a velocity of 15 cm/sec through a $50x10^{-3}$m long and $3x10^{-3}$m internal diameter tubular dye cell pumped by a xenon filled linear quartz flash lamp. This dye cell was placed in a laser cavity formed by 100 % reflection concave mirror and an output coupler of 35% transmission. A 1.5 mm circular aperture was placed near the output coupler for ensuring the lowest order transverse mode (TEM_{OO}) for the dye laser cavity. Three antireflection coated tilted FP etalons had been used for obtaining SLM oscillation. The cavity configuration used by Gale is given in figure 2.4. All the optical components were mounted rigidly on a stainless steel rail and this cavity was placed inside a pressure chamber for isolating the laser from changes in atmospheric pressure. The change in frequency of the dye laser due to air pressure change is ~ 20 MHz/mm Hg. He had obtained single mode bandwidth of 8 ± 2 MHz, pulse duration of 100 ns and a pulse repetition frequency of 0.2 Hz. The thermal distortions for the dye laser were minimized by shorter duration of the pump pulse and smaller thermal expansion coefficient of the water based dye solution.

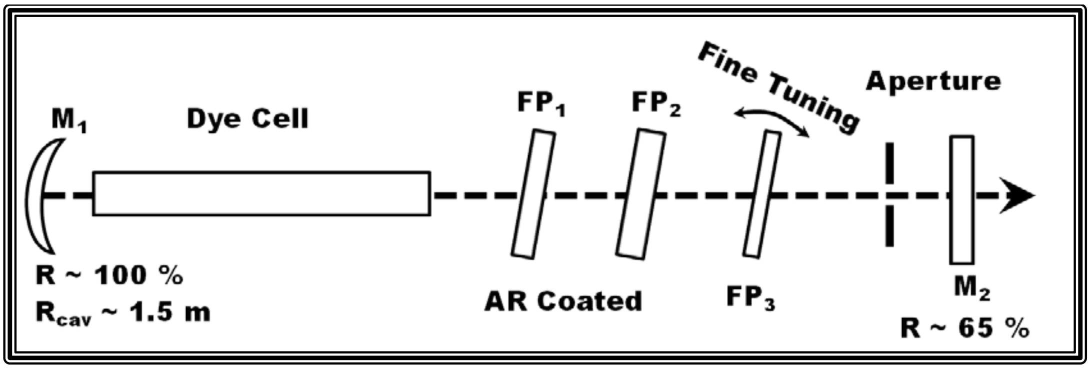

Fig 2.4 Pulsed single mode dye laser pumped by flash lamp [Ref 2.7].

Marowsky had used a Fox – Smith interferometer in combination with an interference filter and two quartz FP etalons of 0.25 mm and 4 mm thickness for obtaining the single mode oscillation in the flashlamp pumped dye laser [2.12]. He had used Rhodamine 6G dissolved in water with Ammonyx LO 30 to obtain laser output parameters of peak wavelength 600 nm, peak power of 1 kW and linewidth of 0.05 pm. The short term wavelength stability of this single mode dye laser for 10 successive pulses was 0.02 pm. The main advantage of Fox – Smith reflector over the tilted FP etalons for the selection of single mode is eliminating the walk off losses, which are inherently present with the FP etalons. Figure 2.5 shows the mechanism of the single mode selection in the Fox – Smith selector and FP etalons used by Marowsky.

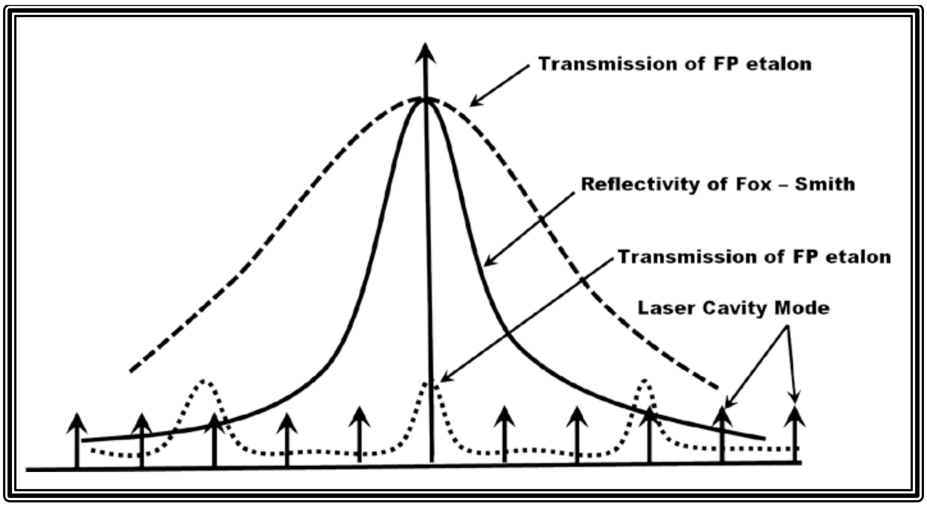

Fig 2.5: Schematic of resonator mode selection by FP etalons and Fox – Smith selector

The peak reflectivity of the Fox – Smith reflector can be matched with the transmission maxima of the FP etalons inside the resonator cavity by precisely adjusting the FP etalon tilt. The combined reflectivity of Fox – Smith reflector and FP etalon's transmission maxima results in the single mode oscillation. The insertion of high finesse FP etalons severely reduces the efficiency of the single mode dye laser due to higher cavity loss introduced by the FP etalons.

2.4.1 Low Repetition Rate Narrow Band Dye Lasers

For operation of SLM dye laser two design goals need to be achieved, which are reduction of cavity length such that the number of round trips within cavity should be large for short available gain and restricting the gain volume so that the cavity Fresnel number should be less than one.

Iles et al. have reported nitrogen laser pumped tunable dye laser operated in a stable SLM based on the Hansch type cavity. Time averaged bandwidth of 0.021 cm^{-1} and single short bandwidth of 630 MHz with a conversion efficiency of 0.5 % have been obtained. On increasing the dye concentration by nearly 4 times from 5 mM to 20 mM the bandwidth of the single mode dye laser increased up to the single pass bandwidth of the cavity and the conversion efficiency increased by 3 times. In the Hansch type cavity, the spectral narrowing and tuning were achieved by a diffraction grating in Littrow configuration. The wavelength selectivity and linewidth narrowing are further improved by an intracavity beam expansion by several methods: lens telescope [2.9], prism expander [2.10] and mirror telescope [2.13]. Hansch had used intracavity beam expanding telescope with tilted F P etalon for his grating based dye laser cavity and obtained a linewidth of 0.004 Å. This dye laser was pumped by a nitrogen laser with a pulse repetition rate of 100 Hz [2.9]. The role of the telescope is to expand the laser beam inside the resonator cavity, so that a larger grating width can be illuminated to obtain higher resolution. It reduces the super-fluorescent beam divergence incident on the grating, which results in reduction of the dye laser linewidth. Two dimensional intracavity expansion used by Hansch increases the cavity length, which is more sensitive to thermal variations. For the nitrogen pump dye laser, the available gain time duration is only a few tens of nanoseconds in which only a few cavity round trips are possible. Hence the linewidth of the dye laser does not reduce much compared to the single pass linewidth of the passive cavity. The cavity single pass linewidth is proportional to the beam divergence of super-fluorescent and inversely proportional to the angular dispersion provided by the frequency selective element in the cavity.

Eesely and Levenson used a mirror telescope with magnification of 18 by employing a combination of convex mirror (f_1 ~ 2.5 cm) and concave mirror (f_2 ~ 46 cm) in the confocal configuration for reducing the intracavity beam divergence and obtained a linewidth of 1.5 cm^{-1} for nitrogen pumped dye laser. The linewidth obtained by them was relatively larger because they used longer cavity length for a short gain, duration available from nitrogen pumped dye laser [2.13]. The main advantages of reflective beam expanders are reduction in the insertion losses, elimination of chromatic aberrations and spurious reflections.

Corney et al. [2.14] had used a rare halide excimer laser for pumping the dye laser and obtained an output bandwidth of as low as 0.012 Å. This simple narrow band dye laser was tuned from 335 nm to 345 nm. In a subsequent development, Sorokin and Lankard (1967) and also independently Schmidt and Schafer (1967) replaced the high intensity laser pumping source with flash lamp. Snavely and Schafer (1969) established the feasibility of continuous wave dye laser pumped by flash lamp [1.3]. This experiment disproves the notion, that a CW dye laser was not feasible because of metastable triplet state losses. In general, uncontrolled triplet losses limit the operation of the dye laser to pulse outputs of approximately 10^{-7} to 10^{-6} sec duration.

In a short cavity with grazing incidence grating (GIG) configuration, it is possible to obtain efficient single mode operation with only one dispersive element grating. A very short cavity is desirable as with shorter cavity length the cavity mode separation is very large. It is to be noted that this cavity is more sensitive to mechanical vibrations which affect the frequency stability of the single mode oscillator. Replacing a dye cell with the commonly used dye jet for CW dye lasers can further reduce the cavity length to obtain large axial mode separation. Reduction in the dye gain length needs higher dye concentrations for commonly used laser dyes to overcome higher losses at grazing incidence. The temporal profile of the single mode pulsed dye laser is smooth because there is no mode beating.

Hanna et al. used a single prism beam expander for their nitrogen laser pumped dye laser, which can generate narrow linewidth similar to those obtained with the telescope beam expanded cavities [2.10]. They had obtained 10 kW diffraction limited tunable output power, 0.01 cm^{-1} linewidth from a dye laser with a single prism beam expander and F P Etalon.

Mory et al. had used optimized holographic grating in grazing incidence with F P Etalon inserted in the diffracted beam of the resonator for spectral narrowing of their dye laser [2.15]. They had obtained about 31 kW output power and 4 pm spectral width from nitrogen pumped Rhodamine 6G dye laser.

Lawler et al. had studied various configurations of Hansch type dye laser pumped by short pulse duration (~ 4 – 5 ns), high power (~ 0.5 MW) nitrogen laser for obtaining narrower linewidth in the range of 0.05 nm to 0.0005 nm [2.17]. If the bandwidth required from the dye laser is 0.01 nm or greater, a low magnification telescope and a diffraction grating are adequate. It is advantageous to use F P etalon inside the dye laser cavity if the required bandwidth is in the range of 0.001 – 0.1 nm. The etalons introduce more wavelength dispersion inside the cavity for generating narrower bandwidths. If the bandwidth requirement is less than 0.001 nm with higher conversion efficiencies it is necessary to use an internal etalon followed by an external etalon and a dye amplifier. They had found that the conversion efficiency of etalon based dye laser can be improved greatly by adjusting the temporal distribution of the pump pulse. They had used a single dye cell in the dye laser system first used as an oscillator and then as an amplifier.

Stokes et al. had demonstrated a dye laser tunable from ultraviolet (UV ~ 350 nm) to infrared (IR~ 730 nm) wavelength region using a variety of laser dyes and their mixtures. The lower limit of wavelength region of the dye laser is extended by 244 nm with efficient second harmonic generation of dye laser output using a cooled ADP crystal.

Wallenstein and Hansch had used aluminized reflection grating in Littrow configuration with intracavity etalon and external invar spaced confocal resonator having a free spectral range of 2 GHz and finesse of 200 for their nitrogen pumped single mode dye laser [2.18]. This single mode dye laser had a bandwidth of 25 MHz, which could be continuously pressure scanned over 150 GHz without any mechanical movement. For example, nitrogen gas (n = 1.000278 at 20 ^{O}C) is used for tuning a laser at a tuning rate of 188 MHz/Torr at 600 nm. The tuning range was further increased by using different scan gas having higher refractive index. When the nitrogen gas was changed to propane gas (n = 1.001023 at 20^{O} C), the scanning was increased to 524 GHz from 150 GHz for the same pressure change of 1 atm. The scanning range was further improved to 850 GHz at 600 nm by modifying the pressure chamber, which allows the pressurization up to 5 atm. The linewidth of the single mode dye laser increased to 750 MHz from 25 MHz without an external confocal filter. For pressure scanning of this single mode dye laser grating and F P etalon was enclosed in an air tight common pressure chamber, whose pressure was varied by a regulating valve connected to a nitrogen gas cylinder. The external confocal cavity was also kept in a separated pressure chamber and both the chambers were connected by copper tubing. Tilted quartz wedge plates with broadband antireflection coating on both the surfaces having a wedge angle of 30′ and surface flatness of $\frac{\lambda}{20}$ have been applied to optically isolating the pressure chambers. These pressure chambers were evacuated to a few torr pressure with a rotary pump. For continuous scanning of the single mode dye laser, the pressure inside the chamber was regulated by a needle valve. The pressure scanning of the air spaced F P interferometers is mostly linear. The scan rate of the single mode dye laser was regulated by controlling the leak rate of the pressure chamber.

Bourne and Rayner had designed and reported the pressured tuned SLM dye laser [2.19]. This SLM dye laser was pressure tuned linearly over a range of 3.75 cm^{-1}.

Dinev et al. had demonstrated two wavelength single mode dye lasers pumped by a nitrogen laser for which both the wavelengths can be tuned independently over the entire tuning range [2.20]. They confirmed simultaneous single mode operation in two wavelengths by tuning the single mode laser at two different wavelengths by their respective resonant reflectors. One resonant reflector was tuned for red wavelength and the other was tuned for yellow wavelength and the combined output was separated using an appropriate filter. This dye laser is highly sensitive to the alignment of the components, as very slight de-tuning results in two mode oscillations. The single shot bandwidth of this single mode dye laser was measured to be 310 ± 50 MHz. The salient features of the low repetition rate SLM dye lasers pumped by a flash lamp or nitrogen / Nd:YAG / Excimer are summarized in table 2.2.

Table 2.2: Low Repetition Rate Pulsed dye Laser Pumped by Flashlamp or Nd:YAG / Excimer/ Nitrogen laser

S.No.	Gain Medium	Cavity Type for Single Mode	Flow cell /Jet	Wavelength / Tuning Range	Bandwidth	PRF Pulse / Duration	Output Power/ Conversion efficiency	Authors
1.	0.1 mM Rh6G in Water with ~ 3 % Ammonyx LO	Concave & 35% output coupler, Three AR coated Tilted Etalon	Flowing Dye Cell 50 mm long, 3mm dia	*Not Reported*	8 ± 2 MHz	100 ns / 0.2 Hz,	*Not Reported*	M Gale (1973)
2.	Rh6G in Water with Ammonyx LO	Fox Smith Interference filter with two FP Etalons of 0.25 mm and 4 mm	*Dye Cuvette*	600 nm	0.02 pm	10 Hz	1 kW	Marowsky (1973)
3.	5 mM Rh6G	GIG Configuration and Blazed Grating at Littrow end mirror replaced with third grating	Quartz Dye cell of 1 cm	*600 nm*	0.021 cm^{-1} 630 MHz single Pulsed Bandwidth	5 ns	0.5 %	Iles et al. (1980)
4.	Rhodamine and Oxazine	GIG Cavity	Dye Cell with 1 mm flow channel	Mode hops free scan 15 cm^{-1}	150 MHz	Pulsed	3 %	Littman (1984)
5.	*Not Reported*	Single Prism Expander, and F P Etalon	Dye Cell	400 – 600 nm	0.01cm^{-1}	Pulsed	10 kW	Hanna et.al, (1975)
6.	5 mM Rh6G in EtOH	GIG cavity with F P Etalon	Dye Cuvette 12 mm	490 – 680 nm	4 pm	2 Hz / 4.5 ns	31 kW / 10 %	Mory et.al, (1981)
7.	Rh6G in Hexafluoro Isopropanol	GIG Cavity with 89^{O} and another grating in Littrow	Dye Cell	570 nm Tuning range 40 nm	0.1 cm^{-1}	*Not Reported*	5 kW	Shoshan Oppenheim (1978)

S.No.	Gain Medium	Cavity Type for Single Mode	Flow cell /Jet	Wavelength / Tuning Range	Bandwidth	PRF Pulse / Duration	Output Power/ Conversion efficiency	Authors
8.	5 mM 7D4MC in EtOH, 5 mM FDS in MeOH, 5mM Rh6G in EtOH, 5 mM RhB in EtOH	Hansch Cavity, cavity length 15 cm, etalon	SS Dye Cell, with fused silica window fixed with Hysol epoxy	480 nm	0.001 nm and 0.0005 nm with external etalon	60 Hz / 4 – 5 ns	0.5 MW/ 10 %	Lawler et al., (1976)
9.	5 mM Rh6G in EtOH	Littrow Cavity with internal Etalon and External confocal cavity FSR 2 GHz	Dye cell	600 nm / Pressure Scanned over 150 GHz	25 MHz with external Confocal cavity and 750 MHz without	50 Hz	*Not Reported*	Wallenstein, Hansch (1974)
10.	3 mM Rh6G DN in absolute alcohol	GIG Cavity with two resonant reflector	Dye Cell 1 cm	Simultaneous operation two wavelengths Red and Yellow, 560 – 600 nm	Single shot bandwidth 310±50 MHz	10 Hz / 8 ns	500 kW	Dinev et al., (1980)
11.	*0.1 mM Mixture of DTCDT and DTNDCT in Pyridine*	Grating intracavity etalon	*Dye cell 2 cm long and 4 cm diameter with 1^{O} tilted window*	760 – 770 nm / 100 Å	0.5 Å, < 500 MHz	*6 ns*	*0.25MW / 4%*	Bradley et al., (1968)
12.	Rh6G in EtOH	Four prism tuning systems	Quartz dye cell 6 mm ID	595 nm 571 – 616 nm	0.17 nm	100 Hz	0.14 J	Strome and Webb (1971)
13.	*5 mM Rh6G EtOH*	Intracavity Telescope M 20 tilted FP Etalon, Littrow cavity	*Pyrex tube dye cell 12 mm dia. 10 mm long*	*600 nm*	300 MHz or less than 0.004Å	100 Hz / 5 – 10 ns	*2 – 4 kW / 4 %*	Hanach (1972)
16.	1 mM Rh6G in EtOH	Prism expander at Grazing incidence	2.5 cm long Dye Cell	*Not Reported*	0.9 Å	20 Hz / 5 ns	*Not Reported*	Mayer (1971)
17.	0.3 mM Rh6G in	Littrow Cavity with Mirror telescope M	Dye Cell	*Not Reported*	1.5 cm^{-1}	10 Hz / 7	17.5 k W	Eesely and Levenson

S.No.	Gain Medium	Cavity Type for Single Mode	Flow cell /Jet	Wavelength / Tuning Range	Bandwidth	PRF Pulse / Duration	Output Power/ Conversion efficiency	Authors
	EtOH	18				ns		(1976)
18.	2.5 mM Rh6G in Hexafluoro Isopropanol	GIG Cavity	Dye Cell	570 nm	0.08 cm^{-1}	10 Hz / 4 ns	4 kW	Shoshan et al, (1977)
19.	*Coumarin 500, DCM and 0.2 mM Rh6G*	Pressure Tuned Littman Cavity Single mode Laser	*Quartz Dye Cell*	520 nm and 620 nm 3.75 cm^{-1} pressure tuned	*0.019 cm^{-1}*	100 Hz / 1.8 ns	*0.2μJ*	Bourne and Rayner (1987)
20.	*Not Reported*	Prism Beam expander and Grating	*Not Reported*	*Not Reported*	0.1 cm^{-1}	*Not Reported*	*Not Reported*	Novikov et al., (1975)
21.	10mM Coumarin 500 in EtOH	GIG with prismatic beam expander	Fused Silica Dye Cell	490 – 530 nm	0.01Å ,0.008Å with double prim expander	Low PRF, 6 ns	0.16 mJ /PP 7 – 10 %	Duarte and Piper (1980)
22.	06 mM Rh6G, dye Mixture (Rh6G + Cresyl Violet)	GIG Cavity, incidence angle 89.2^{O}	Dye Cell with tilted face (Molectron DL051)	600 nm	1.25 GHz	10 Hz / 6 ns	10 kW	Littman and Metcalf (1978)
23.	Dye Rh6G doped MPMMA Solid Medium	MPL cavity, cavity length 55 mm	Trapezoidal wider dim 10 mm	562 -613 nm MPL	SLM ≤ 700 MHz	3 – 4 ns	5-7% HMPGI	Duarte (1995)
24.	0.3 mM Rh 610 in methanol (2 l) water(½ l) mixture	Short Cavity GIG, Cavity length 4 – 5 cm, incidence angle 89^{O} – 89.5^{O}	Quartz Dye Cell with 1mm NSG cell	582 - 599 nm, 1.7 cm^{-1} mode hop free589 nm	58 MHz, time averaged Bandwidth240 MHz	10 Hz / 20 ns	*Not Reported*	Corless, et al., (1997)
25.	1.5 mM Coumarin 522 in ethanol	Littman Cavity incidence angle 88.6^{O} cavity length 4 cm	Dye cell with gain 1.5 mm	*Not Reported*	*Not Reported*	1.2 – 2 ns	1 – 3 %	Jianzhao et al., (2000)

S.No.	Gain Medium	Cavity Type for Single Mode	Flow cell /Jet	Wavelength / Tuning Range	Bandwidth	PRF Pulse / Duration	Output Power/ Conversion efficiency	Authors
26.	2.5 mM Rh6G in EtOH	GIG cavity at 89.2^{O} and another grating at Littrow	Dye Cell	600 nm	300 MHz single Pulse , 750 MHz time averaged	10 Hz / 6 ns	2 – 3%	Littman (1978)
27.	Dye in Mixture of ethylene and water for SCL and RhB in EtOH for NBA	Short Cavity Laser (SCL), cavity length 1-2 mm, Longitudinal pumping	Dye Cell with two mirrors	Continuous scanning 34 cm^{-1} limited by PZT	250 MHz	10 ns	100 kW	Ewart and Meacher (1989)
28.	1 mM Rh6G Coumarin 485	Littrow cavity with Intra cavity etalon, M 25	Dye Cell 10 mm long	Pressure Scanning of dye laser, Δp = 7 bar, scans 3895 GHz	260 MHz and 100 MHz with filtering by confocal filter	5 – 6 ns	4 mJ / 0.8 %	Wallenstein and Zacharias (1980)
29.	1 mM Rh6G in EtOH	GIG Cavity, cavity length of 10 cm	Dye Cell 1 cm	560 – 670 nm	385 MHz	10 Hz	3 %	Hung and Brechignac (1985)
30.	0.3 mM Rh6G EtOH	GIG Cavity	Triangular dye cell	550 – 575 nm	580 ± 50 MHz	100 Hz	15 %	Koprinkov et al, (1982)
31.	0.9 mM 3,3' dimethyl 2, 2' oxatricarbocyanine iodide in aceton	Littrow cavity, with beam expander M 5.3,	Teflon Dye cell 35 mm long with AR coated Windows	720 nm – 750 nm	0.16 Å	15 ns	100 kW/ 6 %	Owyoung (1974)
32.	*Not Reported*	GIG cavity with beam expanding telescope and etalon	Dye cell with 20mm long	*Not Reported*	500 MHz	2- 3 ns	*Not Reported*	Chang and Li (1980)
33.	*Not Reported*	GIG cavity with resonant reflector	Dye Cell 3.4 cm long	519 – 575 nm	420 ±30 MHz	30 Hz / 1.1 ±0.1 ns	1 kW/ 2 %	Saikan (1978)

2.4.2 High Repetition Rate Dye Oscillators Pumped by Copper Vapor / Copper Bromide Laser

CVL pumped dye laser has the unique potential to operate at high average power at a high pulse repetition rate and good overall conversion efficiency. The high pulse repetition frequency CVL pumped dye laser was reported by Pease and Pearson in 1977 [1.35]. They obtained time averaged bandwidth of 1.3 GHz, which was the desired bandwidth for the uranium isotope separation technique. This dye laser system was the first transversely pumped dye cell, which was operated at a pulse repletion frequency of 6 kHz. This dye laser consists of 8 mm long dye cell placed at an angle of 3^{O} with respect to the resonator axis to avoid the parasitic oscillations, Echelle grating with groove spacing of 600 lines/mm blazed at $54^{O}\,6'$, 3 mm thick quartz solid etalon having finesse of 20, a telescope with magnification of 22.5 and uncoated wedged quartz as an output coupler. A cylindrical lens of 100 mm focal length was used to line focus the CVL pump beam on the dye cell. About 2.25 mM Rhodamine 6G dissolved in ethanol was circulated through the dye cell at a sufficiently large flow velocity so that the clearance ratio of one was obtained for the focused pump beam width of 300 μm. The typical laser parameters for CVL pumped narrowband dye laser is pulse energies of hundreds of μJ, peak power of tens of kilowatt, pulse repetition rate of a few tens of kHz and pulse duration in tens of nanoseconds.

Sun et al. had longitudinally pumped the dye jet of Kiton red dissolved in ethylene glycol by Cu/CuBr laser operating at 20 kHz pulse repetition rate and obtained nearly 40 % conversion efficiency [2.21]. The flow velocity of the jet stream was maintained at 18 m/s. They had studied theoretically and experimentally the dependence of pump power on the laser output power for different dye concentration and different reflectivities of output coupler.

Petrov et al. had used copper bromide laser for pumping a dye jet stream of 0.8 mM Rhodamine 590 in ethylene glycol and obtained a conversion efficiency of 63 % in broadband cavity [2.22].

Huang and Namba had used longitudinal pumping for the dye jet of Rhodamine 6G with CVL operating at 5 kHz pulse repetition rate and obtained 0.86 Watt of tunable output power with conversion efficiency of 31% [2.23]. The dye jet dimensions were 0.1 x 4.3 mm with jet stream flow velocity of 13 m/s. The dye laser efficiency was increased with increasing pump power initially; it was clamped to a constant value of 31 % when pump power was increased beyond 2 Watt.

Morey had compared the performance of CVL pumped dye lasers with broadband cavity in two pumping configurations as shown in figure 2.6 and figure 2.7. He had used 5 Watt CVL beam to pump the dye laser oscillator in two configurations, longitudinal as well as transverse [2.24]. He had eliminated the thermal lensing in the dye oscillators by replacing the dye cell windows and tuning prisms materials by non absorbing fused silica. He obtained conversion efficiencies of nearly 57 % in longitudinal pumping and 59 % in transverse pumping configuration with Rhodamine 6G dissolved in ethanol.

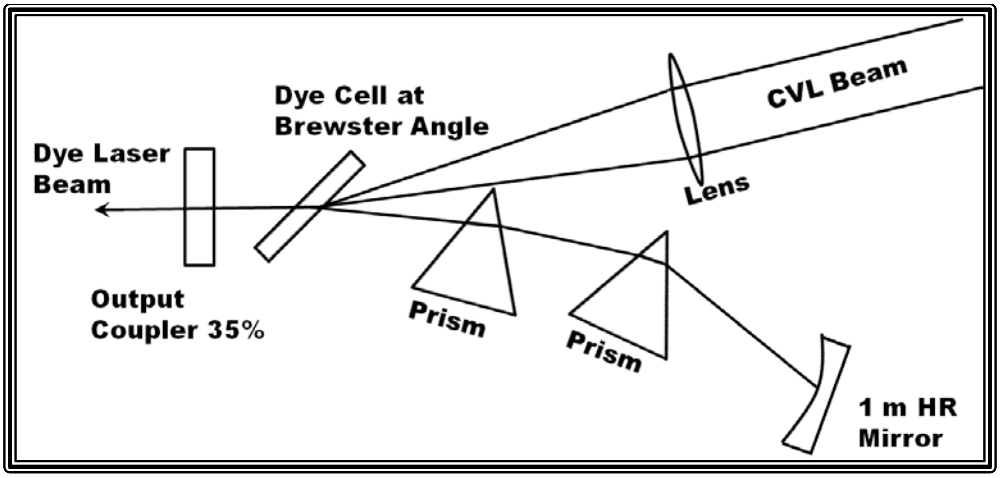

Fig 2.6: Longitudinal pumped broadband dye laser oscillator (Ref [2.24])

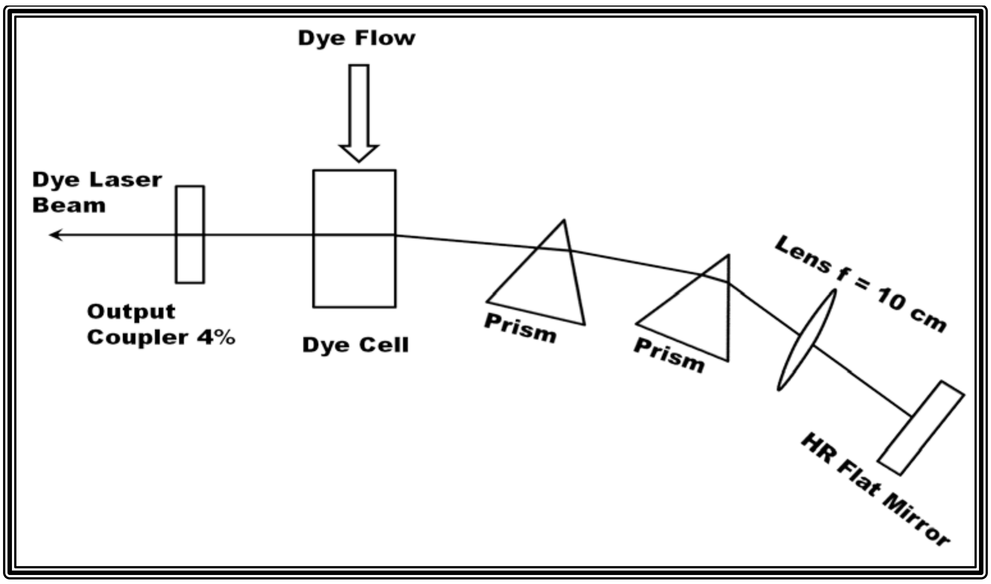

Fig 2.7: Transversely pumped broadband dye laser oscillator. (Ref [2.24])

Morey observed exceptionally long lifetimes for the laser dyes in comparison to the UV pumped dye laser. In fact, there was no photo degradation observed for accumulated pump pulse energies of 2.5 x 10^6 J/liter. The elliptical beam generated with transverse pumping had 21 mrad divergence in the vertical plane and 12.5 mrad in the horizontal plane, while with longitudinal pumping the beam was circular and the beam divergence was 1.53 mrad, close to the diffraction limited beam. The beam profile was close to Gaussian having far field intensity six times larger than the beam generated with transverse pumping. The longitudinal pumped dye laser has low beam divergence and smooth intensity profile [2.25, 2.26].

Owyoung has demonstrated longitudinally pumped tunable laser having a linewidth of 0.16 Å, full angle divergence of 0.95 mrad and peak power of 100 kW with conversion efficiency of 6 % [2.26]. These studies showed that the longitudinal pumping of a dye laser is superior to the transverse pumping, particularly in terms of beam propagation parameters.

Broyer and Chevaleyre had developed a CVL pumped dye laser for spectroscopic application; this dye laser was optimized for different laser dyes for achieving the tuning range from 530 nm to 890 nm [2.27]. They have obtained conversion efficiencies ranging from 40 % to 20 %, depending on the cavity architecture; 40% conversion efficiency was obtained with broadband resonator, while 20 % was obtained with grazing incidence configuration. They had used second harmonic generation (SHG) method for obtaining a tunable ultra violet laser radiation from their dye laser.

Zherikin et al. had demonstrated a narrow band dye laser operation with a minimum linewidth of 0.04 cm^{-1} pumped by CVL operating at 10 kHz pulse repetition rate [2.28]. They had used several laser dyes such as Rhodamine 101, Rhodamine 6G, Rhodamine B and Oxazine 17 dissolved in ethanol to obtain the tuning range of 530 – 720 nm from their dye laser system. The Rhodamine dyes were pumped by only green components of CVL, while the Oxazine 17 was pumped by both green and yellow components of the pump beam. Their dye laser system consists of a diffraction grating having a groove density of 1200 lines/mm, a wedge glass plate and six prisms having an antireflection coating as a beam expander. The dye laser linewidth was measured to be 0.8 cm^{-1}, which was further reduced to 0.04 cm^{-1} without significant reduction in the output power of the dye laser by insertion of F P etalon with FSR of 1 cm^{-1} and finesse of 15.

Lavi et al. reported a dye laser pumped by CVL with 4 kHz pulse repetition rate and 2 – 6 mJ of pump pulse energy having operational parameters such as variable bandwidth in the range of 0.4 – 2 GHz, low wavelength drift, beam divergence less than twice the diffraction limit [2.29]. They had used Hansch type cavity with 10 mm long dye cell, beam expander with magnification of 20, output coupler with 4% reflectivity, diffraction grating and several combinations of F P etalons for reducing the bandwidth. The dye laser bandwidth was obtained nearly 2 GHz with insertion of F P etalon in the cavity having FSR of 0.25 cm^{-1} and finesse of 13. The bandwidth was further reduced to 0.4 GHz with the insertion of another etalon of 1 cm^{-1} FSR and finesse of 25. They were able to reduce the bandwidth of the dye laser from 0.7 GHz to 0.4 GHz by just increasing the finesse of the second etalon from 13 to 25. This dye laser was continuously tuned over the wavelength range of 575 – 620 nm by the use of two laser dyes namely Rhodamine 6G and Rhodamine B dissolved in ethanol.

Duarte and Piper had compared the operating characteristics of several narrowband oscillators transversely pumped by CVL for Rhodamine 590 dye [2.30]. The cavities used for their studies are single prism expander open cavity, double prism expander closed cavity in Littrow configuration, grazing incidence open as well as closed cavity and grazing incidence cavity with a single prism beam expander. The linewidth of ~ 0.01 Å with conversion efficiency of 10 % was obtained in the prism beam expander grazing incidence cavity. The salient features of the high repetition rate narrow band dye lasers pumped by Copper Vapor / Copper Bromide lasers are summarized in table 2.3.

Table-2.3: High Repetition Rate Pulsed Narrow Band Dye Lasers Pumped by CuBr/CVL Lasers

S. No.	Gain Medium	Cavity Type for Single Mode	Flow cell /Jet	Wavelength/ Tuning Range	Bandwidth	PRF Pulse, Duration	Output Power/ Conversion efficiency	Authors
1.	2.25 mM Rh6G in Ethanol	Littrow cavity with Quartz Solid Etalon, Telescope M - 22.5	Dye Cell Transversely pumped	*Not Reported*	1.3 GHz	6 kHz	*Not Reported*	Pease and Pearson (1977)
2.	Kiton Red in ethylene glycol	Longitudinal Pumping	Dye jet with flow velocity18 m/s	*Not Reported*	*Not Reported*	20 kHz	40 % conversion efficiency	Sun et al., (1986)
3.	Used several Rhodamine dyes in EtOH	Grazing incidence cavity	Dye cell of 16 mm long and flow channel 13.5 x 6 mm^2	530 – 890 nm	0.16Å (~ 3GHz)	6 kHz	20 % conversion efficiency	Broyer et al, (1984)
4.	0.8 mM Rh590 in ethylene glycol	*Not Reported*	Dye Jet	*Not Reported*	*Not Reported*	*Not Reported*	63 % in broad band cavity	Petrov et al., (1992)
5.	1 – 3 mM Rh6G in Ethylene Glycol	Compared longitudinal pumping with transverse pumping geometry resonator length of 3 – 4 cm	Dye Jet 0.1 x 4.3 mm at flow velocity 13 m/s	575 nm	*Not Reported*	5 kHz	0.86 W / 31 % conversion efficiency	Huang and Namba (1981)
6.	Several dyes Rh101, Rh6G, RhB, Oxazine 17 in EtOH	Grating, wedge glass plate with 6 prism beam expanders with AR coating and FP Etalon	Rectangular Quartz dye cell with 15 x 0.5 mm	530 – 720 nm	0.04 cm^{-1}	10 kHz	0.6 W/ 7 %	Zherikin et al., (1981)
7.	Rh6G and RhB in EtOH	Hansch type cavity, beam expander with M 20 and FP etalons	10 mm long dye cell	575 – 620 nm	0.4 – 2 GHz 0.7 - 0.4 GHz with finesse increased 13 to 25	4 kHz	*17%*	Lavi et al., (1985)
8.	0.6 mM Rhodamine	Littrow configuration, 30% output coupler, four prism expender M 40 and two solid F	Quartz Dye cell 0.3 x 8 mm	572 nm /560 – 600 nm	60 MHz, 16 GHz Mode hop free	6 kHz / 30 ns	230 mW /5.2 %	Bernhardt Rasmussen (1981)

S. No.	Gain Medium	Cavity Type for Single Mode	Flow cell /Jet	Wavelength/ Tuning Range	Bandwidth	PRF Pulse, Duration	Output Power/ Conversion efficiency	Authors
		P Etalons						
9.	*Not Reported*	Littrow configuration, prism expander, FP Etalon, Quarter wave plate	Dye cell	550 – 650 nm	2.5 kW MOPA operation	26 kHz	*Not Reported*	Bass et al., (1992)
10.	2 mM Rh590 in ethanol,	Compared Littrow and GIG, with Prismatic beam expender M 25, cavity length ~ 150 mm	Trapezoidal fused Quartz dye cell of flow velocity 5 m/s	575 nm	650 – 800 MHz with Expander M 25 and with M 40 less than 500 MHz, with Littrow 1.4 GHz	8 kHz	4 – 5 % , Conversion efficiency improved with pumping of P-polarized	Duarte and Piper (1984)
11.	1 mM Rh6G	Short Cavity Littrow	1mm dye cell	560 – 590 nm	~ 650 MHz	6 kHz	8%	Rawat and Manohar (2000)
12.	Rh6G with Fiber optic pumping	GIG cavity, cavity length 5 cm, incidence angle 80^{O} – 85^{O}, Expander M 10	Dye cell 2 mm active medium	*Not Reported*	SLM operation	12 kHz / 12 ns	250 – 270 mW / 6 %	Vasil'ev et al., (1997)
13.	RhB im methanol and 0.2 mM Rh6G	Short Cavity GIG	2 mm dye cell T74 NSG	570 – 590 nm 546 – 574 nm with Rh6G	150 ±40 MHz, 500 MHz	6 kHz / 30 ns	5 mW, 50 mW / 1 %	Berry et al., (1990)
14.	0.4 mM DCM in methanol Rh6G & RhB in Methanol	Short Cavity GIG, with incidence angle 88.5^{O} – 89.5^{O}	Quartz Dye cell	639.2 nm / 619.3 – 655.9 nm	< 150 MHz, 130 MHz 163 – 198 MHz	6.5 kHz	100 mW / 1.38 % Polarization Ratio 40:1	McKinnie et al., (1991)
15.	1g/l Rh6G in Ethylene Glycol	GIG Cavity incidence angle 89^{O}	Dye jet thickness 0. 2 mm	*Not Reported*	1 GHz	6 kHz / 4 ns	*Not Reported*	Maruyama et al., (1991)
16.	1 mM DCM in methanol	GIG Cavity with Prism beam expander	Dye cell 1 cm long	*Not Reported*	1.2 GHz	6.5 kHz / 23 ns	120 mW	Koprinkov et al. (1994)
17.	Rh6G, DCM,	GIG Cavity with	SS dye Cell 2	564.6 nm	700 MHz	10 kHz	120 mW with	Kostritsa

S. No.	Gain Medium	Cavity Type for Single Mode	Flow cell /Jet	Wavelength/ Tuning Range	Bandwidth	PRF Pulse, Duration	Output Power/ Conversion efficiency	Authors
	Rh640,Rh610	retarder plate	mm				Rh6G 60 – 80 mW with DCM,Rh640, Rh610 / 1- 3 %	and Mishin
18.	0.5 mM RhB in MeOH	Short Cavity GIG	Dye Cell 2x2x8 mm	Tuned over 20 nm	< 200 MHz	6 kHz / 5 ns	12%	McKinnie et al. (1992)
19.	2 mM Rh6G in EtOH	GIG Cavity with prism beam expander	Dye Cell	570 nm	0.03 cm^{-1}	6.5 kHz	180 mW	Singh et al., (1993)
20.	Rh6G in Ethylene Glycol in amplifiers Phenalemine 512 in ethanol	Three stage amplification	Dye cell 0.5 mm and 2 cm long	600 – 615 nm	45 MHz	12 kHz / 10 ns	3 W in amplification / 17 %	Bokhan, et al., (2001)
21.	Mixture of Rh590 and Rh640 in EtOH	End pumping configuration with etalon	Dye Cell 6 mm thick and 2 mm wide	592 – 622 nm	*Not Reported*	10 kHz / 9 ns	550 mW / 16 %	Mcgonigle et al., (2003)
22.	Pyrromethene 597	GIG cavity with beam expander, Cavity length of 35 cm	Dye Cell 10 x 0.35 mm, quartz	550 – 640 nm	1 – 1.5 GHz	10 kHz / 20 ns	500 – 600 mW / 45 %	Grigor'ev et al. (2004)
23.	0.6 mM Rh6G chloride in EtOH	Littrow cavity with quad prim expander M 40 and etalon, Cavity length 13 cm	Quartz Dye Cell 8 mm length	575 nm 550 – 600 nm	100 MHz	5 kHz 10 - 30 ns	10 mW, amplified output 300 mW	Arai et al., (1986)
24.	Dye cocktail of RH6G and Rh640	*Not Reported*	Dye cell of laminar flow design	616 nm	7 GHz with bandwidth stability of 1GHz	6.5 kHz / 33 ns	20 %	Evans and Webb (1994)
25.	2 mM Rh6G in EtOH	GIG cavity with beam expander M 22 and etalon, Cavity length 17 cm	SS dye Cell	*Not Reported*	100 MHz	5.5 kHz	*Not Reported*	Prakash et al., (2010)

2.5 Dye Laser Resonators

Every filter like tuning element shows a considerable degree of spectral narrowing, when compared with the laser bandwidth $\Delta\lambda_{laser}$ with transmission width $\Delta\lambda_O$ of the tuning element. There are no losses at the desired wavelength in the passive bandwidth $\Delta\lambda_O$ of the tuning element. After insertion of the filter into the resonator cavity as shown in figure 2.8, the laser will exceed the threshold at λ_1 and λ_2 and $\Delta\lambda_{laser}$ will become considerably smaller than $\Delta\lambda_O$. The insertion of wavelength dependent losses into the resonator cavity leads to fine tuning of the laser system. Concentration tuning has been used to achieve a spectral shift in the dye laser by Schafer et al. [1.2]. Several resonator configurations have been reported in the literature for spectral narrowing and tuning of the dye lasers.

Bradley et al. had used grating and an intracavity F P etalon to obtain bandwidth less than 0.5Å and tunability over more than 100 Å for their longitudinally pumped dye laser system. They obtained a beam divergence of nearly 1 mrad [2.31].

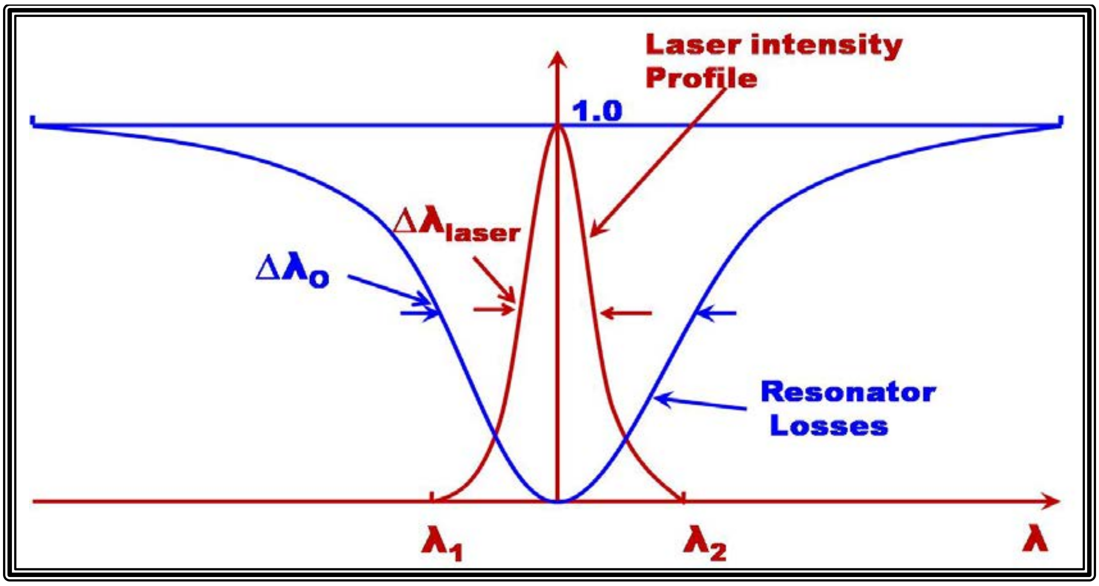

Fig 2.8: Spectral narrowing of laser intensity profile for a filter inserted into the laser resonator

Strome and Webb reported four prism tuning system for their flashlamp pumped Rhodamine 6G dye laser. They obtained dye laser bandwidth of 0.17 nm, tunability over 571 – 615 nm and pulse energy of 0.14 J at peak wavelength of 595 nm [2.32]. Mayer had used a prism at a very high angle of incidence nearly 90^O inside the resonator for his nitrogen laser pumped Rhodamine 6G dye laser. The dye laser output was obtained from one face of the prism and the linewidth was reduced to 0.9 Å [2.33].

Hanna et al. had used prism expander and F P etalon to obtain a single frequency output of 10 kW in a linewidth of less than 0.01 $cm^{-1}$for their nitrogen pumped dye laser [2.10].

Shoshan et al. had used diffraction grating at grazing incidence angle without any intracavity beam expander. The large angular dispersion provided by grating at grazing incidence reduced the dye laser linewidth to 0.08 cm^{-1} [2.11]. On increasing incidence angle the grating diffraction efficiency decreases rapidly. According to the authors, for high gain lasers, efficient lasing is possible if the output coupler is replaced by a 100 %, reflecting mirror and laser output is obtained from the zeroth order of the diffraction grating.

Novikov et al. had used multiple prism beam expander along with the diffraction grating, which improved considerably the selectivity for their longitudinally pumped dye laser. This dye laser was continuously tuned over a wide range and the linewidth of the laser was measured to be less than 0.1 cm^{-1} [2.34]. Multiple prism beam expanders have been successfully implemented for pulse dye laser with very good conversion efficiency (~10%) and narrow linewidth.

Duarte and Piper had calculated the overall dispersion provided by a combination of multiple prisms and grating for pulsed dye lasers [2.15]. Their calculation shows that the contribution of multiple prisms to the dispersion is as small as 2%. This smaller contribution can be further reduced by arranging the prisms in compensation pairs. They had reduced the cavity losses by suitable choice of the angle of incidence for both prism and grating resulting in relatively higher conversion efficiencies of 7 – 10 % and linewidth of less than 0.01Å for Coumarin 500 laser dye pumped by a nitrogen laser [2.35]. They had incorporated a double prism expander instead of the single prism expander for their dye laser to obtain narrower linewidth of 0.008 Å. The prism dispersion is usually neglected in comparison to the grating dispersion. The prism expander cavities are either open cavity or closed cavity. In the open cavity, the output is obtained from the reflective losses in the incident face of the prism, while in closed cavity, an output coupler is utilized from which the tunable laser output is obtained. Typical closed and open cavities are shown in figure 2.9 and figure 2.10.

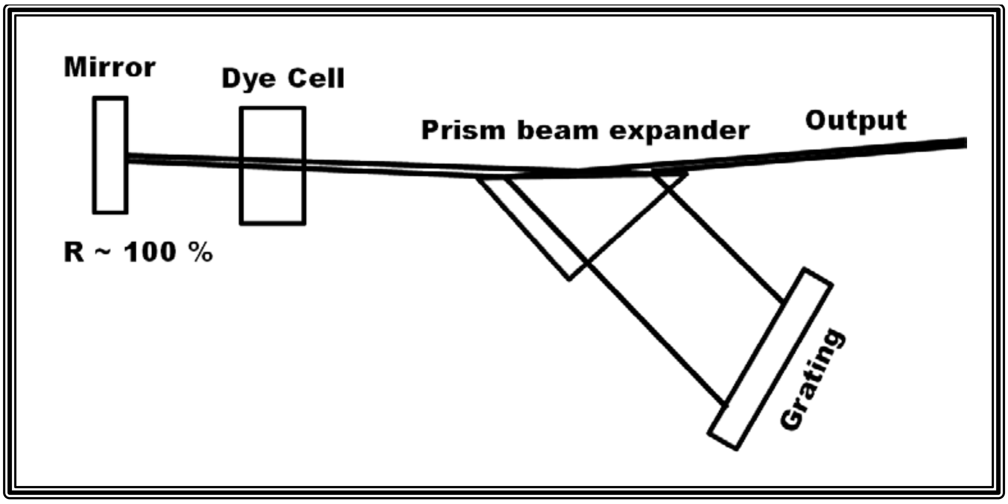

Fig 2.9: Typical open dye laser cavity with prism beam expander.

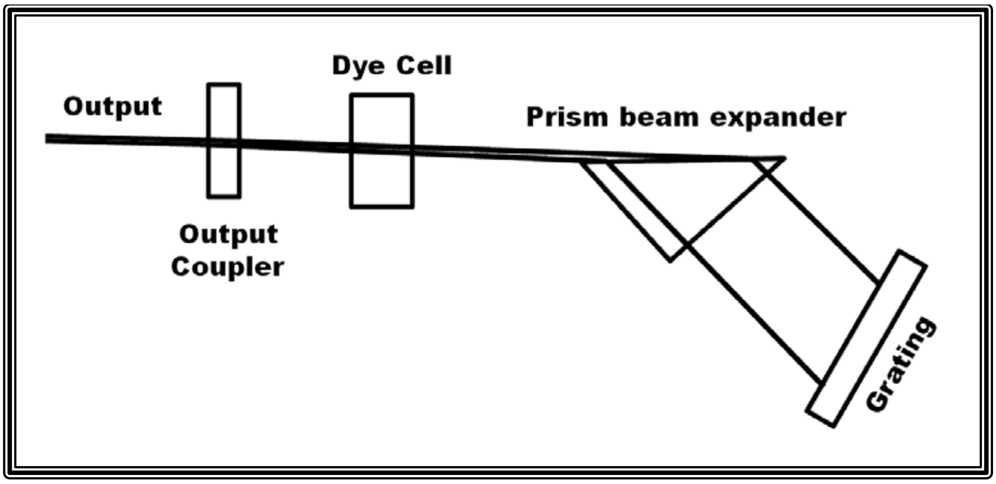

Fig 2.10: Typical closed dye laser cavity with prism beam expander

Although good conversion efficiencies can be achieved from open cavities, the output contains a large amount of amplified spontaneous emission (ASE). In closed cavities, the conversion efficiency is relatively low, but spectral purity is high. The diffraction grating used in these cavities is in Littrow configuration in which a particular wavelength is reflected back exactly along its direction of incidence. For a certain angle of incidence, the feedback from the grating is reduced eventually to a point where an ASE from the rear mirror overcomes grating feedback. This eventually clamps the available tuning range for a given dye laser output.

Nair had reported that the dispersion of a prism beam expander at a very high angle of incidence has a significant contribution on the cavity dispersion, where it exceeds the grating dispersion as the angle of incidence approaches 89^{O} [2.36]. The single pass cavity dispersion offered by the prism grating combination depends on the relative orientation of the grating and prism. If the incidence angle is increased very near to 90^{O}, the prism dispersion exceeds the grating dispersion and the linewidth of the dye laser is further reduced.

Iles et al. [2.8] had used all grating cavity in which a 5 cm long, 2400 line/mm holographic grating were used in grazing incidence, which provides beam expansion and another blazed grating (1200 lines/mm) in second order in Littrow configuration. The end mirror was replaced by a third grating in Littrow configuration as shown in figure 2.11. The laser parameters such as linewidth, conversion efficiency, tuning range and beam divergence obtained from this cavity are comparable to Hansch type cavity with intracavity beam expansion. This grazing incidence cavity has some advantages over Hansch type multiple prism beam expander cavity.

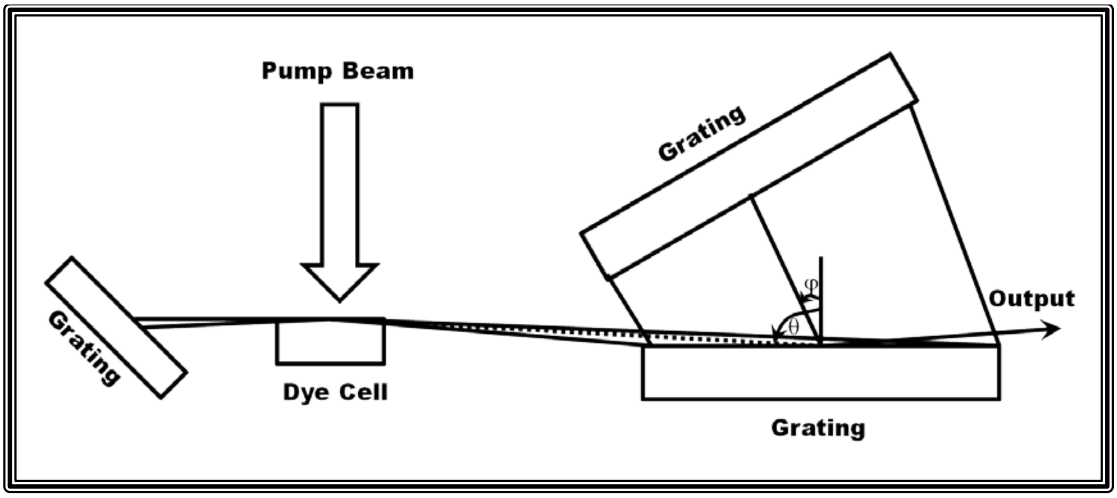

Fig 2.11 All grating cavity dye laser used by Iles

The main advantage is that the cavity does not contain any glass component other than the dye cell. Hence the cavity is less sensitive to the temperature with high power and wavelength dispersion in prisms. The numbers of reflecting surfaces are reduced, so that, the Fresnel losses and undesirable reflections are greatly reduced. The reduced number of cavity components entails ease of alignment. The main disadvantage of this open cavity is a high level of ASE present in the dye laser output. This higher ASE couples to the output of the dye laser from the reflection losses at the grazing incidence grating. Another disadvantage of the open cavity is that it is particularly sensitive to the optical coupling from external components which can destabilize the laser output wavelength.

Dinev et al. had demonstrated a novel double grazing incidence configuration, in which twofold reduction in a single pass linewidth is obtained in comparison to the single grazing incidence grating configuration [2.37]. The double grazing incidence design increases the cavity dispersion by two fold resulting in stable single mode dye laser operation with a linewidth of 210 ± 50 MHz. This dye laser was pumped by a nitrogen laser with peak power of 500 kW, pulse duration of 8 ns and a pulse repetition rate of 10 Hz.

Shoshan and Oppenheim used two gratings for their dye laser cavity as presented in figure 2.12 the output was obtained from the zeroth order. The cavity losses were minimized by choosing the grating in grazing incidence having only a single diffraction order [2.16]. They had used a 40 mm long grating with groove spacing 0.5 μm (2000 line/mm) as beam expander and another grating of 316 lines/mm in 10^{th} order in Littrow mode as tuning grating. They found that the laser linewidth was strongly dependent on the incidence angle. The laser line width increased to ten times from 0.1 cm^{-1} to 1.1 cm^{-1} with decreasing incidence angle from 89^{O} to 83^{O} respectively. This laser was tuned over 40 nm with very high spectral purity even at the extreme of the tuning range.

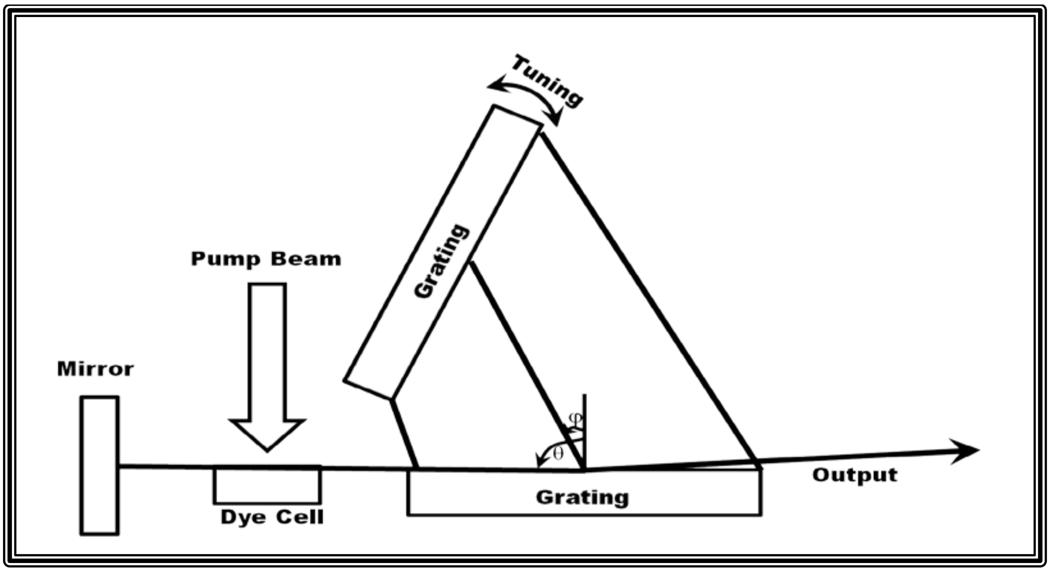

Fig 2.12: Dye laser cavity with two gratings used by Shoshan and Oppenheim [2.16]

Littman and Metcalf had reported a pulsed dye laser which had spectral linewidth of 1.25 GHz and peak power of 10 kW at 600 nm [1.15]. In this dye laser the diffraction grating was used as a grazing incidence and the diffracted beam is returned to the grating by a plane mirror. This reflected beam reduces to its original size and travels towards the gain medium for further amplification. The diffraction grating disperses the wavelengths, two times in one round trip in the cavity so that a narrow spectral component sees the gain. As the diffraction grating is utilized twice per pass, the net efficiency of the dye laser is roughly the square of the grating efficiency. The potential problem of multiple reflections between the grating and the tuning mirror for this cavity can be eliminated by making rulings of the grating exactly perpendicular to the laser optical axis.

Liu and Littman had found the magical geometry for scanning the dye laser for the entire tuning range without mode hop. In this geometry on the rotation of the tuning element, it is possible to change simultaneously cavity length and diffraction angle, which is a necessary and sufficient condition for mode hop free scanning of single mode dye laser [1.16].

2.6 Single Mode Oscillations

A mode of the resonator is the energy distribution inside the resonator, which is self-consistent, reproduces itself after every round trip in the resonator. The energy distribution transverse to the resonator axis is referred to as the transverse mode. A dimensionless number which determines the number of transverse modes in a resonator cavity is known as Fresnel number (N_F). The Fresnel number is defined by the cavity parameters as

$$N_F = \frac{\omega_o^2}{\lambda L} \tag{2.1}$$

where resonator length L, beam size ω_o and oscillating wavelength λ.

For single transverse mode (TEM_{OO}) oscillation the Fresnel number should be close to one. Restricting the resonator to oscillate in a single transverse mode is the first step for the design of the SLM laser. The number of half wavelengths of light fitting along the resonator axis is known as longitudinal modes. These longitudinal modes are separated by a frequency equal to $\frac{C}{2L}$, where c is the velocity of light. The resonator has much larger dimension compared to the laser wavelength, hence a large number of closely spaced longitudinal modes exist. If the gain medium is placed inside the resonator, it exhibits gain at several of these mode frequencies. The number of oscillating longitudinal mode is the ratio of gain bandwidth to the longitudinal mode spacing. In a short cavity laser, when grating is the frequency selective element, it restricts the gain bandwidth to a few GHz, while the shorter cavity widens the longitudinal mode spacing. An alternative approach for obtaining single mode oscillation is to optimize the beam divergence and to increase the intracavity dispersion instead of reducing the cavity length.

2.7 SLM Dye Laser Resonators

Several resonator configurations have been used to obtain high quality single mode oscillation from pulsed dye lasers. The resonators for single mode oscillation can be classified into two categories: short cavity resonator and long cavity resonator. The long cavity resonators use control of beam divergence by the prismatic beam expander and a smaller angle of incidence on the frequency selective element, which results in higher diffraction efficiencies. While the shorter cavity resonators widen the longitudinal mode spacing with a larger angle of incidence on the grating for selecting the single mode. In grating tuned cavities the wavelength of the laser is determined by the angle of the grating, while the modes of the cavity is determined by the geometrical configuration of the oscillator. The bandwidth of the laser is determined by the grating geometry, cavity losses and dye gain medium [2.38].

2.7.1 Short Cavity Resonators

The shortest possible cavity consists of three components, holographic grating in Littrow configuration, the output coupler and a dye cell. Rawat and Manohar had reported a short cavity pulsed dye laser pumped by a CVL at 6 kHz with diffraction grating in Littrow configuration [1.21]. In this design, the laser cavity was made as compact as possible with low losses. The cavity length of about 30 mm offered a large axial mode separation (0.17 cm^{-1}). The spectral narrowing and tuning were achieved by the use of diffraction grating in Littrow configuration as shown in figure 2.13.

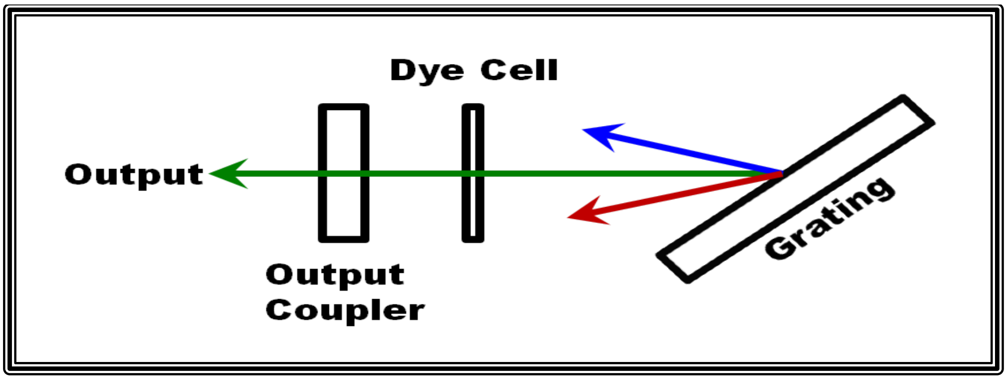

Fig 2.13: Simple short cavity SLM dye laser

Coarse wavelength tuning was achieved by a 30 mm square holographic grating with 600 lines / mm in the fifth order. The output coupler is an un-coated glass plate fixed onto the piezo actuator, which was used to adjust the cavity length and fine tune the SLM dye laser wavelength. The SLM dye laser uses 1 mM Rhodamine 6G in ethanol. This dye laser was longitudinally pumped by the green (510 nm) beam of the CVL with pulse duration of 40 ns. The pump beam was focused using a spherical lens of focal length of 200 mm. The dye cell is kept at an angle of 8^{o} with respect to the resonator axis for avoiding parasitic oscillations. The metallic dye cell made of SS had two replaceable optical quality quartz windows of 2 mm thickness with 1 mm dye flow channel. A SLM bandwidth of ~ 650 MHz was obtained. They had also used higher viscosity solvents for improving the mode stability of the SLM dye laser.

Further reduction in the bandwidth of the SLM dye laser can be achieved by inserting one or two F P etalons in the resonator cavity. The cavity configuration with FP etalons is illustrated in figure 2.14.

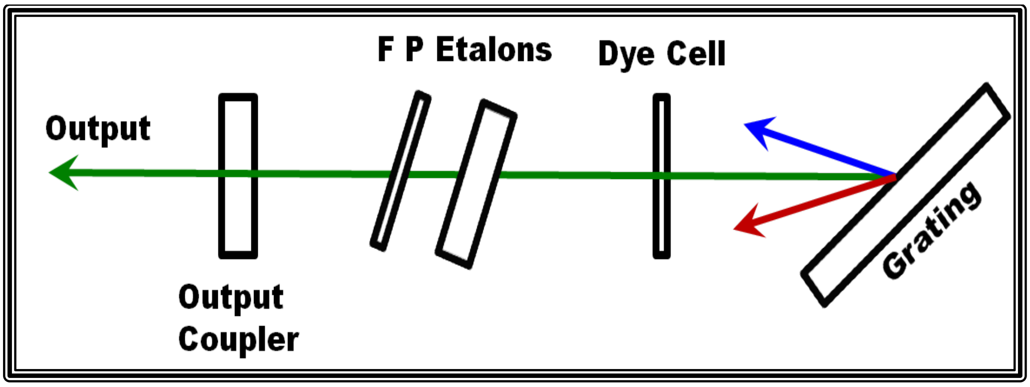

Fig 2.14: Modified Littrow cavity with two F P etalons for obtaining SLM

Insertion of F P Etalon inside the resonator cavity provides additional option of fine tuning of the wavelength through rotation of the etalons. Synchronization of many tuning elements together makes the system more complex. The main disadvantage of this class of lasers in pulsed mode is very high intracavity photon flux, which can induce thermal damage to the grating and etalon coatings.

The SLM oscillator without beam expander uses only natural beam divergence for illuminating the diffraction grating. Grating at grazing incidence provide very high spectral selectivity to select the SLM. With an increasing incidence angle of the grazing incidence cavity the single mode laser efficiency decreases due to decrease in diffraction efficiency of the grating as well as decrease in the input aperture of the diffraction grating. The typical grazing incidence cavity is illustrated in figure 2.15.

Basiev et al. have shown by theoretical calculation that the SLM laser operation can be achieved if the cavity length is less than 70 mm with a free spectral range of the cavity of nearly 2 GHz and the gain aperture is less than 500 µm [2.39]. The smaller gain, aperture limits the maximum pulse energy to a few tens of mJ. This smaller input power and lower diffraction efficiency of the grating reduce the conversion efficiency of the single mode lasers. The pointing stability of the pump laser is another key parameter for single mode lasers as small transverse displacement of gain medium can cause mode hop in the laser.

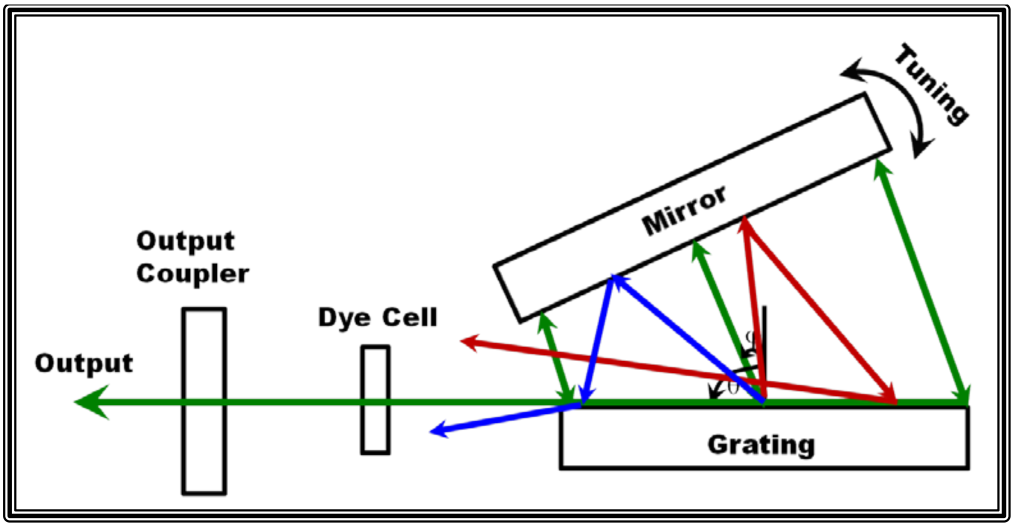

Fig 2.15: Wavelength selection in the grazing incidence grating (GIG) cavity

Kostritsa and Mishin had obtained moderate power of 16 W single mode dye laser pumped by CVL from GIG master oscillator followed by two stage amplification [2.40]. They had used short cavity GIG laser for obtaining single mode bandwidth of 700 MHz, conversion efficiencies of 1 – 3 % and output beam divergence of 0.5 mrad.

Littman had demonstrated pulsed single mode dye laser longitudinally pumped by the second harmonic of Nd:YAG laser [1.17]. This single mode laser has a time averaged linewidth of 150 MHz, a nearly TEM_{OO} spatial mode, mode hop free scanning over 15 cm^{-1}, a very small ASE of ~ 0.01% and conversion efficiency of nearly 3% at the peak of the tuning range. He had operated this dye laser with a variety of Rhodamine and Oxazine laser dyes. The shorter cavity length offers multiple round trips which is analogous to CW dye laser cavity. Here, also the bandwidth of the dye laser can be further reduced by inserting another frequency selective element inside the cavity. The typical resonator cavity with FP etalon is shown in figure 2.16.

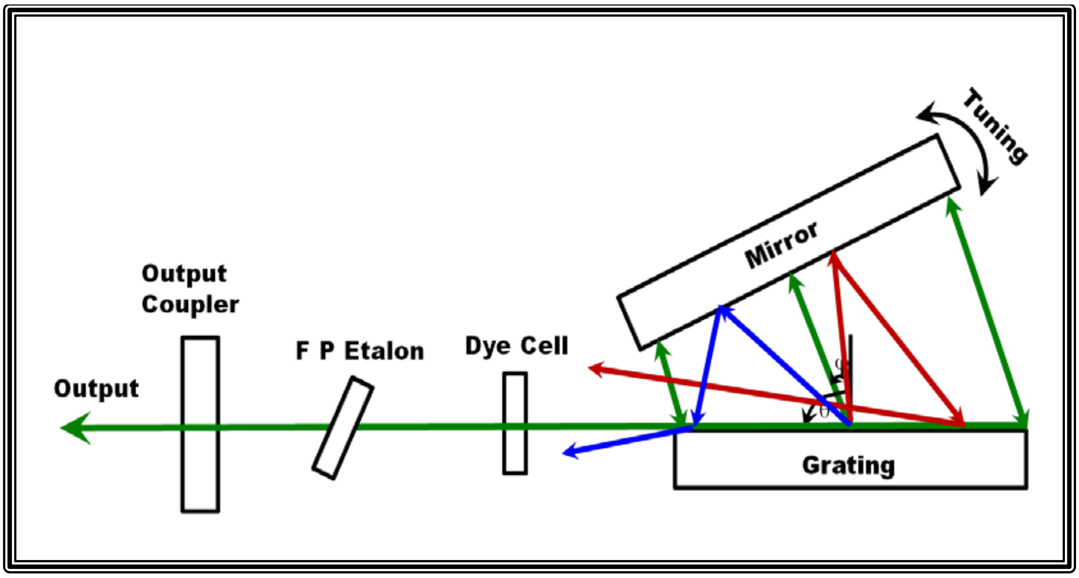

Fig 2.16: Bandwidth narrowing and wavelength selection in the etalon based GIG cavity

Saikan had obtained single mode oscillation in the nitrogen pumped dye laser with a short cavity length, having a diffraction grating in near grazing incidence and an uncoated resonant reflector as an output coupler [2.41]. He had used two uncoated wedges of glass for the resonant reflectors, which were aligned like F P etalon in the backscattering with diffuse illumination. The free spectral ranges of resonant reflectors were 0.14 cm^{-1} and 0.07 cm^{-1}. He had replaced resonant reflector by totally reflecting mirror and single mode operation was obtained only near the lasing threshold and the number of oscillating modes depends on the pump power. The author had found that with resonant reflector stable single mode oscillation is obtained up to fairly high pump powers and the axial mode selectivity had increased; the calculated reflectivity of the quartz resonant reflector was 0.13 at 524 nm, while the reflectivity for two quartz resonant reflectors was 0.41. The combined reflectivity of the grating and tuning mirror was relatively smaller compared to the resonant reflectors, which results in a very low Q factor of the cavity. In low Q cavity with pulsed excitation the population inversion suddenly reduces and laser oscillation ceases, which results in very short duration of single mode laser pulse.

2.7.2 Long Cavity Resonators

Higher dispersion along with high diffraction efficiency of the grating can be achieved by the illumination of larger grating length at relatively smaller angle of incidence. These types of oscillators are commonly known as a multiple prism Littrow (MPL) grating laser. The main disadvantage of this type of cavity is a long cavity length, which reduces the intracavity longitudinal mode spacing and needs additional frequency selective intracavity component such as F P etalon for achieving SLM oscillation. The typical Hansch type cavity with F P etalon is given in figure 2.17.

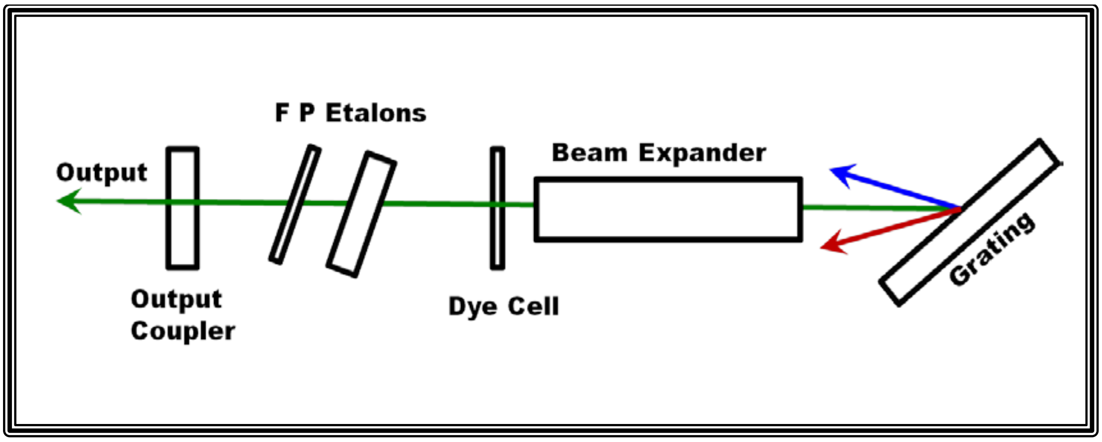

Fig 2.17: Typical Hansch type single mode dye laser cavity with intracavity beam expansion and F P etalon

Commonly used prism beam expanders utilized in a dye laser consists of either two prisms or four prisms depending on the required beam expansion. These prisms are arranged in the compensating mode for minimizing the prismatic dispersion at the desired wavelength. The prismatic beam expander provides large intracavity magnification in the range of $100 \leq M \geq 200$.

Arai et al. had used this type of cavity for their SLM dye laser pumped by CVL; they obtained SLM bandwidth of 100 MHz, pulse width from 10 – 30 ns with a pulse repetition rate of 5 kHz [2.42]. They had used four prism beam expander and F P Etalon for their single mode dye laser with Rhodamine 6G dissolved in ethanol. The dye solvent temperature was controlled within a temperature band of $\pm$ 0.05 ^{O}C to keep the single mode frequency band less than 200 MHz. The dye laser pulse resembles the pump pulse except the delay for the buildup period is 10 ns.

Bernhardt and Rasmussen had reported pulsed single mode dye laser pumped by CVL at 6 kHz with 230 mW average output power [1.20]. They had used blazed (angle 61^{O}) holographic grating in the fifth order at Littrow configuration, a partially transmitting output coupler (~30%), four prism beam expander of magnification of 40 and 5 mm solid etalon with FSR of 20 GHz and finesse of 13 which forces the laser to oscillate in SLM having a bandwidth of 60 MHz. The etalon was placed in the expanded portion of the cavity beam so that walk off losses could be minimized. The efficiency of this SLM dye laser was 5.2 % with 4 watts of the green beam of CVL. The single mode power was maximized and mode hopping was suppressed by keeping the F P etalon passband at the center of the cavity mode. This single mode dye laser was continuously tuned without mode hopping over 16 GHz at a rate of 1.6 GHz/s.

Bass et al. reported the highest average power dye laser in the history of dye laser which was operated in MOPA configuration pumped by CVL at Lawrence Livermore National Laboratory [1.39]. They have used, modified Hansch type master oscillator cavity, which uses grating in Littrow configuration, prism beam expander, F P etalon, quarter wave plate and output coupler. The dye cell was pumped by a CVL MOPA beam delivered by 600 μm core diameter optical fiber. They had generated 2500 Watt of broadly tunable dye laser over 550 – 650 nm pumped by 7000 Watt CVL operating at 26 kHz.

Maruyama et al. had demonstrated wavelength stabilized single mode pulsed dye laser with double prism beam expander pumped by CVL with long term frequency drift of 30 MHz and a single mode bandwidth of 60 MHz [1.30]. They reduced the cavity length so that the axial mode spacing was larger than the etalon passband. The gain length of 8 mm was utilized in a dye cell, which was kept at 3^{O} with respect to the optic axis to avoid the sub cavity resonances within the dye cell. The frequency jitter in the single mode dye laser output was linked to the flow turbulence in the dye solution at the higher Reynolds number.

Another class of dye laser oscillators is an intracavity beam expander with grazing incidence grating (GIG) cavity. This cavity is called the hybrid multiple prism grazing incidences grating (HMPGI) and widely used for obtaining narrow band dye laser. This cavity is inherently compact as the grating used in the near grazing incidence, which reduces obligatory magnification of double prism beam expanders deployed in compensating mode.

Vasilev et al. had achieved the SLM operation with Rhodamine 6G longitudinally pumped by 5 W CVL operating at 12 kHz pulse repetition rate [2.43]. They had used silica optical fiber of core diameter of 400 µm for transporting the pump beam to their SLM dye laser. The fiber coupling efficiency was measured to be 80 – 85 %. The longitudinal pumping demands sufficiently high quality (lower beam divergence) pump beam, so that, it can be focused to the required gain diameter and constant position (good pointing stability) of the active region relative to the cavity components. They used dye cell of 2 mm width and overall cavity length of 50 mm corresponding to the cavity free spectral range of nearly 3 GHz. They had used an incidence angle of 85^{O} and expander magnification of 10 for obtaining overall efficiency of 12 % for the combination of grating and tuning mirror. The typical hybrid multiple prism grazing incidence cavities is shown in figure 2.18.

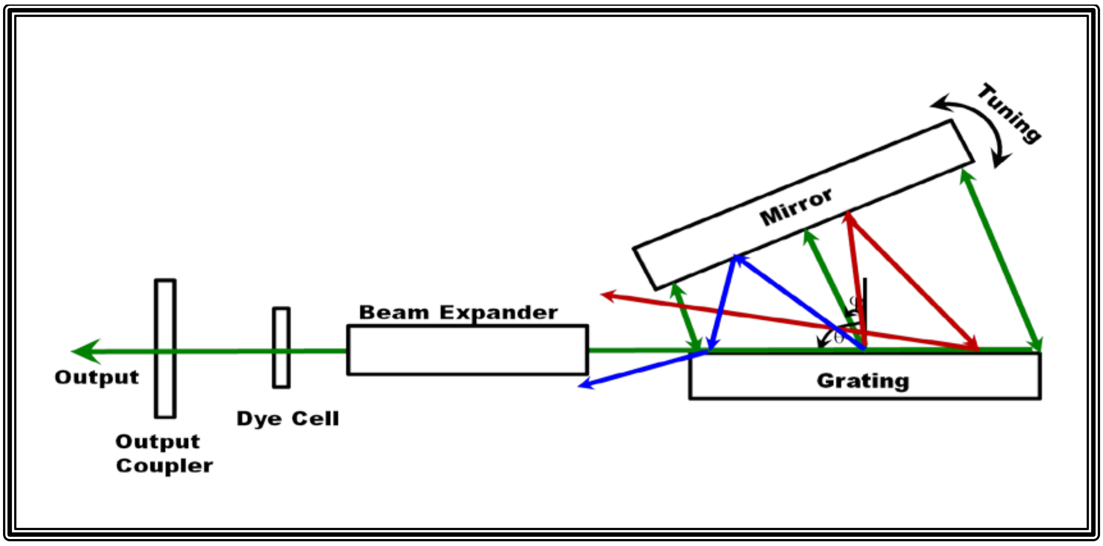

Fig 2.18: Typical HMPGI cavity used for achieving SLM in pulsed dye lasers.

The MPL and HMPGI grating cavities can be directly used in other tunable high power laser such as Excimer laser and carbon dioxide laser. Mostly external cavity semiconductor diode lasers use near grazing incidence cavity rather than pure grazing incidence. For pure grazing incidence the grating diffraction efficiency is very small to sustain the laser oscillation in semiconductor diode lasers.

Duarte and Piper had reported high pulse repetition rate CVL pumped dye laser operating at peak wavelength of 575 nm with conversion efficiency of 4 – 5 %. They had compared two dye laser output parameters obtained from two separate cavities in Littrow configuration and grazing incidence cavity with double prism expander magnification of ~ 25 [1.29]. The trapezoidal dye cell made of fused quartz was used for both types of dye laser cavities. The 2 mM Rhodamine 590 dissolved in ethanol was circulated through the dye cell at a flow velocity of 5 m/s. The CVL pump beam comprising both green and yellow was line focused on the dye cell by 100 mm focal length cylindrical lens. The overall cavity length for both Littrow and grazing incidence cavity was nearly 150 mm. The dye laser linewidth was measured to be 650 – 800 MHz in grazing incidence cavity with double prism beam expander. This linewidth was further reduced to less than 500 MHz by increasing the magnification of the double prism beam expander to 40 from 25 but the conversion efficiency was correspondingly reduced. The linewidth obtained for Littrow cavity with the highest possible magnification of 100 was limited to ~ 1.4 GHz, while the conversion efficiency at peak wavelength of 575 nm was 5% at 8 kHz pulse repetition rate. The linewidth was measured to be 2 – 3 GHz with cavity magnification of 25 while the conversion efficiency improved to 10 % from 5 %. The conversion efficiency of the dye laser was further improved by pumping the dye laser with the p-polarization of the pump beam matched with prism beam expander and grating combination. They had found that the flow turbulences result in two mode oscillation, increased frequency jitter leading to higher effective linewidth and intensity fluctuations in the dye laser output. The dependence of conversion efficiency on the pulse repetition rate of the pump laser for both the dye lasers have been studied and found to be inversely proportional to pulse repetition rate. The conversion efficiency was reduced by four times when the pump pulse repetition rate was increased to 13 kHz from 8 kHz for the same dye flow velocity inside the dye cell. ASE was nearly one order smaller for the grazing incidence cavity in comparison to Littrow cavity. The pulse duration for both dye laser oscillators was measured to be 10 – 15 ns, beam divergence of ~ 4 mrad and buildup time of 2 – 3 ns. They have concluded that for obtaining narrower linewidth form a dye laser pumped by high pulse repetition rate CVL the grazing incidence cavity is advantageous over the Littrow cavity.

Another modification to the HMPGI cavity is the introduction of the F P etalons on the resonator for obtaining the single mode oscillation. Chang and Li had inserted intracavity etalon in their grazing incidence cavity for selecting single mode and obtained an output linewidth of the order of a few hundred MHz (below 0.006 Angstrom) [2.44].

Prakash et al. had obtained a single mode time average bandwidth of 100 MHz for their GIG cavity with intra cavity double prism beam expander and etalon [2.45]. They had used holographic grating at 84^{O} angle of incidence with prismatic beam expander of magnification of 20 and an intracavity etalon FSR of 10 GHz with reflective finesse of 12.

The typical schematic of the intracavity beam expander and etalon is shown in figure 2.19. Duarte and Piper had compared operating characteristics of several cavities for Rhodamine 590 dye laser oscillators transversely pumped by pulsed copper bromide laser. They obtained line widths of ~0.01 Angstrom with conversion efficiency of up to 10% for prism expanded grazing incidence cavity [2.30]. The MPL and HMPGI cavity yields very high spectral purity for the SLM dye laser as they yield very small ASE.

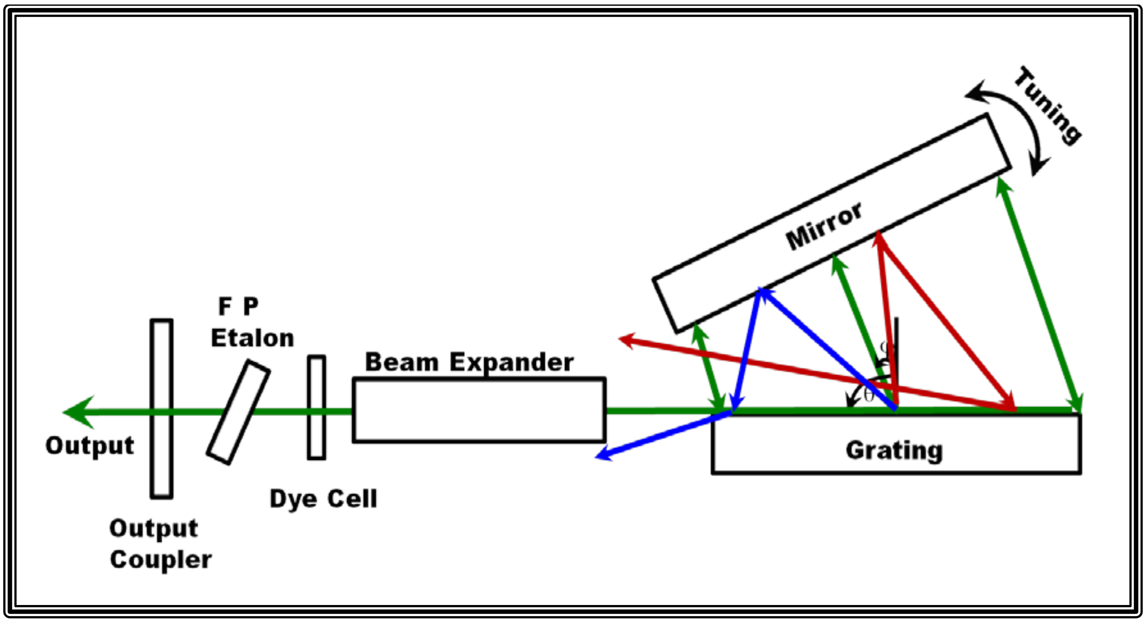

Fig 2.19: Typical HMPGI grating dye laser oscillator with intra cavity F P Etalon

2.8 Other Techniques for Single Mode Operation

Hansch et al. had used external filtering of narrow band tunable dye laser pumped by a nitrogen laser with a piezoelectrically tunable confocal FPI, which acts as an ultra narrow band pass filter outside the dye laser cavity. This technique had reduced the linewidth from 300 MHz to 7 MHz full width at half maximum (FWHM) [2.46]. This laser was operated with peak power of several watts, pulse repetition rate of 100 Hz, nearly diffraction limited output beam.

Black et al. used a very short cavity laser (SCL) of optical length of ~ 4.5 mm, which provided a mode spacing of 33 GHz. They have obtained SLM operation, which yields > 12 mJ pulses of 6 ns duration with conversion efficiency of 10 % and 2.7 times transform limited linewidth of less than 200 MHz with seamless, single mode tunability over 20 cm^{-1} [2.47] This laser was pumped by the second harmonic of Nd:YAG laser.

Ewart et al. had demonstrated a widely tunable, SLM pulsed dye laser. They had selected a single mode from the multimode output of a short cavity laser in a narrow band amplifier having linewidth of 250 MHz and continuously tuned over 34 cm^{-1}[2.48]. They had obtained a wide tuning range by scanning the SCL where the narrow band amplifier (NBA) tracks the selected mode of SCL.

Binks et al. had used four arm grazing incidence cavities, which ensured single mode operation in pulsed laser system by interferometrically enhancing mode selection [2.49]. Pinard et al. obtained SLM for their dye laser with double or triple Michelson reflectors instead of F P etalons inside the standing wave dye laser cavity [2.50]. Mandl et al. had achieved single mode oscillation from a linear optical cavity with twisted mode configuration pumped by long pulse ~ 700 ns flash lamp with an output energy of 350 mJ [2.51]. Beltyugov et al. had used dye laser whose resonator consisted of a grazing incidence grating and Troltskii interferometer for obtaining single mode oscillations and achieved SLM bandwidth of 0.02 cm^{-1} with an output power of 10 kW at 580 nm wavelength with pulse duration 3 ns [2.52]. Shevchenko et al. had obtained single mode oscillation by introducing intracavity Fox Smith interferometer. In this way, they obtained 5 ns pulse duration at a wavelength of 590 nm with pulse energy of 6 mJ and single mode bandwidth of 100 MHz at FWHM [2.53].

2.9 Pulse Amplification of Single Mode CW Laser

Pulse amplification of CW single mode dye laser is another important technique, which can generate a transform limited bandwidth with very small amount of ASE. The CW single mode dye laser focused on the amplifier dye cell with a spherical lens and the dye amplifier pumped by pulsed pump sources, can generate a transform limited bandwidth of the amplifier dye laser. The bandwidth of the amplifier dye laser is limited to the pump pulse duration. Ni and Kung had used a CW dye master oscillator and dye pulsed amplifier system that generated 4 ns 100 mJ pulses with a pulse repetition rate of 30 Hz, SLM output bandwidth of 275 MHz with undetectable ASE for the entire tuning range. They had used backward stimulated Brillouin scattering to control the growth of ASE [1.10].

Namba and Ida, had used pulsed dye amplifier pumped by CVL with CW dye oscillator and obtained an efficient tunable source with high average power, good spectral purity and excellent tunability for several laser dyes such as Rh6G, RhB and DCM. They had used two stage amplifier to cover the spectral range of 575 – 670 nm with conversion efficiency of greater than 7% [2.54].

Lavi et al. had used three stage pulsed amplifier pumped by CVL for pulse amplification of their CW dye laser. They had obtained conversion efficiency of 32% for Rhodamine 6G pumped by the green beam of CVL and 25% for Rhodamine B pumped by both yellow and green beam of CVL. The temporal pulse followed the pump pulse and bandwidth of 30 MHz was obtained [2.55].

Hahn and Yoo had used four pass dye amplifier pumped by injection seeded frequency doubled Nd:YAG laser for pulsed amplification of 100 mW, 10 MHz bandwidth at 572 nm wavelength CW dye laser [2.56]. In a four pass amplification system they obtained the ASE ratio less than 1.5 % for a pumping energy up to 4.2 mJ.

Eesley et al. had obtained 20 kW diffraction limited laser with a linewidth of 17 ± 4 MHz from pulsed amplification of CW dye oscillator pumped by argon laser [5.57].

2.10 Selection of SLM Configuration for Development and Study

Due to the difficulties in the design of a single mode pulsed dye laser with higher average power, high conversion efficiency, high repetition rate, diffraction limited beam divergence (a very good spatial profile) and transform limited bandwidths, a careful selection has to be made for the research work. On reviewing the literature, it is found that the short cavity pulsed single mode lasers are the simplest class of device with the minimum optical components, which can generate narrow linewidth in the range of hundreds of MHz, pulse repetition rate as high as tens of kHz, output powers in the range of hundreds of mW, conversion efficiency in the range of 3 – 5% and beam divergence close to diffraction limited. These lasers can be tuned without mode hop for the entire tuning range of available gain medium with very high spectral purity. The GIG cavity is the smallest possible resonator cavity with grating at grazing incidence, which can be tuned without any mode hop, while arranged in the magical configuration shown by the Littman and Metcalf. In GIG cavity the grating provides the required angular dispersion for developing single mode oscillation without any other frequency selective element. This cavity eliminates the movement of the frequency selective element unlike the other cavities where the frequency selective elements need to be either rotated or displaced. With a smaller number of optical components the laser alignment becomes simpler and more easily repeatable. In the short GIG cavity the axial mode separation is comparable to the single pass bandwidth of the grating. The combination of grating and tuning mirror provides a predetermined range of frequency bandwidth to the laser beam back and forth inside the laser cavity. The short cavity laser provides a large number of cavity round trips within the duration of tens of ns and provides smaller bandwidth, much less than the single pass bandwidth of the frequency selective element. The grazing incidence also does not require any magnifying element to expand the beam for generating a spectrally narrow high power laser beam. As in this cavity the grating diffracts the incident beam twice only a narrow spectral component is developed inside the cavity. The rotation of the tuning mirror scans the dye laser wavelength, while the rotation of the grating results in variation of laser bandwidth.

The short cavity provides a simple, smaller and more compact design of single mode pulsed dye laser. In summary, this short cavity GIG SLM has following advantages

i. This design eliminates the magnifying components from the cavity.

ii. As there are only three optical components the laser alignment becomes simple.

iii. The cavity does not contain any other components except the dye cell, so that the laser is much less sensitive to temperature.

iv. The elimination of the beam expander reduces the number of optical surfaces present inside the cavity, which results in less loss, fewer reflections and shorter cavity length.

v. Implementation of pivot point suggested by Littman and Metcalf provides mode hop free tuning for the entire tuning range.

vi. Replacing the output coupler with 100 %, reflecting mirror increases the laser efficiency and the laser output can be obtained from the zeroth order of the diffraction grating. The zeroth order from the grating as an output eliminates the unavoidable zeroth order losses in the GIG cavity.

vii. The laser can be made extremely compact so that short duration gain can be utilized efficiently and a very small amount of feedback from the grating mirror pair is sufficient to generate the laser at the desired wavelength.

viii. The longitudinal pumping provides excellent beam quality with small beam divergence to the SLM dye laser.

The design of a pulsed narrow band dye laser as proposed by Littman and Metcalf is chosen for generating SLM dye laser. This SLM dye laser was designed to be compact, engineered, rugged, stable, less expensive to construct and relatively less complex in design, which can be adopted either vertical or horizontal mounting. The schematic of short cavity GIG SLM laser is shown in figure 2.20.

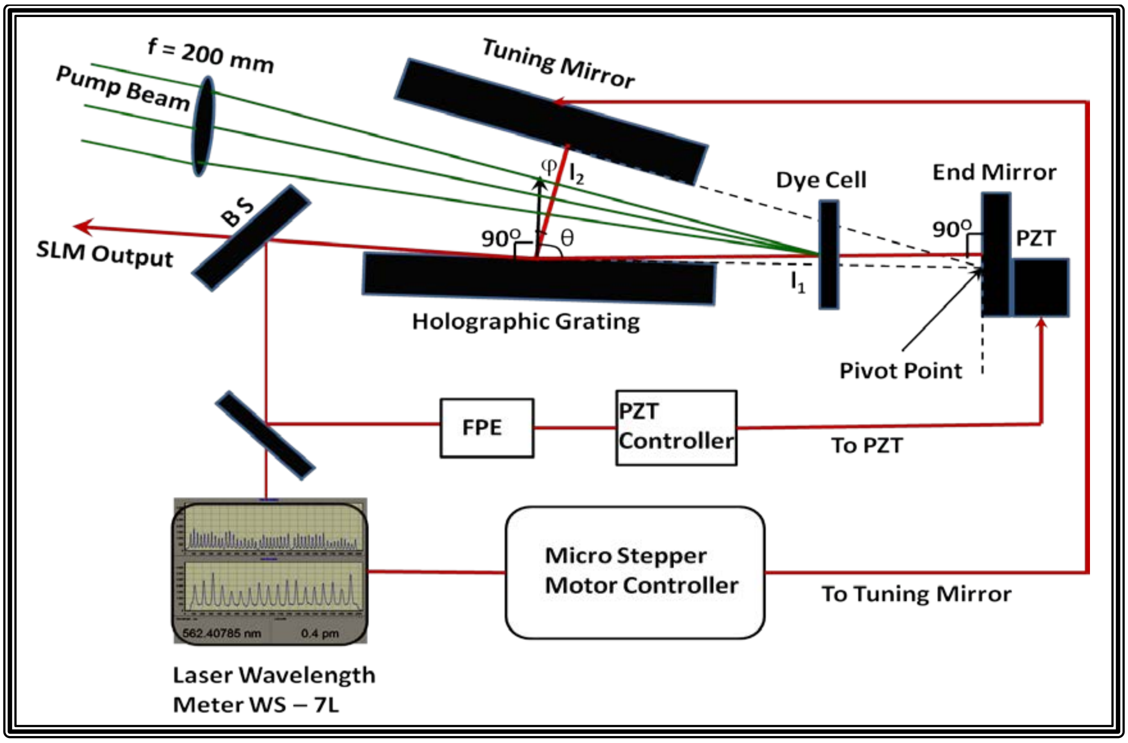

Fig 2.20: Schematic of the short cavity grazing incidence SLM dye laser

References

[2.1] R R Lewis, G A Naylor, A J Kearsely, "Copper Vapour Lasers reach high power" Laser Focus, 92 – 96, 1988.

[2.2] M Hercher, H A Pike, "Tunable dye laser configurations", Optics Comm. 3, 65 – 67, 1971.

[2.3] S M Jarrett, J F Young, "High efficiency single frequency cw ring dye laser", Opt., Let., 4, 176 – 178, 1979.

[2.4] T F Johnston, R H Brady, W Proffitt, "Powerful single frequency ring dye laser spanning the visible spectrum", Appl. Opt. 21, 2307 – 2316, 1982.

[2.5] S Liberman, J Pinard, "Single-mode cw dye laser with large frequency range tunability", Appl. Phys. Lett., 24, 142 – 144, 1974.

[2.6] M Pinard, C G Aminoff, F Laloe, "Double Michelson mode selector and pressure scanning of a cw single mode dye laser", Appl. Phys. 15, 371 – 375, 1978.

[2.7] G M Gale, "A Single mode flashlamp pumped dye laser", Optics Comm. 7, 86 – 88, 1973.

[2.8] M K Iles, P Arthur, P D'Silva, V A Fassel, "Single mode nitrogen pumped dye laser", Opt., Comm., 35 133 – 136, 1980.

[2.9] T W Hansch, "Repetitively pulsed tunable dye laser for high resolution spectroscopy", Appl., Opt., 11, 895 – 898, 1972.

[2.10] D C Hanna, P A Karkkainen, R Wyatt, "A simple beam expander for frequency narrowing of dye lasers" Opt., Quantum Electronics, 7, 115 – 119, 1975.

[2.11] I Shoshan, N N Danon, U P Oppenheim, "Narrowband operation of a pulsed dye laser without intracavity beam expansion", J Appl. Phys. 48, 4495 – 4497, 1977.

[2.12] G Marowsky, "Reliable Single mode operation of a flashlamp pumped dye laser", Rev., Sci. Instr., 44, 890 – 892, 1973.

[2.13] G L Eesley, M D Levenson, "Dye laser cavity employing a reflective beam expander", IEEE J Quantum Electron, QE – 12, 440 – 442, 1976.

[2.14] A Corney, J Manners, C E Webb, "A Narrow bandwidth pulsed, ultra violet dye laser", Opt., Comm., 31 354 – 358, 1979.

[2.15] S Mory, A Rosenfeld, S Polze, G Korn, "Nanosecond dye laser with a high efficiency holographic grating for grazing incidence", Opt. Comm., 36, 342 – 346, 1981.

[2.16] I Shoshan, U P Oppenheim, "The use of a diffraction grating as a beam expander in a dye laser cavity", Opt. Comm. 25, 375 – 378, 1978.

[2.17] J E Lawler, W A Fitzsimmons, L W Anderson, "Narrow bandwidth dye laser suitable for pumping by a short pulse duration N_2 laser", Appl. Opt. 15, 1083 – 1090, 1976.

[2.18] R Wallenstein, T W Hansch, "Linear pressure tuning of a multi-element dye laser spectrometer", Appl., Opt., 13, 1625 – 1628, 1974.

[2.19] O L Bourne, D M Rayner, "Pressure tuned single longitudinal mode dye laser", Opt., Comm., 64, 461 – 466, 1987.

[2.20] S G Dinev, I G Koprinkov, K V Stamenov, K A Stankov, C Radzewicz, "Two wavelength single mode grazing incidence dye laser", Opt., Comm., 32, 313 – 316, 1980.

[2.21] W Sun, C S Tang, X B Zhuge, M S Chen, "Theory and experiment of dye lasers longitudinally pumped by copper vapor laser (CVL)", Opt. Comm., 58, 196 – 200, 1986.

[2.22] T Petrov, N Sabotinov, S Trendafilov, "Efficient dye jet laser pumped by CuBr vapor laser" Opt. Comm. 92, 291 – 294, 1992.

[2.23] Z G Huang, K Namba, "High power efficient dye laser pumped by a copper vapor laser", Jpn. J Appl., Phys. 20, 2383 – 2387, 1981.

[2.24] W W Morey, "Proceedings of the international conference on Laser'79", STS, McLean VA, 365 – 373, 1980.

[2.25] K Kato, A Fujisawa, "Longitudinally pumped high power dye laser in the Blue", Optics Comm. 10, 21 – 22, 1974.

[2.26] A Owyoung, "An efficient ruby laser pumped, diffraction limited dye laser", Optics Comm. 11, 14 – 17, 1974.

[2.27] M Broyer, J Chevaleyre, G Dclacretaz, L Woste, "CVL – pumped dye laser for spectroscopic application", Appl. Phys. B, 35, 31 – 36, 1984.

[2.28] A N Zherikin, V S Letokhov, V I Mishin, V P Belyaev, A N Evtyunin, M A Lesnor, “High repetition rate tunable dye lasers pumped by copper vapor laser”, Sov. J Quantum Electron., 11, 806 – 808, 1981.

[2.29] S Lavi, M Amit, G Bialolanker, E Miron, L A Levin, “High repetition rate high power variable bandwidth dye laser”, Appl., Opt., 24, 1905 – 1909, 1985.

[2.30] F J Duarte, J A Piper, “Comparison of prism expander and grazing incidence grating cavities for copper laser pumped dye laser”, Appl., Opt., 21, 2782 – 2786, 1982.

[2.31] D J Bradley, G M Gale, M Moore, P D Smith, “Longitudinally pumped, narrow band continuously tunable dye laser”, Phys., Lett.,26A, 378 – 379, 1968.

[2.32] F C Strome Jr, J P Webb, “Flashtube pumped dye laser with multiple prism tuning”, Appl., Opt., 10, 1348 – 1353, 1971.

[2.33] S A Mayers, “An Improved line narrowing technique for a dye laser excited by a nitrogen laser”, Opt. Comm. 4, 187 – 189, 1971.

[2.34] M A Novikov, A D Tertyshnik, “Tunable dye laser with a narrow emission spectrum”, Sov. J Quantum Electron, 5, 848 – 849, 1975.

[2.35] F J Duarte, J A Piper, “Prism pre-expanded grazing incidence grating cavity for pulsed dye lasers”, Appl., Opt., 20, 2113 – 2116, 1981.

[2.36] L G Nair, “On the dispersion of a prism used as a beam expander in a nitrogen laser pumped dye laser”, Opt., Comm., 23, 273 – 274, 1977.

[2.37] S G Dinev, I G Koprinkov, K V Stamenov, K A Stankov, “A Novel double grazing incidence Single mode dye laser”, App., Phys. 22, 287 – 291, 1980.

[2.38] P McNicholi, H J Metcalf, “Synchronous cavity mode and feedback wavelength scanning in dye laser oscillators with gratings”, App., Opt., 24, 2757 – 2761, 1985.

[2.39] T T Basiev A G Papashvilli, V V Fedorov, S V Vassiliev, W Gellermann, “Single Longitudinal Mode LiF:F_2^- Color Center Laser for High Resolution Spectroscopy”, Laser Physics, 14, 23 – 29, 2004.

[2.40] S A Kostritsa, V A Mishin, “Tunable narrow band moderate power laser system pumped by copper vapour laser”, Sov, Quantum Electronics, 25, 516 – 520, 1995.

[2.41] S Saikan, “Nitrogen laser pumped single mode dye laser”, Appl. Phys. 17, 41 – 44, 1978.

[2.42] Y Arai, H Niki, S Adachi, T Takeda, T Yamanaka, C Yamanaka, “Development of single mode dye laser pumped by a copper vapor laser”, Technology reports of the Osaka University, 36, (1986), 361 – 367.

[2.43] S V Vasilev, V A Mishin, T V Shavrova, “Single frequency dye laser with fiber optic pumping”, Sov, Quantum Electronics, 27, 126 – 128, 1997.

[2.44] T Chang, F Y Li, “Pulsed dye laser with grating and etalon a symmetric arrangement”, Appl., Opt., 19, 3651 – 3654, 1980.

[2.45] O Prakash, R Mahakud, P Saxena, V K Dubey, S K Dixit, J K Mittal, “A study on the control of dye solution temperature on the linewidth and wavelength stability of copper vapor laser pumped single mode dye laser”, Opt., Comm., 283, 5099 – 5106, 2010.

[2.46] T W Hansch, I S Shahin, A L Schawlow, “High resolution saturation spectroscopy of sodium D lines with a pulsed tunable dye laser”, Phys., Rev., Lett., 27, 707 – 710, 1971.

[2.47] J F Black, J J Valentini, “Development of a single longitudinal mode high peak power tunable pulsed dye laser”, Rev. Sci. Instrum., 65, 2755 – 2761, 1994.

[2.48] P Ewart, D R Meacher, “A novel widely tunable single mode pulsed dye laser”, Opt., Comm., 71, 197 – 201, 1989.

[2.49] D J Binks, D K Ko, L A W Gloster, T A King, “Pulsed single mode laser in four arm grazing incidence cavity”, J Mod., Opt., 45, 1249 – 1258, 1998.

[2.50] M Pinard, M Leduc, G Trenec, C G Aminoff, F Laloe, “Efficient single mode operation of a standing wave dye laser”, Appl., Phys., 19, 399 – 403, 1979.

[2.51] A Mandl, D E Klimek, H P Chou, L Litzenberger, Y Wang, “Single mode operation of a long pulse flashlamp pumped dye laser”, IEEE J Quantum Electronics, QE – 31, 346 – 351, 1995.

[2.52] V N Beltyugov, V I Nalivaiko, A I Plekhanov, V P Safonov, “Single Mode pulsed dye laser”, Sov. J. Quantum Electronics, 11, 837 – 839, 1981.

[2.53] A Shevchenko, P Ryytty, T Kajava, M Hautakorpi, M Kaivola, “Single longitudinal mode selection in a nanosecond pulsed dye laser”, Appl., Phys., B74, 349 – 354, 2002.

[2.54] K Namba, J Ida, “Copper vapor laser pumped dye amplifier of a CW dye laser”, Jp J Appl., Phys. 23, 1330 – 1335, 1984.

[2.55] S Lavi, G Bialolanker, M Amit, D Belker, G Erez, E Miron, “Characterization of a pulse amplifier for CW dye laser”, Opt., Coummn., 60, 309 – 313, 1986.

[2.56] J W Hahn and Y S Yoo, “Suppression of amplified spontaneous emission from a four pass dye laser amplifier”, Appl. Opt., Vol. 37, No.21 4867 – 4870, 1998.

[2.57] G L Eesley, M D Levenson, D E Nitz, A V Smith, “Narrow band pulsed dye system for precision nonlinear spectroscopy”, IEEE J Quantum Electronics, QE – 16, 113 – 115, 1980.

Chapter – III

DESIGN ASPECTS OF SLM DYE LASER

3.1 Introduction

Many current and prospective applications demand that laser sources must have high power, narrow bandwidth (transform limited) and small beam divergence (diffraction limited). For several reasons the high power and narrow band output are contradictory for standard cavity designs, and the usual approach to meeting both the requirements is the use of the MOPA configuration. Hence all the narrow band oscillators generate a small output power with very narrow linewidth. As discussed in chapter – II, the Littman Metcalf cavity because of its simplicity is of interest for SLM dye laser [1.15]. The design concepts of this cavity will be discussed at length in this chapter.

A feature of this simple cavity design is the use of diffraction grating at grazing incidence (~ 88 – 89.5^{O}) to the laser beam, which allows a larger grating illumination length without any intracavity beam expander. The short cavity length provides a large inter mode spacing and higher grating illumination provides high selectivity. The short cavity SLM GIG laser consists of mainly four components: a holographic grating in grazing incidence, a high reflectivity stripe plane mirror, a high reflectivity end mirror and a fluctuation free dye flow cell. The stripe plane mirror (tuning mirror) is rotated for tuning the SLM dye laser wavelength. The cavity mode structure of a grating tuned oscillator generally does not scan synchronously with the feedback wavelength from tuning mirror. For smooth scanning (mode hop free) of SLM dye laser it is necessary that while rotating the tuning mirror, the mode index number of longitudinal mode does not change. In order to establish a mode hop free smooth wavelength scanning in the SLM dye laser, the cavity mode frequency should exactly match the feedback frequency determined by the grating pass band [3.1].

It has been demonstrated by Liu and Littman that if the optical components of GIG laser are mounted in such a way that the surface planes of three optical components (tuning mirror, grating and end mirror) intersect at a common point and the axis of rotation of the tuning mirror passes through this point, which is known as the pivot point, no mode hop will take place in the entire tuning range of the SLM dye laser [1.16].

3.2 Requirements of Design Architecture

Designing a SLM dye laser requires some well defined steps to arrive at the specifications, such as bandwidth, tuning range, scanning rate, wavelength, beam divergence, spectral purity, pulse repetition frequency, power requirement etc. of the laser system. A coarse selection of the dye laser wavelength is possible by judicious choice of the laser dye, solvent and the resonator type. A small linewidth and fine tuning can only be obtained by wavelength selective resonators. The steps involved in designing an efficient SLM laser are discussed here [1.6].

i. The specification of the wavelength is the determining factor in selecting the pumping source and the type of laser dye. Ideally, the pumping source emission wavelength must match with the absorption transition of the dye utilized. The efficiency of the laser depends on the ratio of the emitted wavelength of the molecular gain media to pump wavelength. The small Stokes shift, i.e., the difference between the pump wavelength and emitted wavelength, also increases the life of the gain medium in the visible range.

ii. The specification of pump power for any laser system is dictated by the cavity components. As a rule of thumb, the intensity inside the resonator must be higher than the saturation intensity and must be lower than the damage threshold of the optical components used inside the resonator. The laser emission that starts at one end and transits to the other end depends upon the amount of gain available.

iii. Between longitudinal pumping and transverse pumping, longitudinal is preferable for SLM dye lasers because here, as the gain dimension is matched with the beam waist, an essential requirement for the TEM_{OO} mode. The smaller gain dimension also facilitates the shorter cavity length to obtain the larger inter longitudinal mode spacing. The gain size acts as a slit for the spectrometer formed by the grating and the tuning mirror; the smaller the slit width the larger the spectral resolution.

iv. Different longitudinal modes travel in slightly different paths inside the resonator. For oscillation of single transverse mode the Fresnel number for the cavity must be close to unity as defined by equation 2.1. It is important to note that the gain dimension should not be so small that the diffraction losses dominate or the increase in the energy density inside the resonator is high enough to cause damage to the cavity components. The beam waist is a product of the focal length of the focusing lens and the divergence of the pump beam. The divergence of the pump beam must be small to achieve the required beam waist.

v. The TEM_{OO} mode is best achieved, when the Rayleigh length associated with the gain diameter (beam waist) is approximately equal to twice the cavity length [2.26].

$$\frac{\pi\omega_o^2}{\lambda} \approx 2\,L \tag{3.1}$$

This equation provides the optimum cavity length. For example, the cavity length of $4x10^{-2}$ m, laser wavelength of 580 nm and the beam waist ω_o is $0.12x10^{-3}$ m.

vi. Selection of cavity components is another important step for designing the SLM dye laser. The groove density of a diffraction grating sets the upper and the lower cutoff wavelengths for SLM laser and also provides the possible resolution for selecting a single mode, as given below

$$\frac{\Delta\lambda_o}{\lambda} = \frac{1}{mN} \tag{3.2}$$

where m is the order of the grating, N is the total number of illuminated lines, d * w, here d is the groove density lines/mm and w is the length of the grating in mm.

$$1 \leq (\lambda/d) \leq 2 \tag{3.3}$$

For example, the groove density of 2400 lines/mm has a lower cutoff λ_{min} ~ 416 nm and an upper cutoff λ_{max} ~ 833 nm.

vii. Dye cell is the heart of the SLM dye laser; hence the design of the dye cell is one of the important design steps. Generally, the dye solution exposed to the pump pulse should get volumetrically renewed in the cell at least twice between two pump pulses to overcome the temperature effects. It is required to minimize the index gradient in the dye cell to obtain high beam quality. The design details and temperature effects on the SLM are discussed in length in Chapter – IV and Chapter – VI respectively in this thesis.

viii. Selection of oscillator configuration is one of the key steps for generating SLM laser output. For higher cavity dispersion, the grating incidence angle is increased. It also reduces the diffraction efficiency of the holographic grating.

ix. In the next step, the cavity length and axial mode separation for the cavity are estimated. The single pass linewidth ($\Delta\nu_{single}$) is calculated using, incidence angle, diffraction angle, groove density and illuminated grating length of the desired wavelength. This single pass linewidth should be smaller than the axial mode separation ($\delta\nu_{cavity}$) for selecting one axial mode. If this condition is not matched one should resize the oscillator to attain shorter cavity lengths.

$$\Delta\nu_{single} \leq \delta\,\nu_{cavity} \tag{3.4}$$

x. The tuning mechanism can be implemented for mode hop free scanning over the entire tuning range by mounting all the optical components in a specific manner. The details of fixing of these components are discussed later in this chapter.

The pump beam alignment is another important aspect of design for obtaining single mode is the measurement of the laser parameters such as wavelength, bandwidth, tuning range, conversion efficiency, beam divergence and ASE etc. The parametric characterization of SLM dye laser pumped by 9 kHz CVL is presented in Chapter – V of this thesis. The feedback control of the SLM to actuate on output the effects of various disturbances described in Chapter – VII of this thesis. This chapter addresses the design for passive, free running operation of the laser without external environmental disturbances.

3.3 Scanning of SLM Dye Laser

In the GIG configuration a rotation of the tuning mirror by 0.001^{O} results in change of the SLM wavelength by around 3 cm^{-1} (~ 90 GHz). This frequency is too large to perform any high resolution spectroscopy; hence it is necessary to use a kinematic element that provides an angular resolution smaller than 0.1”. For continuous scanning the variation in the lasing wavelength selected by the grating, the feedback wavelength (λ_G) and the wavelength selected by the optical path length of the cavity $\left(\lambda_L \approx \frac{2L}{q}\right)$ the cavity wavelength (λ_L) should be so synchronized that a mismatch in these wavelengths is avoided. Due to mismatch, when the feedback wavelength and the cavity wavelength are shifted relative to each other by exactly one cavity mode separation, an adjacent mode then becomes more centered in the gain profile and the wavelength jumps discontinuously and abruptly to the adjacent mode. For example, if the cavity length is 5 cm then the cavity mode separation would be ~ 3 GHz. Hence, when the abrupt jump or mode hop occur a wavelength jump of ~ 3 GHz will be seen.

The principal longitudinal mode begins to dominate in the GIG cavity at large angles of incidence. Near the lasing threshold, the principal mode accumulates nearly 50% of the laser output power. In a standard GIG configuration, the gain diameter is limited by the grating input aperture. A small transverse displacement of the active region position can cause hop in the laser mode. Thus, for the stable SLM operation, high pointing stability of the pump beam is essential.

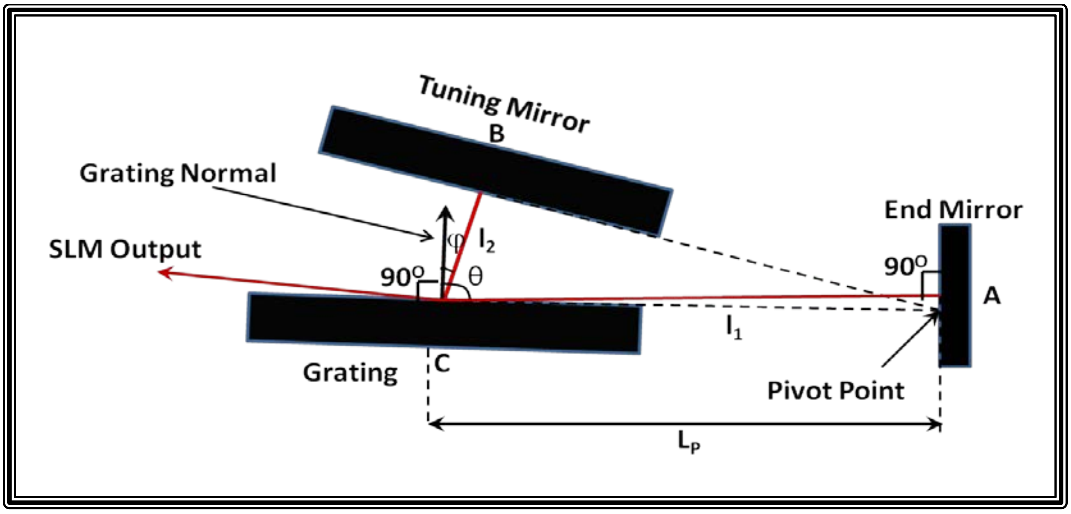

Fig 3.1: Schematic of the GIG cavity for pulsed dye laser with self tracking geometry

In the self tracking geometry, as stated earlier, the optical components of GIG cavity are mounted in a manner that the plane of grating, the plane of tuning mirror and the plane of end mirror intersect at a common point. The rotation axis of the tuning mirror coincides with this point.

In figure 3.1, the total cavity length $L(\varphi)$ can be defined as the fixed length plus a variable length.

$$L(\varphi) = l_1 + l_2(\varphi) \tag{3.5}$$

The lasing wavelength (λ_L) supported by the cavity length of $L(\varphi)$ is expressed as

$$\lambda_L = \frac{2L(\varphi)}{q} = \frac{2\,[l_1 + l_2(\varphi)]}{q} \tag{3.6}$$

where q is the mode index number. If the distance between the grating center and the pivot axis is L_P, the l_1 and l_2 can be defined as

$$l_1 = L_P \sin\theta \tag{3.7}$$

$$l_2 = L_P sin\,\varphi \tag{3.8}$$

From equations 3.7 and 3.8

$$\frac{l_1}{l_2} = \frac{sin\ \theta}{sin\ \varphi} \tag{3.9}$$

Hence,

$$L(\varphi) = l_1 \left[\frac{sin\ \theta + sin\ \varphi}{sin\ \theta}\right] \tag{3.10}$$

The wavelength supported by the grating, defined by grating master equation, must be the same as the wavelength supported by the cavity. For synchronization, from equation 3.6

$$q = \frac{2L(\varphi)}{\lambda} = \frac{2\,m l_1}{d\ sin\ \theta} \tag{3.11}$$

Equation 3.11 indicates that the longitudinal mode index number (q) neither depends on the diffraction angle (φ) nor on the lasing wavelength, hence it does not change with the rotation of the tuning mirror. This scheme needs highly precise rotation of the tuning mirror, since a linear mechanical displacement of only half wavelength can result in mode hopping. The mirror is placed on a fine rotating table. For a grazing incidence $sin\ \theta\ \approx 1$, d = 2400 lines/mm, order of grating m = 1, cavity length 5 x 10^{-2} m, the mode index number q is around $2.4\text{x}10^5$.

3.3.1 Tuning Mechanism

A very small band of wavelength is diffracted due to angular dispersion and reflected back from the tuning mirror along the direction of the incident beam. This back reflected beam is further diffracted by the grating and returned to the dye cell, while the zeroth order of diffraction becomes the laser output. The laser is tuned by rotating the tuning mirror. For tuning the laser, one can selectively auto collimate the first order diffracted beam back to the grating by rotation of the tuning mirror (retro mirror). The selection of the wavelength and the mode in the GIG cavity is shown in figure 3.2.

These processes follow the following equations derived from the grating master equation

$$m\lambda = d(\sin\theta_1 + \sin\theta_2) \tag{3.12}$$

$$m'\lambda = d(\sin\theta_3 + \sin\theta_4) \tag{3.13}$$

For use of diffracted light as feedback to the dye lasing medium, the incident angle of the laser light from the dye gain medium onto the diffraction grating (θ_1) must be equal to the diffraction angle of the light reflected back to grating by the tuning mirror (θ_4).

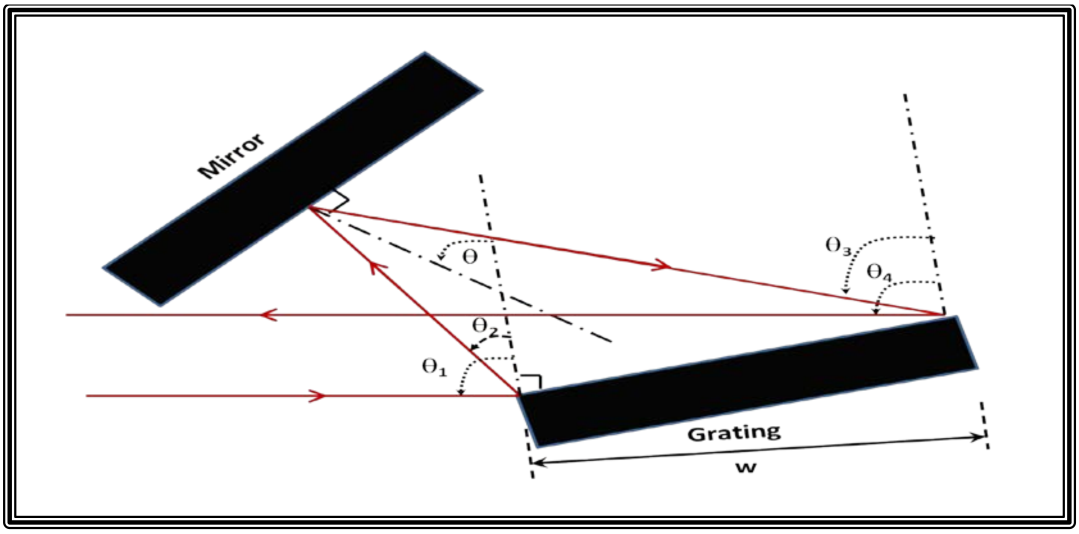

Fig 3.2: The wavelength selection on the GIG cavity of dye laser

For maximum efficiency, the diffraction order during the two diffraction processes must be the same, that is, $m = m'$. Hence the diffraction angle (θ_2) for the first diffraction must be equal to the incident angle (θ_3) for the second diffraction. Hence $\theta_2 = \theta_3 = \theta$. With these above conditions the lasing wavelength is determined by

$$\lambda_{laser} = \frac{d}{m}(\sin\theta + \sin\varphi) \tag{3.14}$$

The main problem with the GIG dye laser is the practical realization of tuning mechanism for continuous tuning over the tuning range, as it has a very high tuning rate of frequency (ν). The tuning rate is derived from grating equation as

$$\frac{d\nu}{d\varphi} = -\frac{c}{d}\frac{\cos\varphi}{(\sin\theta + \sin\varphi)^2} \tag{3.15}$$

where c is the velocity of light and m = 1. For an incidence angle of 89.5^{O}, grating groove spacing of 2400 lines/mm, grating length of $60\text{x}10^{-3}$ m and laser wavelength of 560 nm, the diffraction angle is 20.13^{O}. The tuning rate is estimated to 2.25 x 10^4 GHz deg^{-1}; implying that 1 degree angular displacement of tuning mirror will cover half the tuning range of the SLM dye laser. Hence the laser frequency tuning with a resolution of 10 MHz requires that tuning mirror must be rotated with a resolution of 4.44 x 10^{-6} degree (~ 0.016″), which is technologically a challenging task.

Kostritsa and Mishin achieved a fine tuning by an optical reducer in the form of a wedge placed in between the grating and tuning mirror; a wedge with vertex angle of 2^{O} allowed mode hop free tuning over 30 GHz by angular rotation of 1^{O} about its axis [3.2].

The tuning can also be achieved by changing the cavity length. Let us assume that the cavity linewidth Δλ remains constant at two relatively close but different wavelengths. This is a reasonable assumption for a laser emitting a diffraction limited beam. Under these circumstances the spacing of the intracavity modes will change within the pass band of the grating.

$$\delta\lambda_1 = \frac{\lambda_1^2}{2L} \tag{3.16}$$

$$\delta\lambda_2 = \frac{\lambda_2^2}{2(L \pm \Delta L)} \tag{3.17}$$

For SLM oscillation the mode index number should be the same for both wavelengths hence

$$\lambda_2 \approx \lambda_1 \left(1 \pm \left(\frac{\Delta L}{L}\right)\right)^{\frac{1}{2}} \tag{3.18}$$

This equation indicates that tuning by changing the cavity length depends on the $\frac{\Delta L}{L}$ ratio. The tuning of the SLM dye laser is discussed in chapter – V in detail. The cavity length of the SLM dye laser must be controlled carefully to ensure the stability in the frequency domain.

For wavelength 570 nm, d = 2400 lines/mm, θ = 89.5^{O} m = 1 for first order

$$5.7 \times 10^{-7} * 2.4 \times 10^{6} = (\sin 89.5 + \sin\varphi) \tag{3.19}$$

$$\varphi = 21.59467^{O}$$

For tuning step of 6 MHz at 570 nm the change in diffraction angle is calculated from grating master equation.

$d\varphi = 1.677 \times 10^{-8}$ radian or 0.003461 arc-sec

For tuning the SLM dye laser frequency with a resolution 6 MHz the minimum angular change required is 0.003461 arc-sec.

3.3.2 Optimum Cavity Length

A narrow linewidth is achieved when the principal diffraction lobe of the slit function just fills the holographic grating. The single pass linewidth (FWHM) has a minimum value when the separation between the dye cell and the grating equals the Rayleigh length (L_R) [1.14]. The resultant linewidth of the laser output has contributions of angular dispersion and the resolving power of the frequency selective element of the cavity [2.16]. The single pass linewidth of a grating cavity is much like that of a spectrometer; the pass band is a convolution of the entrance / exit slit function and the angular dispersion of dispersive element used in the spectrometer [3.3]. The figure 3.3 shows the laser beam path for the GIG cavity. The pass band is defined by equation 3.20 for an active region of ω_O with Gaussian intensity profile.

$$\Delta\lambda \approx \Theta\left(\frac{\partial\theta}{\partial\lambda}\right)^{-1} \tag{3.20}$$

The $\left(\frac{\partial\theta}{\partial\lambda}\right)$ is the angular dispersion and Θ is the entrance/exit slit function or divergence. It is clear from equation 3.20 that for narrow bandwidth it is necessary to increase the intracavity dispersion and reduce the beam divergence.

This equation is used extensively to determine the emission linewidth in pulsed narrow linewidth dispersive laser oscillators [3.4]. This equation is also well known in the field of classical spectrometers, where it is introduced using geometrical arguments [3.5]. The beam divergence can be defined as

$$\Theta = [\Theta^2{}_{entrance} + \Theta^2{}_{exit}]^{\frac{1}{2}} \tag{3.21}$$

where the $\Theta_{entrance} = \frac{W\ Cos\ \theta}{d_2}$ and $\Theta_{exit} = \frac{\omega_o}{d_2}$, W is the total illuminated width on the grating, ω_o is the diameter of the gain region and d_2 is the distance between the dye cell and the grating. So the total beam divergence can be defined as

$$\Theta = \left[\left(\frac{W\ Cos\ \theta}{d_2}\right)^2 + \left(\frac{\omega_o}{d_2}\right)^2\right]^{\frac{1}{2}} \tag{3.22}$$

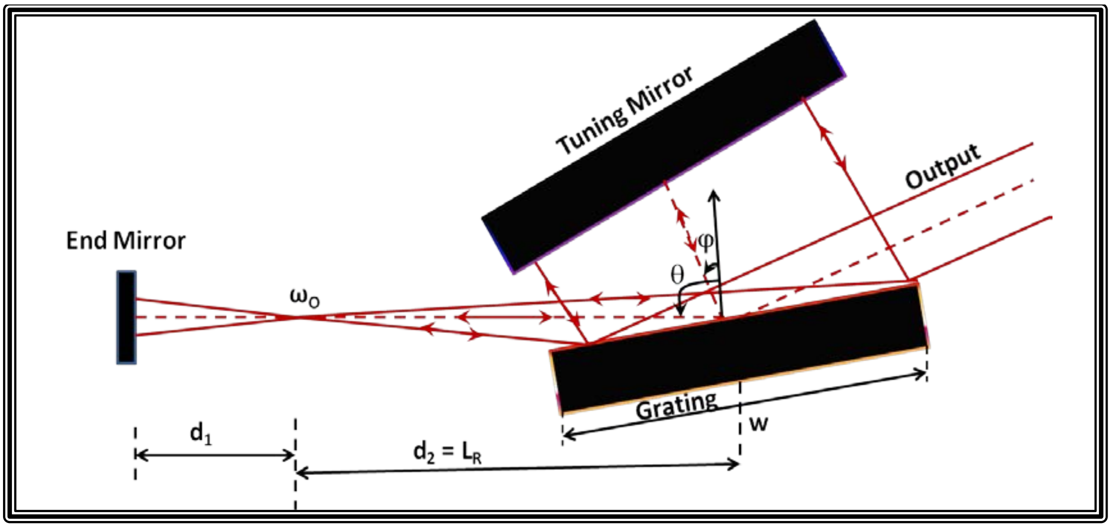

Fig 3.3: Grazing incidence generalized dye laser cavity

Case: $d_2 >> L_R$

For a far field case d_2 is very large i.e., $d_2 >> L_R$, $L_R = \frac{\pi\omega_o^2}{\lambda}$. The diffraction limited beam divergence for a Gaussian beam is defined as (half angle) $\Theta = \frac{\lambda}{\pi\omega_o}$

The second term in equation 3.22 is very small for far field

$$\Theta = \frac{W\ Cos\ \theta}{d_2} = \frac{\lambda}{\pi\omega_o} \tag{3.23}$$

Case: $d_2 << L_R$

For a near field $d_2 << L_R$ for this condition $W\ cos\ \theta = \omega_o$

$$\Theta = \left[\left(\frac{\omega_o}{d_2}\right)^2 + \left(\frac{\omega_o}{d_2}\right)^2\right]^{\frac{1}{2}} = \frac{\sqrt{2}\lambda}{\pi\omega_o}\left(\frac{L_R}{d_2}\right) \tag{3.24}$$

Case: $d_2 = L_R$

The equations 3.22 and 3.24 had the minimum value of divergence if $d_2 = L_R$.

$$\Theta = \frac{\sqrt{2}\,\lambda}{\pi\omega_o} \tag{3.25}$$

For a wavelength $\lambda \sim 600$ nm and gain spot size (ω_o) ~ 0.1x 10^{-3} m the Rayleigh range is nearly 5x 10^{-2} m, which should be equal to the distance between the dye cell and grating. For 5x10^{-2} m cavity length, 2400 lines/mm holographic grating at 600 nm the single pass linewidth is calculated to be 0.076 cm^{-1} or 2.6 pm. For minimum achievable bandwidth, once the optics layout is optimized for diffraction limited beam divergence, one should use the largest width of grating (w) for increasing the intracavity dispersion.

3.4 Optical Components

In the following section, the basic principles of the optical components used in the resonator cavity are briefly discussed. There are mainly three optical components, holographic grating, plane tuning mirror and end mirrors in the SLM GIG cavity.

3.4.1 Grating

In a grating, the distance between the adjacent grooves and the angle of grooves with respect to the substrate influences the dispersion as well as the efficiency. The groove spacing is almost equal or comparable to the wavelength being diffracted. The light incident on a grating surface is diffracted to its discrete constituents. The light diffracted by each groove combines to form a diffracted wave front (surfaces of constant phase). In a master grating equation, by convention the angles of incidence (θ) and diffraction (φ) are measured from the grating normal to the beam as shown in figure 3.4. In a grating whose groove spacing is d, the beam of light with wavelength λ incident on the grating at an angle θ is diffracted by a grating along angles φ_m. The sign convention for these angles depends on whether the diffracted light is on the same side or the opposite side of the incident beam; the plus sign is taken if φ_m and θ are on the same side of the grating normal; otherwise the minus sign is taken. The generalized grating master equation is given by

$$m\lambda = d(\sin\theta \pm \sin\varphi) \qquad (3.26)$$

For a particular wavelength λ all the integral values of m for which $\left|\frac{m\lambda}{d}\right| < 2$ correspond to physically viable diffraction orders. The angles of incidence, diffraction and wavelength are mathematically related for fixed groove spacing. For a particular order "m", the different wavelengths of light wave fronts incident at an angle "θ" are separated in angle by

$$\varphi(\lambda) = \sin^{-1}\left(\frac{m\lambda}{d} - \sin\theta\right) \qquad (3.27)$$

When m = 0 the wavelength dependent factor is neutralized; similarly, the wavelengths are not separated ($\varphi = -\theta$) for all wavelengths. This is known as specular reflection or zero order for the grating, where the incident angle θ equals the reflection angle φ. For $d > \frac{\lambda}{2}$ there exist two lowest diffraction orders in the incident plane for a specific incidence angle θ. A special condition for which the diffracted light diffract back towards the incident light, that is, the angle of incidence is equal to the angle of diffraction (θ = φ).

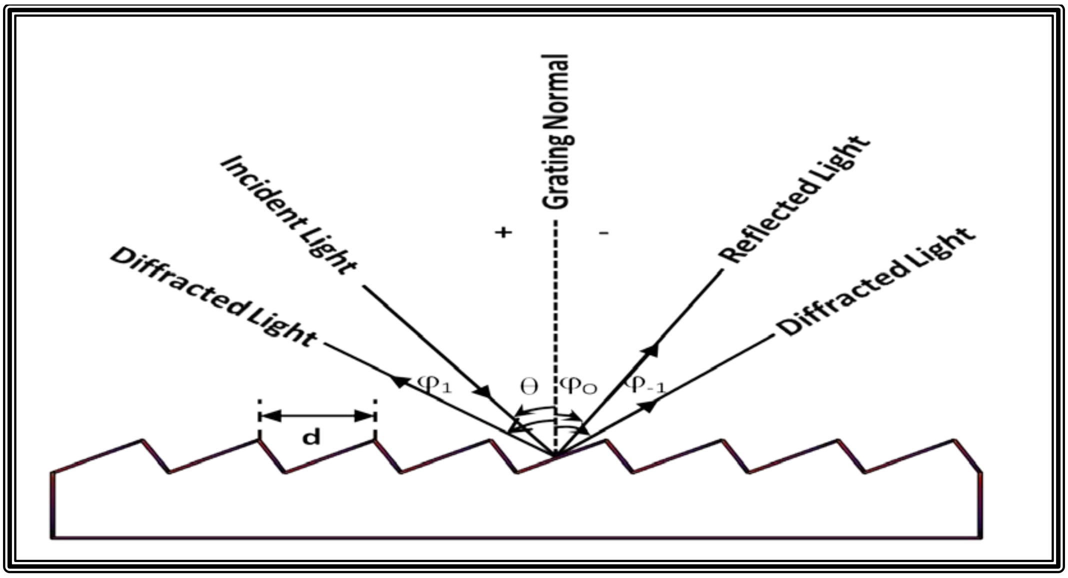

Fig 3.4: Incident, diffracted and reflected beam on the grating and sign convention

In this arrangement known as Littrow configuration, the grating equation is modified as

$$m\lambda = 2\, d\, sin\, \theta \tag{3.28}$$

The diffracted wavelength by equation 3.28 is the feedback wavelength for the Littrow cavity. For a particular set of grating parameters such as groove density d, angles θ and φ, the grating equation is satisfied for more than one wavelength. The constructive interference of diffracted waves by successive grooves simply requires that the each beam is either retarded or advanced in phase with respect to each other, where the corresponding path difference is an integral multiple of the wavelength. The path difference is one wavelength, when the diffraction order is one (m = 1). Similarly, for second order the path difference between the diffracted beams from adjacent grooves equals to two wavelengths and so on. The diffraction order m is usually the first order for maximum efficiency.

Dispersion: Angular dispersion of a grating is the spectral range per unit angle. It is a function of the angle of incidence and groove density. It is obtained by differentiating the grating master equation

$$\left(\frac{\partial\theta}{\partial\lambda}\right) = \frac{m}{d\ cos\ \theta} \qquad (3.29)$$

The angular dispersion can be increased by increasing the angle of incidence or by increasing the groove density. For single mode oscillators a high dispersion leads to narrower linewidth.

For $\theta \rightarrow \frac{\pi}{2}, cos\ \theta\ \rightarrow 0$, if the radiation incident at a grazing angle on to grating surface, then the grating dispersion tends to infinity and strong spatial compression of the incident laser beam occurs.

Substituting the value of $\frac{m}{d}$ from the grating equation in the equation 3.29, yields the general equation for the angular dispersion:

$$\left(\frac{\partial\theta}{\partial\lambda}\right) = \frac{(sin\ \theta \pm sin\ \varphi)}{\lambda\ Cos\ \theta} \qquad (3.30)$$

This shows that the angular dispersion is exclusively a function of the angles of incidence (θ) and diffraction (φ) for a given wavelength.

Resolving Power: The resolving power of a grating is defined by its ability to recognize two separate spectral lines of wavelength. It is expressed as

$$R = \frac{\lambda}{\Delta\lambda_G} \qquad (3.31)$$

The theoretical resolving power of the grating is given by

$$R = mN \qquad (3.32)$$

where m is the diffraction order and N is the total number of grooves illuminated on the surface of the grating. By replacing the value of m from the grating master equation

$$R = \frac{Nd\ (sin\ \theta + sin\ \varphi)}{\lambda} \qquad (3.33)$$

The Nd is simply the illuminated width W of the grating

$$R = \frac{W\ (sin\ \theta + sin\ \varphi)}{\lambda} \qquad (3.34)$$

The maximum value of resolving power regardless of the order m or groove spacing d corresponds to the grazing Littrow condition, (θ = φ, $|\theta| = 90^O$).

$$R_{max} = \frac{2W}{\lambda} \qquad (3.35)$$

The limit of the resolving power not only depends on the angles θ and φ, but also on the optical quality of the grating, uniformity in groove spacing and quality of the associated optics.

The wavelength resolution of the grating is from equation 3.31 and 3.34

$$\Delta\lambda_G = \frac{\lambda^2}{W(\sin\theta + \sin\varphi)} = \frac{\lambda}{mN} \qquad (3.36)$$

$$\frac{\Delta\lambda_G}{\lambda} \approx \frac{1}{mN} \qquad (3.37)$$

$$\Delta\nu = -\frac{c}{\lambda^2}\Delta\lambda_G = -\frac{c}{W(\sin\theta + \sin\varphi)} = \frac{c}{mN\lambda} \qquad (3.38)$$

This expression predicts a linewidth about 30% smaller than that expected for the Hansch laser.

Magnification: For a given wavelength λ we may consider the ratio of the width of a collimated diffracted beam to that of a collimated incident beam to be a measure of the effective magnification of the grating.

$$M = \frac{b}{a} = \frac{\cos\varphi}{\cos\theta} \qquad (3.39)$$

Since θ and φ depends on wavelength through a grating master equation the magnification will vary with wavelength. The ratio $\frac{b}{a}$ is called the anamorphic magnification for a given wavelength λ; it depends only on the angular configuration in which the grating is used. A large magnification factor can be achieved when the incident beam is near grazing (θ →90^{O}). As already discussed the GIG can be used as a very strong intracavity frequency selector as well as beam expander. The beam expansion obtained by this method is accompanied by a reduction in the beam divergence as shown in figure 3.5.

This can be obtained by differentiating the grating master equation. An incident monochromatic beam with divergence Θ is diffracted with smaller divergence δΘ given by

$$\delta\Theta = -\frac{\cos\theta}{\cos\varphi} = -\frac{\Theta}{M} \qquad (3.40)$$

Beam expansion and reduction in beam divergence occur only in one dimension, therefore, narrowing the line width. Beam expansion for the dye laser is required only in the plane of incidence of the grating. At higher angle of incidence the grating input aperture becomes smaller than the gain size in the resonator, leading to an additional loss. The small input aperture limits the transverse (spot) size of the laser active region and in turn, the maximum output power of the laser. In the GIG configuration, the grating input aperture (A_1) is

$$A_1 = w \cos \theta \tag{3.41}$$

where w is the grating length and θ the incidence angle.

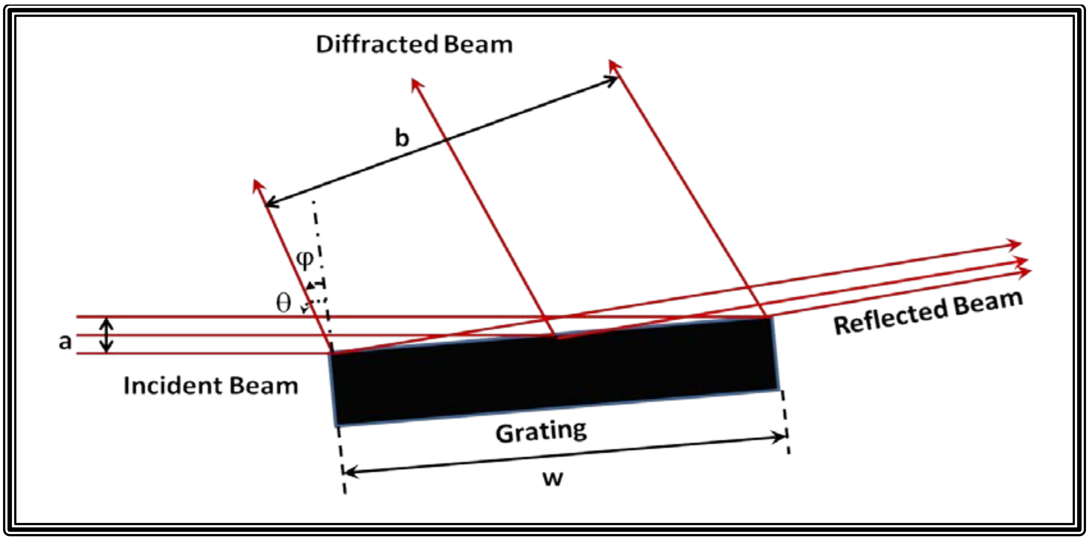

Fig 3.5 Magnification of input beam by a grating at grazing incidence

For example, in the SLM dye laser for the 62.5×10^{-3} m long grating with incidence angle of 89.5^{O}; the grating aperture is nearly 545 μm, which limits the maximum pump pulse energy to ~ 2 mJ based on the damage of dye cell windows.

3.4.2 Selection of Tuning Mirror and End Mirror

Selection of the tuning mirror and end mirrors are of importance to the design of SLM laser. In this design, both the mirrors are high reflectivity mirrors, for which dielectric coatings are used on highly polished substrates. The main interest in dielectric mirror is that they have extremely low losses at optical frequencies as compared to ordinary metallic mirrors. Dielectric coatings are optically stable, free of scattering and absorption, mechanically strong and chemically inert. A dielectric mirror consists of identical alternating layers of high and low refractive indices. The optical thicknesses are typically chosen to be quarter wavelength ($\lambda/4$) long for operating wavelength. As the number of bilayers increases the reflection response becomes flatter within the bandwidth Δλ, and has sharper edges and tends to be100%. The bandwidth Δλ represents the asymptotic width of the reflecting band. To estimate the losses for the high reflectivity mirror one requires to find its reflectance, transmittance, absorption and scattering by the coating. For a particular mirror the following relationship between the power coefficients holds

$$A' + S' + R' + T' = 1 \tag{3.42}$$

where A' is the fraction of losses due to absorption, S' the fraction lost due to scattering, R' the reflectance and T' the transmittance. The scattering losses for high reflectivity coatings can be divided into three major groups according to the scatterer size. For example,

Mie Scattering : particle size in the range of 100 – 1000 nm

Rayleigh Scattering : Particle size in the range 10 – 100 nm

Raman Scattering : Particle size < 1nm.

The total scattering is a simple number describing the amount of scattered light integrated over an entire hemisphere.

$$S' = \left(\frac{4\pi\delta_r}{\lambda}\right)^2 \tag{3.43}$$

where δ_r is the surface roughness of the thin film and λ is the wavelength of the light [1.23]. Absorption is an important parameter for the high reflectivity mirror: even very weak absorption can cause failure of the optical components of the laser system. There are several methods used to measure the weak absorption in the coating, such as photo thermal deflection and surface thermal lens technique. Among the three losses, the contribution from absorption is the highest and the transmission is the lowest.

The high reflectivity mirrors are generally prepared by ion beam sputtering methods. The coating substrate needs to be polished with surface roughness better than λ/2. High reflectivity tuning and end mirrors used in the SLM cavity have nearly zero or less than a few ppm transmissivity.

3.5 Mechanical Design of SLM Dye Laser

For tuning the SLM dye laser ultra high precise backlash free rotary mechanisms are required for rotating the tuning mirror with milli arc second accuracy. Obtaining such a high resolution is a challenging task. The mounting of optical components such as grating, tuning mirror and end mirrors is very important and should have the same order of accuracy as the rotary mechanism. To match the wavelength tuning requirements of SLM dye laser a rotary tuning mechanism has been designed in-house and developed with a resolution of 0.001 arc second. This rotary mechanism consists of two stage differential table having angular motion within $\pm 13^{o}$ limited to one quarter of the table. On this differential table three numbers of optical components are mounted to form an optical resonator cavity, namely, holographic grating, end mirror and tuning mirror. The holographic grating and the end mirror are mounted on the fixed table while tuning mirror was mounted on the rotary table. All these components need to be fixed in such a manner that the surface planes of all the three optical elements should intersect at the axis of rotation. This point of intersection is known as the pivot point. To locate the pivot point accurately each mount is placed on linear translation tables, which has positional accuracy of 10 µm. To obtain the absolute positioning accuracy of the optical components a special type of mount based on flexural design has been developed. Each optical component is mounted on its individual mount for precise alignment. The rotary table is attached to a stepper motor which is rotated by a computer controlled micro stepping drive.

3.6 Rotary Tuning Mechanism

A standard rotary table commercially available driven by a worm and worm gear mechanism provides an absolute accuracy of only 0.1 arc second. However, for tuning the SLM dye lasers in steps of a few MHz require a resolution of one hundredth of an arc second or better. Such a high-resolution rotary motion cannot be achieved by direct mounting of the stepper motor on the rotary table because of the limited number of micro steps available for stepper motor drive. The stepper motor having 50,000 micro steps provides the angular resolution of 26 arc sec, which is almost 10^4 times higher than the required resolution for the SLM dye laser. The rotation of the tuning mirror by one micro step (~26 arc sec) changes the SLM dye laser frequency 45 GHz. To match the tuning requirement of a few MHz per step by rotary table needs a mechanical gear with a gear ratio of 1:1000 in between the table and the stepper motor. Higher gear ratio makes the rotary table bulky with very high backlash, which is not acceptable, particularly for mode hop free scanning.

In this design, required resolution of 0.0013 arc sec has been achieved by two stage differential indirect drives. This high resolution was achieved by a rotary mechanism, which has two stages of drives. In the first stage of a stepper motor with 50,000 micro steps is directly attached to the shaft of the rotary table, which provides an angular resolution of 26 arc sec per step; this is used for coarse tuning. The second stage is rotated by an indirect drive, which rotates the fine table with respect to the coarse table. In indirect drive, the rotary motion is transferred to the fine table through an eccentric disc and backlash free worm and worm wheel arrangement. Eccentric disc is mounted just above the worm and worm wheel and the eccentricity of the disc pushes the lever of rotary table suitably as shown in figure 3.6. The cam follower is mounted on a fine table, which is connected to the cam with the help of a tensile spring.

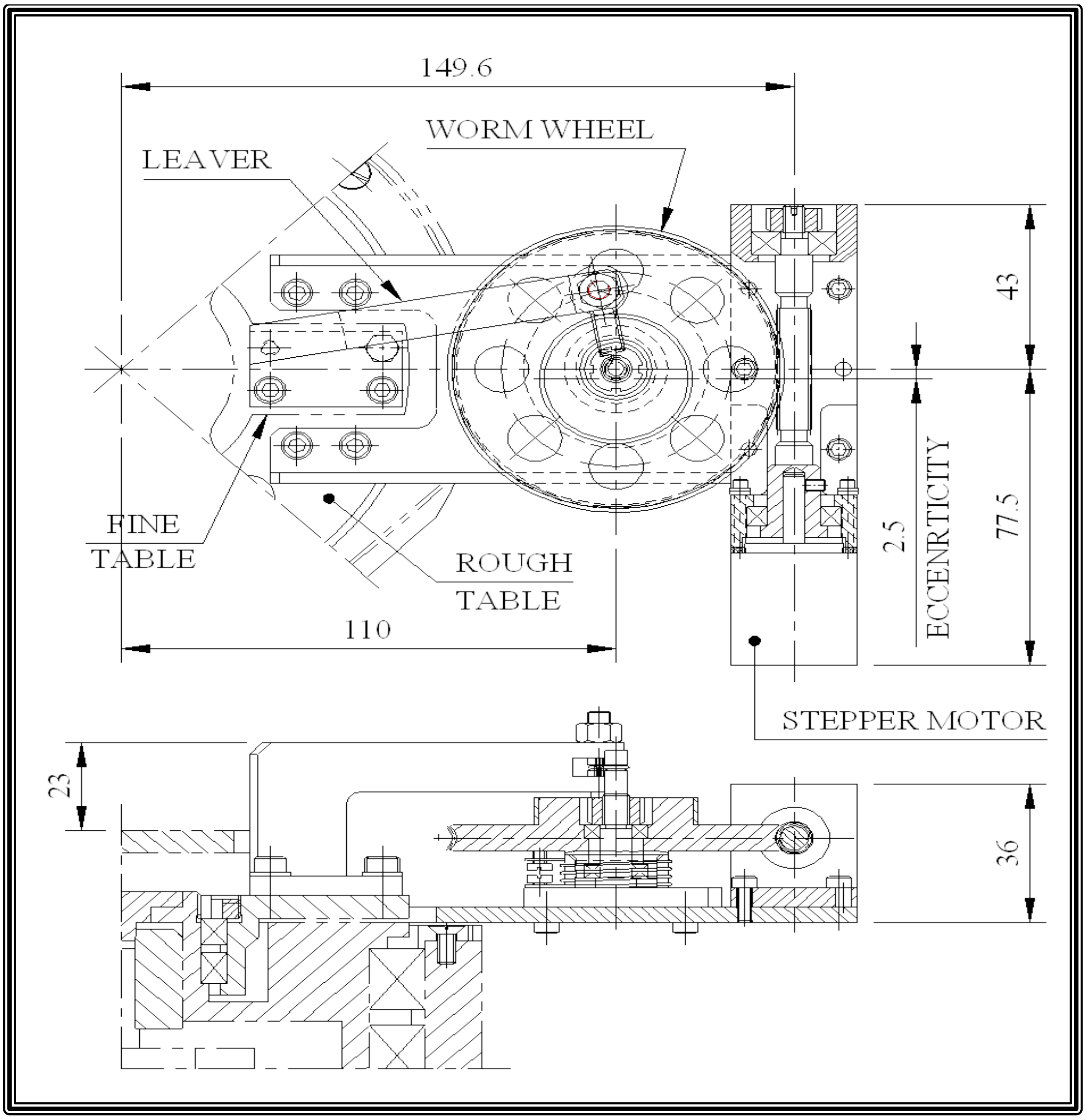

Fig 3.6: High precision wavelength tuning mechanism for SLM dye laser

The worm wheel is preloaded with the help of a spiral spring which eliminates the backlash. The tuning mirror mount is fixed on the rotary table, which can scan the SLM dye laser in steps of 10 MHz. This precise and compact design has been fabricated and implemented for tuning the SLM dye laser. For mounting of optical elements the standard kinematic mounts available commercially do not offer high accuracy which can match the precision and accuracy obtained by rotary tuning mechanism. These mounts are also not rigid enough to match the required high value of natural frequency. These mounts are designed based on flexure design with fine adjustments and the planes can be adjusted against the flexure hinge (detailed in para 3.7). These planes have angular adjustment within $\pm 2^0$ with a resolution of 10 arc sec. Each mount has two such types of unit mounted in a perpendicular direction for adjustments in two perpendicular planes. The arrangement of optical components is shown in figure 3.7.

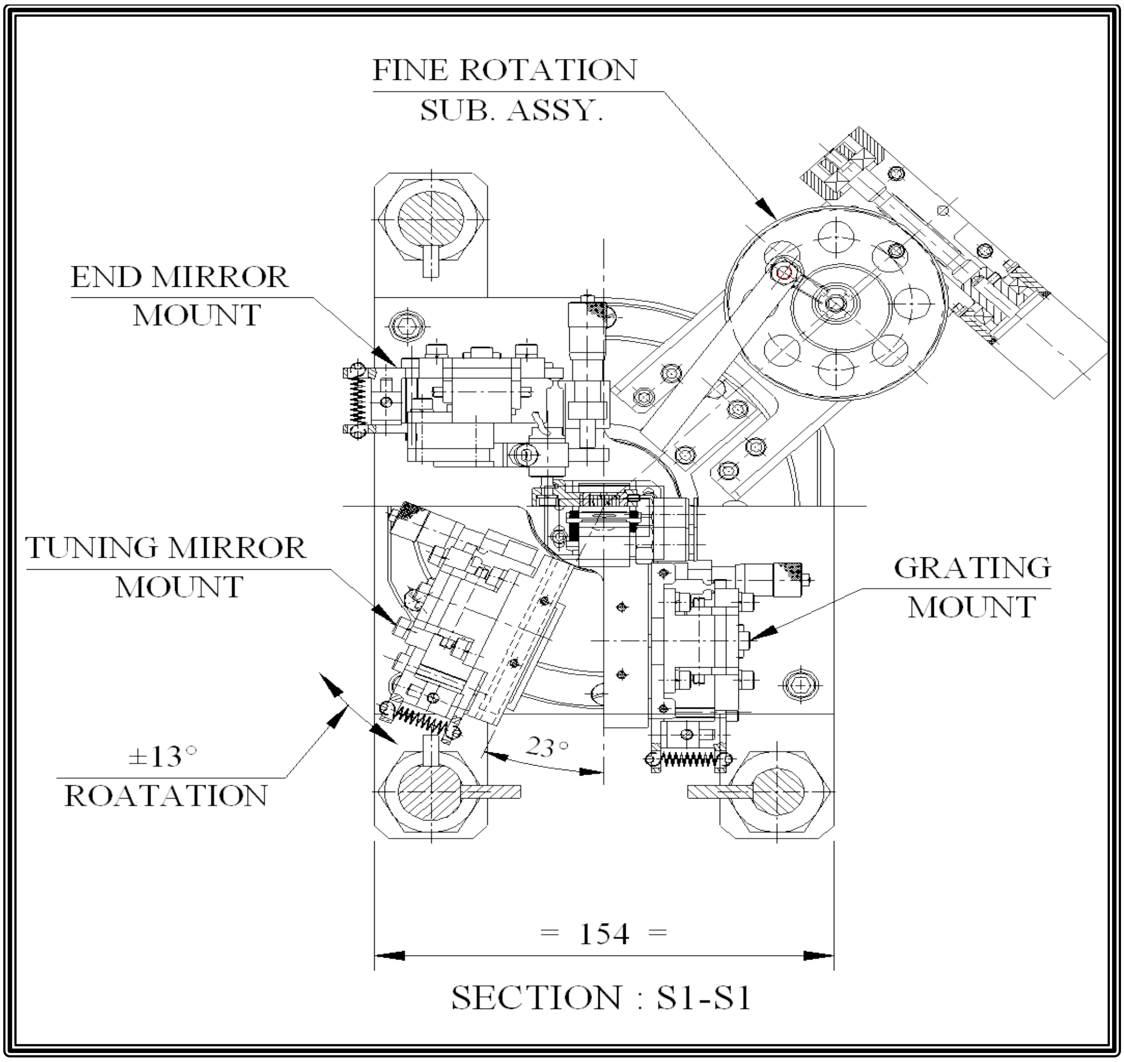

Fig 3.7: Optical components fixed on the high precision rotary table

This SLM dye laser can be mounted on a vertical wall or can be kept on a horizontal table without any deterioration of performance. Computer controlled tuning mechanism is used for scanning the SLM dye laser wavelength. The total tuning range of this tuning mechanism is limited to the ± 13^{O}, which provides the wavelength tuning range of the SLM dye laser in the band of ~ 100 nm.

3.6.1 Coarse Tuning Subassembly

The coarse tuning sub assembly consists of a rotary table shaft attached directly to the stepper motor. This table is fixed onto the main housing by two preloaded cross roller THK bearings. This table is coupled with stepper motor, which can be driven by a 50,000 micro-stepping driver of Ms Slo-Syn D6. The stepper motor directly rotates this table and keeps the laser wavelength fixed by actively locking the stepper motor with a holding torque.

The Slo-Syn motor (KLM091E) with 50,000 micro stepper drive gives a resolution of

$$\frac{360^{O}}{50{,}000} = 0.0072^{0} \text{ and } 0.0072 \times 3600 = 25.92 \text{ arc} - \text{sec} \qquad (3.44)$$

Thus the minimum tuning achieved by the coarse tuning is ~ 44.93 GHz/step or 44.93 pm or 1.49 cm^{-1}/ step

3.6.2 Fine Tuning Subassembly

The worm shaft is driven by a stepper motor having 50,000 micro stepping. The eccentricity in the cam rotator is 1.5×10^{-3} m, which provides maximum displacement of nearly 3×10^{-3} m. The gear ratio in this worm and wheel tuning arrangement is 1:120. One complete revolution of the cam follower shaft provides the displacement of nearly 25 µm. The combined effect of arm length of 110×10^{-3} m, eccentricity (1.5×10^{-3}m), gear ratio (1:120) and micro stepping (50,000) results in nanometer movement of the fine table. The combination of these parameters provides minimum linear displacement of 0.5 nm. This fine tuning subassembly has a rotary resolution of 0.0012 arc sec, which has a capability to tune the SLM dye laser in the steps of 1.7 MHz. The linear movement for the fine tuning subassembly, which results in an angular displacement, has an option of replacing the worm and wheel arrangement by either PZT or the motorized micrometer. In this tuning assembly the worm and wheel was replaced by motorized micrometer, which has a minimum linear resolution of 0.3 µm resulting in angular resolution of 0.68 arc sec. There is a provision of replacing the motorized micrometer with a PZT for fine movements, which has no gear and motor movements involved. The fine movement by PZT does not have any backlash.

Fine Tuning with PZT

There are three PZT's utilized for the fine tuning of the SLM dye laser. One at the end mirror and another two at the tuning mirror (cascaded) with 100×10^{-3} m arm length. The input signal for PZT drive was generated from a digital to analog converter having 14-bit resolution (1×10^{-4}).

PZT at Tuning Mirror

The tuning mirror was rotated by PZT around a pivot point with 100×10^{-3} m arm length. The minimum resolution obtained by 20 µm PZT at tuning arm is calculated.

For 20 µm PZT the maximum rotation of tuning mirror for maximum stroke length of PZT is $20 \times 10^{-6} / 100 \times 10^{-3} = 2 \times 10^{-4}$ radian or 41.27 arc-sec. This angular displacement of the tuning mirror will tune the SLM dye laser by 71.54 GHz or 2.38 cm^{-1}. The 1 µm displacement of PZT will tune the SLM dye laser by ~ 3.6 GHz. The minimum tuning step with 14 – bit input signal to the PZT driver provides linear displacement of 20×10^{-10} m that changes tuning mirror angle by 0.00412 arc-secs, corresponding to a frequency change of 7.14 MHz.

PZT at End Mirror

Tuning of the SLM dye laser with end mirror is mainly used for wavelength stabilization at the dynamic frequency of nearly ~ 1 kHz.

The cavity length tuning is given by

$$\frac{dL}{L} = \frac{d\nu}{\nu} \tag{3.45}$$

where dL is a change in cavity length, L is the total cavity length, dν is the change in frequency and ν is laser frequency.

$$L = n_a l_a + n_g l_g + n_d l_d \tag{3.46}$$

Here n_a is an air refractive index, l_a is the cavity length in air, n_g refractive index of the glass window, l_g is window thickness, n_d is the refractive index of liquid and l_d is the dye cell width.

$$\mathrm{L} = 1 \times 45 + 1.5 \times 4 + 1.33 \times 1 = 52.33 \text{ mm} \tag{3.47}$$

The cavity free spectral range is

$$\frac{c}{2L} = \frac{3 \times 10^{8}}{52.33 \times 10^{-3}} = 2.87 \text{ GHz} \tag{3.48}$$

For given $\nu = 5.26 \times 10^{14}$ Hz (at λ~570 nm) and L = 52.33×10^{-3} m full tuning range with 8 μm PZT at the end mirror

$$d\nu = \frac{8 \times 10^{-6} \times 5.26 \times 10^{14}}{52.33 \times 10^{-3}} = 80.41 \text{ GHz} \tag{3.49}$$

The minimum resolution achieved with 14-bit input signal to the PZT driver is 8×10^{-10} m, that corresponds to tuning range by this length is

$$\frac{8 \times 10^{-10} \times 5.26 \times 10^{14}}{52.33 \times 10^{-3}} = 8 \text{ MHz} \tag{3.50}$$

For dν = 6 MHz,

$$dL = \frac{6 \times 10^{6} \times 52.33 \times 10^{-3}}{5.26 \times 10^{14}} = 0.597 \text{ nm} \tag{3.51}$$

The change in cavity length required to compensate for the 6 MHz change in the SLM dye laser frequency is 0.6 nm. The angular resolution achieved by various methods has been tabulated in a table 3.1.

3.7 Opto-Mechanical Mounts

The system performance depends on the precision of the optics, their mounts and their positioning accuracy [3.6]. The parameters that determine the performance of the mounts are adjustment range, resolution, repeatability, orthogonality of the motion, stability and thermal drifts. The tuning mirror, grating and end mirror mounts are specially designed for θ_x and θ_y plane adjustment of mounts. These two adjustments are independent. A flexure base design has a minimal cross axis coupling between the X and Y, where the cross axis coupling refers to any motion along the Y direction in response to an actuation along the X direction and vice versa. A notch is provided in a U-plate, which acts like a centerline for the plane adjustment. The notch works as a hinge axis, which defines the angle of the plane of rotation. One arm of the U plate is clamped to a fixed plate while the transmission arm is rotated with the help of wedge mechanism with respect to the clamped arm. The two U-plates with notch are clamped orthogonally to each other allowing tip / tilt motion that is constrained in all other dimensions. The actuation flexure is physically one piece of stainless steel that has been cut using electro discharge machining (EDM). These types of mounts are compact and offer exceptional mechanical and thermal stability. The wedge mechanism is implemented for precise movement in both planes in all the opto-mechanical mounts. With the help of the wedge mechanism, the planes of the tuning mirror, the grating and the end mirror are aligned to the optical axis of SLM dye laser resonator cavity. This arrangement provides maximum $\pm 2^0$ of angular (tip / tilt) adjustment in each opto mechanical mount. The mounting scheme must support the optics, while providing adequate safety margins for the stresses developed in the optics due to mounting [3.7]. Hence, each optical element is fixed onto the stainless steel casing and the casing is fixed on the respective mounts. A locking screw ensures no unintentional movement of the optics.

3.8 SLM Dye Laser Assembly

The final SLM assembly is mounted on three numbers of studs welded to the stainless steel base plate. The base plate is clamped onto the vertical wall, which is a monolithic concrete structure along with the vibration isolated floor. The assembly is self balanced by a proper distribution of mass of different components around the axis of rotation, which minimizes the torque requirement by the stepper motor. The SLM assembly with worm and wheel tuning mechanism is shown in figure 3.8. The figure 3.9 shows the SLM dye laser mounted on the vertical wall is being pumped by the green beam of CVL.

3.9 SLM Dye Laser Control Unit

The objective is to design a rugged and reliable control system for the remote operation of tunable dye laser by the stepper motor, PZT’s etc. The closed loop control system controls the disturbances that could destabilize the SLM dye laser wavelength. The disturbances present in the SLM dye laser output and their dynamic responses are discussed in Chapter – VII of this thesis.

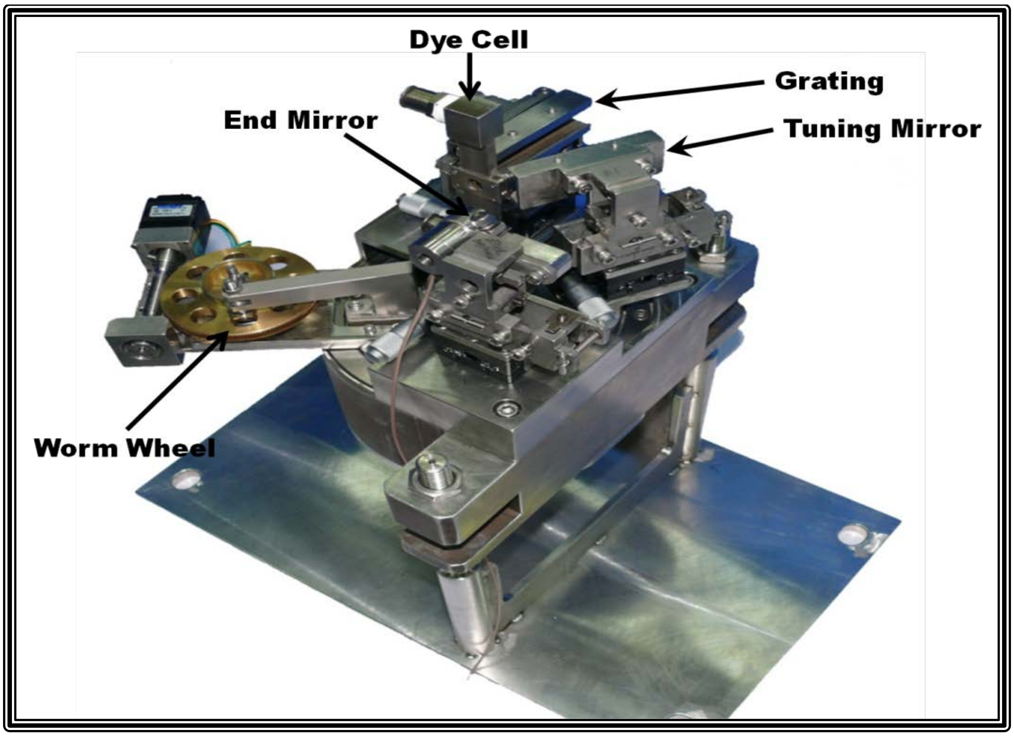

Fig.3.8**:** SLM Assembly with opto mechanical mounts

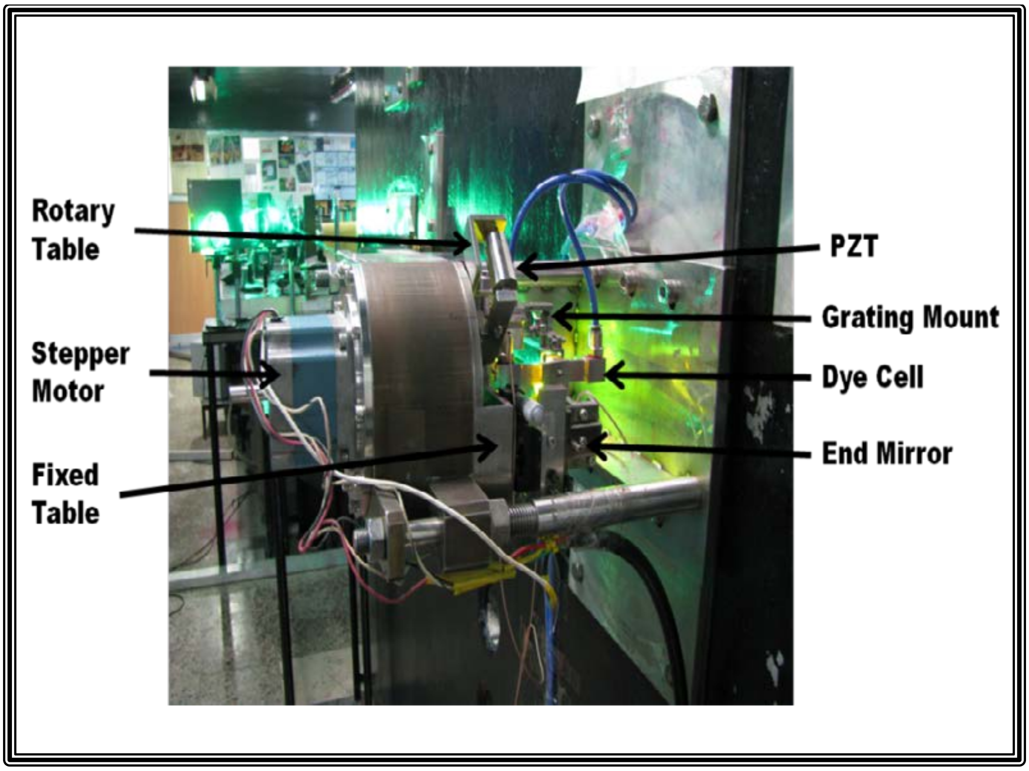

Fig 3.9: SLM dye laser assembly mounted on a vertical wall

Table 3.1: Tuning Range Obtained for SLM Dye Laser by Various Components

S. No.	Tuning Device	Minimum Displacement	Maximum Displacement	Minimum Tuning Step	Maximum Tuning Range
1.	Stepper Motor (50,000 micro steps)	25.92 arc sec	20^{O}	44.93 GHz	10^6 GHz
2.	End Mirror PZT	0.8 nm with 14 bit Input signal	8 µm	8 MHz	80.41 GHz
3.	Tuning Mirror PZT	2 nm with 14 bit Input signal	20 µm	7.14 MHz	71.54 GHz
4.	Tuning Mirror PZT	8 nm with 14 bit input signal	80 µm	28.56 MHz	286.17 GHz
5.	Cascaded PZT at Tuning Mirror	10 nm with 14 bit input signal	100 µm	7.14 MHz	357.72 GHz
6.	Motorized Micrometer	0.3 µm 0.6875 arc sec	10×10^{-3} m	2.45 GHz	3.6×10^4 GHz
7.	Stepper Motor and wedge at 80 mm arm length	1.744 nm with 50,000 micro steps	20×10^{-3} m	6 MHz	7.2×10^4 GHz
8.	Tuning with Worm Wheal gear reduction 1:120	0.5 nm with 50,000 micro steps	3×10^{-3} m	1.7 MHz	1.08×10^4 GHz

The control system is necessary to establish the remote operation of SLM dye laser in closed loop control. The automated operation reduces the need for a highly skilled operator. The automated control system has an inbuilt embedded intelligence with all necessary functionality and interlocks, considering all the system constraints which will guarantee safe and reliable operation. The control panel for the remotely tunable SLM dye laser is shown in figure 3.10. The remote operation requires user interactive GUI and rugged control system. The SLM dye laser can be tuned to an absolute wavelength using coarse tuning by a stepper motor and fine tuning by PZT actuators, resolution of 45 pm with coarse of 7.14 fm with fine control. The detail characterization of this SLM dye laser is discussed at length in Chapter – V of this thesis.

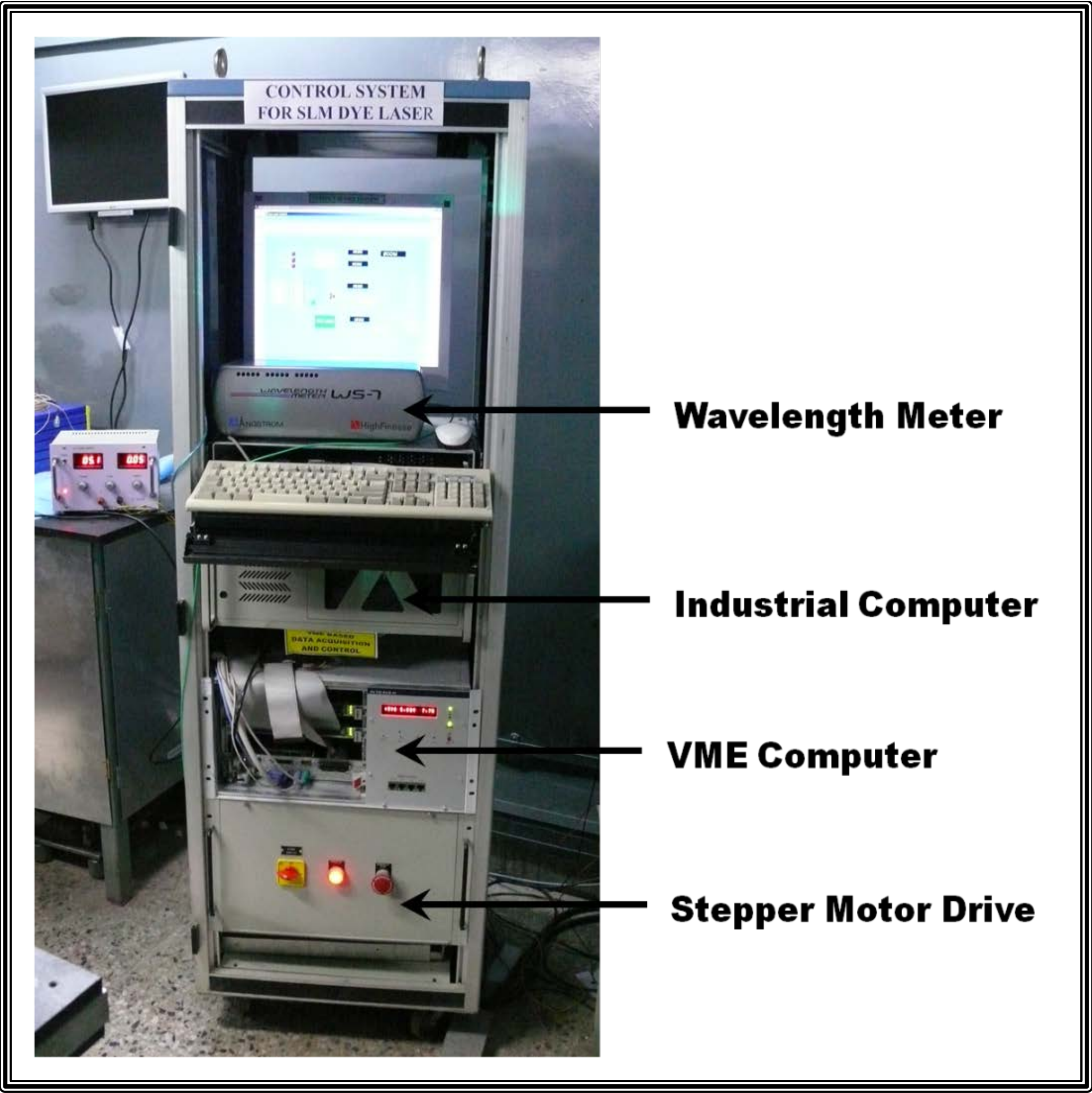

Fig 3.10: VME control panel for SLM dye laser.

3.10 Conclusions

The short cavity GIG SLM dye laser has been designed and fabricated. A precision differential rotary movement with micro stepping of 50,000 steps per revolution was used for the first time for tuning the SLM dye laser, which can generate angular displacement of a few milli arc sec. This angular displacement provides a tuning resolution of a few MHz per step to the SLM dye laser. The pivot point for the mode hop free tuning of the SLM dye laser is located at the center of the rotary table and the planes of the three optical components: grating, tuning mirror and end mirror intersect at this point. The opto mechanical mounts of these three components are fixed on the linear motion tables for precisely locating the pivot point. Four types of actuators, namely, PZT of different stroke lengths, motorized actuator, stepper motor with wedge, worm wheel and hybrid mechanism, a cascade of PZT and motorized actuator have been successfully implemented for fine tuning of the SLM dye laser. The PZT has been found to be the best choice for dynamic control of the SLM dye laser over ~ 12 cm^{-1}. The flexure based opto mechanical mounts for grating, tuning mirror and end mirror have been implemented to obtain the required angular displacement, repeatability, orthogonality of motion, stability and uniform thermal drifts. A VME based control system has been implemented for controlling the stepper motors and PZT's attached to the tuning assembly of the SLM dye laser.

References

[3.1] P McNicholl, H J Metcalf, "Synchronous cavity mode feedback wavelength scanning in dye laser oscillators with gratings", Appl., Opt., 24, 2757 – 2761,1985.

[3.2] S A Kostritsa, V A Mishin, "Narrow band tunable pulsed dye laser for isotope separation", Quantum Electronics, 24, 464 – 466, 1994.

[3.3] M L Iles, "Unified single pass model of linewidths in a Hansch single and double grating grazing incidence dye lasers", App Opt., 20, 985 – 988,1981.

[3.4] F J Duarte, "Cavity dispersion equation$\Delta\lambda \approx \Delta\theta \left(\frac{\partial\theta}{\partial\lambda}\right)^{-1}$: a note on its origin, App. Opt., 31, 6979 – 6982, 1992.

[3.5] J K Robertson, "Introduction to Optics: Geometrical and Physical", Van Nostrand New York 1955.

[3.6] P Griffith, D Silberman, “Optical Mounts: Ignore Them at your Peril”, Photonics Spectra September 1998.

[3.7] J Fitzsimmons, D Erickson, A Hill, R Bartos, J K Wallace, “Design and analysis of flexure mounts for precision optics”, Proc. of SPIE, 7018, 70181K-1- 8, 2008.

Chapter – IV

DESIGN AND DEVELOPMENT OF DYE FLOW CELL FOR SLM

4.1 Introduction

In this chapter several conceptual dye cell geometry designs are discussed. CFD modeling as well as flow visualization studies are reported for selected designs.

Several dye cell geometries such as converging, diverging, straight, trapezoidal, parallelogram, rectangular and cell with convex inner surfaces have been extensively used to achieve high flow velocities in the dye active region [4.1 – 4.7]. The dye cell design has to be such that the flow channel in the dye laser reduces the thermal and pressure variations in the flowing dye solution particularly in the vicinity of the active volume. To some extent the power and repetition rate can be augmented by increasing the flow velocity of the dye solution in the flow channel. Excessive self-heating due to wall friction, disturbances to the streamline, eddies due to the turbulence, local cavitation in the dye solvent are some of the limiting conditions of increasing the flow velocity for a high repetition rate laser. A judicious design of the dye cell flow channel and appropriate selection of active volume will help to solve the problems related to dye flow.

A more serious problem for a SLM dye laser is the instantaneous flow velocity and pump power fluctuations. As the pump pulse energy absorbed by the dye medium degrade the optical quality of the flowing dye, it is imperative that every pump pulse must see a fresh dye volume. The high repetition rate operation demands relatively high flow velocity in the dye cell. A well known consequence of the continuity equation is that, the reduction in the cross section area results in higher flow velocities; increase in velocity is always at the expense of the static pressure. The increase in the flow velocity in a constricted channel causes turbulence to set in the dye solution flow. Such turbulences lead to non-uniformity in the dye refractive index [4.8], resulting in a change in the optical path length of the cavity. It is important to eliminate the turbulence by design and ensure high optical quality laminar flow. The imbalance between the heating rate and cooling rate of the active volume is primarily responsible for temperature fluctuations in the dye lasers. The heating is caused primarily by the radiation less transitions in the dye molecules, while the cooling is achieved predominantly by heat transfer from the dye solution to the walls, as well as replacement of the volume. It is reported in the literature that high flow velocities in the dye cell can suppress the thermal effects in the dye laser [1.2, 4.1, 4.2, 4.9, 4.10]. High flow velocities may generate local flow induced vibrations which are difficult to eliminate. The flow velocity allows several active volume clearances between pump pulses. Operation at high repetition rate demands a high average flow velocity. The maximum dye flow velocity is limited by cavitations, which destroy the optical homogeneity of the dye medium.

In case of narrow linewidth dye lasers, it is advantageous to utilize the dye cell where its windows are tilted at an angle relative to the optic axis. The wedge type geometry is quite effective in reducing parasitic oscillation in the dye cell. The antireflection coatings are used to diminish the unwanted parasitic oscillations. Roncin and Dammay have designed demountable trapezoidal dye cell to avoid such unnecessary effects [4.5]. Duarte and Piper had used trapezoidal dye cell cross section area of 11 mm x 1 mm with the end window tilted at ~ 77.7^{O} to the long (optic) axis. An alternative to the trapezoidal dye cells parallelogram and rectangular dye cells oriented at an angle to the plane formed by the cavity axis could be used [1.29].

4.2 Fluid Flow

The fluid can flow through a channel as a laminar or a turbulent flow. In a laminar flow there is no lateral mixing, thus all fluid elements keep their position relative to the cross section of the flow channel, the viscosity effects are more dominant than the inertial effects. The fluid in contact with the surface at the boundary is stationary, but all the other layers slide over each other. At higher flow velocities, turbulence appears and vortices form which leads to lateral mixing. In a turbulent flow, the velocity of the fluid particles at a point continuously undergoes change in both magnitude and direction. Between laminar and turbulent flow regimes there is also a transitional regime with turbulence in the center of the region and laminar near the boundaries. The velocity profile between the two flow boundaries of a channel is parabolic in shape for laminar flow. Figure 4.1 shows the velocity profile of laminar and turbulent flow in a circular pipe. The critical velocity where laminar flow changes to turbulent flow depends on four parameters; the hydraulic diameter of the flow channel, viscosity, density and average linear flow velocity of the fluid. The combination of these four quantities provides the dimensionless Reynolds number given by

$$R_e = \frac{\rho v D}{\mu} \tag{4.1}$$

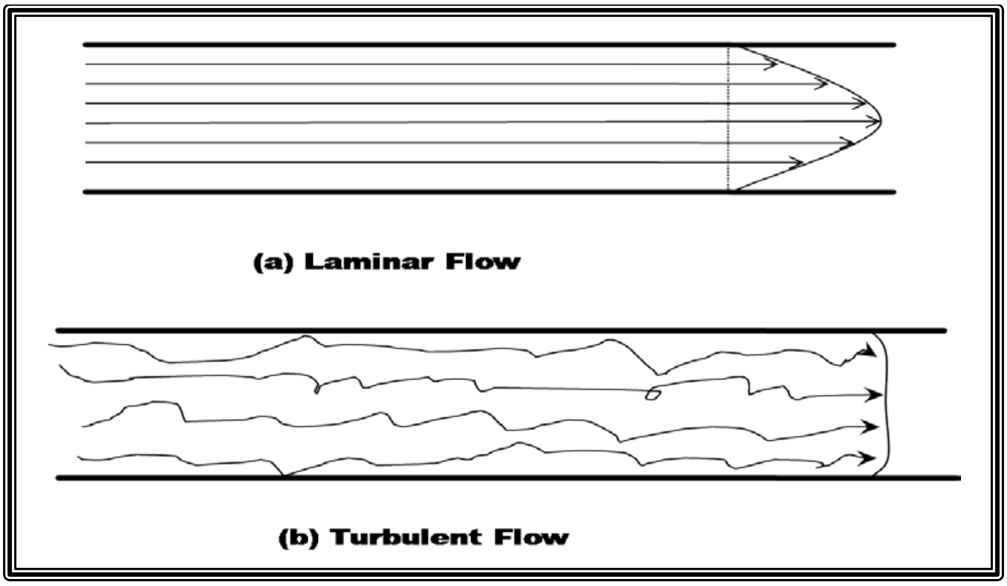

Fig 4.1: Velocity profile of a laminar and a turbulent flow in a pipe

where D is the hydraulic diameter, v is the average velocity of the fluid, ρ is the density of the fluid and μ is the viscosity of the fluid. The Reynolds number can be used for identifying the fluid flow velocity either in laminar or turbulent region. In a pipe flow, if the Reynolds number is below 2100, the flow is laminar. The Reynolds number is above 4000 for turbulent flow. The Reynolds number in between 2100 to 4000 is said to be in the transitional zone [1.5, 4.11 – 4.14].

4.2.1 Boundary Layers

A boundary layer is defined as that part of a moving fluid in which the fluid motion is influenced by the presence of a solid boundary due to the viscosity of the fluid and adhesion of fluid at the surface. If the fluid layer does not adhere, the velocity should be free stream velocity U_∞ everywhere in the flowing fluid. However, most fluids exhibit no slip condition at the surface, that is, the fluid velocity at the solid-fluid interface is zero and the velocities close to the solid surface are small. In the boundary layer, velocity gradients are large enough to produce significant viscous stresses and dissipation of mechanical energy. Outside the viscous boundary layer, in the free stream, velocity gradients and viscous stresses are negligible. The fluid velocity varies from zero at the wall to a velocity almost equal to that of the free stream (99% of U_∞) [4.15]. In a closed channel, boundary layer extends to the center of the flow channel. At the onset of the turbulence, a turbulent boundary layer is formed, which consists of three zones: the flow in the boundary layer very near the surface, the viscous sub layer is essentially laminar; the zone between fully developed turbulence in the turbulence zone and the region of viscous sub layer is a transition zone called the buffer layer. For flow in a pipe or duct the boundary layers will eventually meet at the center and at this point they cannot grow further. The velocity profile reaches an asymptotic state where the flow is said to be fully developed. The effects of viscous friction are then felt over the whole cross section of the tube. The length of the entrance region of the pipe necessary for the fully developed flow to be established, is called the transition length [4.13 – 4.15].

The boundary layer thickness for laminar and turbulent boundary layer can be approximately estimated [4.13 – 4.15].

Laminar boundary layer $$\frac{\delta}{x} \sim \frac{5}{\sqrt{Re_x}} \qquad (4.2)$$

Turbulent boundary layer $$\frac{\delta}{x} \sim \frac{0.16}{(Re_x)^{1/7}} \qquad (4.3)$$

Flow Induced Vibration

The fluid induced vibration can originate from a number of system conditions such as

- High turbulence
- Pressure pulsation
- Cavitation

The high turbulence can excite the vibrations. An inherent feature of the turbulent flow is a random pulsation of pressure. This process generates a broad spectrum of frequencies, which rise with increasing fluid velocity. The formation and shedding of eddies in places where fluid is forced to change flow direction abruptly causes additional pressure pulsations. The broad spectrum of frequencies generated by a turbulent flow increases the risk of resonance.

Pressure pulsation originates from the operation of fluid handling equipment like pumps. In the gear pump, the pressure of the liquid delivered by the pump pulsates at the frequency at which teeth of the gear pump pass through the pump discharge. Thus, this frequency depends on the number of gear teeth and rotational speed (RPM). If one of the natural frequencies of the components in the flow system is close to a frequency of the flow induced vibration, resonance may increase vibration amplitudes to an unacceptable level.

4.2.2 Cavitation

Cavitation is a term to describe the process, which includes nucleation, growth and implosion of vapour filled cavities and is important in fluids, which have significant vapour pressure. Cavitation takes place in the dye cell when the static pressure of the liquid falls below the vapor pressure of the liquid at a given temperature. When the pressure in the liquid is reduced vapor bubbles appear. The vapour bubbles grow till low pressure occurs. Later, the pressure in the flow channel rises due to decrease in average velocity; the cavities repeatedly collapse leading to local high pressure and cause sonic waves. The degree of cavitation can be determined by a dimensionless parameter typically known as cavitation number K

$$K = 2\frac{(P_d - P_v)}{\rho v^2} \tag{4.4}$$

where P_d is the pressure, P_v vapor pressure, ρ density and v bulk velocity

The numerator in the above equation corresponds to the static pressure, which resists the cavitations while the denominator corresponds to the dynamic pressure, which promotes cavitations. Hence the reduction in the local pressure inside the dye cell should be limited to the vapor pressure of the solvent. Because of sudden changes in flow conditions, local heating and lower surface energy can also cause the generation of cavitation (vapour bubble) in the flow. The cavitations result in vibrations as well as noise, which cause short term frequency fluctuations [4.15]. The formation of vapour bubbles (cavitation) contributes to damage of the dye cell windows in several ways.

- The bubble harshly affects the heat transfer at the solid-liquid interface from the quartz window to flowing dye solvent.

- The bubble degrades the optical quality of the lasing cavity and increases the possibility of scattering for pumping and lasing radiations.

The flow geometry, the operating pressure and the pressure drop, the solvent properties are chosen judiciously to eliminate cavitation.

4.3 Flow Requirement for SLM Dye Laser

Ideally, the liquid exposed to the pump beam should be replenished in the dye cell before the arrival of the next pulse, so that the gain medium is fresh. It is important to minimize thermal induced refractive index gradient in the dye cell to achieve high beam quality of the dye laser. The pump beam energy absorbed in the dye medium, at least one fourth of the energy results in heating of the dye solvent. The temperature gradient due to heating produces a refractive index gradient ($\frac{dn}{dt}$), which results in a deflection of the dye laser beam. The value of $\frac{dn}{dt}$ depends on the thermo optical properties of the solvent. The pump beam does not get absorbed uniformly throughout the dye cell due to Beer Lambert exponential law. The cell width and dye concentration determine the energy deposition in the dye solvent. The flow rate is sufficient to flush out the optically pumped dye solution volume after each pump pulse. The velocity profile again is not uniform in the dye cell. A boundary layer of very slow moving dye solution exists at the window surface. The velocity must be sufficiently high to remove the slow moving layer, where the laser beam intensity would be the maximum. Thus,

$$v_g > \frac{V}{T_1} \tag{4.5}$$

where v_g is the average volume flow rate, V is the cell volume being optically pumped and T_1 is the repetition period. The number of cell volumes replaced per pump pulse is recommended to be two or more for eliminating the thermal effects.

Optical damage to the dye cell windows occurs in most dye lasers at some point because the intensities of the lasing beam and pump beam intensities are generally very close to the damage threshold of the dye cell windows. The damage threshold depends on window material, surface quality, cleanliness of the window, heat transfer, flow conditions and laser power density. In practice, for a given pump power density liquid-solid interface suffer higher damage at much lower power densities than vapor solid interfaces. One of the important causes of damage at lower power densities is the deposition of photo degraded products on the dye cell windows. The dye cell windows are not merely passive surfaces that collect the photo degraded products, but they also actively participate in the photochemical reactions. The thermal conductivity of the dye cell windows may also play an important role in the damage mechanisms by affecting the local heat transfer. The normally used quartz has less thermal conductivity than magnesium fluoride. It has been observed that the damage threshold of the quartz windows shows major improvement, when the solvent used is Dioxane. However, it should be remembered that the photochemical stability is generally poor under higher power densities.

To avoid extensive time consuming experimental studies it was decided to study the dye cell design suitable for high repetition rate SLM pulsed dye laser, through computational modeling, in a general purpose computational fluid dynamics (CFD) software. The rectangular dye cell geometry was chosen for the study of single mode dye laser.

4.4 Computational Fluid Dynamics (CFD)

CFD is a powerful tool used for the prediction and analysis of fluid flow. It is able to offer three dimensional, time dependent and fairly accurate solutions to the highly coupled differential equations that govern fluid flow in a domain and help conduct computational experiments. Thus a large number of designs can be tested rapidly without spending any time or money for tedious experimental investigations.

4.4.1 Overview of CFD Study and the Software

The main aspects of numerical modeling performed within the scope of this thesis are presented here for a general physical and mathematical understanding of the simulations used. The CFD code contains discretisation techniques suitable for the treatment of the key transport phenomena, convection and diffusion as well as the source terms and the rate of change with respect to time. The underlying phenomena are complex and non-linear, so an iterative solution approach is required. Following steps are taken to use the CFD package to carry out the analysis on hand [4.16].

A control space is defined where the equations are to be solved. A geometrical model is built using Solid Works [4.16], pre-processing the model to generate the grid; each grid point is given an initial value chosen by the user. The grid generation for the dye cell flow domain was carried out with ANSYS ICEM CFD and ANSYS CFX [4.16]. One of the important factors when it comes to obtaining convergence when performing CFD simulations is the use of good quality mesh. Quality of hexahedral mesh in ICEM is calculated as the relative determinant of each cell. The relative determinant is the ratio of the smallest determinant of the Jacobian matrix divided by the largest. A determinant value of one would indicate a perfect regular mesh element; zero would indicate one or more degenerate edges and minus one would indicate completely inverted elements. The other aspects that should be considered for the quality of the mesh are aspect ratio, the skewness and the internal angles for the element. The better this guessed starting point is the faster a solution is reached.

Boundary conditions are specified for the flow domains at the walls, inlets, outlets and openings. These are known values of velocity, mass flow, heat load etc, at the inlet, outlet and the walls.

Next is to set the time steps and selecting numerical sub-models. The domain is split up into a number of cells (control volumes around a grid point) known as meshing. The mesh does not necessarily have to have the same density in the entire domain. The equations are discretised in the centre of the computational cells. This means that the partial differentials are translated into equations with coefficients that form a matrix. The algorithm in the solver solves this matrix.

Monitoring the iterative solution process

For each cell of the mesh the governing equations of mass, momentum and energy are solved together with the model related equations, before the computation moves on to the next cell. When the calculation is finished for all the cells, one iteration step is finished. The results are compared to the solution of the previous step. If the difference between the two solutions is larger than the specified accuracy, calculation for all cells is repeated, starting from the last solution as the start condition.

Analyzing the solution obtained

The results can be organized, displayed and analyzed by post processing tools. Most of them work with graphical user interface.

The main elements of the CFD code are shown in figure 4.2. It contains three main elements.

i. A pre-processor
ii. A Solver
iii. A Post Processor

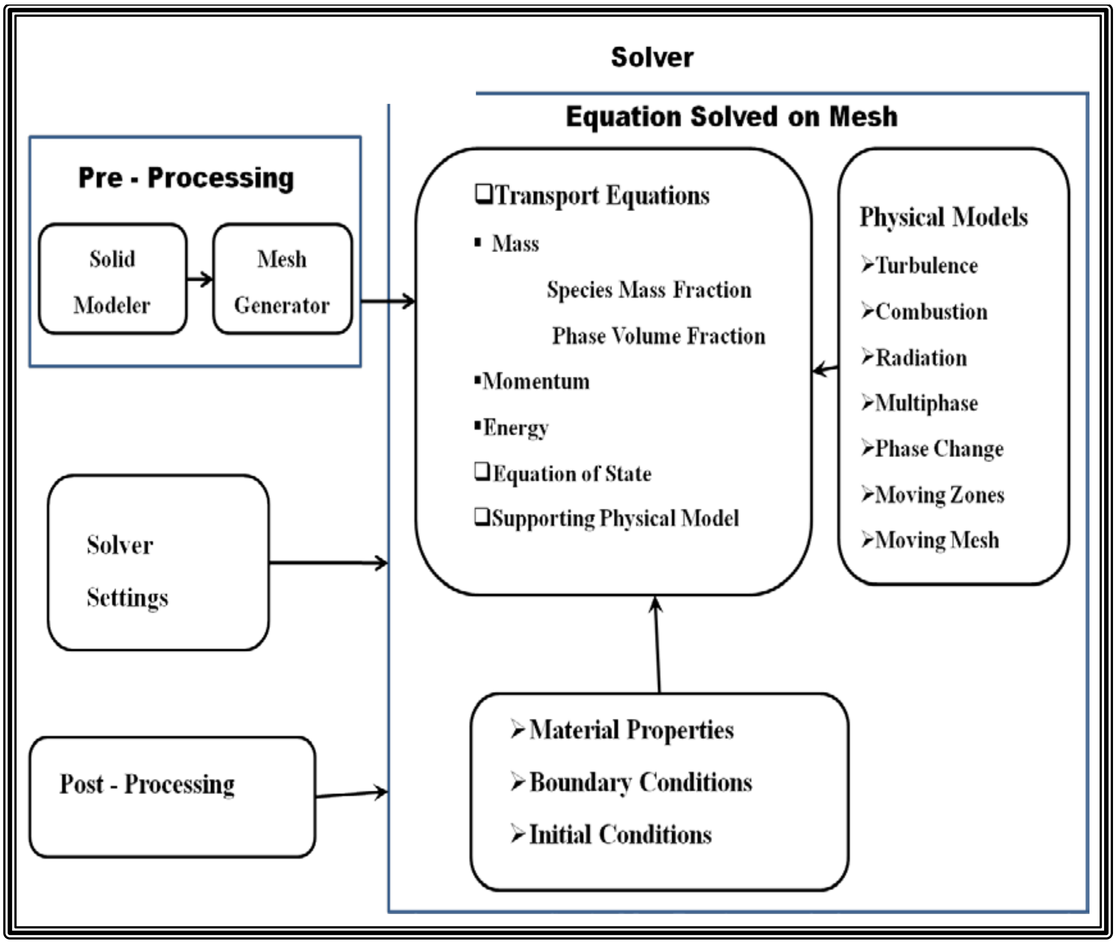

Fig 4.2: Computational Fluid Dynamics (CFD) main components

4.4.2 Pre-processor

The pre-processor consists of the flow problem to a CFD program by means of an operator friendly interface and the subsequent transformation of this input into a form suitable for use by the solver. The steps involved in the pre-processor stages are definition of flow geometry or computational domain, grid generation, selection of physical and chemical phenomena, defining fluid properties and specifying boundary conditions [4.15].

4.4.3 Solver

ANSYS CFX is a finite volume method code. The approach involves discretising the flow domain into finite control volumes using ANSYS ICEM CFD mesh.

4.4.4 Selection of Physical Sub Model

The fluid flow equations solved in a general purpose CFD code are not the exact governing Navier Stokes equations. This is because the exact equations either cannot be solved for physical flows of interest as is the case with turbulent flow or because the exact governing equations are not completely known. Hence simplified physical sub models are employed. They consist of a set of approximate equations in part derived from empiricism and physical reasoning. One has to select the proper sub model for turbulence to be implemented in the simulation.

4.5 Turbulence Models

It is very crucial that the user must have a good understanding of the physical mechanism of some of the turbulence sub-model as well as good knowledge of the limitations of the sub model. The turbulent flow contains a wide range of length and time scales. For fluid flow, the scales are dependent on characteristics of flow and the flow dimensions. Several approaches for turbulence modeling have been proposed. They are broadly classified into three categories.

Direct Numerical Simulation (DNS)

All the turbulent motions are resolved by solving directly the Navier Stokes equations that govern fluid flow without additional modeling. This approach requires a very large number of grid cells and thus requires large computational resources for practical applications.

Large Eddy Simulation (LES)

Although, this approach allows employing fewer grid cells than DNS but still impractical for complex flow geometries. In this model, the smallest turbulent motion is resolved by Navier Stokes equations. The finest eddies are either ignored or modeled.

Reynolds Averaged Navier Stokes Model (RANS)

The Navier Stokes equations are time averaged and thus the equations so obtained do not aim to resolve the turbulent motions, but to provide the time averaged characteristics of flow quantities. Since, the RANS model is not trying to resolve the turbulent motions, the grid needs only to be fine enough to capture the important time average feature of the fluid flow.

4.6 The Two Equation Model

Two equation models are the most commonly used models for turbulence and engineering problems. They introduce two new transport equations that represent the turbulent properties of a flow, like convection and diffusion of turbulent energy. The most common transport variables are the turbulent kinetic energy and either the turbulent dissipation or the turbulent specific dissipation. The turbulence dissipation determines the length or time scales of the turbulence. The velocity scale is often modeled using an extra transport equation for the turbulent kinetic energy, given by

$$k_1 = \frac{1}{2}\,\overline{u'^2} \tag{4.6}$$

where u' represent the turbulent velocity fluctuations. The length scale is calculated as a function of the turbulent kinetic energy dissipation (ϵ) or the turbulent kinetic frequency (ω).

4.6.1 The k-ϵ Model

The k-ϵ model assumes that the eddy viscosity is related to the turbulent kinetic energy and turbulence dissipation rate according to relation

$$\mu_t = C_\mu \rho \frac{k_1^2}{\epsilon} \tag{4.7}$$

The values of the turbulent kinetic energy and the eddy dissipation come directly from their differential transport equations respectively

$$\rho \frac{Dk}{Dt} = \nabla.\left[\left(\mu + \frac{\mu_t}{\sigma_k}\right)\nabla k\right] + P_k - \rho\epsilon \tag{4.8}$$

$$\rho \frac{D\epsilon}{Dt} = \nabla.\left[\left(\mu + \frac{\mu_t}{\sigma_\epsilon}\right)\nabla \epsilon\right] + \frac{\epsilon}{k}\left(C_{\epsilon 1} P_k - C_{\epsilon 2}\rho\epsilon\right) \tag{4.9}$$

where $C_{\epsilon 1}$, $C_{\epsilon 2}$, σ_k and σ_ϵ are constants P_k is the turbulence production due to viscous and buoyancy forces.

The main drawback of this model is a poor prediction of the flow behavior in the case of non-equilibrium boundary layers. The reattachment point during separation flow calculation is usually under predicted. Errors occur in the magnitude of the local heat transfer and as a consequence, the overall device performances are solved incorrectly [4.14, 4.15, 4.17].

4.6.2 The k-ω Model

The k-ω model was developed in order to improve the predictions in the near wall region and reduce the errors in adverse pressure gradient calculations. In order to define the turbulent eddy viscosity, the k-ω model uses a frequency scale (ω) called also specific turbulent dissipation rate.

$$\mu_t = \rho \frac{k_1}{\omega} \tag{4.10}$$

In this model instead of eddy dissipation a turbulent eddy frequency (ω), which is related to the length scale, is used for the formulation of equations.

$$l = \frac{{k_1}^{1/2}}{\omega} \tag{4.11}$$

instead of the formulation used for the k – ϵ model

$$l = \frac{{k_1}^{3/2}}{\epsilon} \tag{4.12}$$

So the turbulent kinetic energy equation is written

$$\rho \frac{Dk}{Dt} = \nabla.\left[\left(\mu + \frac{\mu_t}{\sigma_k}\right)\nabla k_1\right] + P_k - \beta' \rho k_1 \omega \tag{4.13}$$

And the equation for the eddy dissipation rate ω is written

$$\frac{D\omega}{Dt} = \nabla.\left[\left(\mu + \frac{\mu_t}{\sigma_\omega}\right)\nabla \omega\right] + \alpha \frac{\omega}{k} P_k - \beta \rho \omega^2 \tag{4.14}$$

The major advantage of the k – ω model is the robust and simple way the near wall region is handled. Contrary to the k – ϵ model the k – ω model does not involve complex non-linear damping functions to take into account the near wall low Reynolds effects. The main weakness of the k – ω model is the strong sensitivity of the solution to the free stream ω values [4.14, 4.15].

4.6.3 The Shear Stress Turbulence Model

In order to get the best from the k – ϵ and the k – ω models, a new blended model called Shear Stress Turbulence (SST) model is available in the ANSYS CFX. The SST model calculates the flow in the near wall region using a k – ω formulation whereas in the bulk flow the high Reynolds k – ϵ formulation is employed. A smooth transition between the two formulations is ensured by the use of additional blending factors, which are functions of the wall distance. The SST model has good merits for accounting for adverse pressure gradients and separating flow, but tends to produce too large turbulence levels in the stagnation region and regions with strong acceleration. To make the switch between the models, the equations are multiplied with blending functions and the final result for kinetic energy and the eddy dissipation is

$$\rho\frac{Dk}{Dt} = \nabla.\left[\left(\mu + \frac{\mu_t}{\sigma_{k3}}\right)\nabla k_1\right] + P_k - \beta'\rho k_1\omega \qquad (4.15)$$

and

$$\frac{D\omega}{Dt} = \nabla.\left[\left(\mu + \frac{\mu_t}{\sigma_{\omega 3}}\right)\nabla\omega\right] + (1 - F_1)2\rho\frac{1}{\sigma_{\omega 2}\omega}\nabla k_1\nabla\omega + \alpha_3\frac{\omega}{k}P_k - \beta_3\rho\omega^2 \qquad (4.16)$$

As in the k – ω model, the CFX implementation of the SST model permits the automatic shifting from the low Reynolds number formulation to the wall function scheme according to the grid resolution. It is obvious that special attention has to be paid to modeling the near wall region. Near the wall, turbulence is dampened and the velocity decreases to zero as viscous forces start to influence the flow. The SST model is used in this thesis for evaluating the dye cell geometries for single mode operation. [4.14,4.15,4.18, 4.19].

4.7 The Finite Volume Method

ANSYS CFX is a finite volume method – FVM code. The finite volume method was originally developed as special finite difference formulations. Each mesh element is translated into a bonded assembly of finite volumes, each of which has its unique form and address and enclose its appropriate node as shown in figure 4.3. In the finite volume method, the volume integrals in a partial differential form of the governing (momentum, energy, mass) equations that contain divergence terms are converted to surface integrals, using the divergence theorem. These terms are then evaluated as fluxes at the surfaces of each finite volume while ensuring the principle of conservation [4.20, 4.21]. For example, the integral form of the continuity equation for steady incompressible flow is reduced to

$$\int_S \vec{V} . \hat{n} \, dS = 0 \tag{4.17}$$

The integration over the surface S of the control volume and n is the outward normal to the surface. Physically, this equation means that the net volume flow into the control volume is zero. Let us consider a rectangular cell

The velocity at the face I is taken to be $V_i = u_i \, \hat{\imath} + v_i \, \hat{\jmath}$. Applying the mass conservation equation (4.17) to the control volume defined by the given cell

$$-u_1 \, \Delta y - v_2 \Delta y + u_3 \, \Delta y + v_4 \, \Delta y = 0 \tag{4.18}$$

This is the discrete form of the continuity equation for the cell. Hence the cell values at the cell centers are stored. The face values u_1, v_2, etc are obtained by suitably interpolating the cell centre values for adjacent cells. Similarly, one can obtain discrete equations for the conservation of momentum and energy for the cell.

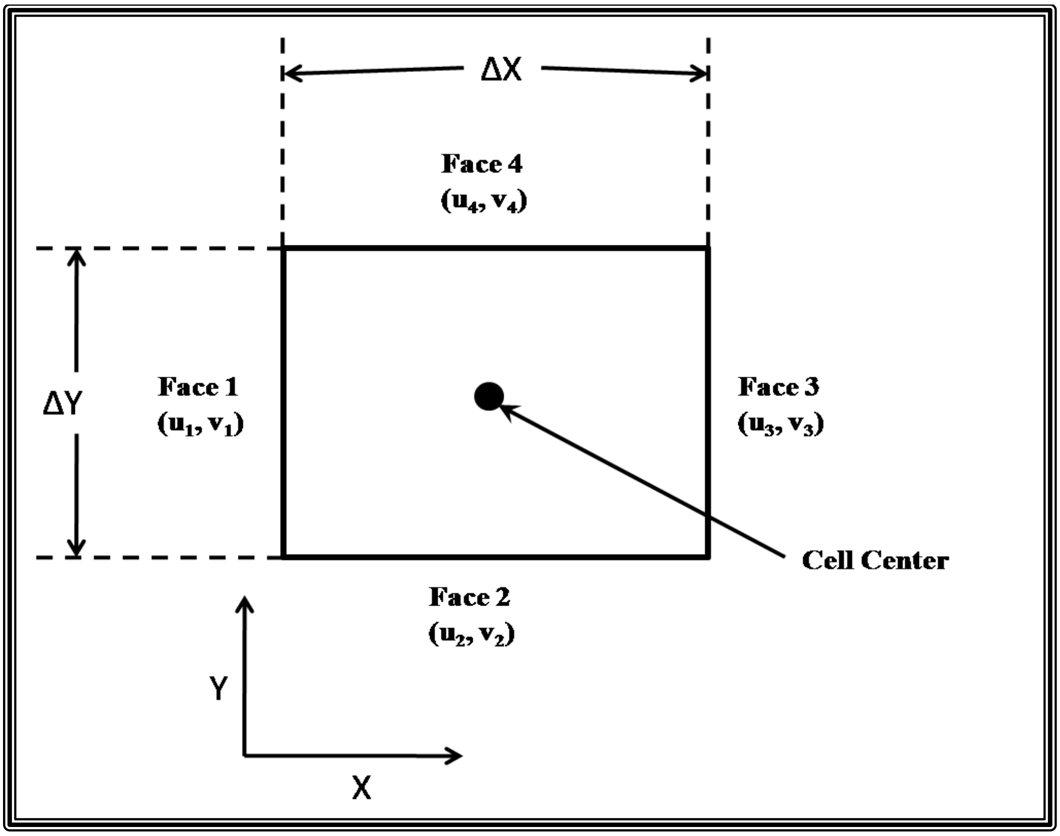

Fig 4.3: Control volume defined by a cell

4.8 Conjugate Heat Transfer

ANSYS CFX allows for incorporation of solid domains and modeling of the liquid – solid interaction within one simulation model. In a solid domain the equation for the conservation of energy is simplified since there is no flow within or in and out of a solid and conduction is essentially the only mode of heat transfer. Fluid and solid domains are coupled in ANSYS CFX via conservative domain interface allowing for momentum and energy transfer across the boundaries [4.22]. The conjugate heat transfer will be presented in this thesis for absorption of pump beam in the dye solution. In which the pump beam energy is deposited in a cylindrical volume. This heat source is treated as exponentially decaying volumetric heat source and will be discussed in detail in chapter – VI of this thesis.

4.9 Convergence Criteria

As the number of grid points increases, the error in the numerical solution would decrease and the agreement between the numerical and exact solutions would get better. When the numerical solutions obtained on different grids agree to within the specified level of tolerance specified, they are referred to as grid converged solutions; convergence becomes independent of the grid as the cell size is reduced. Further, refinement of the grid is carried out for a better agreement between the numerical solution and the exact solution. As the guessed value of u_g tends to u, the linearization and matrix inversion errors tend to zero. The residual R_1 is the RMS value of the difference between the u and u_g on the grid, given by

$$R_1 = \sqrt{\frac{\sum_{i=1}^{N}\left(u_i - u_g\right)^2}{N_1}} \tag{4.18}$$

It is useful to scale this residual with the average value of u in the domain. In a good simulation, both iterative convergence error and truncation error would be of comparable level and less than the tolerance level chosen.

4.10 The Dye Cell Geometries and Flow Analysis

The restriction in flow area by the convex-convex, convex-plane, or plane-plane surfaces increases the flow velocity in the region of active volume [2.29, 4.3 – 4.7, 4.10, 4.23 – 4.27]. As an alternative to the experimental methods, detailed CFD studies were undertaken for several rectangular dye flow channels of cross sectional area ranging from 5 x 1 mm^2 to 20 x 1 mm^2 and cell lengths from 30 mm to 80 mm. The entrance to flow channel was either rectangular or tubular. The fluid entering in a flow channel requires a certain length to develop the velocity profile in the flow channel. This length is known as entry length, depends on the type of flow channel, flow velocity and solvent properties. The entrance of the flow channel was rounded to avoid an initial disturbance to the entering flow stream. A FVM with ANSYS CFX solver of general purpose CFD software was used to visualize the flow velocity vectors in the flow domain. The ANSYS CFX – 12 solved the Navier – Stokes equation for the flow domain, which was uniformly, meshed using ICEM CFD mesh. The mesh element consists of tetrahedral cells and prismatic cells near solid-liquid interface. The SST model was used to solve the k-ω model at the wall and solve k-ϵ model in the bulk flow, where k is the turbulent kinetic energy, ϵ turbulent eddy dissipation and ω turbulent frequency. A blending function ensures a smooth transition between the two models. The quality of meshing has a significant effect on the accuracy of results [4.28 – 4.31]. Theoretically, higher number of mesh elements in the flow geometry provide better accuracy of the results, but the computational time is higher. The grid independent results were obtained by refining the mesh element of flow domain so that with further refinement of the grid the computational result does not change significantly. The grid size near the wall was ~ 25 µm and in the bulk ~ 250 µm. The Intel Pentium Quad Core, 2.8 GHz, 4 GB RAM and 1 TB HDD was used for all runs. A typical solid works flow domain is shown in figure 4.4. The typical mesh for SLM dye laser shell is shown in figure 4.5.

It was observed that the solution obtained from ANSYS ICEM CFD mesh has better convergence than the mesh generated by ANSYS CFX mesh generator. The typical meshes generated by ANSYS CFX and ANSYS ICEM CFD mesh generator are shown in fig 4.6 and fig 4.7 respectively. The convergence time for ANSYS ICEM CFD mesh has almost 50% less than the convergence time for ANSYS CFX mesh for the same geometry, mesh element size and boundary conditions.

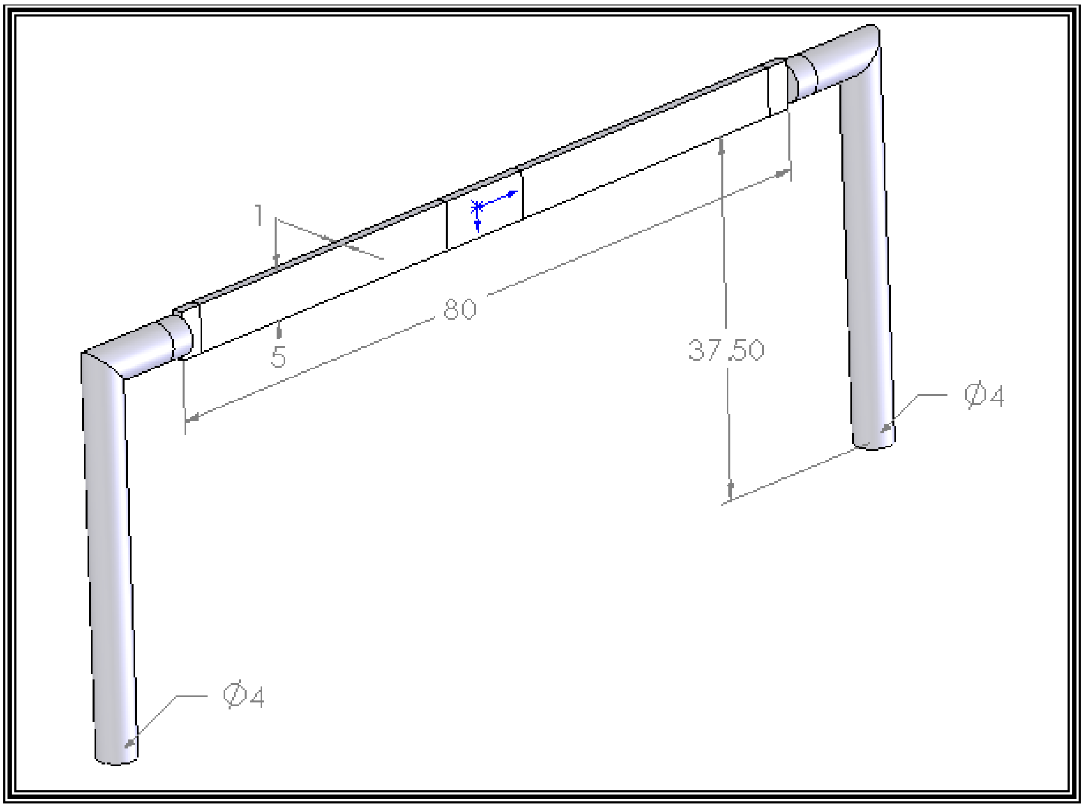

Fig 4.4: Typical SLM dye cell flow geometry with tubular entry.

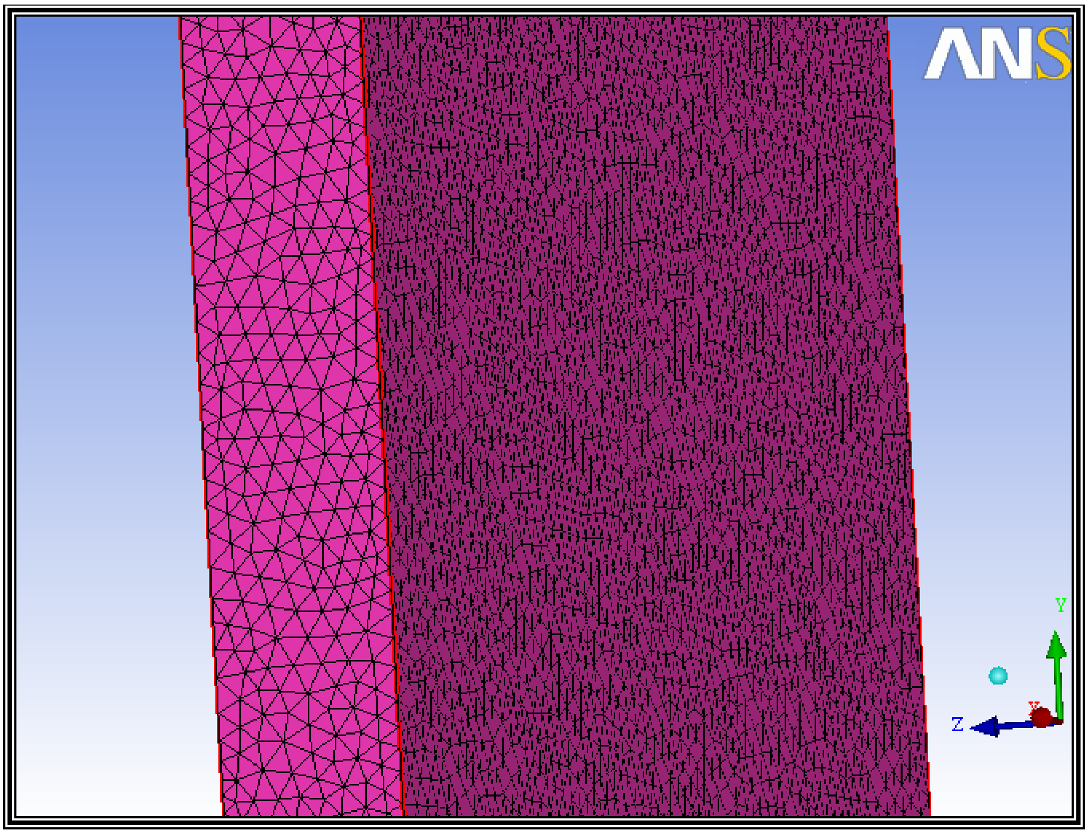

Fig 4.5: Typical unstructured mesh for SLM dye cell with mesh element size of 175 μm.

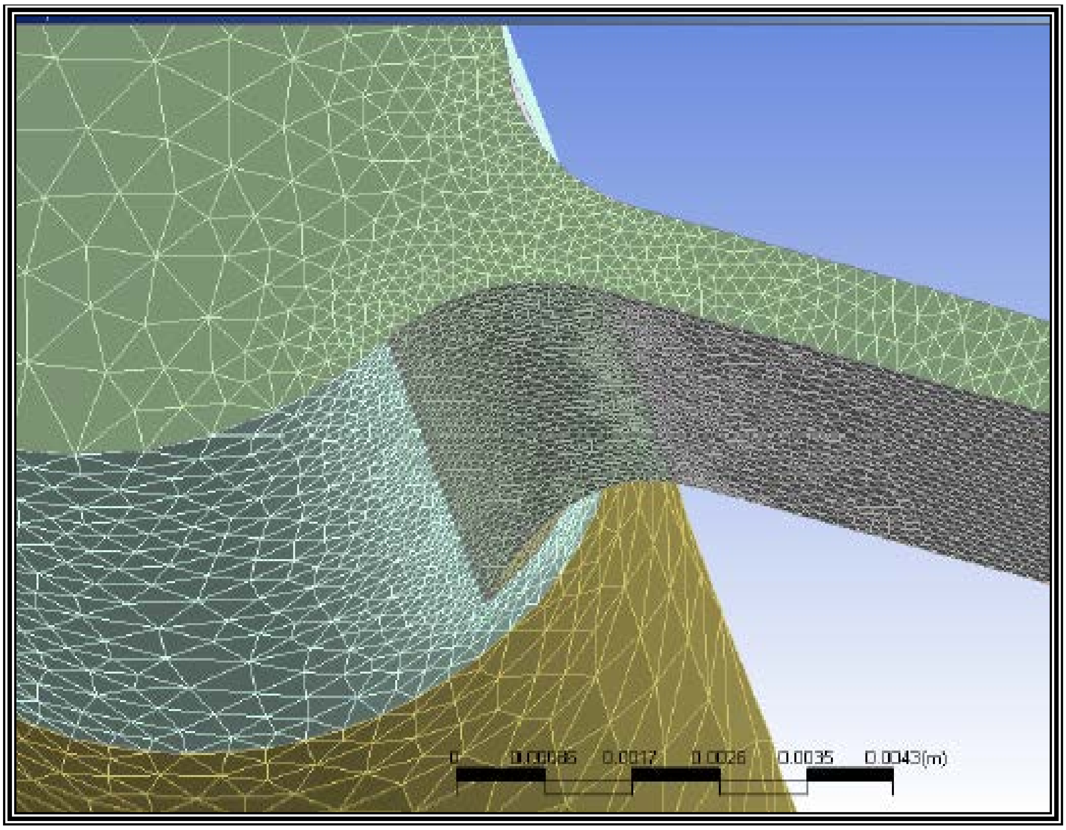

Fig 4.6: Grid generated by ANSYS CFX

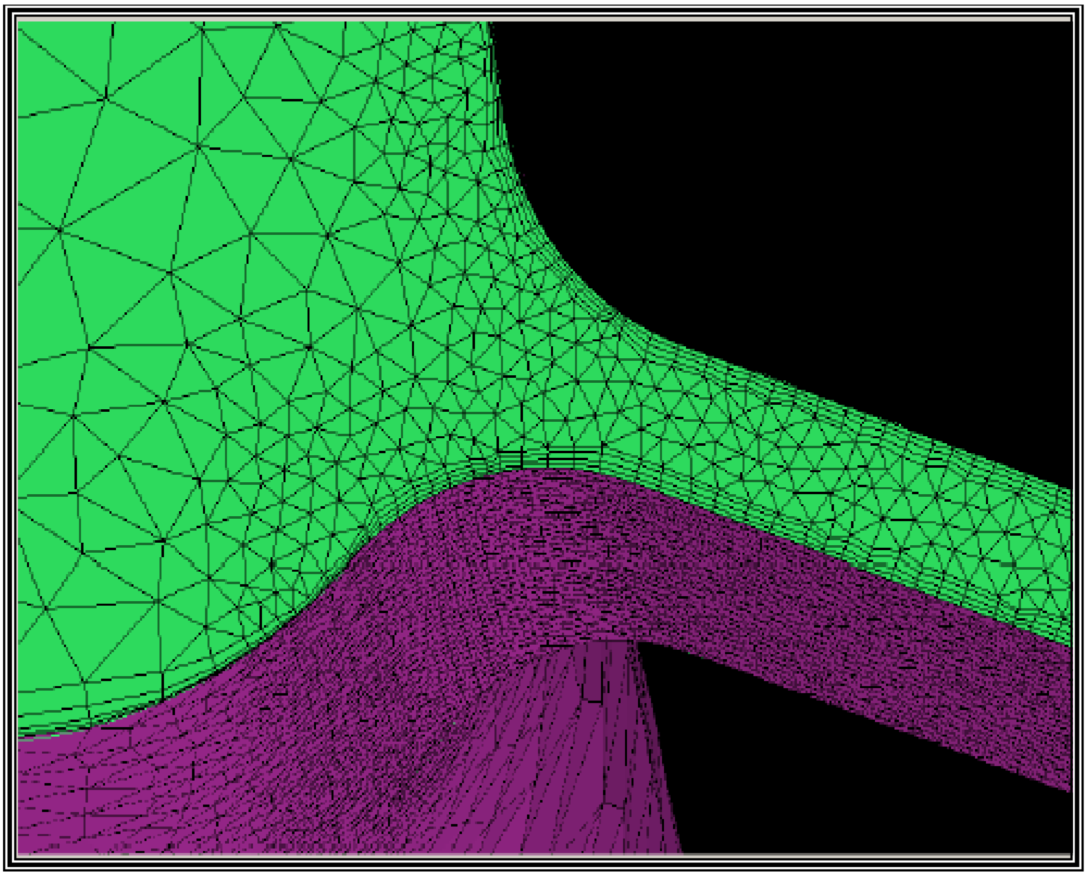

Fig 4.7: The grid generated by ANSYS ICEM CFD

4.11 Inputs and Boundary Conditions

The following boundary conditions were used for these simulation studies: inlet flow velocity 2 m/s, outlet pressure of 1 atm and no slip condition at the solid liquid interface. The no slip condition defines the flow velocity at the solid surface as zero. Here, it is also assumed that at the surface the fluid temperature will be equal to the temperature of the surface. The liquid properties used for simulation were molar weight, density, viscosity, thermal conductivity, specific heat, etc. The simulations were carried out for four different types of dye solvents employed in the calculation. The flow properties (viscosity and density) of the different solvent are listed in the following table 4.1.

	Ethanol	**Glycerol**	**Ethylene Glycol**	**Binary Solvent Ethanol and Glycerol (50:50)**
Viscosity	1.087 cP	1200 cP	20 cP	200 cP
Density	789 kg/m^2	1261 kg/m^2	1115 kg/cm^2	1023 kg/m^2

Table 4.1: Solvent Properties Used for Computational Fluid Dynamics Analysis

4.12 Dye Cell Geometries and Flow Simulation

Several dye cell geometries have been analyzed and studied with their velocity vector visualization. Some of the typical cell geometries and their velocity vectors are presented in the table 4.2. In all the cases, the flow medium is ethanol. The referred design numbers correspond to those indicated in the table.

Design – I

In this cell of uniform cross section of 19 mm x 1 mm and length of 70 mm, the inlet and outlet headers are circular channel of 8 mm diameter. The simulation results show flow circulation (vortex) near the entrance of the dye cell whose length is approximately one fourth of the cell. The pressure drop across the cell was computed to 101.314 kPa at 1 m/s inlet flow velocity.

Design – II

For this design the flow cross section area was reduced from 19 mm^2 to 10 mm^2 (10 mm x 1 mm) and the flow header diameter was reduced from 8 mm to 4 mm. It was observed that flow circulation up to 20 mm and 25 mm length from the inlet was obtained for flow velocities of 2 m/s and 4 m/s respectively. The pressure drop across the flow cell increased from 112.756 kPa to 146.957 kPa with an increase in the flow velocity from 2 m/s to 4 m/s; the increase in the pressure drop was nearly 30 %, indicating the major pressure loss in the secondary flow.

Design – III

In design III, the flow length was increased to 80 mm for the cross sectional area of 10 mm^2. For this design flow circulation near the entry of the flow cell was seen. The flow circulation extended up to almost 40 % of the flow length for inlet flow velocity of 2 m/s. On increasing inlet flow velocity the flow circulation length was increased. The pressure drop across the cell was nearly 116.55 kPa.

Design – IV

In design IV, the flow cross section area was reduced to 5 mm^2 (5 mm x 1 mm) from 10 mm^2 and the flow length was reduced to 65 mm from 80 mm. For this design, there was no flow circulation observed. On reduction of cross sectional area the flow circulation was eliminated. The pressure drop across the dye cell was computed to be 122.964 kPa at an inlet flow velocity of 1 m/s.

Design – V

In design V, the change from the preceding design was that the inlet flow header tube diameter was increased to 8 mm from 4 mm and the flow channel length was varied from 70 mm to 30 mm in steps of 10 mm. The flow velocity inside the flow channel was the same for all the dye cells of different flow channel lengths while the pressure drop increased with increasing flow channel length for the same inlet flow velocity. The pressure drop across the cell was 138.604 kPa for 30 mm cell length and it was 152.708 kPa for 70 mm cell length. There was no vortex present in the flow cell for slit entry as well as tubular entry to this flow cell.

Design – VI

For Design VI, the flow channel length and the flow cross section area were kept the same as in design V. The flow entry to the cell was smoothened with the introduction of 2 mm radius fillet. The maximum flow velocity components were 2.24 m/s and 11.71 m/s for inlet flow velocities of 0.198 m/s and 0.994 m/s respectively. No flow circulation was observed for all the five simulations carried out for different inlet flow velocities. The pressure drop across the flow cells was 104.04 kPa and 162.773 kPa for 0.198 m/s and 0.994 m/s inlet flow velocities respectively.

Design – VII

For Design VII, converging, straight and diverging sections were introduced in the flow geometry and the flow width was kept 19 mm. The inlet header tube diameter was 8 mm. The flow circulation near the inlet as well as at the outlet was observed. The flow circulation starts immediately after the diverging section of the flow. The pressure drop across the cell was 102.625 kPa at an inlet flow velocity of 1 m/s. The pressure drop across the flow cell was relatively small due to converging and diverging flow sections. Due to convergence and divergence geometry, higher flow velocity was achieved with a smaller pressure drop.

Design – VIII

For Design VIII, the flow channel width was reduced to 5 mm^2 (5 mm x 1 mm) from 19 mm^2 (19 mm x 1 mm) and flow channel length was 90 mm. This design had also converging, straight and diverging sections in the flow domain. The velocity vectors show flow circulation both near inlet as well as at the outlet of the flow cell. The maximum flow velocity was in the straight region of the flow cell. The pressure drop across the flow cell was 108.118 kPa at an inlet flow velocity of nearly 2 m/s. For converging and diverging flow channels the pressure head loss is minimized due to recovery of pressure in the diverging section.

Design – IX

For this design IX, triangular converging and diverging sections were introduced; the diverging angle was kept 30^{O} for both diverging and converging angles. Total flow domain length was kept 25mm in which 10 mm length was kept straight. The inlet and outlet header areas were also kept 25 mm^2. A flow circulation in the outlet was observed at an inlet flow velocity of 1 m/s. The maximum velocity of 4.43 m/s was obtained in the straight section of the flow domain.

Design – X

For this design X, the triangular geometry was changed to a smooth radius of 30 mm with 30^{O} convergence angle and 30^{O} divergence angle. The other dimensions remained the same as in the design IX. Flow circulation at the outlet of the flow channel was observed and the flow velocity was the same as in design IX as the flow cross section dimensions remained unchanged.

Design – XI

For design XI, the converging and diverging channel radii were reduced to 15 mm from 30 mm and keeping all the other dimensions the same. In this design also the flow circulation at the outlet of the flow cell was present while the flow velocity was the same as in designs IX and X.

Design – XII

In design XII, the converging and diverging radius was changed to 151 mm and straight length was kept10 mm. The flow channel gap was reduced to 0.5 mm from 1 mm unlike in all the other designs; the flow channel length was 124 mm with inlet and an outlet header area of 200 mm^2. Flow circulation was observed immediately after straight section at the outlet of the flow cell. The pressure drop across the flow cell was only 103.83 kPa despite relatively higher flow velocities of 19.5 m/s in the straight section.

Design – XIII

In design XIII, a smooth flow entry with 2 mm radius fillet was introduced before the straight section of the flow domain, followed by a diverging section with a divergence angle of 14^{O}. There was a flow circulation at the outlet of the flow channel as seen in the earlier designs. The pressure drop across the flow channel was computed to be 106.645 kPa at a flow velocity of 5.32 m/s in the straight section of the flow channel.

Design – XIV

For design XIV, the fillet radius was increased to 3 mm, straight length reduced to half and diverging angle also reduced to 6.73^{O} with flow channel length of 55 mm to keep the inlet and the outlet header area the same. The entry and exit in the cell were with a tube of 4 mm diameter. The maximum flow velocity component was 1.42 m/s for inlet flow velocity of 1 m/s. No flow circulation was observed in this flow geometry. The pressure drop across the flow cell was 101.95 kPa at an inlet flow velocity of 1 m/s.

The converging and diverging flow geometries are useful for high flow velocities in the flow channel as the pressure drops are smaller in higher flow velocities. These types of flow cell geometries can be used for high repetition rate lasers where the flow velocity requirements are high without significant pressure head loss.

Table 4.2: Design Number – I

Flow channel gap 1 mm, width 19 mm and length 70 mm, Inlet outlet tube diameter 8 mm. Flow channel area 19 mm^2 with slit entry from nearly 50 mm^2 inlet header.

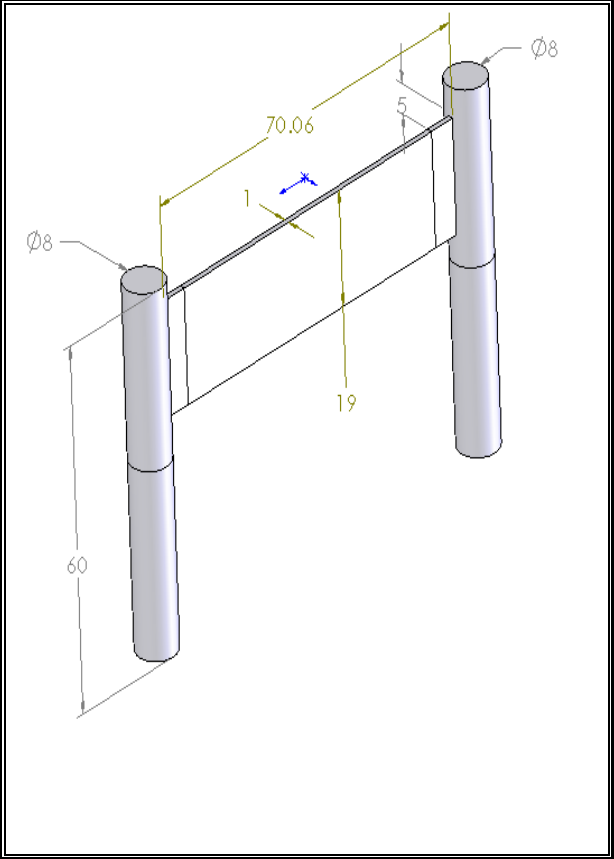	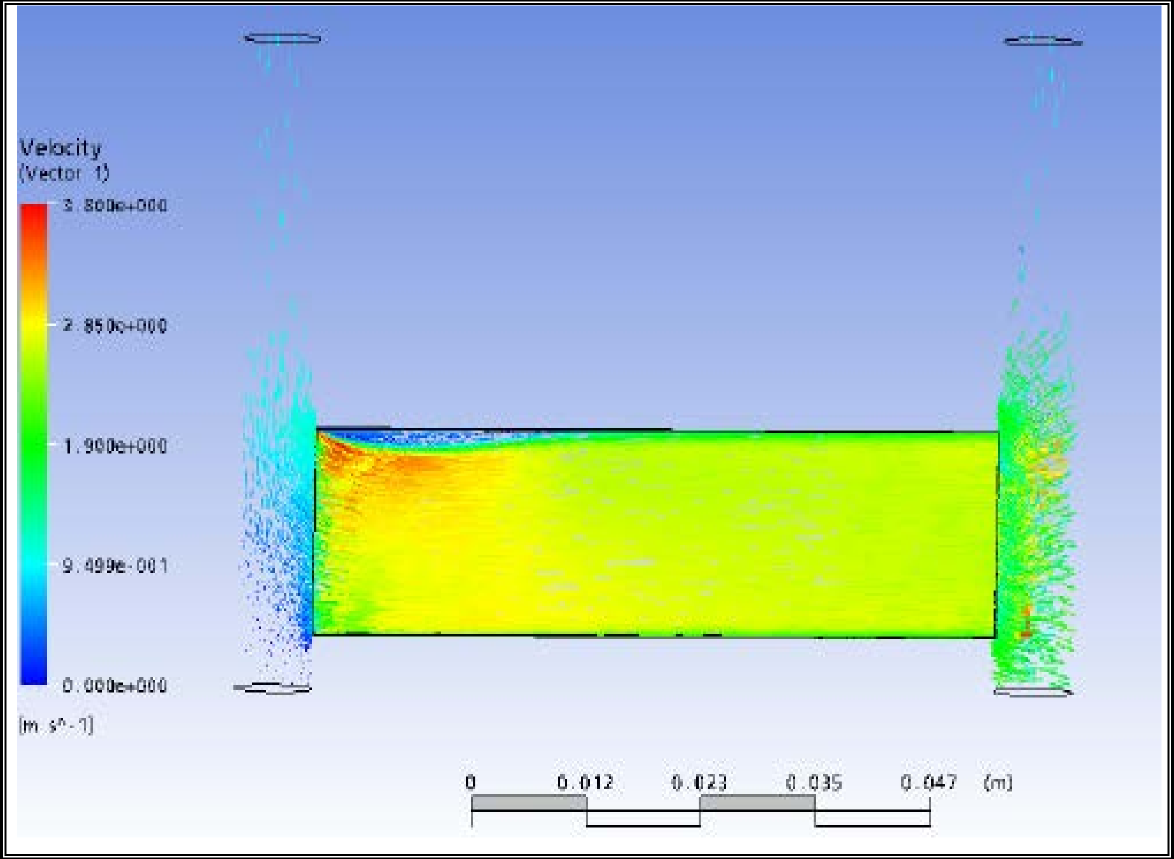
Flow Domain	**Velocity Vectors**

Table 4.3: Design Number – II

The flow channel cross section area was 10 mm^2 with flow channel length of 76 mm. The inlet tube diameter was kept 4 mm to match the flow channel area. The entry to the flow channel was kept slit area of 10 x 1 mm^2.

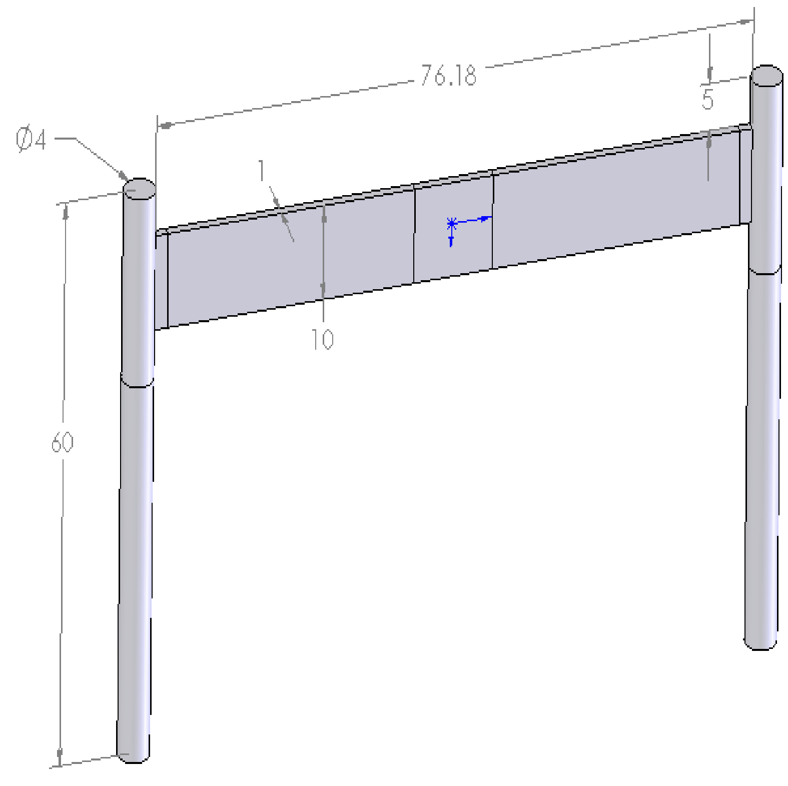

Flow Domain

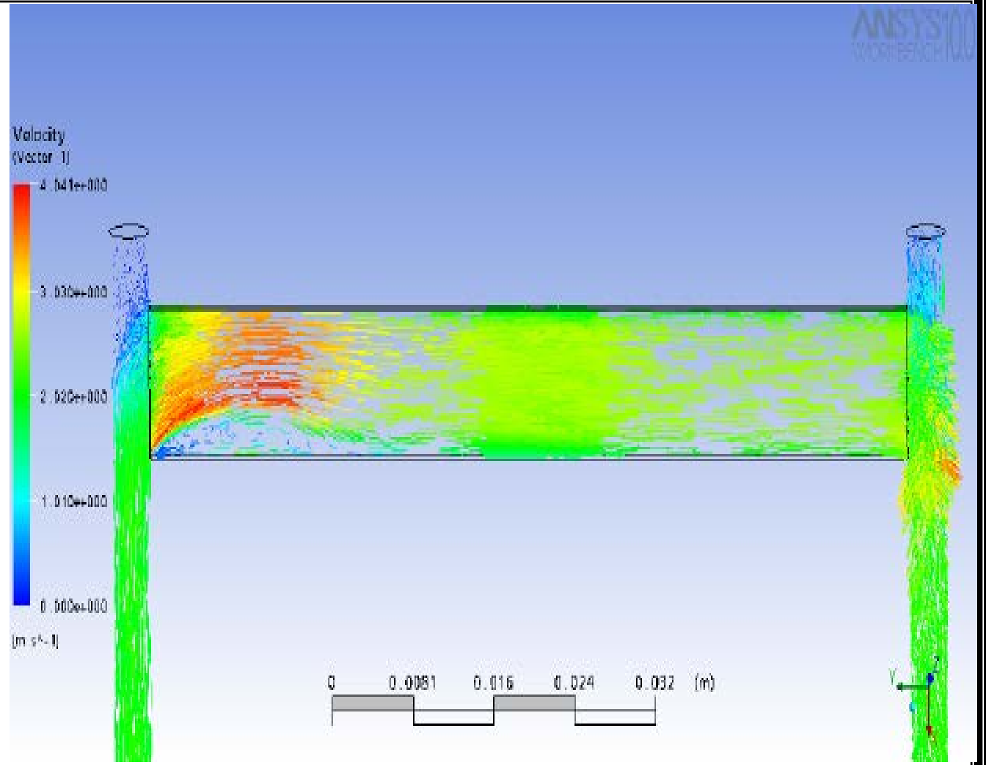

Velocity Vectors

Table 4.4: Design Number – III

For this design the flow channel area was also kept 10 mm^2 with flow channel length of 80 mm, inlet as well as the outlet tube diameter was 4 mm with slit entry.

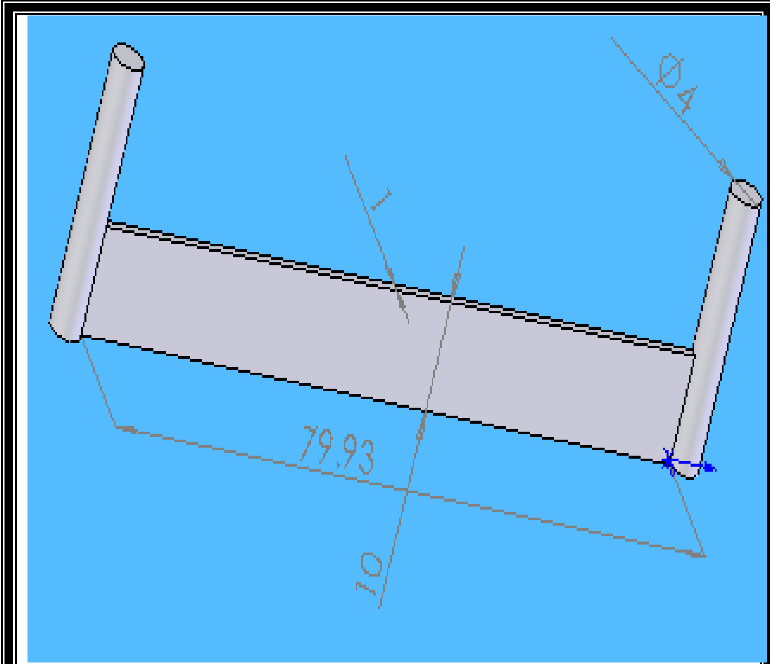

Flow Domain

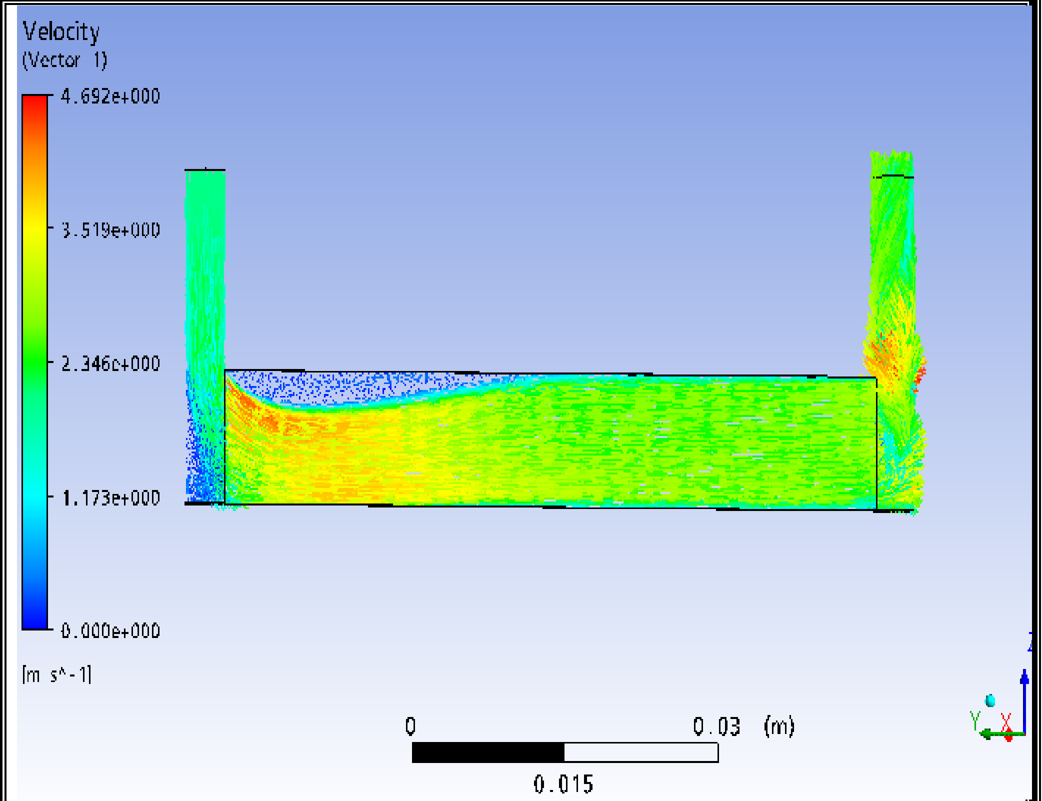

Velocity Vectors

Table 4.5: Design Number – IV

For this design the flow channel area was reduced to 5 mm^2 with flow channel length of 65 mm. The entry to the flow channel was kept from tube of 4 mm diameter with a slit entry.

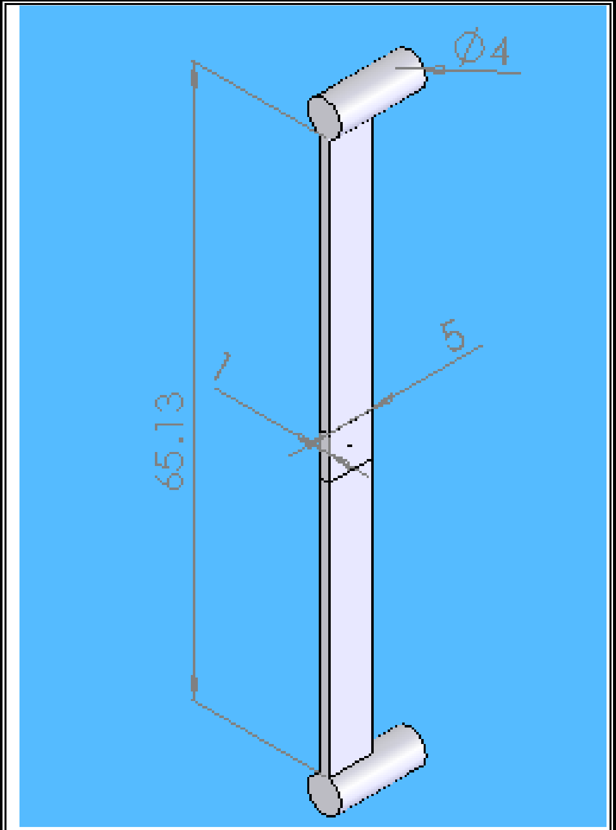	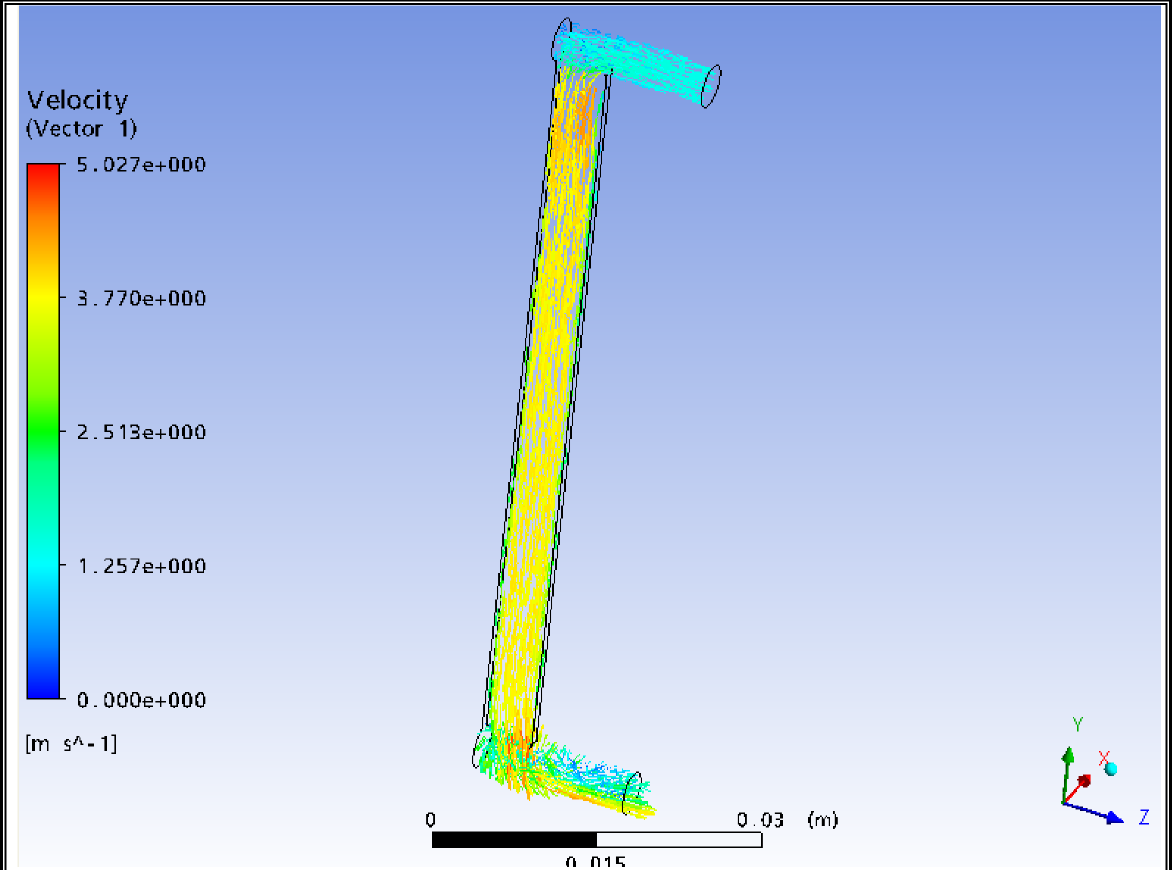
Flow Domain	**Velocity Vectors**

Table 4.6: Design Number – V

For this design the flow channel area of 5 mm^2, 60 mm tube length 8 mm tube diameter with slit entry and exit. The flow channel lengths were varied from 70 mm to 30 mm in steps of 10 mm for different simulations.

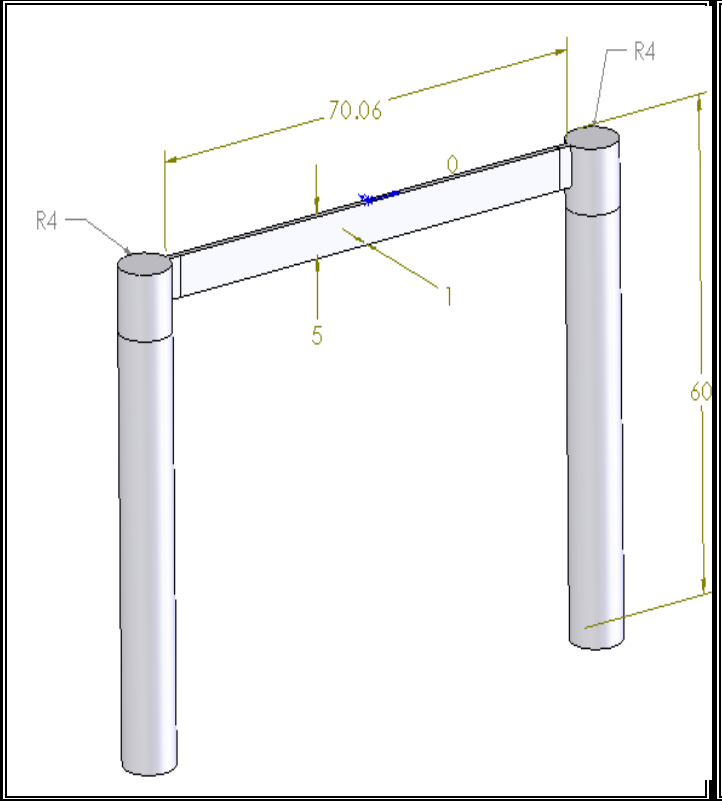

Flow Domain

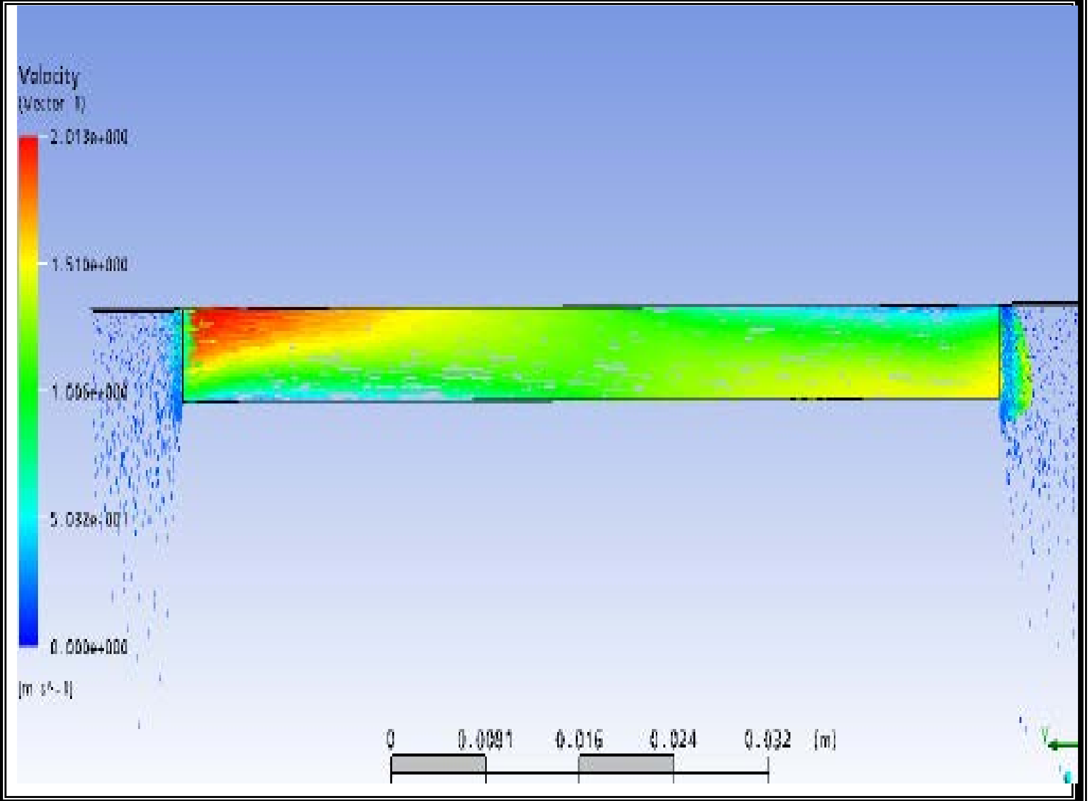

Velocity Vectors

Table 4.7: Design Number – VI

The flow channel length was kept 30 mm, flow cell cross section area was kept 5 mm^2 and the entry to the cell was made by slitting 8 mm diameter tube. The flow entry to the cell was smoothened with the introduction of 2 mm fillet to avoid the initiation of the turbulence in the flow channel. The inlet flow velocity was altered from 0.198 m/s to 0.994 m/s to obtain the required flow velocities in the flow channel.

<table>
<tr>
<td>
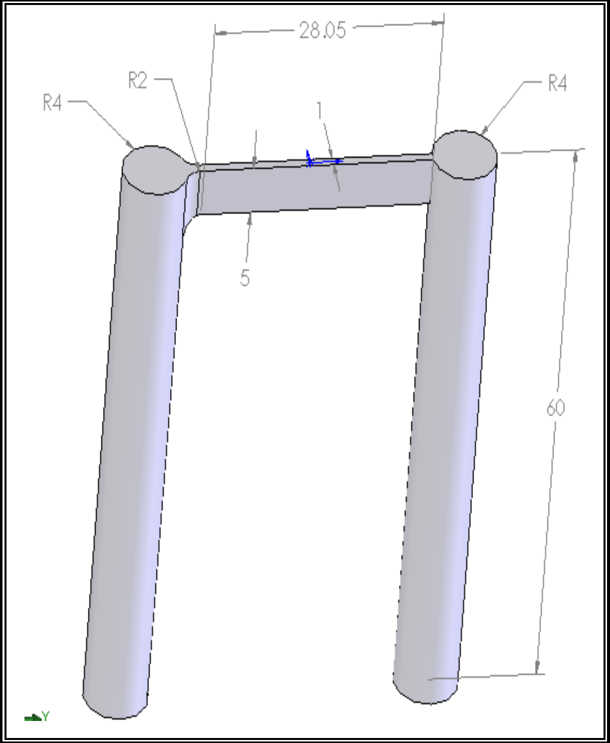

</td>
<td>
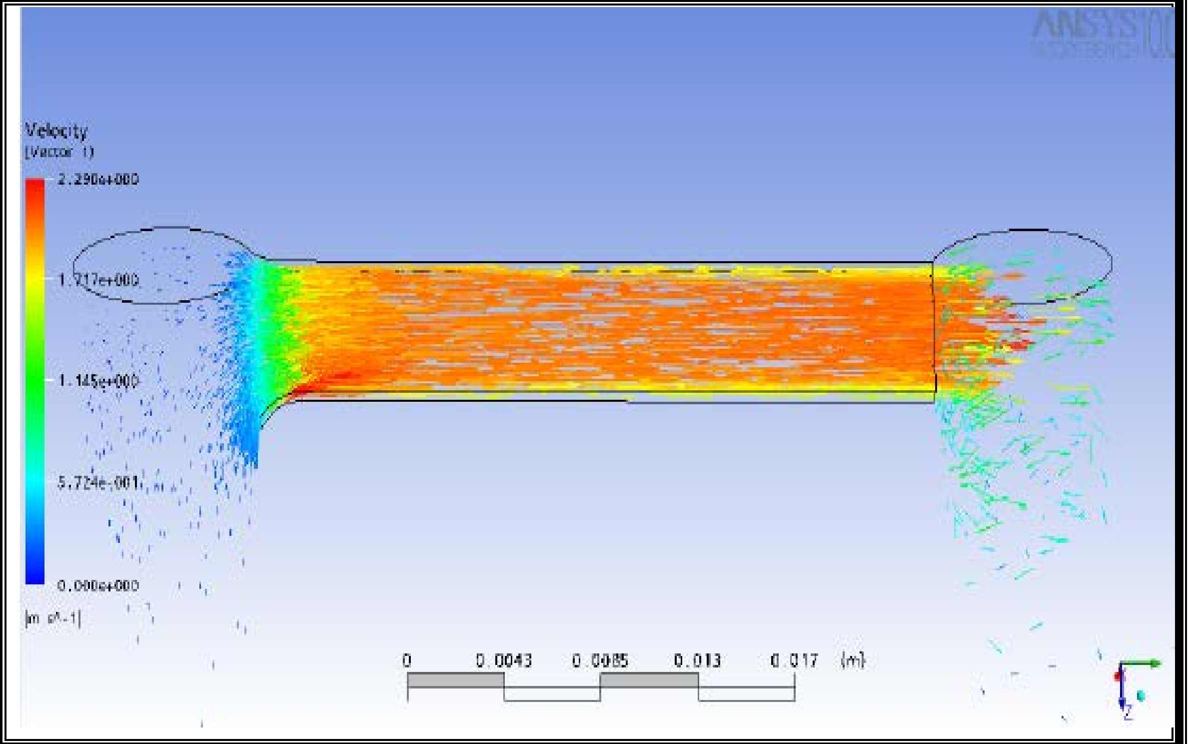

</td>
</tr>
<tr>
<td>Flow Domain</td>
<td>Velocity Vectors</td>
</tr>
</table>

Table 4.8: Design Number – VII

Flow channel gap of 1 mm, 19 mm flow width and total flow channel length was kept ~ 75 mm with 5 mm straight section. Inlet tube diameter was 8 mm and 64 mm tube length with converging-diverging flow geometry.

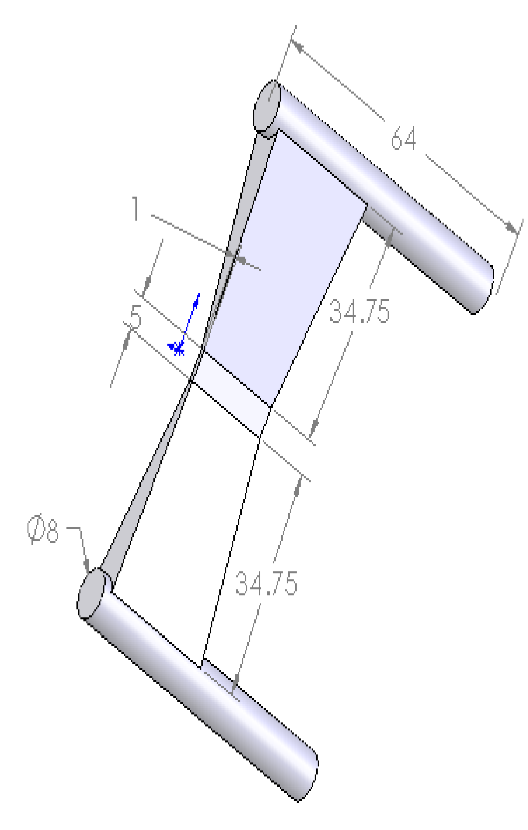

Flow Domain

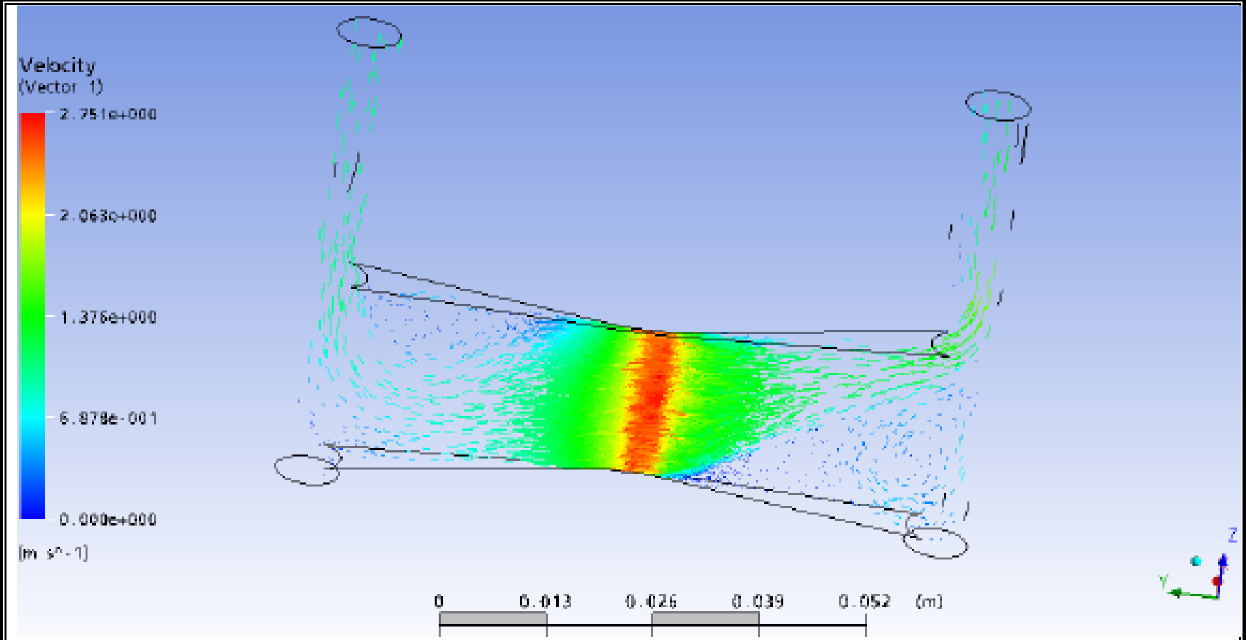

Velocity Vectors

Table 4.9: Design Number – VIII

For this design the flow channel gap was kept 1 mm, flow channel area of 5 mm^2, flow channel length of 90 mm with 5 mm straight length having converging-diverging flow channels. The flow entry to the dye flow cell was tubular with tube diameter of 5 mm.

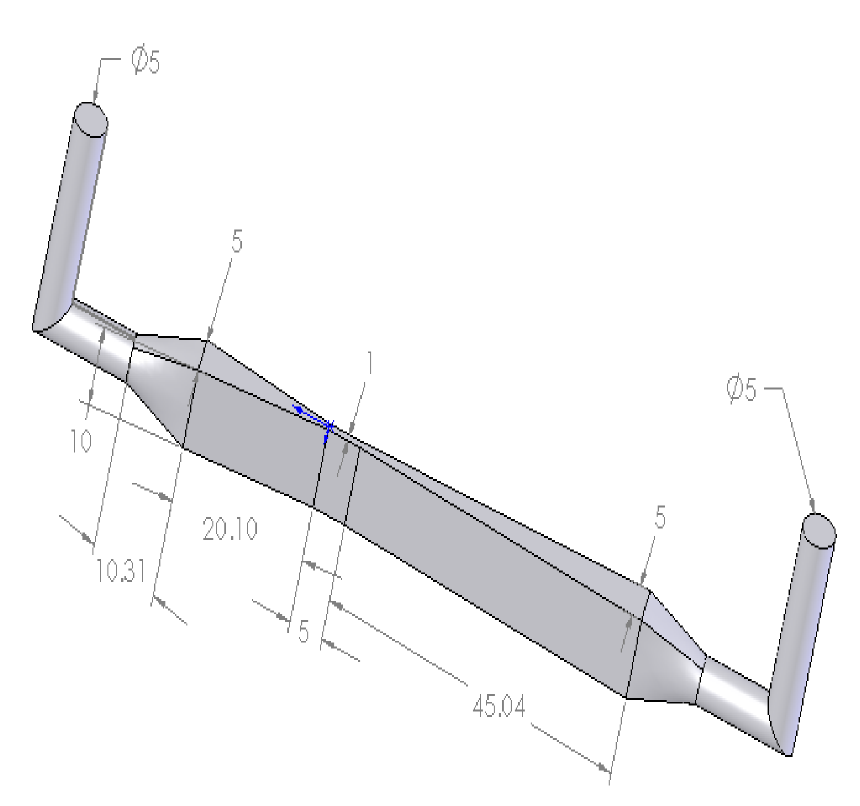	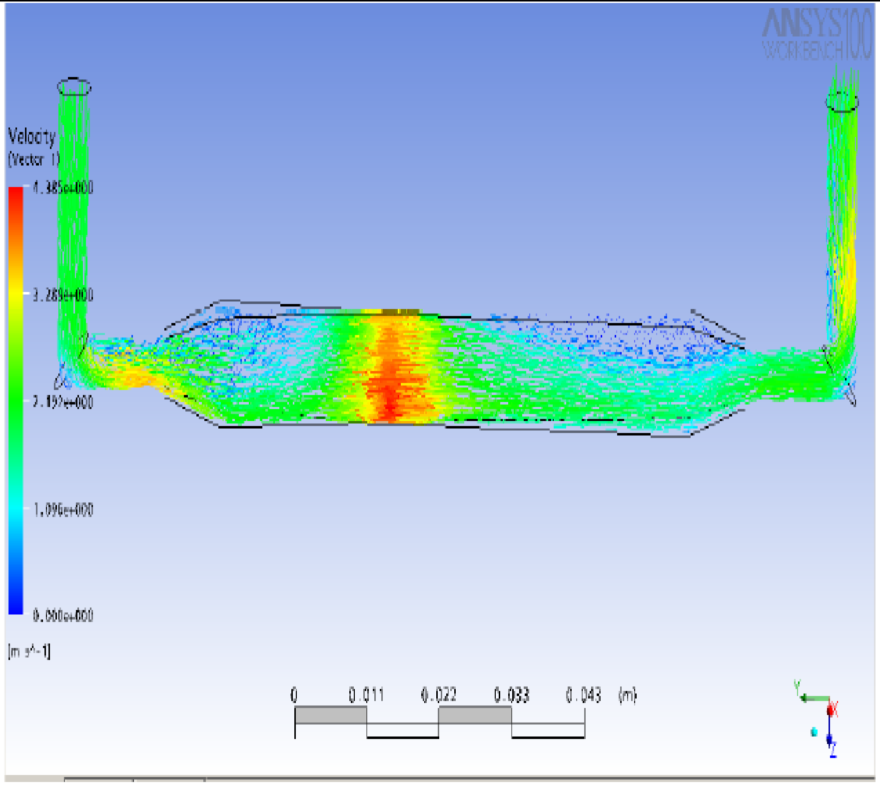
Flow Domain	**Velocity Vectors**

Table 4.10: Design Number – IX

This flow channel consists of three sections triangular; converging, straight and triangular diverging. The diverging angle was kept nearly 30^{O} for both converging and diverging sections. The flow cell width was kept 5 mm, flow length 10 mm, flow channel gap 1 mm and both inlet and outlet out areas is 25 mm^2.

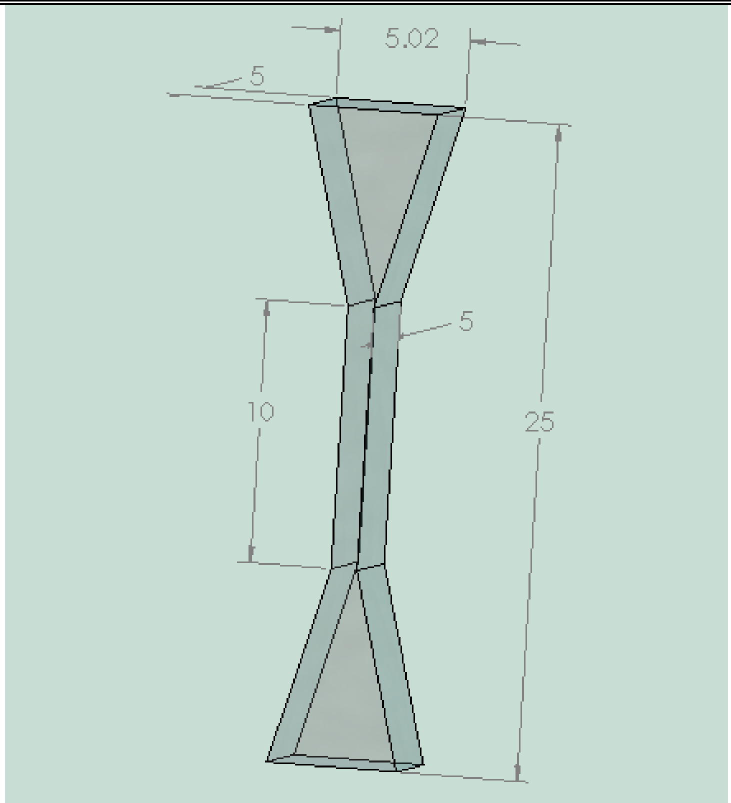	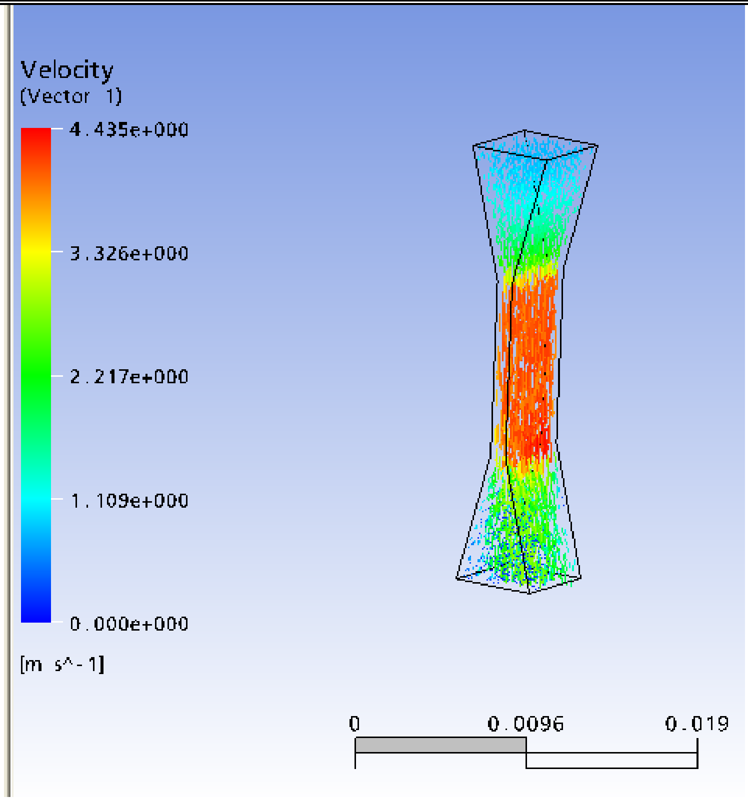
Flow Domain	**Velocity Vectors**

Table 4.11: Design Number – X

This flow cell had converging, diverging and straight sections. The converging and diverging section has 30 mm radius with 30^{O} angle. The inlet and outlet areas were the same ~ 25 mm^2. The flow cell gap was kept 1 mm and flow cell length 25 mm.

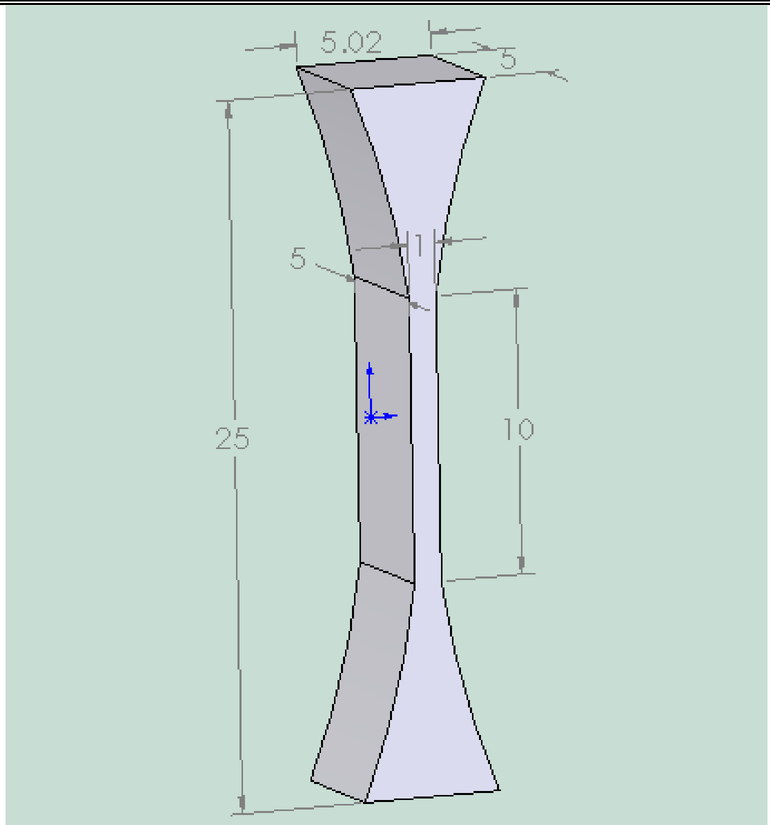

Flow Domain

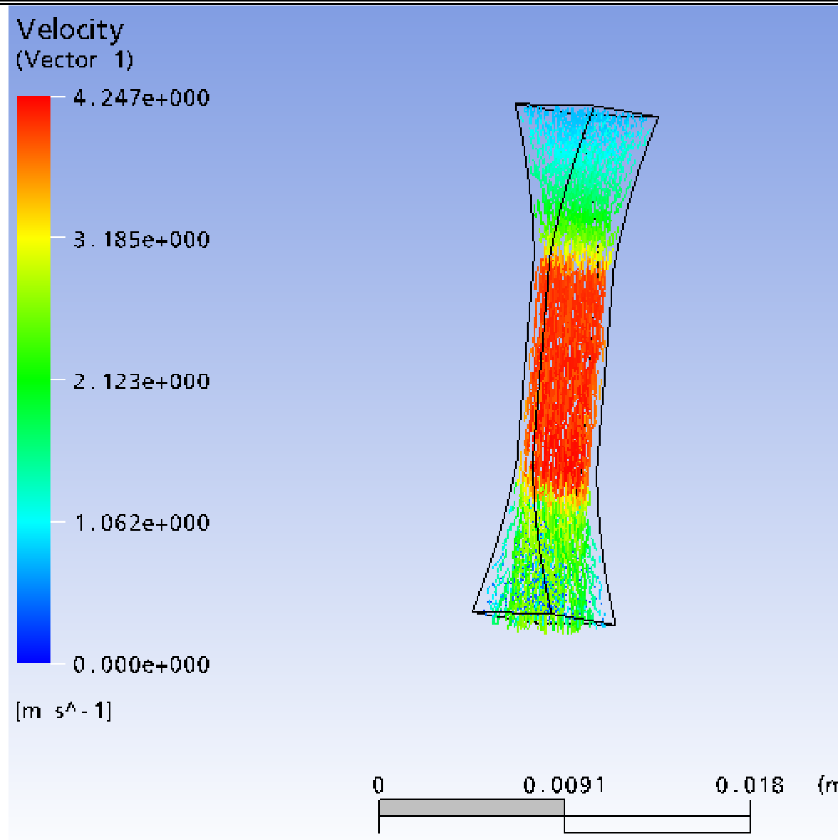

Velocity Vectors

Table 4.12: Design Number – XI

This flow cell has three sections: Converging, straight and diverging, the converging and diverging section radii were 15 mm with inlet and outlet flow areas of 25 mm^2. The straight channel flow area was 5 mm^2, with a flow channel length of 25 mm.

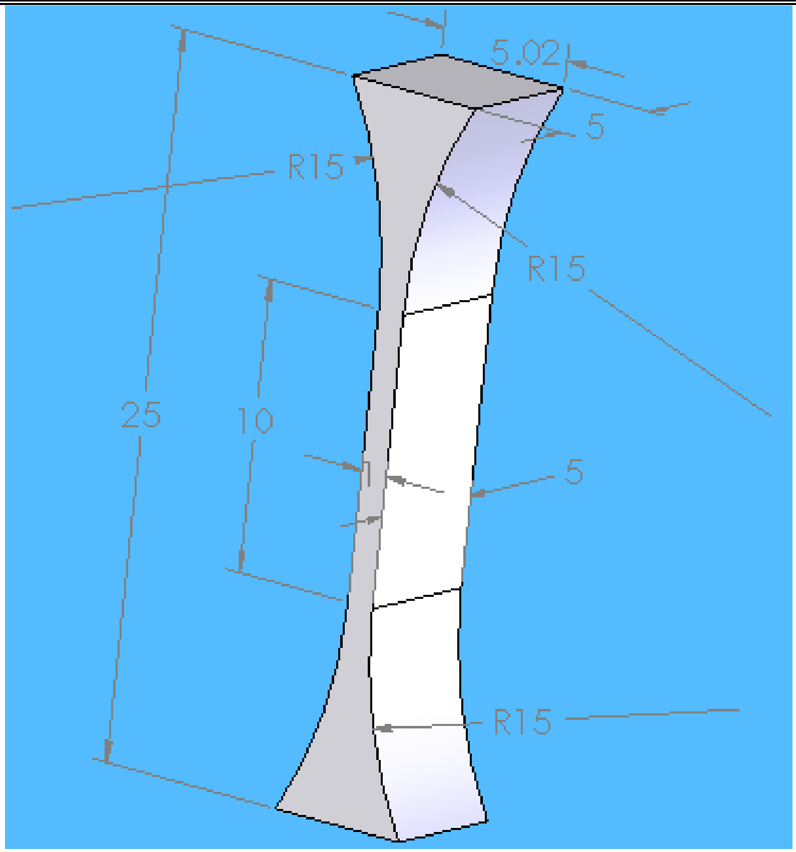	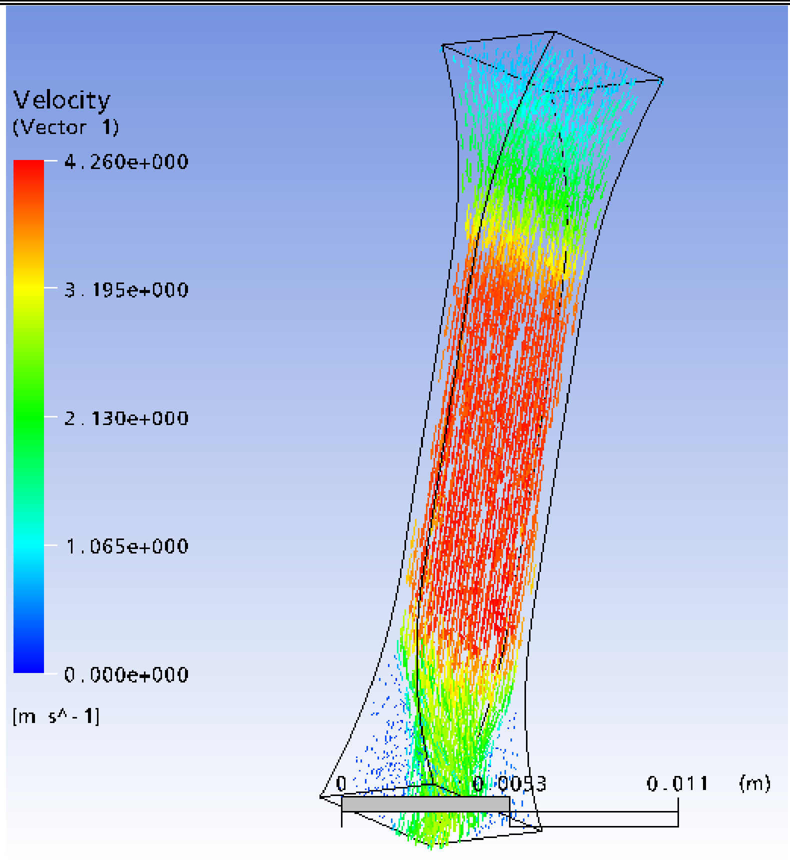
Flow Domain	**Velocity Vectors**

Table 4.13: Design Number – XII

This flow cell design has converging, diverging radius of 151 mm and a straight section of 10 mm length with inlet and outlet areas of nearly 200 mm^2. The straight channel had an area of 8 mm^2 with straight length 10 mm, flow channel gap 0.5 mm and total flow channel length of 124 mm.

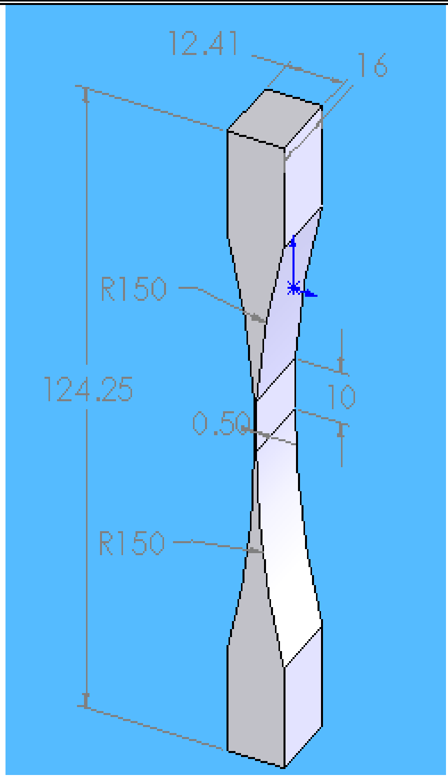

Flow Domain

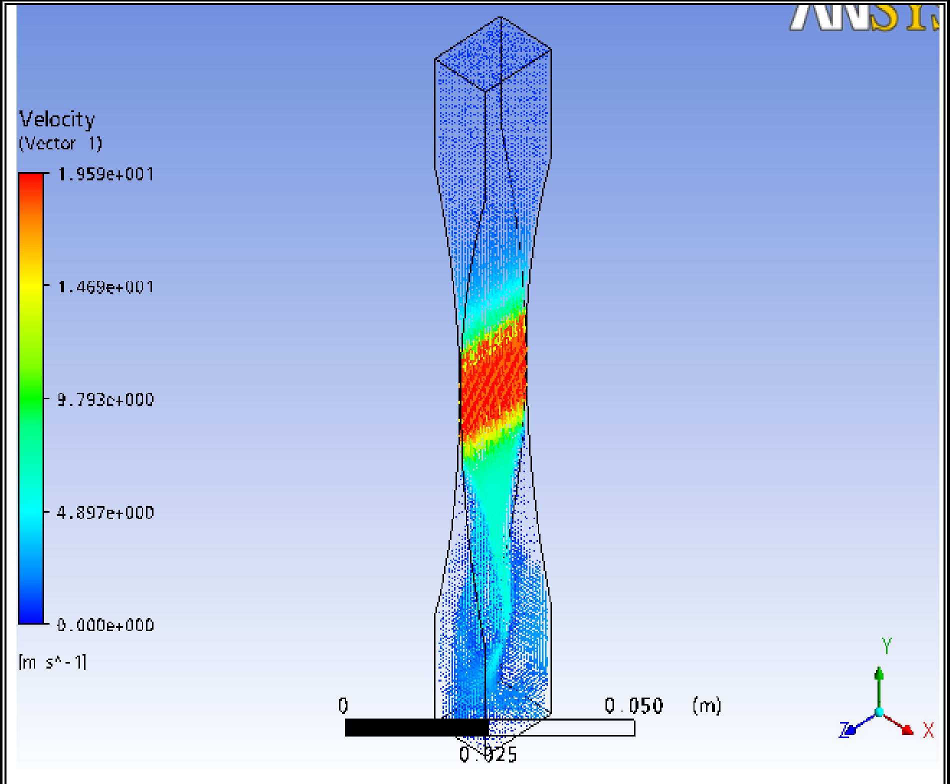

Velocity Vectors

Table 4.14: Design Number – XII

For this design the flow channel gap of 1 mm in the straight section, flows entry with 25 mm^2 flow areas having 2 mm fillet radius had been analyzed. The total flow channel length of 40 mm, straight section of 12 mm and the divergence angle of 14^{O}.

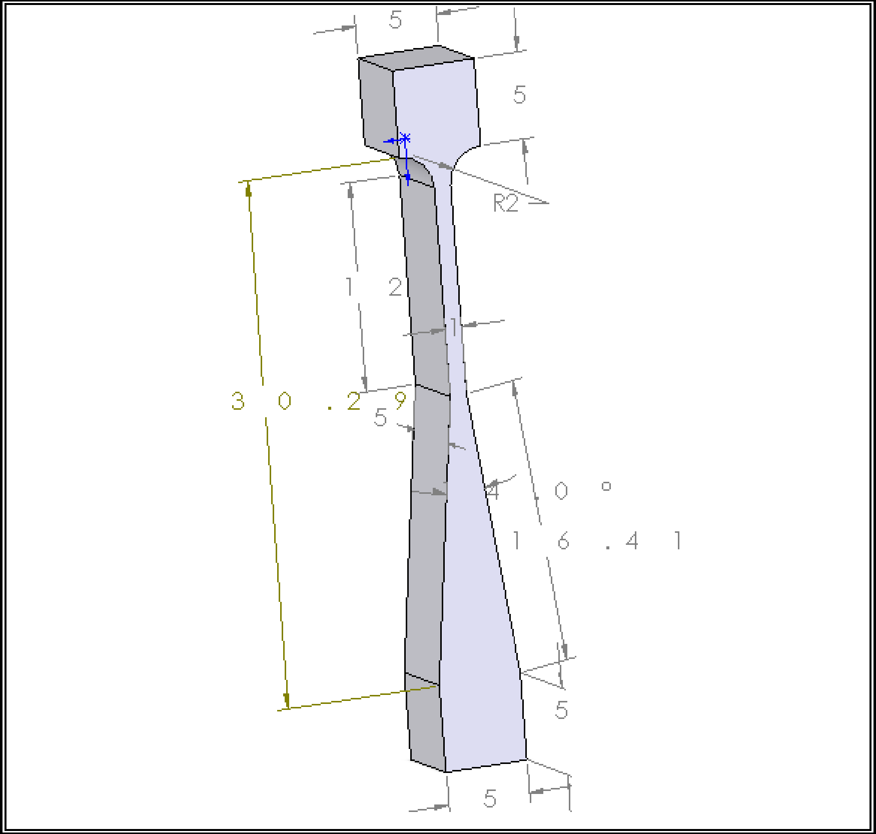	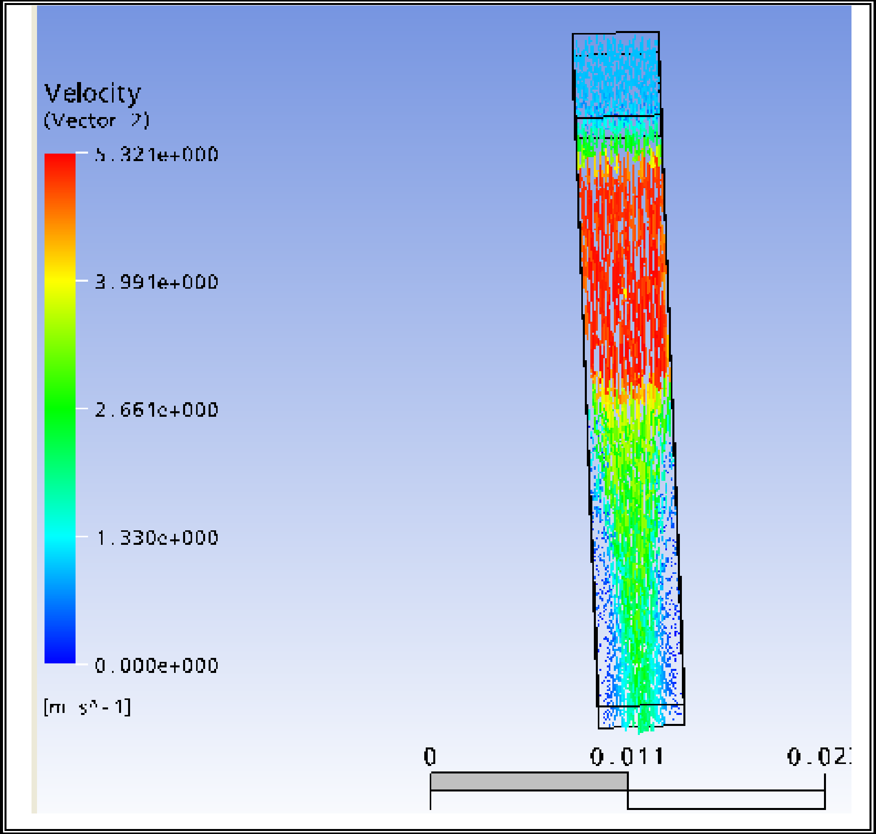
Flow Domain	**Velocity Vectors**

Table 4.15: Design Number – XIV

The inlet has a fillet of 3 mm radius; flow channel gap of 1mm for straight length of 6 mm, diverging angle of 6.73^{O}, flow channel length of 55 mm. The flow cell inlet area was 35 mm^2 and the flow entry was 4 mm diameter tube.

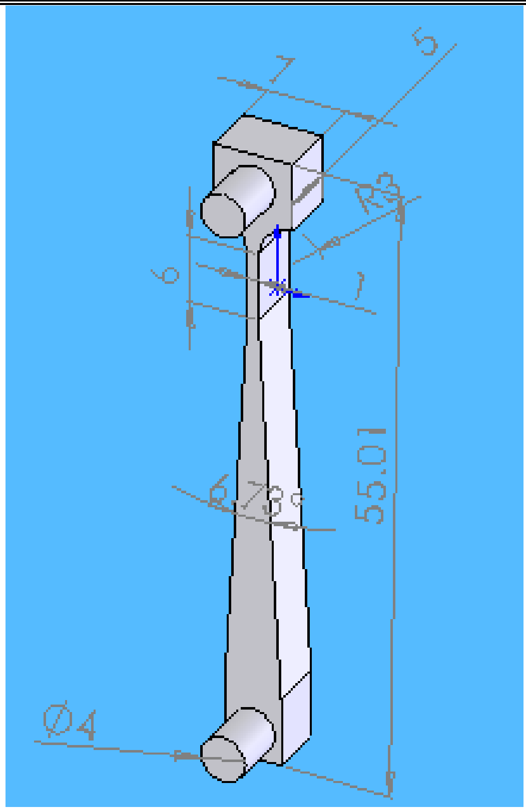

Flow Domain

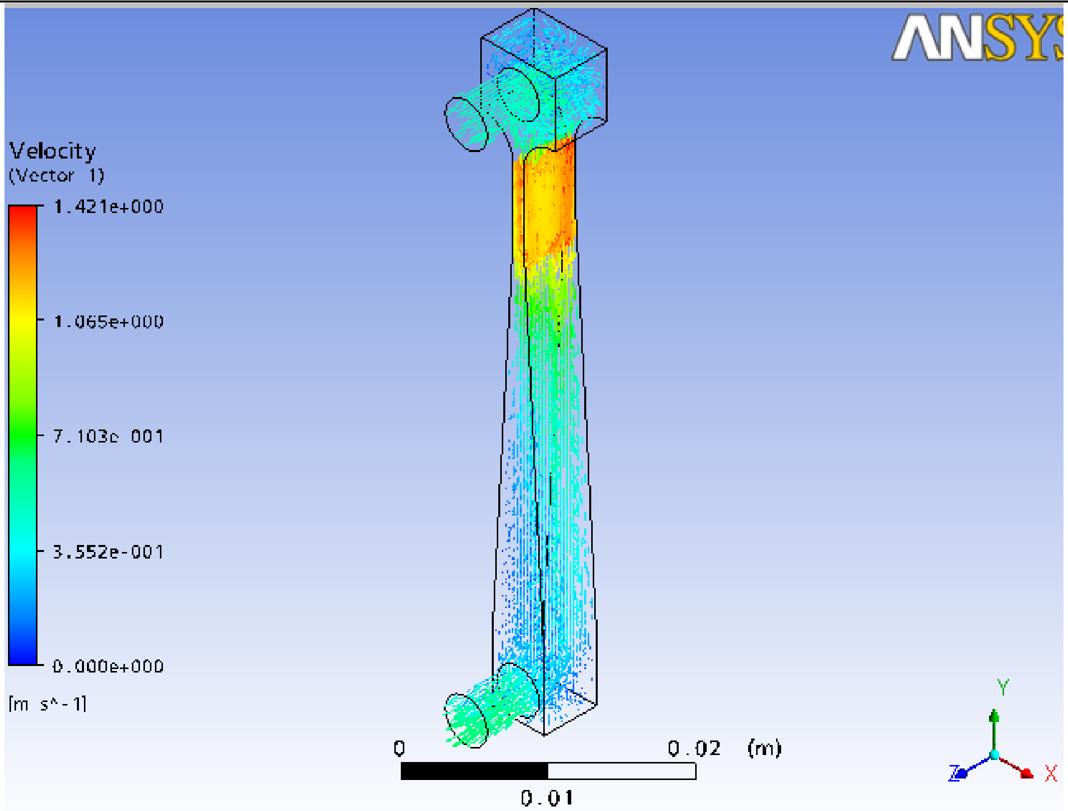

Velocity Vectors

4.13 Selection of Dye Cell for Detailed Analysis

Of the several designs investigated two dye cells with different flow cross section and different flow entries were chosen for fabrication, mainly because of the simplicity in fabrication. These were simulated in detail by the CFD model. The velocity vectors obtained for these two dye cells of dimensions 10 mm x 1 mm x 70 mm (Length, width and height) and 5 mm x 1 mm x 70 mm have been presented in figure 4.8 a, b and figure 4.9 a, b respectively. The velocity vectors for 1 x 10 mm^2 cell in figure 4.8 shows a flow circulation (~ vortex) near the entrance of the dye cell, which is spread over two third length of the dye cell with inlet flow velocity of 2 m/s and ethanol as solvent. This dye cell has a tubular entry with an inlet tube diameter of 4 mm. The circulation length reduced to half the cell length with a slit entry (1 x 10 mm) to the dye cell (1x 10 mm^2) for the same boundary conditions. The mean flow velocity in the flow channel was computed to nearly 2.5 m/s. The circle marked on the dye cell shows the position of active volume for generating the SLM dye laser.

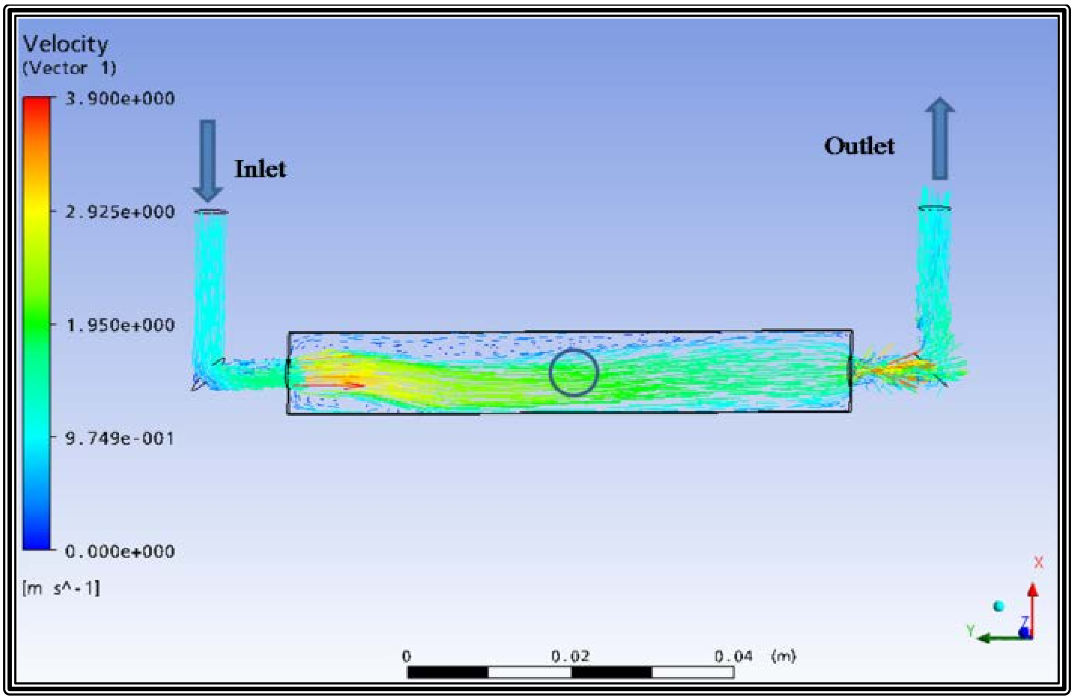

Fig 4.8 a: Flow velocity vectors for ethanol solvent with 2 m/s inlet flow velocity of 10 x 1 x 70 mm dye cell with tubular entry.

When the flow channel cross section area was reduced from 10 mm^2 to 5 mm^2 and tubular entry changed to slit entry, as can be seen in figure 4.9 a; no flow circulation was observed in the velocity vector diagram for the same boundary condition and the same solvent. No flow circulation was observed in the computational results with tubular entry of 4 mm ID in this dye cell (1 x 5 mm^2) as shown in figures 4.9 b.

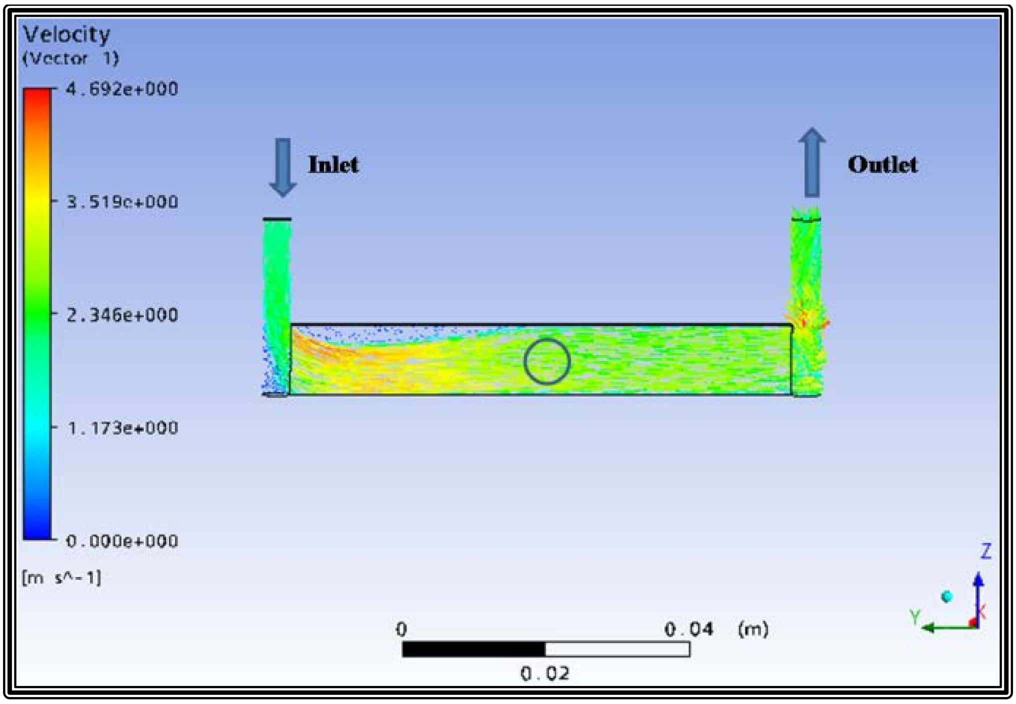

Fig 4.8 b: Flow velocity vectors for ethanol solvent with 2 m/s inlet flow velocity for 10 x 1 x 70 mm dye cell with slit entry.

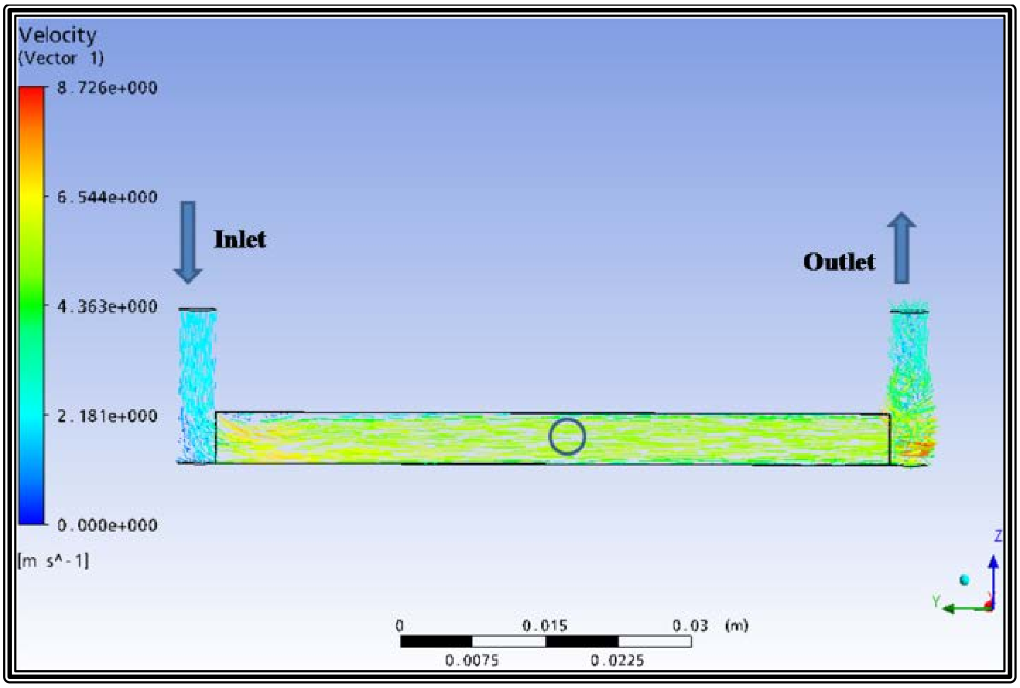

Fig 4.9 a: Flow velocity vectors for ethanol solvent with 2 m/s inlet flow velocity for 5 x 1 x 70 mm dye cell with slit entry.

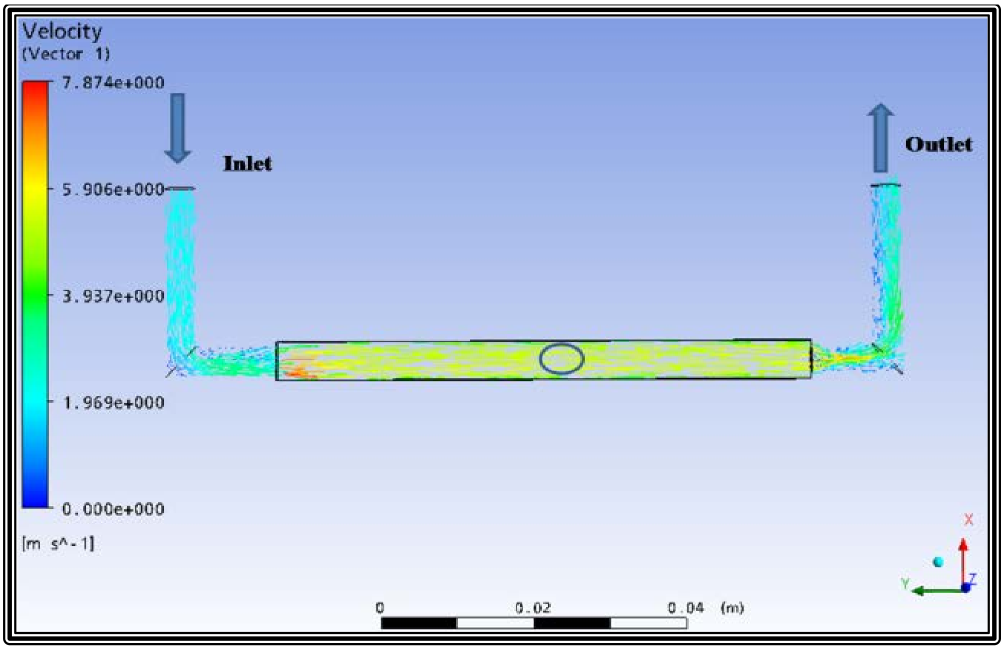

Fig 4.9 b: Flow velocity vectors for ethanol solvent with 2 m/s inlet flow velocity for 5 x 1 x 70 mm dye cell with tubular entry.

The use of solvents with higher viscosity such as binary solvent (50:50 ethanol and glycerol) and pure glycerol allowed elimination of flow circulation in 1 x 10 mm^2 dye cell for the same boundary conditions as simulation results shown in fig 4.10.

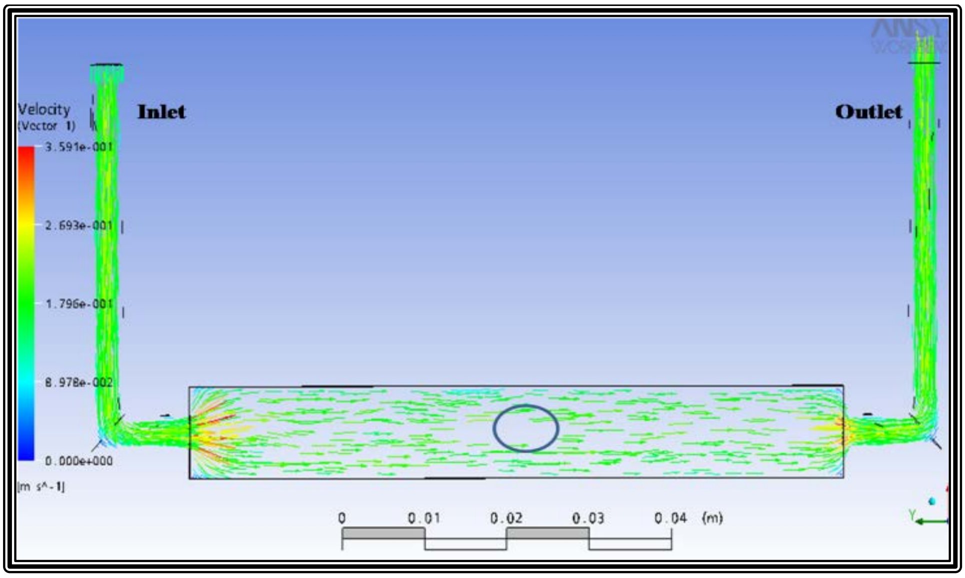

Fig 4.10: Flow velocity vectors for binary solvent (50: 50 Ethanol & Glycerol) with 2 m/s inlet flow velocity of 10 x 1 x 70 mm dye cell with tubular entry.

The pressure drop across the dye cell with glycerol is higher (2.4 kg/cm^2) than the corresponding pressure drop (1.45 kg/cm^2) with ethanol as a solvent for the same boundary condition.

4.14 Boundary Layer Visualization

The simulation results for a range of velocities between 0.2 m/s and 2.5 m/s show boundary layer thickness (99% U_∞) was maximum ~370 µm for inlet flow velocity of 0.2 m/s, while it was minimum ~327 µm for inlet flow velocity of 2.5 m/s. In this thin boundary layer the velocity is small, while the pump power and the velocity fluctuations are large, which severely affects the bandwidth and the wavelength stability of the SLM dye lasers. The flow velocities in the active volume were computed for different inlet flow velocities from 0.2 m/s to 2.5 m/s in steps of 0.2 m/s. It was observed that the maximum flow velocity of 6.5 m/s was obtained for an inlet velocity of 2.5 m/s and the maximum flow velocity of 0.5 m/s was obtained with 0.2 m/s inlet flow velocity. The flow velocity profiles for several inlet flow velocity with ethanol ranging from 0.2 m/s to 2.5 m/s for dye cell geometry of 5 mm x 1 mm x 70 mm have been computed and plotted as shown in figure 4.11.

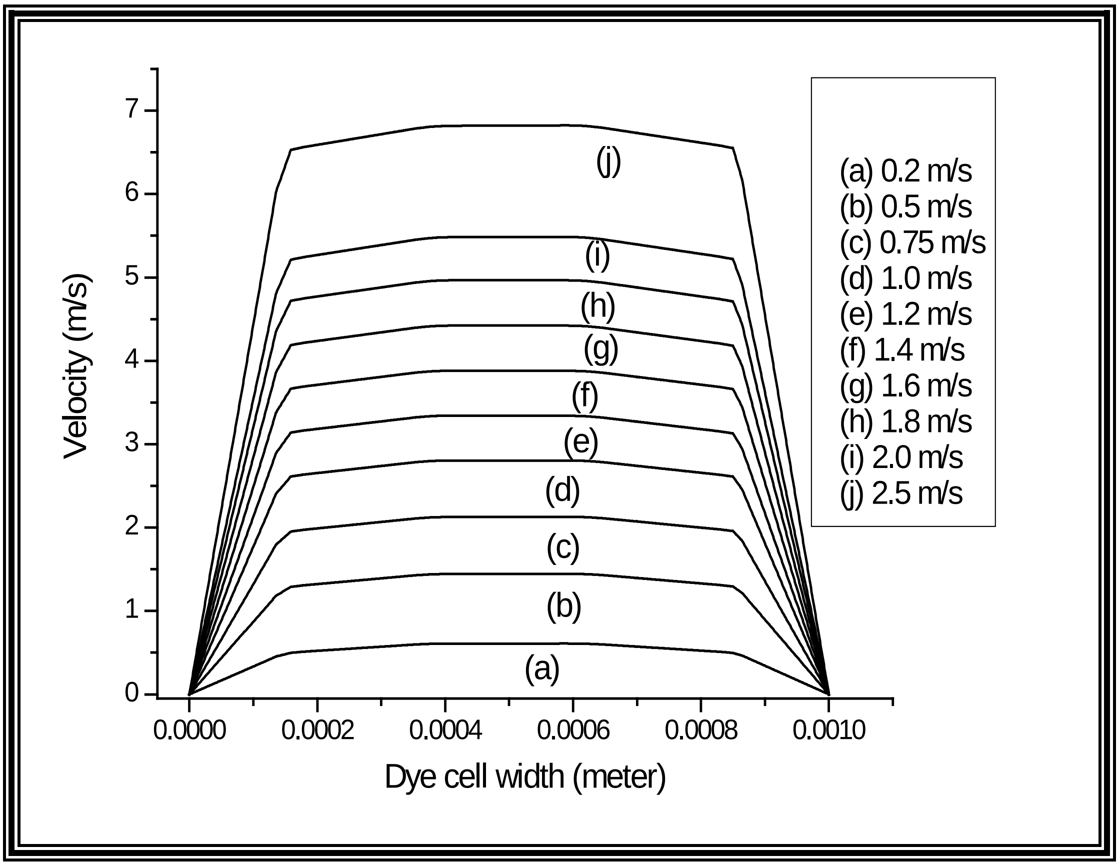

Fig 4.11: Computationally generated velocity profile for 5x1x70 mm dye cell for different inlet flow velocities. (a) 0.2 m/s, (b) 0.5 m/s, (c) 0.75 m/s, (d) 1.0 m/s, (e) 1.2 m/s, (f) 1.4 m/s, (g) 1.6 m/s, (h) 1.8 m/s, (i) 2.0 m/s and (j) 2.5 m/s

The boundary layer thickness was plotted with Reynolds number for the inlet flow velocities ranging from 0.2 m/s to 2.5 m/s as shown in figure 4.12.

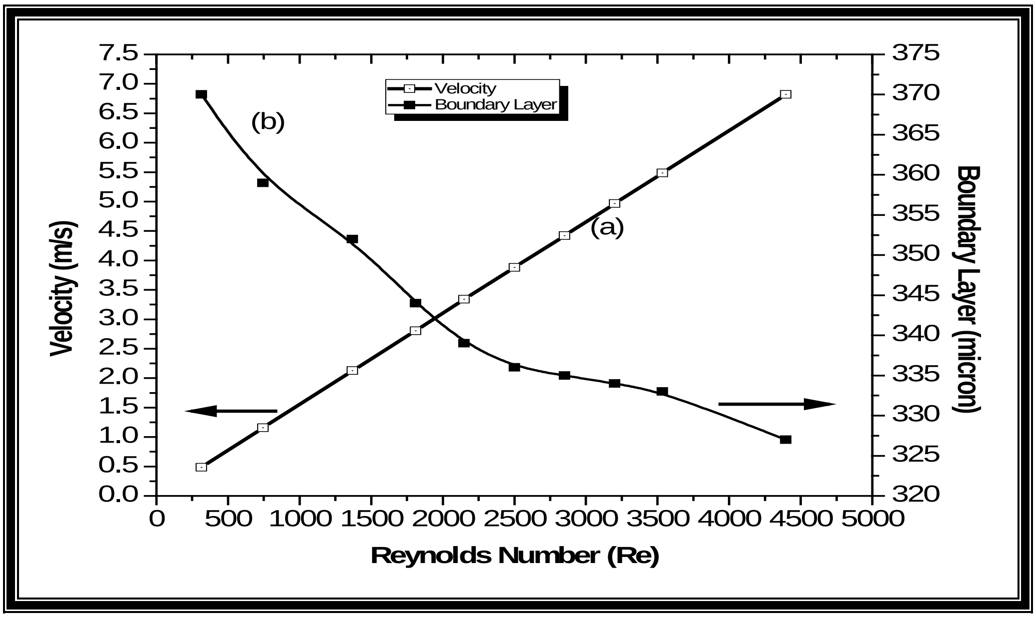

Fig 4.12: Boundary layer thickness and velocity with Reynolds number for 5 x 1 x 70 mm dye cell, (a) velocity (b) boundary layer thickness

The computational results of design – XIV are presented here to show the capabilities of the CFD model. The pressure drop across the dye cell at different inlet flow velocities was plotted as shown in figure 4.13

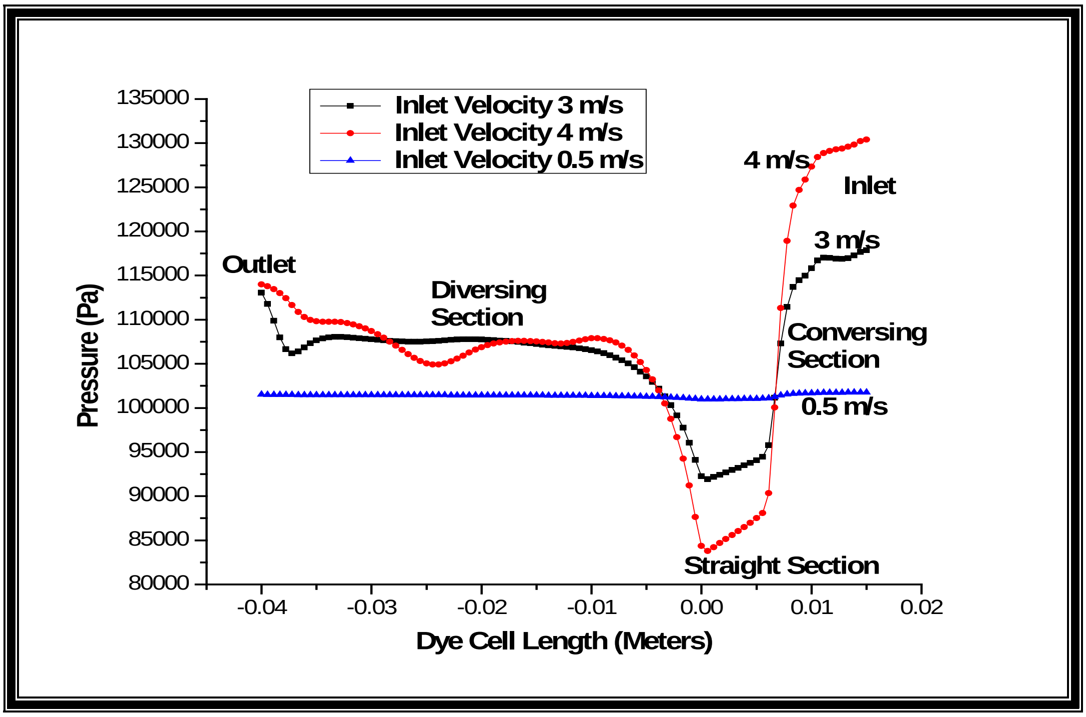

Fig 4.13: Pressure drop across the dye cell (Design – XIV)

It is observed that the pressure drop across the dye cell increases with increasing inlet flow velocity. The static pressure decreases as the flow area decreases from 35 mm^2 to 5 mm^2 and it regains as the flow area increases in the downstream direction. This dye cell has less permanent pressure loss in comparison to the dye cell with straight rectangular channel of 70 mm length. The computational result of pressure drop and recovery for three different inlet flow velocities is shown in figure 4.13.

4.15 Dye Cell Design Considerations

The dye cell used as active volume for dye laser is one of the vital components, which facilitate single mode operation at high repetition rate. The dye cell design has to be such that the flow channel in the dye laser reduces thermal and pressure variations in the flowing dye solution particularly in the vicinity of the active volume. The pump power and repetition rate are related to each other as increasing repetition rate demands increase in the velocity in the flow channel. The higher flow velocity in the dye flow channel results in self-heating due to wall friction. Eddies due to turbulence resulting in disturbances to the streamline and local cavitation in the solvent are some of the limiting conditions for increasing the flow velocity for a high repetition rate laser. The dye cell physical dimensions are very important for single mode operation as larger physical dimensions increase the cavity length, resulting in a smaller cavity FSR, which demands higher resolution from the grating for selecting one longitudinal mode without beam expanders. A judicious design of the dye cell flow channel having smaller physical dimensions and appropriate selection of active volume and pump powers helped solve this problem.

4.16 Fabrication of Dye Cells

Two dye cells were fabricated and the simulation results were verified by operating them in the SLM dye laser with high repetition rate (~ 9 kHz) CVL as the pump source. The dye cell is made of two stainless steel (SS) pieces precisely cut (wire EDM cut from a single SS block), polished (diamond polished surfaces) and welded together to form the flow channel of dimensions 10 mm x 1 mm x 70 mm and 5 mm x 1 mm x 70 mm. The dye solution flow direction was from top to bottom for both the dye cells. The C channels were engraved on two SS plates by wire cutting and they were welded together to form the flow channel. The top and bottom pieces were made from two SS blocks of required dimensions. The 6 mm OD and 4 mm ID SS tube of 30 mm length were welded at each SS block. The orientation can be seen from the fittings on the length side of SS block a rectangular slot was created by spark erosion process up to 5mm depth to accommodate the dye cell flow channel. A through hole of 4 mm ID was made along the length of the slot to match the flow channel area of 10 mm^2 of the dye cell with flow dimensions of 10 x 1x 70 mm. While for 5 x 1x 70 mm dye cell a rectangular slot of 5 mm^2 was created by spark erosion method to match the flow cross-sectional area of 5 mm^2. The 4 mm ID flexible polyurethane tubing **was** used for circulating dye solution through the dye cells.

A photograph of the fabricated dye cell with flow channel of 10 mm x 1 mm x 70 mm is shown in figure 4.14. Two optical quality broadband AR coated quartz windows $\left(\sim \lambda/_4\right)$ of diameter 20 mm and 2 mm thickness are fixed on the dye cell with Viton O rings, maintaining flow cross section area of 10 mm^2. This dye cell was made with tubular entry of 4 mm internal diameter tube to match the cross sectional area of flow channel with the area of flow entry. The flow channel was polished to avoid the flow disturbances in the stream.

Fig 4.14: Photograph of the SLM stainless steel dye cell (10 x 1 x 70 mm)

Fig 4.15: Photograph of the SLM dye cell (5 x 1 x 70 mm)

Two optical quality broadband AR coated quartz windows $\left(\sim \lambda/_4\right)$ of 10 mm diameter and 2 mm thickness are fixed on the dye cell of internal flow channel width of 5 mm x 1 mm x 70 mm with Viton O-ring seal. The fluid enters into the flow channel through a slit of 5 mm x 1 mm area for the 5 mm x 1 mm x70 mm dye cell. The photograph of the dye cell with flow channel of 5 mm x 1 mm x 70 mm is shown in figure 4.15. The performance of these two dye cells was experimentally tested by operating them in the single mode condition with the SLM dye laser system as described below.

4.17 Testing of Dye Cells with SLM Dye Laser

The simulation results with ethanol medium (viscosity 1.078 Cp and density 789 kg/m^3) for the dye flow channel of dimensions 10 x 1 x 70 mm was not able to demonstrate stable SLM operation with 9 kHz pulse repetition rate CVL pumping. There was frequent switching of modes from single mode to two modes for this dye laser. When this laser was operated with binary solvent, a stable single mode operation was established and the bandwidth of this laser was measured to be ~ 650 MHz. The SLM dye cell 5 mm x 1 mm x 70 mm was characterized with a flow system. The flow velocity in the dye cell was varied using a variable frequency drive (VFD) and flow characteristics were plotted as shown in figure 4.16.

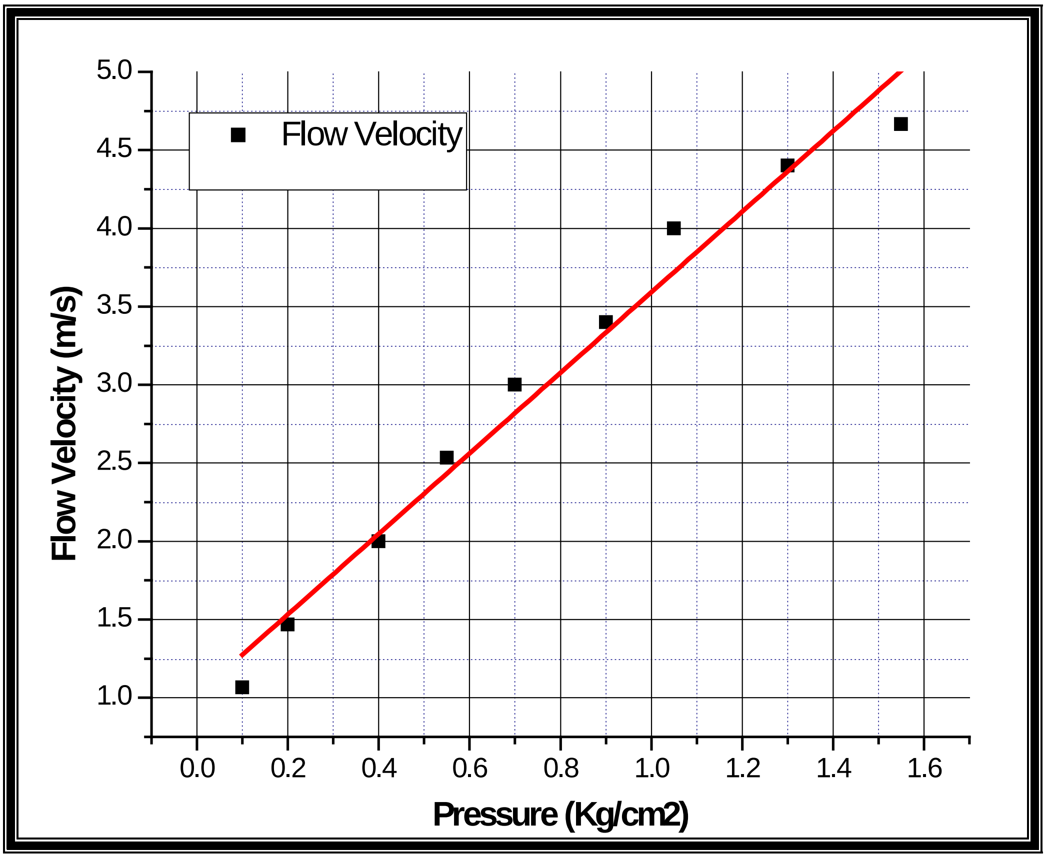

Fig 4.16: The line pressure versus flow velocity for the SLM dye cell.

A stable single mode operation with low viscosity solvent such as ethanol was established on reduction of the cross section area of the dye cell. A minimum time averaged line width of ~ 375 MHz was obtained with this dye cell. This line width is ~ 40% less than bandwidth obtained with binary solvent of 650 MHz for 10 mm^2 cross section dye cell. The dye flow control was done with variable frequency drive (VFD) to change the Reynolds number and thereby improve the passive frequency stability for the present SLM dye laser. The detailed characterization of the SLM dye laser is presented in Chapter – V of this thesis.

References

[4.1] D S Bethune, “Dye cell design for high power low divergence excimer pumped dye lasers”, Appl. Opt, Vol. 20, 1897 – 1899, 1981.

[4.2] R Chaube, “The effect of varying the hydraulic parameters of the flow cell in a dye laser pumped by a copper vapor laser Opt & Laser Tech.”, Vol 42, 819 – 827, 2010.

[4.3] W Wright, I S Falconer, “A transversely pumped prismatic dye cell for high power dye lasers”, Opt. Comm. Vol 67, 221 – 224, 1988.

[4.4] T Bultmann, D Bingemann, N P Emsting, D Shchwarzer, L Nikowa, “A new cell design for off-axis amplification of ultrashot dye lasers which uses total internal reflection”, Rev. Sci., Instruments Vol 66, 4393 – 4394, 1995.

[4.5] J Y Roncin, H Damany “Improved cell design for pulsed dye lasers”, Rev. Sci., Instruments Vol 52, 1922 – 1923, 1981.

[4.6] K A Stankov, “Compact high flow dye cell for laser pumped dye laser”, Rev. Sci., Instruments Vol 59, 666, 1988.

[4.7] P. Burlamacchi, R Pratesi, U Vanni, “Tunable supperradiant emission from planner dye laser”, Appl. Opt., Vol 15, 2684 – 2689, 1976.

[4.8] I G Koprinkov, K V Stamenov, K A Stankov, “High efficiency single mode dye laser”, Opt., Commun., 42, (1982), 264 – 266.

[4.9] F J Duarte, J A Piper, “Narrow linewidth, high prf copper laser pumped dye oscillators”, Appl Opt, Vol. 23, 1391 – 1394, 1984.

[4.10] R Chaube, “Design criteria and numerical analysis of a stable dye laser with a curved flow cell”, Opt. Engg. Vol 47, 014301 – 1, 2008.

[4.11] N Singh, “On the microstructure of thermal and fluid flow field in a lasing medium of a high repetition rate dye laser”, Optik, 121, 1642 – 1648, 2010.

[4.12] R Bhatnagar, N Singh, R Chaube, H S Vora, “Design of a transversely pumped high repetition rate narrow bandwidth dye laser with high wavelength stability”, Rev., Sci., Instru., 75, 5126 – 5130, 2004.

[4.13] E D Fatnes, “Master Thesis in Multiphase System, Process Technology, University of Bergen, May 2010.

[4.14] U Lekic, “Fluid flow and heat transfer in a Helium gas spring Computational Fluid Dynamics and experiment” PhD Thesis University of Twente, 2011.

[4.15] R W Fox, A T McDonald, “Introduction to Fluid Mechanics”, 4th Ed., John Wiley, Singapore, 1995.

[4.16] ANSYS CFX Solver Guide 2006.

[4.17] K S Abdol-Hamid, S J Massey, “Unified process Management system for Computational Fluid Dynamics (UPMS),” in 41st Aerospace Science Meeting and Exhibit, Reno Nevada 6 – 9 January 2003.

[4.18] T Y Song, S Park, B C Lee, Y O Lee, A R Junghans, “Development of a neutron TOF facility at KAERI”, Journal of the Korean Physical Society, 59, 1609 – 1612, 2011.

[4.19] F R Menter, M Kuntz, R Langtry, “Ten years of industrial experience with the SST Turbulence Model”, Turbulence, Heat and Mass Transfer 4, K Hanjalic, Y Nagano, M Tummers (Ed.) Begell House Inc. 2003.

[4.20] Jr J D Anderson, “Computational fluid dynamics – The basics with applications”, McGraw Hill Inc. 1995.

[4.21] J H Ferziger, M Peric, “Computational method for fluid dynamics”, 3rd Ed., Berlin Springer – Verlag 2001.

[4.22] A K Pozarlik, D Panara, J B W Kok, T H vander Meer, “Heat transfer in a recirculation zone at steady state and oscillating conditions the back facing step test case”, 5th European Thermal Sciences Conference, The Netherlands, 2008.

[4.23] Z Burshtein, D Levron, G Bialolenker, “Thermally induced refractive index in dye laser cell”, Comp. Phys. Comm. 51, 349- 353, 1988.

[4.24] I Itzkan, F W Cinningham, ”Oscillator – Amplifier dye laser system using N_2 laser pumping”, IEEE J Quantum Electronics, QE – 8, 101 – 105, 1972.

[4.25] N Singh, “Fluctuations in near 360^O curved and straight channel dye cells for high repetition rate copper vapour laser pumped dye laser”, J Phys, D: Appl. Phys. 39, 2084 – 2089, 2006.

[4.26] R L St Peters, D J Taylor, “Face pumped high average power low distortion dye laser”, Appl., Phys Lett., 23, 90 – 91, 1973.

[4.27] G R Holtom, W M McClain, “Design of a dye laser for nonlinear spectroscopy”, Opt., Comm., 22, 153 – 155, 1977.

[4.28] M F Passos, A R R Bineli, V P Bavaresco, A L Jardini, R M Filho, " Application of CFD simulation to Localized Cure pHEMA Using infrared laser", Chem., Engg., Transactions, 24, 1465 – 1470, 2011.

[4.29] P Apanasevich, D Lucas, T Hohne, "Pre-Test CFD simulations on topflow – PTS experiments with ANSYS CFX 12.0", CFD4NR – 3 Workshop on Experimental Validation and application of CFD and CMFD codes to Nuclear Reactor Safety Issues Washington D.C., USA 14 – 16 September 2010.

[4.30] P M Burban, H A Hegna, "Equipping engineers to solve computational fluid dynamics in senior design: Challenges and successes using a commercial CFD package", American Society for engineering education, IPFW March 31 – April 1, 2006.

[4.31] A R Miroliaei, F Shahraki, H Atashi, "Computational fluid dynamic simulations of pressure drop and heat transfer in fixed bed reactor with spherical particles", Korean J Chem., Eng., 28, 1474 – 1479, 2011.

Chapter – V

CHARACTERIZATION OF SLM DYE LASER

5.1 Introduction

The tunable pulsed dye laser discussed in this thesis was specifically designed for SLM operation using GIG cavity. This SLM dye laser was pumped by CVL operating at 9 kHz pulse repetition rate and pulse width of a few tens nano-seconds (~30 ns). This chapter discusses the characterization and performance of GIG SLM pulsed dye laser based on Littman type configuration.

A schematic of the SLM laser is shown in figure 2.20. It has a cavity of length about 50 mm. The cavity optics consists of an end mirror (R > 99 %), a strip-tuning mirror (R > 99%) and a holographic grating. The details of dye cell design and construction are discussed in Chapter – IV of this thesis. The metallic dye cell is made of stainless steel having two replaceable optical quality quartz windows of 2 mm thickness with 1 mm dye flow channel: the total physical thickness of the dye cell is 5 mm. The dye cell of internal dimensions 5 x 1 x 70 mm was mounted in the center of the rotation table and was tilted with respect to the vertical axis by nearly 5^{O} to prevent parasitic oscillation at the windows. The dye cell windows are an anti reflection coated to avoid sub cavity resonances inside the dye cell. All the components of the SLM dye laser were mounted on a two stage differential rotary table. The first stage provides the coarse movement with a minimum resolution of 25.92 arc-secs (~ 46 pm) with a stepper motor of 50,000 micro-steps per revolution. The second stage, which is used for the fine motion utilizes an 80 μm PZT with drive voltage of 150 V and gives a minimum resolution of 0.0014 arc-secs (~ 4 fm) at 80 mm arm length. A piezoelectric transducer (PZT) stack is fixed to the end mirror with an adapter, which provides a maximum displacement of 8 μm at a drive voltage of 150 V; the details of tuning mechanisms are discussed in the Chapter – III of this thesis. The cavity length of ~ 50 mm provides axial mode separation of ~ 3 GHz, which is larger than the single pass width ~ 1.57 GHz of the dye laser cavity; this makes it possible to obtain lasing of the dye laser in SLM. The green beam (510.6 nm) of CVL operating at 9 kHz repetition rate was focused into the dye cell with a plano convex lens of focal length 200 mm. The focusing lens was mounted on a linear translation stage for precise control over the focal spot. The 0.2 mM Rhodamine 6G in ethanol was circulated in the dye cell with a gear pump of 1 to 10 lpm flow capacity and the flow was controlled between 5 and 50 Hz by a variable frequency drive (VFD).

The flow velocity was measured to be 3.6 m/sec, which provides a clearance ratio of two for 9 kHz pulse repetition rate and gain width of nearly 200 µm. The diameter of the focal spot in the gain medium was ~ 200 µm. The focal spot was located in front of the dye cell, which avoids both damage to the dye cell windows and thermal distortion in the dye active medium. The pump beam diameter should be approximately matched to the mode diameter of the dye laser for maximum utilization of pump power in the single mode dye lasers. The photograph of the SLM dye laser mounted on the monolithic vertical wall with the help of four anchor bolts is shown in figure 5.1.

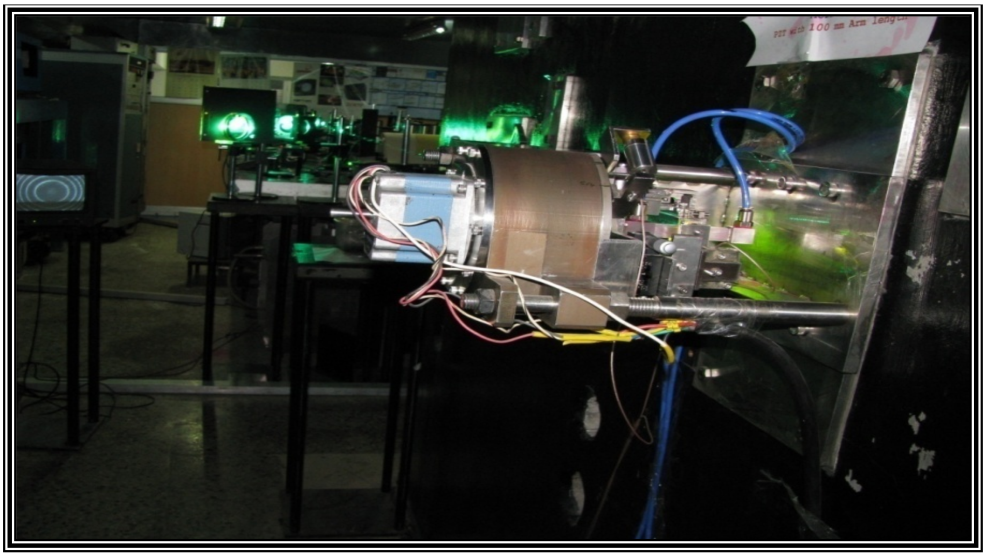

Fig 5.1: SLM dye laser mounted on a vertical wall pumped by CVL at 9 kHz

5.2 Dye Flow System for SLM Dye Laser

The dye flow system consists of a dye solution reservoir (capacity ~ 3 liters), a magnetically coupled gear pump of 10 lpm capacity to circulate the dye solution, a heat exchanger coil fully immersed into the dye solution, a 10 µm polypropylene filter for filtering photo degraded products, a temperature sensor, a pressure gauge, flow switch and a tuning fork based level sensor. The dye reservoir was connected to the inlet of magnetically coupled gear pump. The speed of the three phase motor (ATEX), which is magnetically coupled with gear pump, is controlled by the variable frequency drive (VFD). The main advantages of this pump are absence of dynamic seal; smooth flow, self-priming and a direct relation between pump speed and flow rate.

The schematic of the dye flow system is shown in figure 5.2. The outlet of the gear pump was connected to the inlet of the dye cell. The outlet of the dye cell was connected back to the dye solution reservoir in a closed loop. Legris quick release connectors (QRC) are used in the dye flow system for connecting them to the SLM dye cell at locations A and D and rotatable elbows are used at locations F and G for providing cooling water to the heat exchanger coil in the dye flow system. The dye solvent enters into the dye cell from a slit of 5 x 1 mm^2 cross section with a 6 mm diameter tubular header. The signal from the liquid level indicator in the reservoir and the flow switch status are monitored and recorded. The signal cables and the power cables are terminated separately with shell connectors in a separate plate attached to the dye flow system. A 250 watt explosion proof immersion heater was provided inside the dye reservoir. The heater was powered by a Euro therm thyristor power pack, whose voltage was controlled by proportional integral differential (PID) controller. The temperature sensor PT – 100 measured the temperature and EUROTHERM PID controller provided power to the heater proportional to the difference between the measured temperature and the set temperature.

5.3 Selection of Single Longitudinal Mode

The critical parameters for stable SLM operation are the angle of incidence of the grating and the cavity length. Holographic grating with 89^0 angle of incidence provides large dispersion for the selection of SLM for the dye laser.

The single pass line width ($\Delta\nu_{single}$) of the grating mirror pair is given by [1.16]

$$\Delta\nu_{single} = \frac{\sqrt{2}\,c}{\pi w\,(Sin\ \theta + Sin\varphi\,)} \tag{5.1}$$

where $\Delta\nu_{single}$ is grating pass band, c is the velocity of light, w is the illuminated grating length, θ is the incidence angle and φ is the diffraction angle. The single pass line width calculated from equation 5.1 is 1.56 GHz FWHM for grating length of 60 $x10^{-3}$ m, incidence angle of 89.5^O and the diffraction angle of 26^O. Since the single pass line width is half of the mode spacing, only single longitudinal mode is selected by the cavity. The mechanism for the selection of single longitudinal mode is shown in figure 5.3.

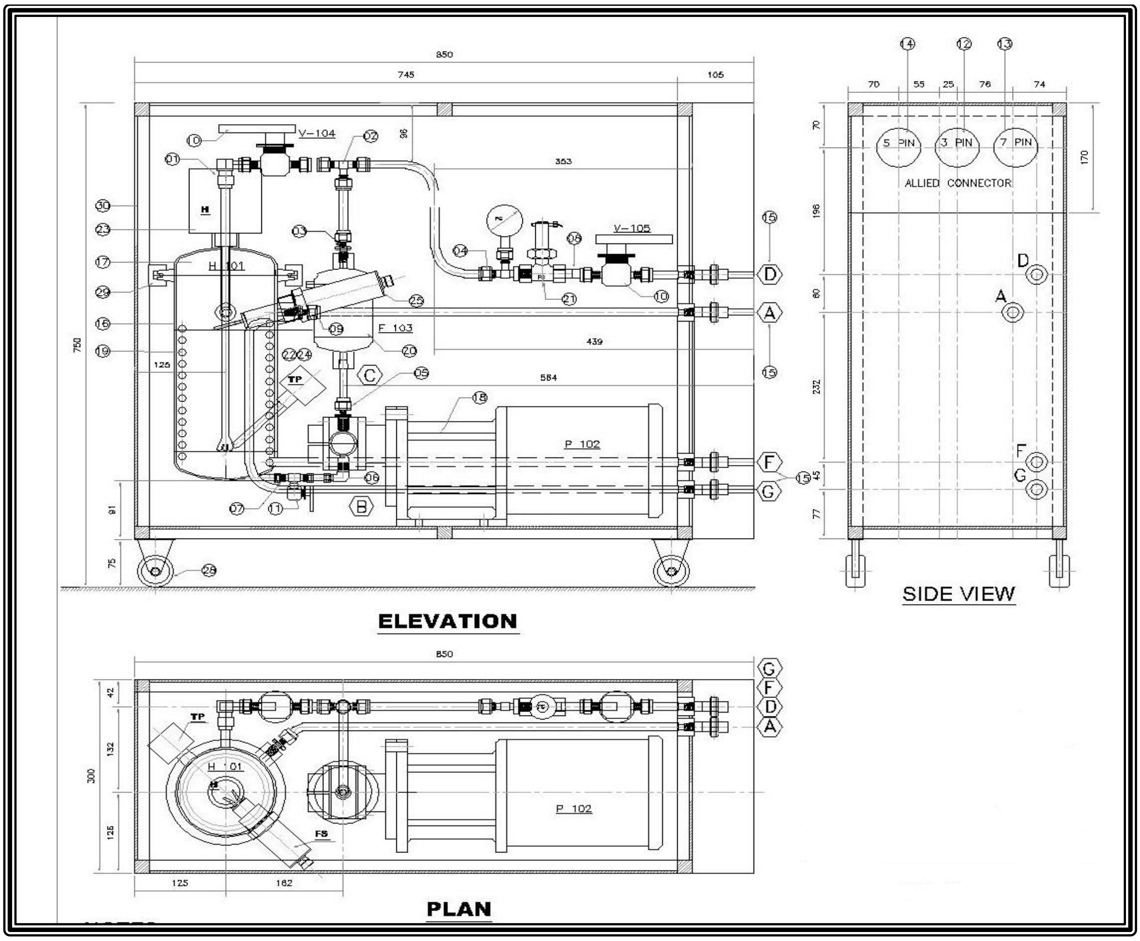

Fig 5.2: Schematic of the dye flow system for SLM dye laser

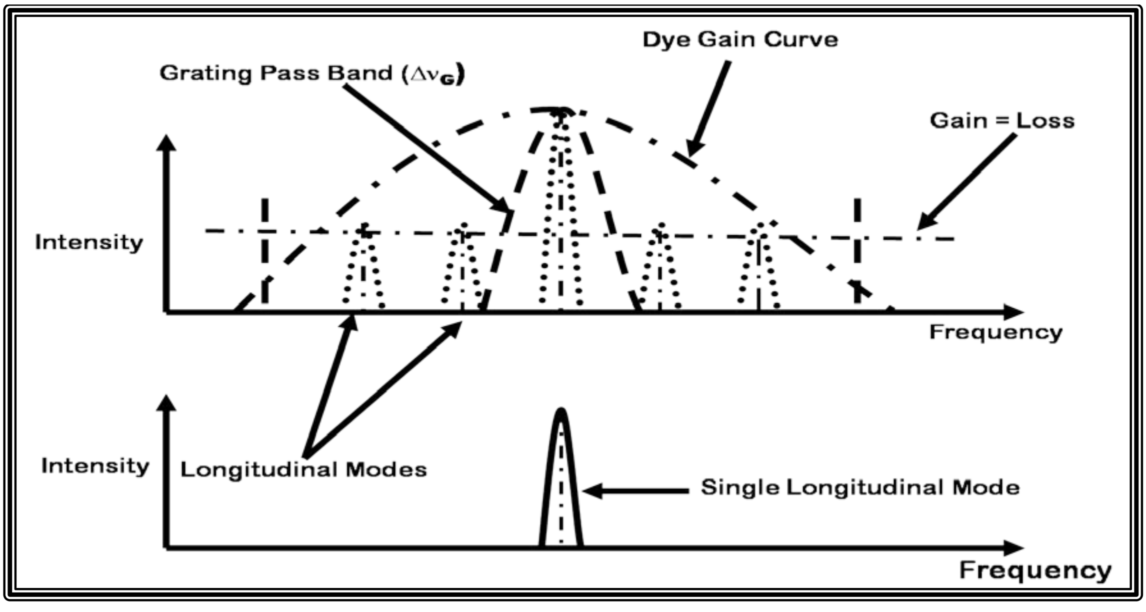

Fig 5.3: Selection of single mode in the SLM GIG cavity

The cavity length tuning of the SLM dye laser is limited to the grating pass band as the spacing of the intracavity modes will change within the transmission window set by the grating. Whenever, the wavelength change was more than the grating pass band, a mode hop takes place to compensate for the wavelength change. This has been experimentally observed and discussed at length in Chapter – VI of this thesis.

5.4 Parametric Characterization of SLM Dye Laser

In this section of the thesis, the parametric characterization of the SLM pulsed dye laser is presented in detail. The green beam (510.6 nm) of CVL operating at 9 kHz repetition rate was focused into the dye cell with a planoconvex lens. The CVL beam size was telescopically reduced from 40 mm to 10 mm and spatially filtered using a pinhole of diameter 700 µm. Two dichroic beam splitters were used to reduce the yellow (578 nm) content below 1% of the pump beam. About 1.5 Watt of the green CVL beam was used for pumping the SLM dye laser. The 0.2 mM Rhodamine 6G dissolved in ethanol was circulated in the dye cell. The cooling water at a constant temperature of 293 K was circulated through the heat exchanger. The cooling water temperature was controlled in the temperature band of ± 0.1 K in the 15 liter capacity tank. The large volume of dye reservoir capacity (~3 liters) was helpful to minimize the temperature drift. The dye solution temperature could be maintained at around 295 ± 0.10 K. Nearly 30 mW of tunable single mode dye laser output was obtained with conversion efficiency of 2 %.

5.4.1 Single Mode Spectrum of SLM Dye Laser

The time averaged linewidth was measured by Fabry Perot etalon for the SLM dye laser. The SLM operation of the dye laser was verified by monitoring the spectral output of Fabry – Perot (FP) etalon of 7.5 GHz FSR and reflective finesse of 30. A small portion of the SLM dye laser was coupled to a 62.5 µm core diameter optical fiber and a diverging output from the optical fiber was directed onto a FP etalon (FSR ~7.5 GHz). The circular fringes at the output of FP etalon were focused with a spherical lens of 500 mm focal length onto a CCD camera. The output of the CCD camera was interfaced to a personal computer (PC) with a frame grabber card. Figure 5.4 shows the FP etalon fringes of SLM dye laser. From the F P fringes the laser was found to oscillate in a single mode. The FP etalon FSR (7.5 GHz) was multiplied by the ratio of width (FWHM) of the second fringe to the separation between the first and second fringe as shown in figure 5.5 for estimating the linewidth. The spectral linewidth of the laser was measured by the F P etalon in conjunction with a wavelength meter (Angstrom WS-7L). The time averaged linewidth measured by F P etalon was 400 MHz. The SLM bandwidth measured by the laser wavelength meter was 0.4 pm (~ 385 MHz), while lasing at 563.65694 nm as shown in figure 5.6. The wavelength was measured with relative accuracy of 60 MHz. The central stepper motor of the tuning assembly was locked by applying holding current to the stepper motor.

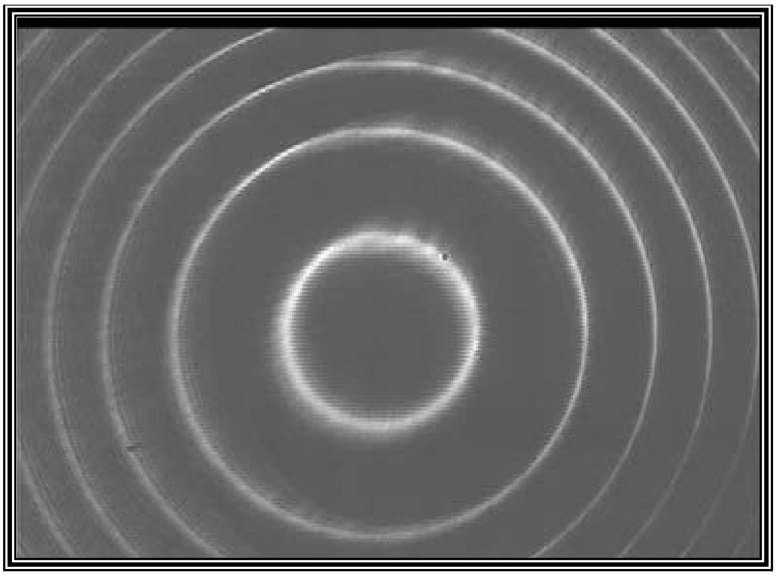

Fig 5.4: Typical Fabry Perot fringe of single mode dye laser with etalon of FSR 7.5 GHz.

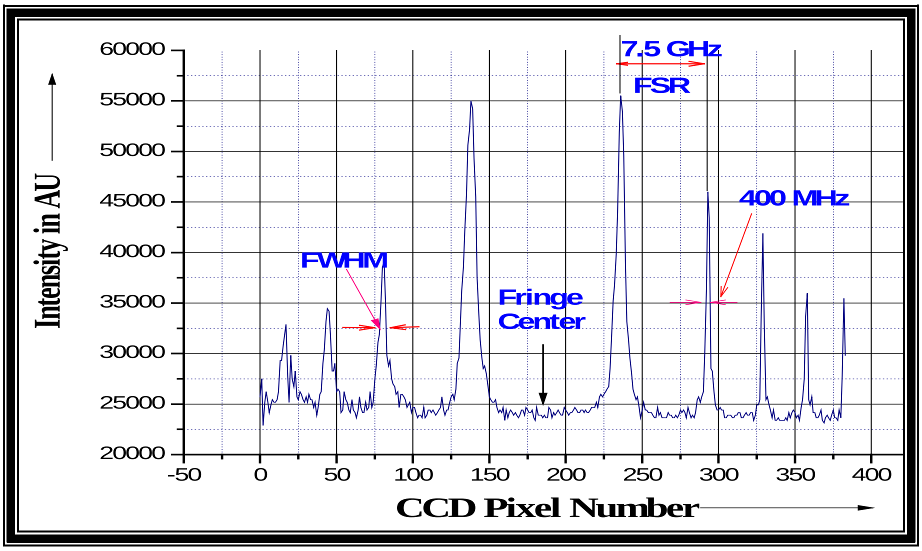

Fig 5.5: Intensity pattern of FP etalon fringe of SLM dye laser, measures time averaged bandwidth of 400 MHz

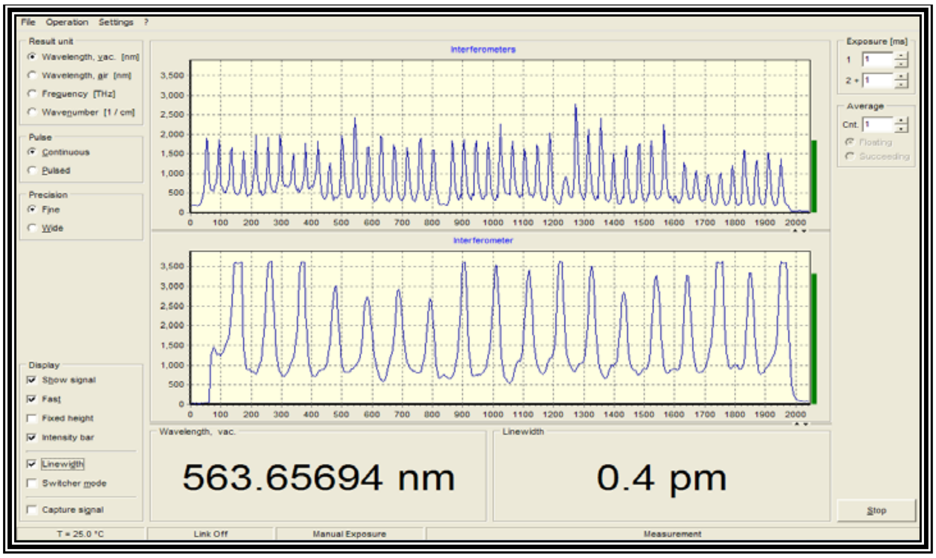

Fig 5.6: Wavelength and bandwidth measured by laser wavelength meter (WS – 7L) for GIG SLM dye laser pumped by 9 kHz CVL

It was observed when the pump power is increased beyond 3.5 Watts; the laser begins to oscillate in two modes. Figure 5.7 shows the two mode oscillation of the SLM dye laser with higher pump power of 4 watts.

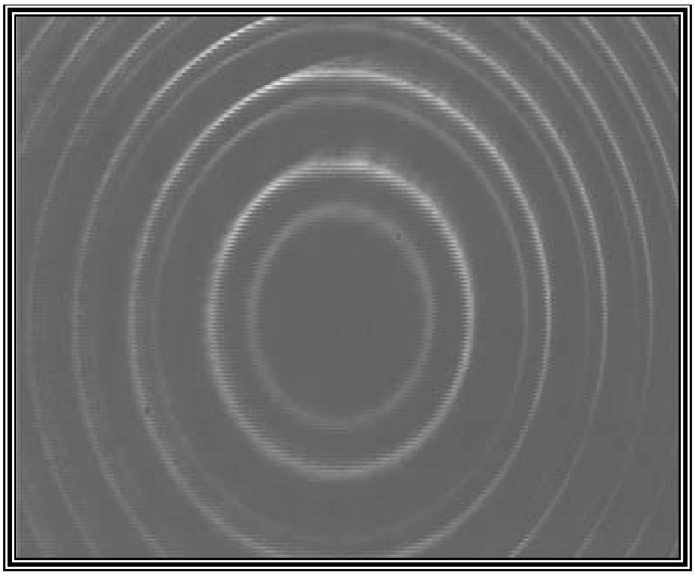

Fig 5.7: Two mode oscillations for SLM dye laser pumped by CVL at a pump power of more than 3.5 Watts

5.4.2 Single Pulse Spectrum of SLM Dye Laser

For capturing single pulse spectrum for SLM dye laser a fast CCD camera (Pixelfly qe, PCO AG) was used. A normal CCD camera was replaced with a fast CCD camera in the linewidth measurement set-up of the SLM dye laser. This fast CCD camera was externally triggered from the trigger signal of the CVL operating at 9 kHz pulse repetition rate to measure the single shot single pulse linewidth of the SLM dye laser using a FP etalon of FSR 7.5 GHz. The single pulse bandwidth of SLM dye was measured to be 315 MHz. Figures 5.8 and 5.9 show the FP etalon fringes and intensity variation along the fringe diameter respectively obtained with external triggering of the fast CCD camera.

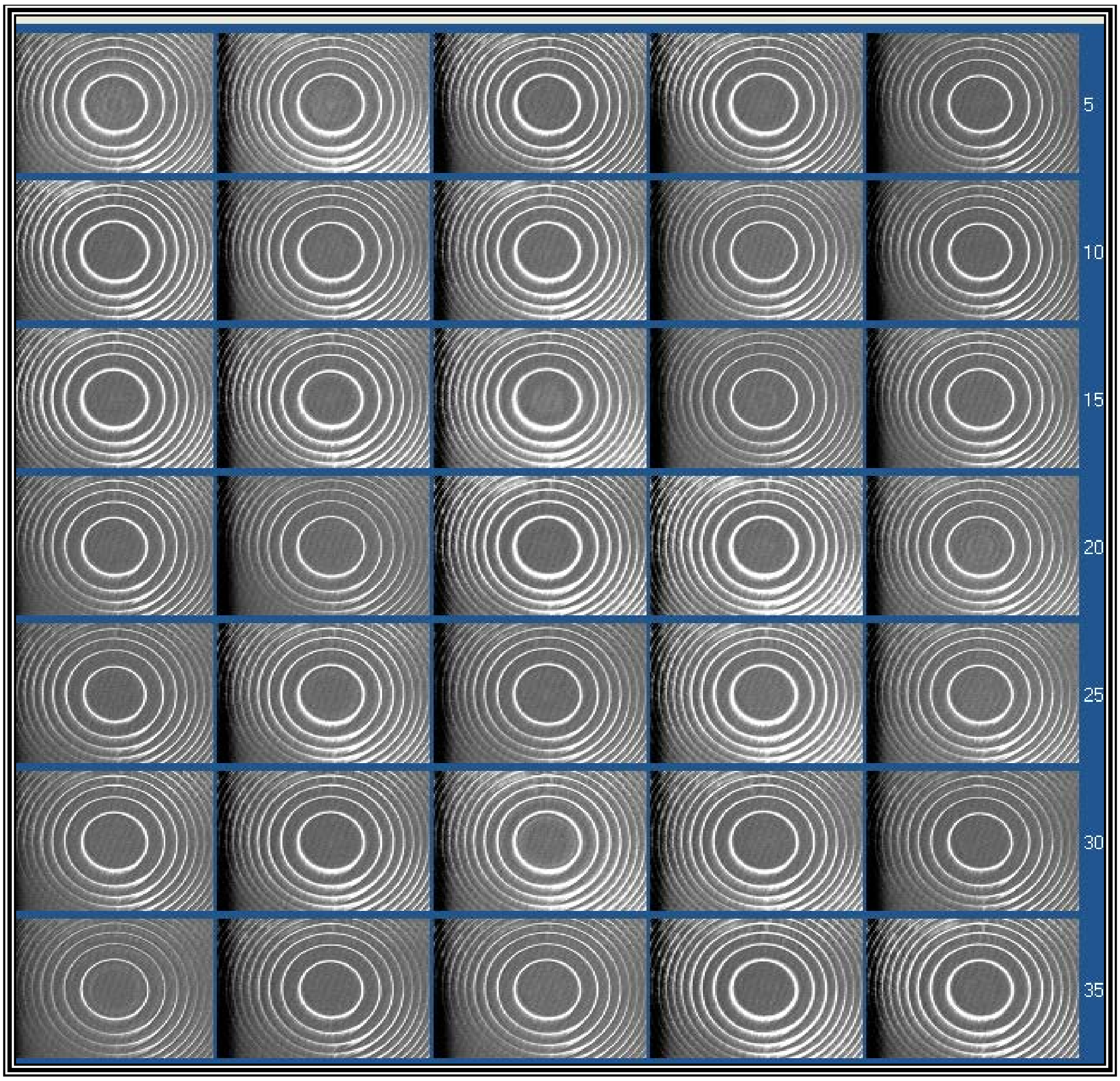

Fig: 5.8: Single pulse spectrum for 35 pulses of the CVL pumped SLM dye laser

All the thirty five frames of the single shot FP etalon fringes show single mode oscillation for every pump pulse. These experimental results show that the single pulse linewidth of the SLM dye laser was nearly 21 % smaller than the time averaged linewidth for the SLM dye laser for the same operating parameters.

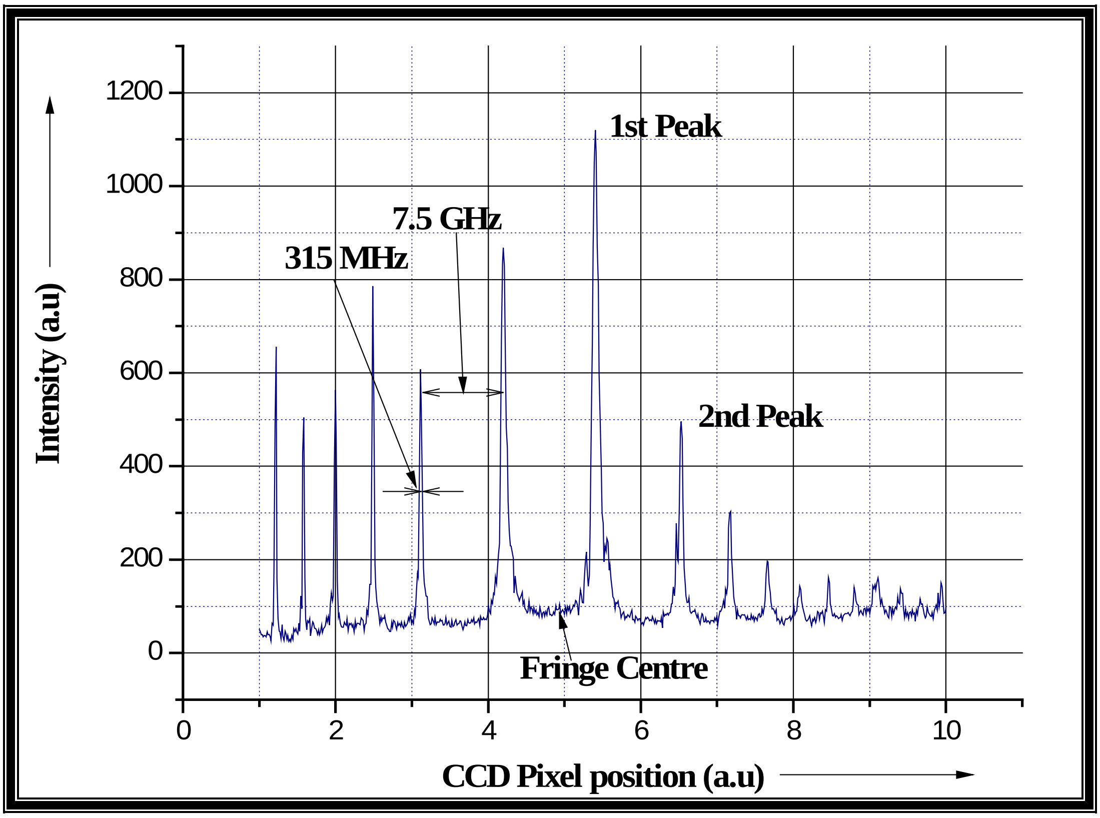

Fig 5.9: Intensity pattern for a FP etalon fringe of a single pulse of the SLM dye laser pumped CVL

5.4.3 Wavelength Tuning for SLM Dye Laser

The wavelength meter (Angstrom WS 7L) measured with an absolute accuracy of 60 MHz and a relative accuracy of 10^{-7}. The tuning range of SLM dye laser was from 554 nm to 566 nm (~ 12 nm) by rotating the tuning mirror of the SLM dye laser with 0.2 mM Rhodamine 6G dye solution in ethanol. The tuning range of SLM at two different pump powers is shown in figure 5.10. At higher pump power the tuning range is seen to increase by 5 nm and increase in the tuning range is more towards the higher wavelength region. It was observed that the tuning range and the peak wavelength of the SLM dye laser are dependent on the dye concentration for Rhodamine 6G in ethanol. The peak wavelength was red shifted by 4 nm as the dye concentration is increased from 0.15 mM to 0.5 mM. The tuning range was measured to be 9 nm (553 – 562 nm) for 0.15 mM dye concentration, while for 0.5 mM dye concentration the tuning range increased to 14 nm (554 – 568 nm) for the same configuration of the SLM. It was observed that the increase in the tuning range was towards the red region as shown in figure 5.11. The pump power needed for higher dye concentration was smaller than that required for the lower dye concentration due to higher availability of gain. The SLM output power is increased by ~ 45 % as the dye concentration is increased by a factor of 3.

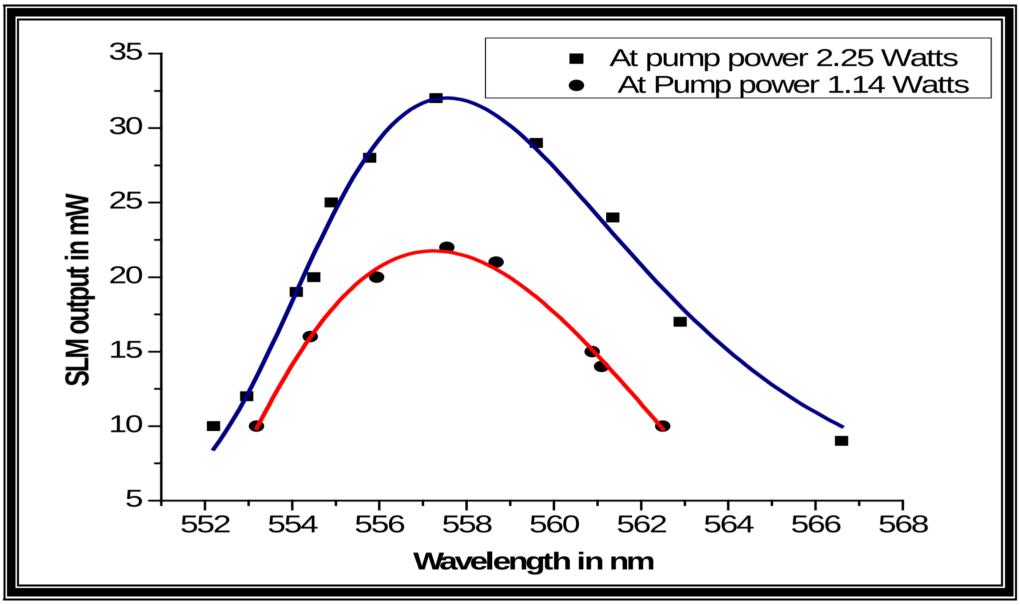

Fig 5.10: Laser tuning range of two pump powers (a) 2.25 Watts (b) 1.14 Watts

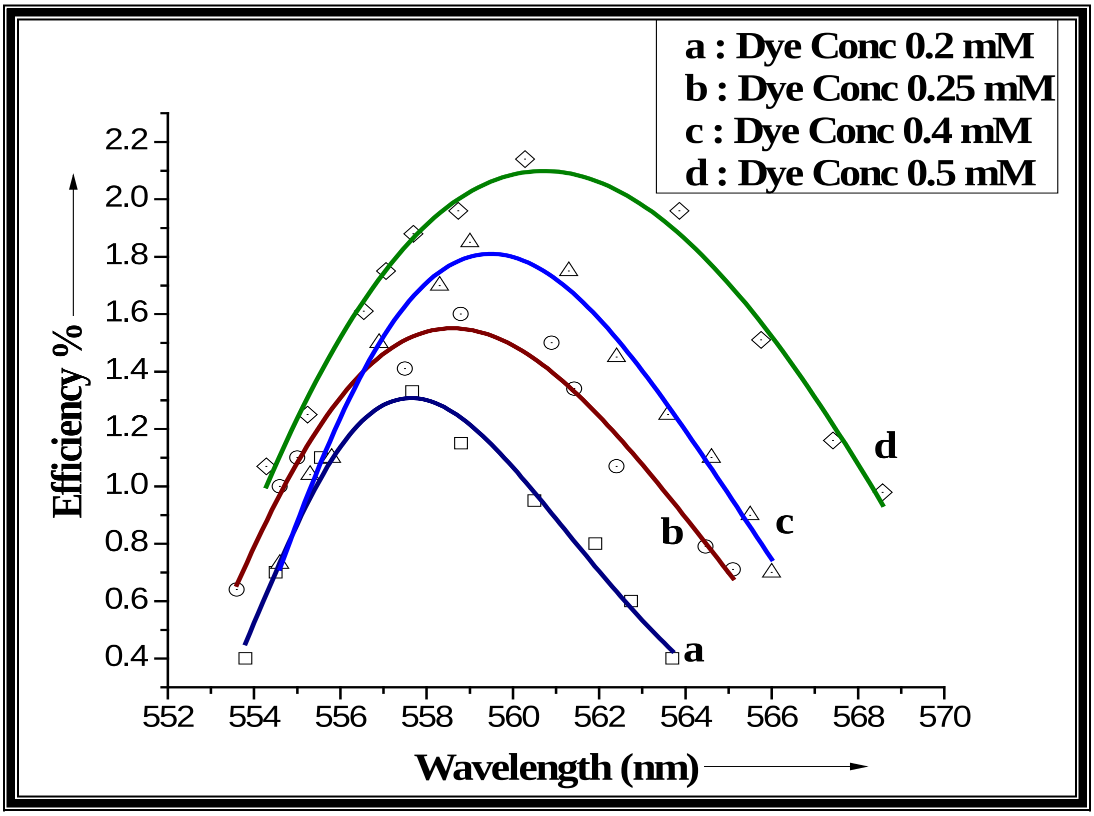

Fig 5.11: Wavelength tuning ranges for different dye concentration of Rhodamine 6G in ethanol. (a) 0.20 mM, (b) 0.25 mM, (c) 0.40 mM, (d) 0.50 mM

The peak wavelength of SLM dye laser is around 560 nm. It is reported that the peak wavelength for Rhodamine 6G is blue shifted in the SLM GIG configuration in comparison to the lower loss cavities such as the Littrow configuration due to its higher lasing threshold [2.30]. The peak wavelength around 570 nm has been observed in the low loss dye laser cavities. At larger diffraction angle, the diffraction efficiency of the grating is reduced, hence the loss line for the resonator is higher. To compensate for the higher losses higher gain is required for the laser oscillation to build inside the cavity. The high gain leads to the onset of the superradiance in a pulsed dye laser [1.24]. There is a competition between the onset of lasing and superradiance inside the laser cavity. At a lower wavelength (~ 554 nm) intracavity photon flux grows faster at the expense of the gain while at higher wavelength (~ 564 nm) the superradiance dominates and lasing reduces to a bare minimum. Hence, a larger incidence angle of the grating (higher threshold) resulted in a blue shift of the peak wavelength and led to a decreased range of tuning.

5.4.4 Mode Hop free Tuning of SLM Dye Laser

When the tuning mirror is rotated to scan the laser frequency, there is a mismatch between the feedback frequency determined by the grating pass band (say λ_G) and the cavity mode frequency (say λ_L) determined by the cavity length. In order to achieve mode hop free smooth wavelength scanning in the SLM dye laser, the cavity mode frequency should exactly match the feedback frequency ($\lambda_0 = \lambda_G = \lambda_L$). When the cavity is tuned, the comb of cavity modes ($\Delta\lambda_L$) shifts proportional to the change in resonator length in the direction of tuning. The dispersion linewidth ($\Delta\lambda_G$) also shifts in the direction of tuning, but is proportional to the angle of the tuning mirror. Single mode tuning without mode hop is achieved when the comb of cavity modes and the dispersion bandwidth shift together [1.16]. This implies that the cavity length and the angle are coupled in the tuning process and must be controlled simultaneously. This can be achieved by rotating the tuning mirror about the common pivot point such that the variation of optical length of the cavity does not alter the index of the longitudinal mode. It is reported in literature, [3.1,5.2] that with the positional accuracy of 50 μm in pivot point frequency scanning of 20 cm^{-1} can be achieved. To achieve mode hop free scanning in the experimental SLM dye laser, the axis of rotation of the tuning mirror passes through a geometrically located point, where the surface planes of the tuning mirror, end mirror and the grating intersect.

Mode hop free scanning requires high precision rotation of the tuning mirror, since the mechanical displacement equivalent to half wavelength, 0.25 to 0.3 μm in this case, can result in mode hopping. This laser was remotely tuned with a 20 μm PZT by applying a slowly varying voltage (ramp) from 0 – 150 V.

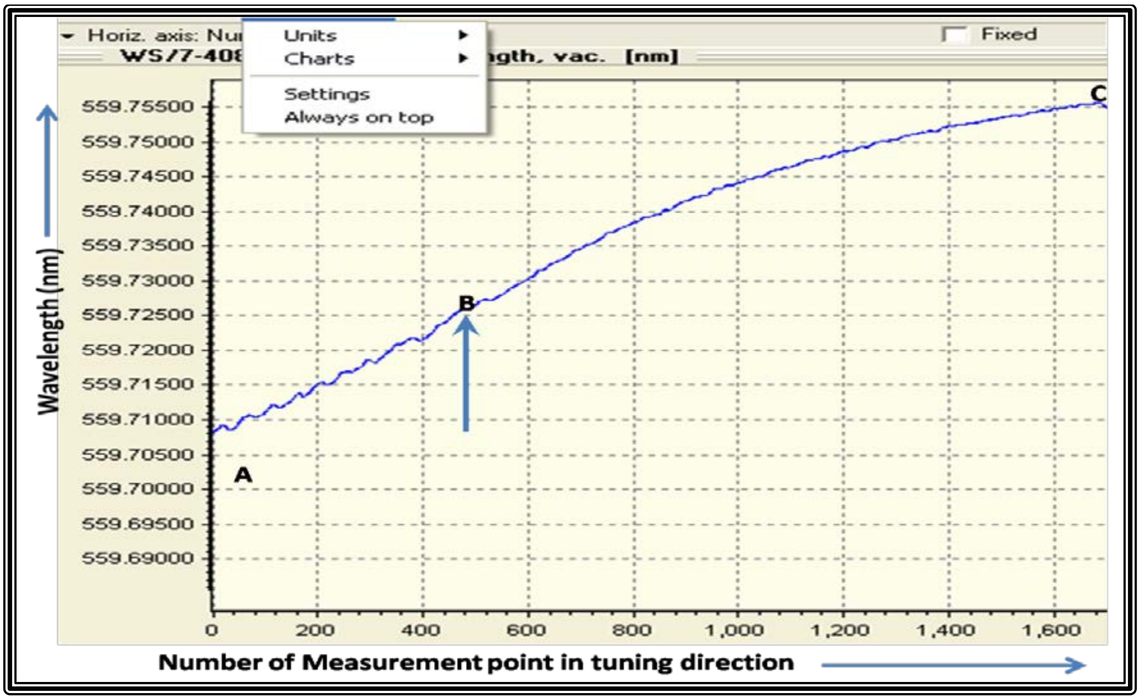

Fig 5.12: Typical tuning of the SLM dye laser pumped by CVL (X-axis wavelength (nm) and Y- axis number of measurements in tuning direction)

The input signal was generated from the computer and fed to the high voltage amplifier of the PZT. The high voltage signal was fed to the PZT actuating the tuning mirror. Using this technique mode hop free tuning over a wavelength range from 559.75556 nm to 559.68245 nm (~ 70 GHz) was achieved. The SLM wavelength and FP fringes were monitored simultaneously, so the sudden jump in the SLM wavelength by one cavity FSR could be detected during scanning. Jump in the SLM wavelength by one cavity FSR, which corresponds to mode hop, was not observed over 70 GHz of scan width.

Figure 5.12 shows the tuning of the SLM dye laser from wavelength 559.708 nm to 559.725 nm point A to point B, shows mode hopping, while from wavelength 559.727 nm to 559.755 nm point B to point C tuning without mode hop for ~ 29 GHz. From point A to point B mode hop occurs 8 times while tuning the SLM dye laser as the pivot point was not precisely matched.

5.4.5 ASE Measurement for SLM Dye Laser

In the output characteristics of a SLM dye laser, apart from the tuning range, bandwidth and fluence, the spectral purity of the laser (expressed in percentage of signal radiation in the total output) is also very important for spectroscopic applications. The main source of spectral impurity is ASE of the oscillator itself. The contrast ratio of narrow band laser output with respect to ASE for conventional transversely pumped dye laser is as high as 100 at the peak of the lasing wavelength and falls to unity at the edges of the tuning range [1.24]. The high gain in the pulsed dye laser results in higher ASE, which may be comparable to the output energy at the edge of the tuning range.

The ASE was measured in the SLM signal at various dye concentrations ranging from 0.15 mM to 0.5 mM for Rhodamine 6G dye in the ethanol. It is seen that the contribution of ASE is always more towards the edges of the tuning curve for each concentration. The contribution of ASE in the SLM signal was also found to increase with increasing dye concentration as shown in figure 5.13.

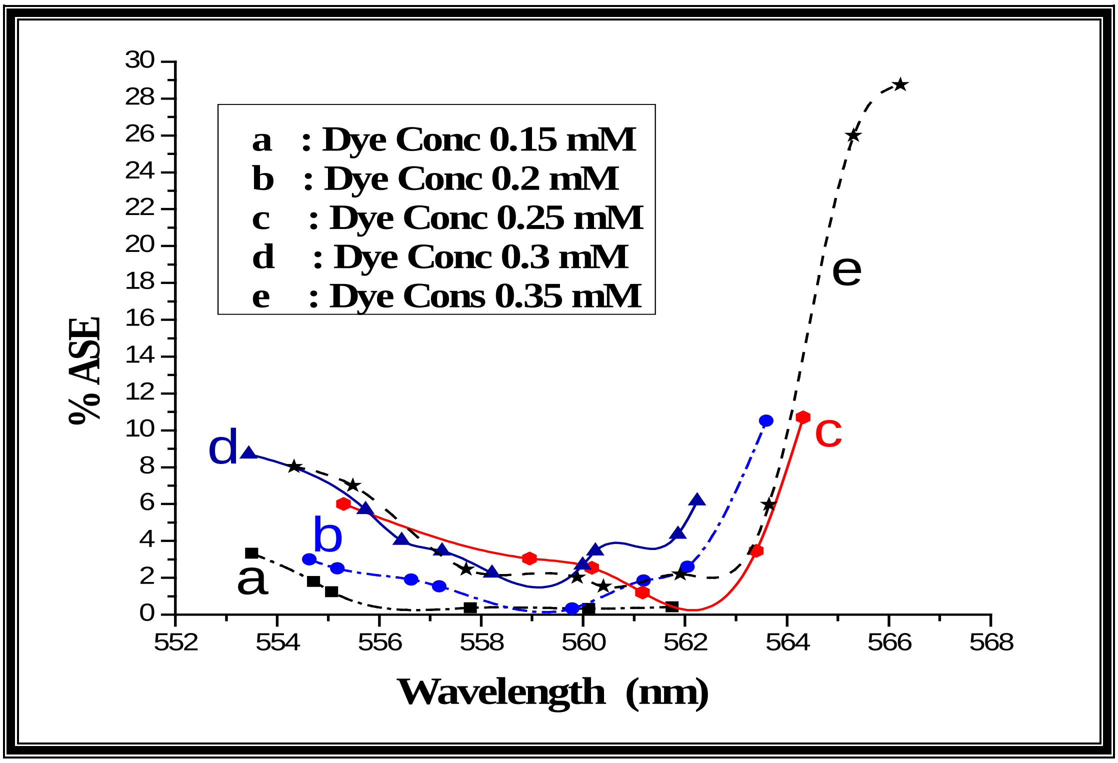

Fig 5.13: ASE present in the SLM signal for different dye concentration of Rhodamine 6G dye (a) 0.15 mM, (b) 0.20 mM, (c) 0.25 mM, (d) 0.30 mM, (e) 0.35 mM

The ASE was measured by feeding the SLM dye laser to a monochromator (Applied Photophysics Ltd, London; model No. F 3.4) that spatially separates the ASE from the signal. The ASE and signal were separately measured by a photodiode. As shown in figure 5.14, the ASE is about 20 – 30 % at the edges of the tuning range and ~ 2% at the centre wavelength for higher dye concentration. Similar behavior is observed at lower dye concentrations also. The ASE is nearly 0.33% at the center wavelength and about 10 – 15 % at the edges of the tuning range. This is due to low effective gain available for the SLM dye laser in the edges. Here the ASE is as high as nearly 50 % at the edges of the tuning range. The ASE was measured with an accuracy of 0.01%.

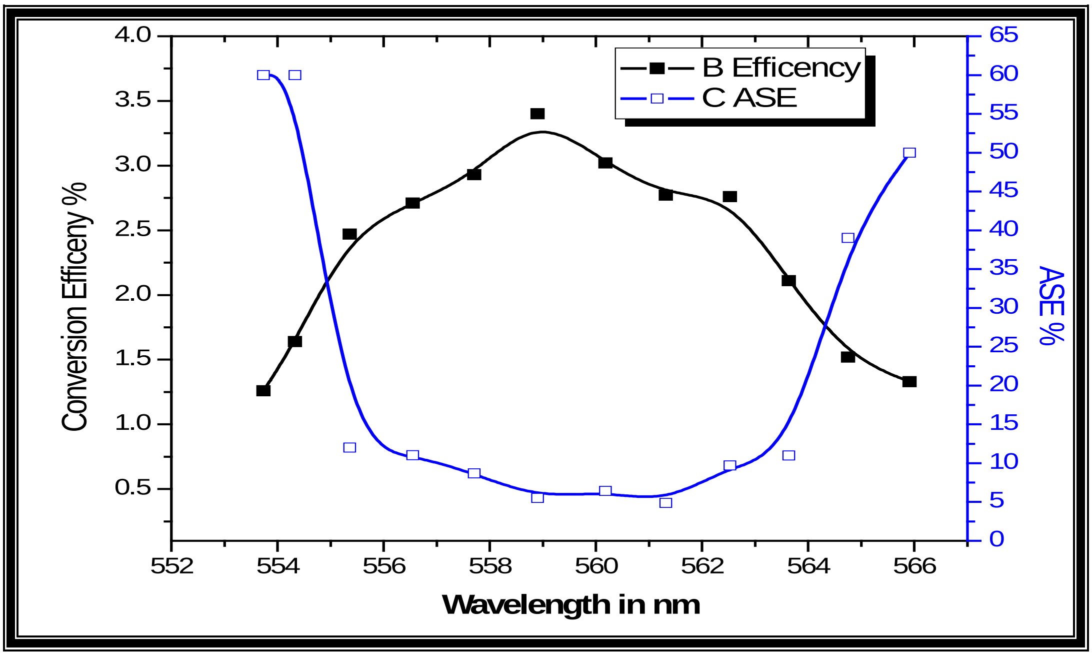

Fig 5.14: ASE versus wavelength for SLM dye laser for Rhodamine 6G

5.4.6 Measurement of Buildup Time of SLM Dye Laser

In the SLM dye laser, the laser pulse is delayed with respect to pump pulse because several round trips are required for building the laser radiation inside the resonator cavity. This delay between the pump pulse and the SLM dye laser pulse is known as the buildup time [5.1]. In order to measure the buildup time, the SLM dye laser and CVL pump laser beams were fed to two photodiodes. The output of lasers was observed on photodiodes (FND 100) in conjunction with a four channel oscilloscope (Tektronix TDS 724D, 500 MHz). The synchronization of the two signals was ensured by appropriately locating the photodiodes for pump and SLM beams and using the same length of BNC cable for both the photodiodes. The SLM pulse buildup time was experimentally observed to be strongly dependent on the pump power, resonator parameters such as grating diffraction efficiency and wavelength of dye laser in the tuning range. The experimental observations are enumerated below.

5.5.6.1 Effect of Pump Power: Figure 5.15 shows the dependence of SLM buildup time on pump power for a laser dye Rhodamine 6G concentration of 0.2 mM in ethanol. It can be seen that the laser buildup time is 11.7 ns for pump power of 3 watts, while the buildup time is 15 ns for pump power of 1 watt.

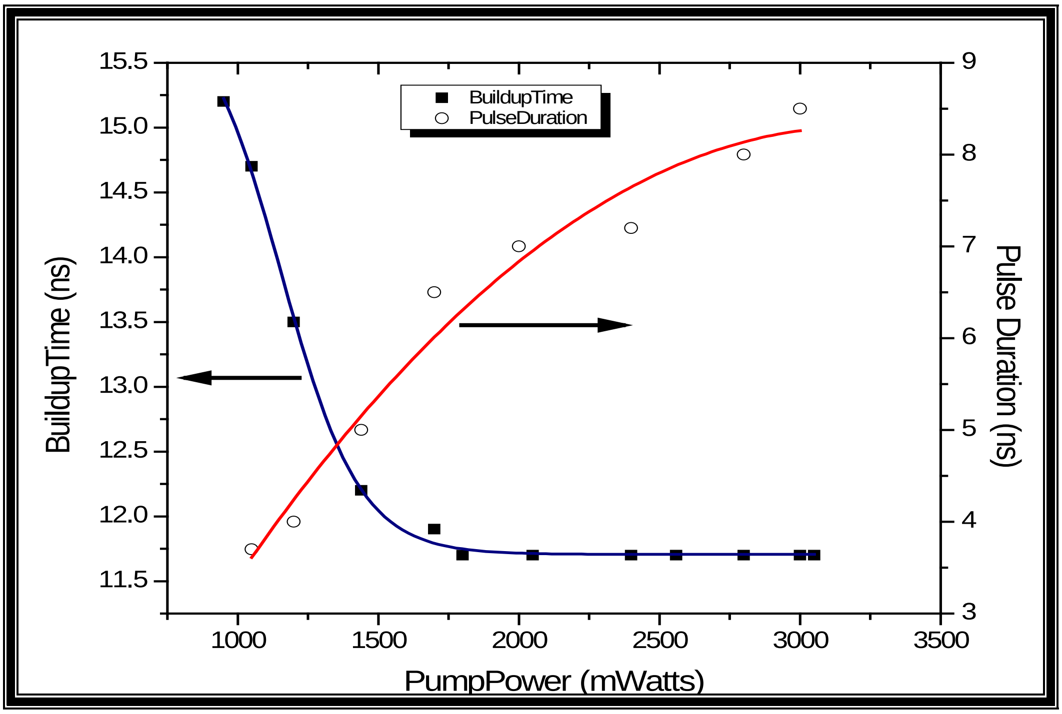

Fig 5.15: Pulse buildup time and pulse duration with pump power of SLM at peak wavelength for Rhodamine 6G

The buildup time decreases as the input pump power increases; this is due to the higher gain available for laser signal to grow faster inside the fixed loss cavity. While lower pump power results in lower gain and the laser signal needs more number of round trips inside the resonator cavity to reach the lasing threshold thus contributing to increase in the buildup time.

5.4.6.2 Effect of Wavelength: At the peak wavelength, the buildup time is small (~ 12 ns) and as the lasing mode is tuned on either side of the line centre the buildup time increases. Longer buildup time at either end of tuning curve is due to smaller gain available to the SLM laser. Figure 5.16 shows the effects of the operating wavelength on the buildup time of the SLM dye laser pumped by CVL with different pump powers.

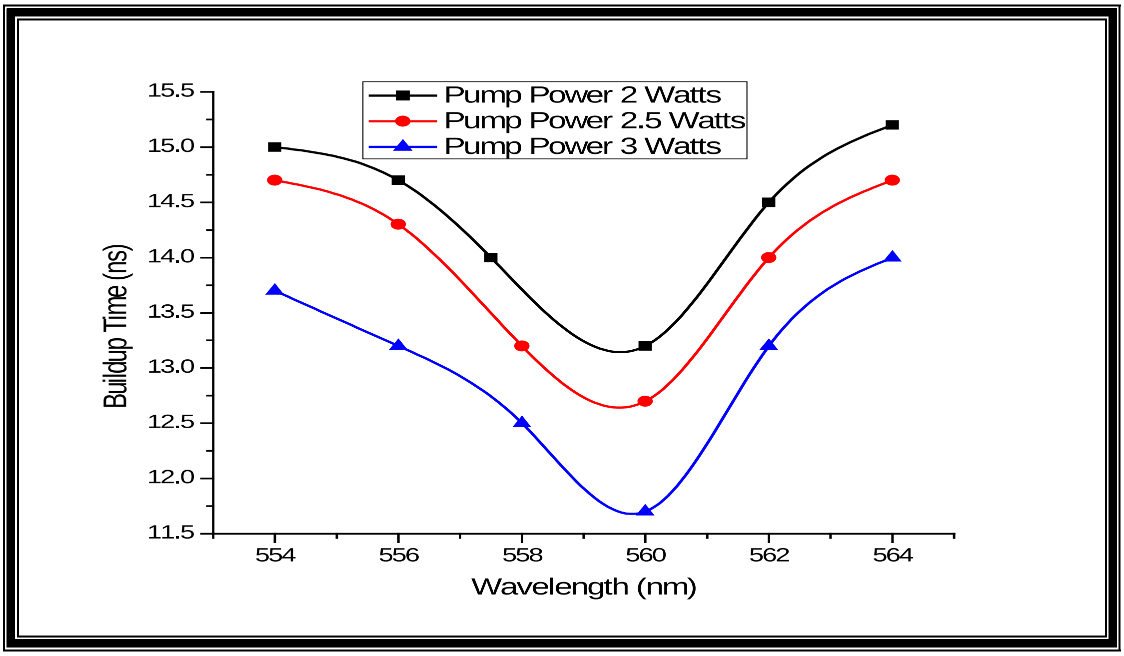

Fig 5.16: Effect of wavelength on buildup time of SLM dye laser

5.4.6.3 Effect of Grating Efficiency: Most of the grating based laser cavities have a rather high lasing threshold due to the lower value of diffraction efficiency at a higher angle of incidence; thus the grating diffraction efficiency plays an important role in the laser buildup time of the SLM dye laser. It was observed that the buildup time of SLM dye laser is reduced to 8 ns from 12 ns for holographic grating of 5% diffraction efficiency in comparison to a conventional grating with diffraction efficiency of 2% at the same incidence angle. It is due to the fact that with higher diffraction efficiency the threshold line for the SLM dye laser is reduced for the same gain.

5.4.6.4 Effect of Pumping Wavelength: An alternate study of buildup time was done by pumping the SLM dye laser with the second harmonic of Nd:YAG laser (532 nm). The buildup time was 5 – 6 ns when the Rhodamine 6G dye was pumped by the second harmonic of Nd: YAG laser as shown in figure 5.17. The buildup time was observed to be shorter ~ 6 ns as compared to ~ 12 ns for CVL pumped SLM dye laser for 0.2 mM Rhodamine 6G dye in ethanol.

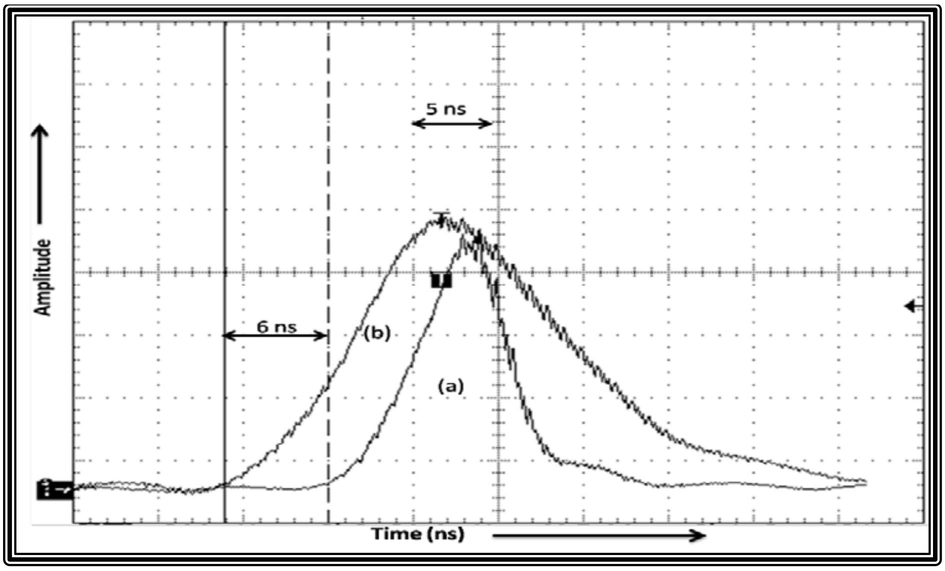

Fig 5.17: Plots of intensity vs time show buildup time of 6 ns for the Rhodamine 6G pumped with second harmonic of Nd:YAG pumped, (a) Dye laser pulse and (b) Nd:YAG pump laser pulse (X-axis Amplitude, Y- axis Time (ns))

5.4.6.5 Effect of Stokes Shift: A different experiment was carried out with Rhodamine 101 dye pumped by the yellow (~578 nm) beam of CVL (9 kHz) peak wavelength of Rhodamine 101 is 600 nm. The buildup time for Rhodamine 101 SLM dye was measured to be ~ 6 ns at the peak wavelength as shown in figure 5.18. It can be concluded that for a smaller Stokes shift (difference between the pump wavelength and lasing wavelength) the build-up time was smaller.

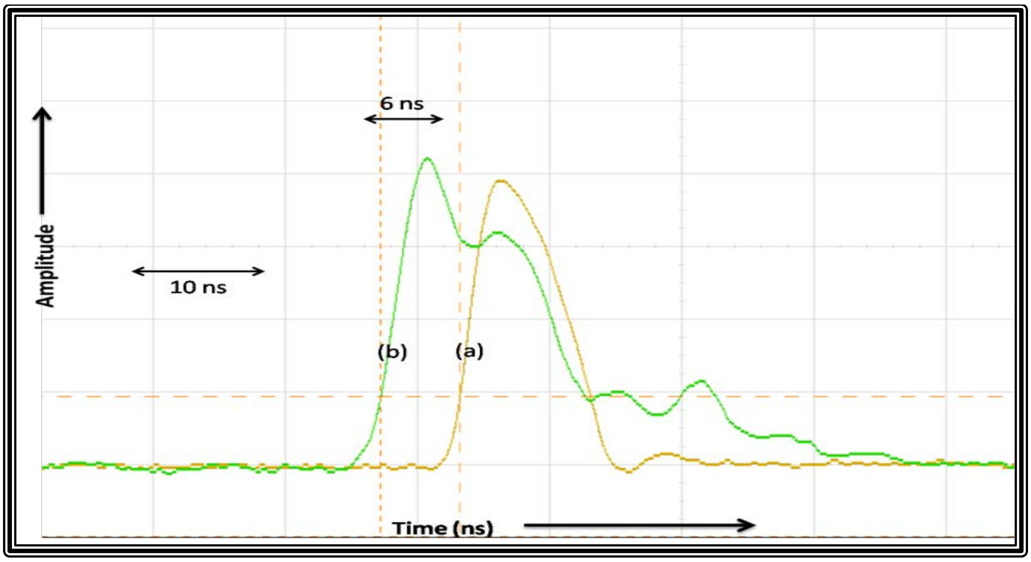

Fig 5.18: Plot shows buildup time of 6 ns for the Rhodamine 101 dye pumped by the yellow CVL beam: (a) SLM dye laser pulse and (b) CVL pump pulse {X-axis Amplitude, Y-axis time (ns)}

5.4.6.6 Effect of dye Concentration: The buildup time was observed to be dependent on the dye concentration for the same pump power. The buildup time was reduced by 3 ns as the dye concentration was increased from 0.15 mM to 0.5 mM of Rhodamine 6G in ethanol as shown in figure 5.19. This reduction in the buildup time was due to the higher gain available with increased dye concentration for the same pump power. The buildup time decreased by 21 % as the dye concentration was increased by nearly 3 times.

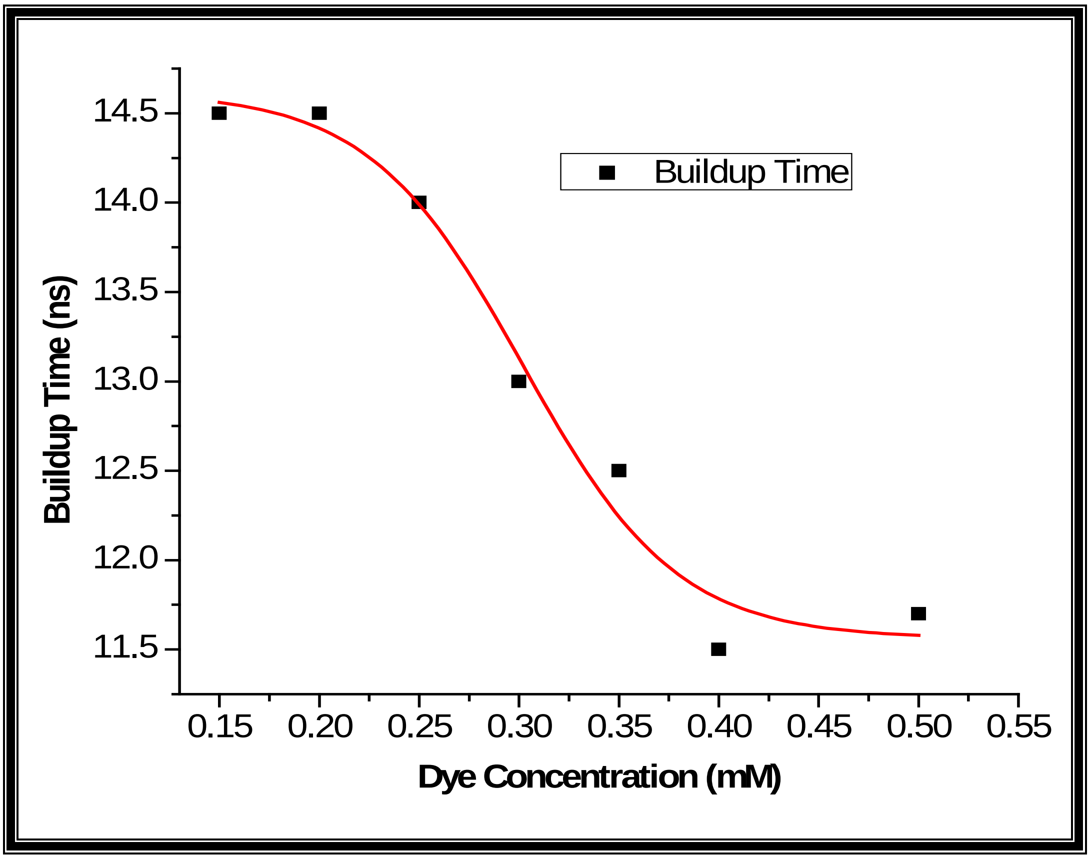

Fig 5.19: Effect of dye concentration at the buildup time of Rhodamine 6G dye pumped with green beams of the CVL

5.4.6.7 Effect of Laser Dye Purity: It was experimentally observed that the buildup time depends on the laser dye purity. The buildup time for Ms Radiant Rhodamine 6G dye is as high as 18 ns, while for the same laser dye of Ms Lambda Chrome it was 12 ns for the same pump power and the dye concentration of 0.2 mM in ethanol. Figure 5.20 and 5.21 shows the buildup time for two laser dyes measured with the same experimental setup and conditions.

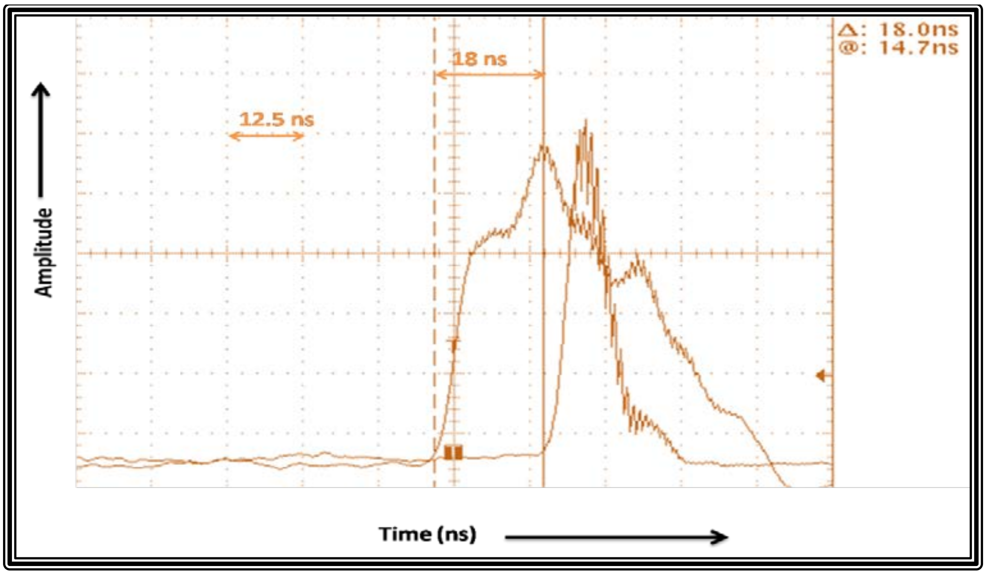

Fig 5.20: Plot shows buildup time of SLM dye laser with Radiant Laser dye (~ 18 ns) {X- axis Amplitide, Y- axis time (ns)}

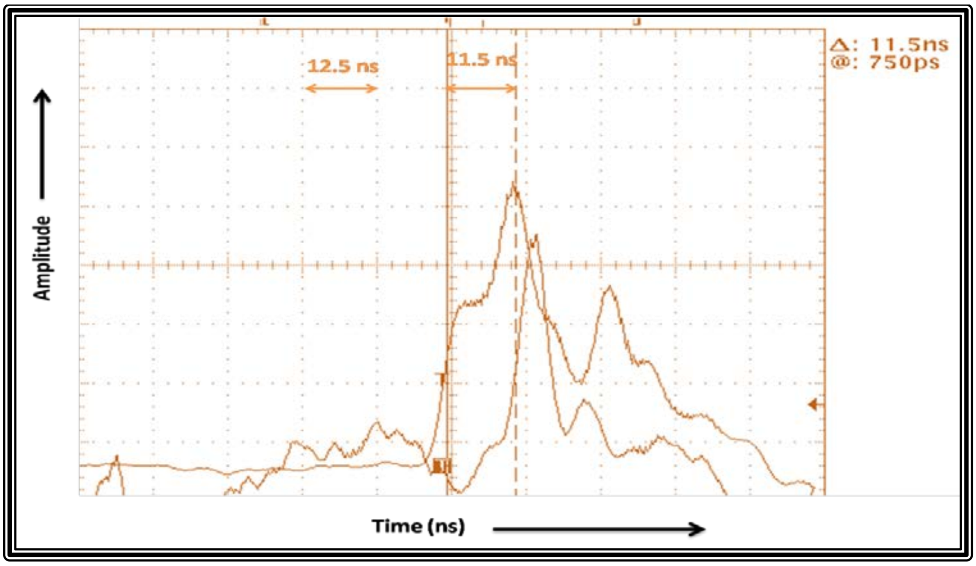

Fig 5.21: Plot shows buildup time of SLM dye laser with Lambda Chrome Laser dye (~ 11.5 ns) {X- axis Amplitide, Y- axis time (ns)}

5.4.7 Measurement of SLM Pulse Duration

The pump pulse and SLM pulse were monitored using a photo diode (FND 100) and oscilloscope (Tektronix TDS 724D, 500 MHz). It was found that the SLM pulse duration increases with increasing pump power. For a pump pulse duration of 33 ns and at higher pump power (~3.5 watts) the SLM pulse duration is 17 ns as shown figure 5.22 while at lower pump power of 1 watt it is 5 ns as shown in figure 5.23.

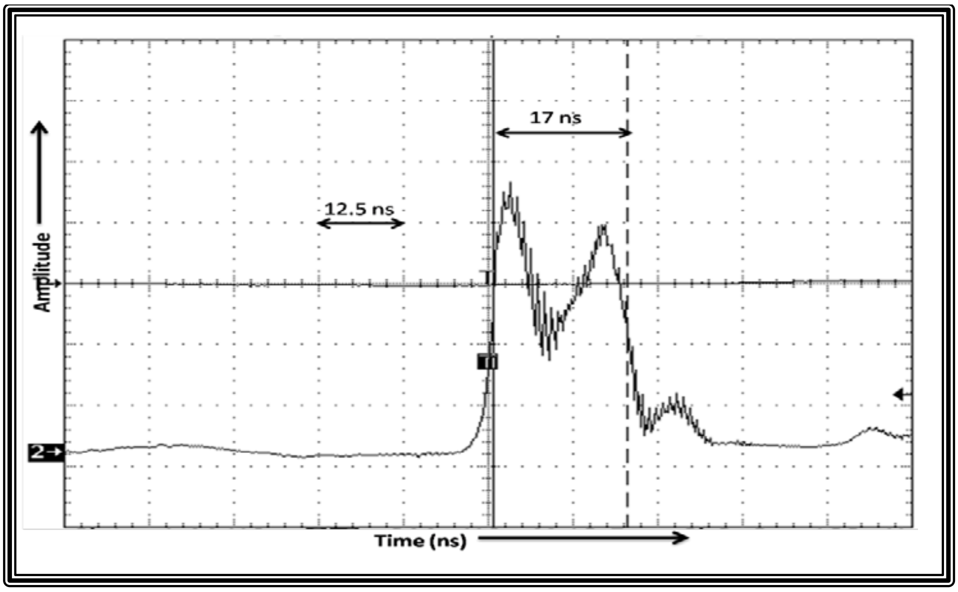

Fig 5.22: Plot of the SLM dye laser pulse at CVL pump power of ~ 3.5 Watts. {X- axis Amplitide, Y- axis time (ns)}

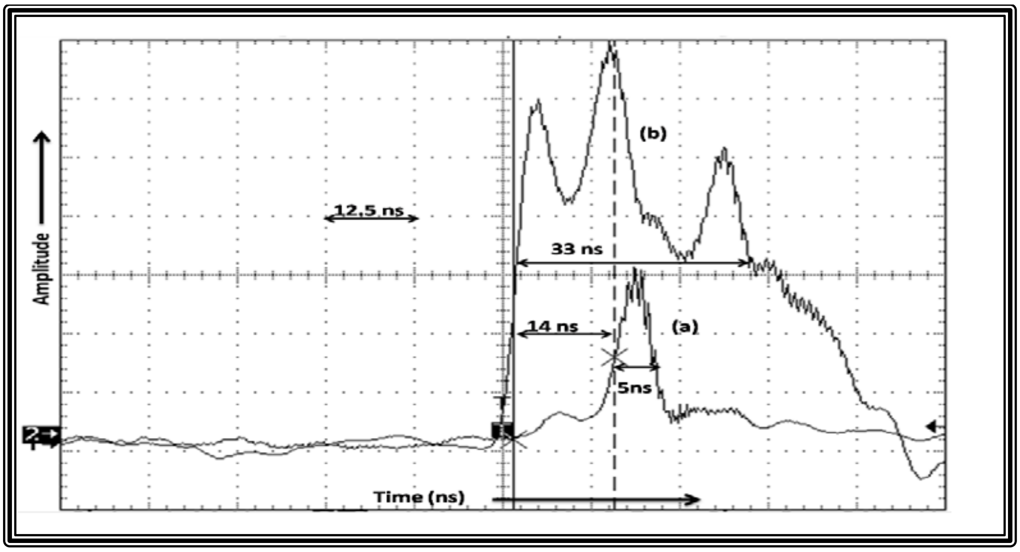

Fig 5.23: Plot shows the SLM dye laser pulse and CVL pump pulse with pump power of ~ 1 watt. (a) SLM pulse and (b) pump pulse {X- axis Amplitide, Y- axis time (ns)}

At higher pump powers, the available gain above the threshold lasts longer, which results in laser emission for longer duration. This has also been experimentally observed that the two peaks in dye laser pulse develop successively for a single pump pulse as shown in figure 5.24. The laser pulse begins to grow during the initial part of the pump pulse and since the gain is still enough after delivering the first pulse (peak a), the population inversion builds again giving rise to the onset of the second pulse (peak b). Measurement of temporal separation of the two pulses {~ 7.7 ns the separation between the peak (a) and peak (b)} led to the confirmation that they did not originate from the round trip peaks of the CVL pump pulse. However, the peaks (a) and (c) appear to originate from the shape of the CVL pulse as the time interval of 16 ns between the two peaks corresponds to the round trip time of the pump pulse in the resonator length of 2.4 meters. At still higher pump power these two peaks merge together, resulting in a single pulse of correspondingly longer duration.

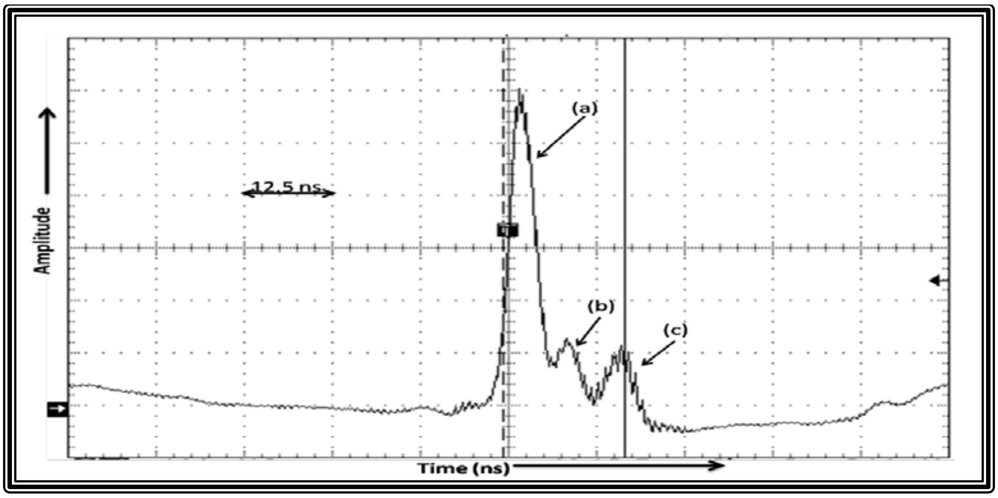

Fig 5.24: Plot of SLM dye laser pulse the at lower pump power of ~ 800 mW. Peak (a) and (b) with separation of 7.7 ns, while separation of peak (a) and (c) is 16 ns, corresponding to the round trip time for CVL pulse. {X- axis Amplitide, Y- axis time (ns)}

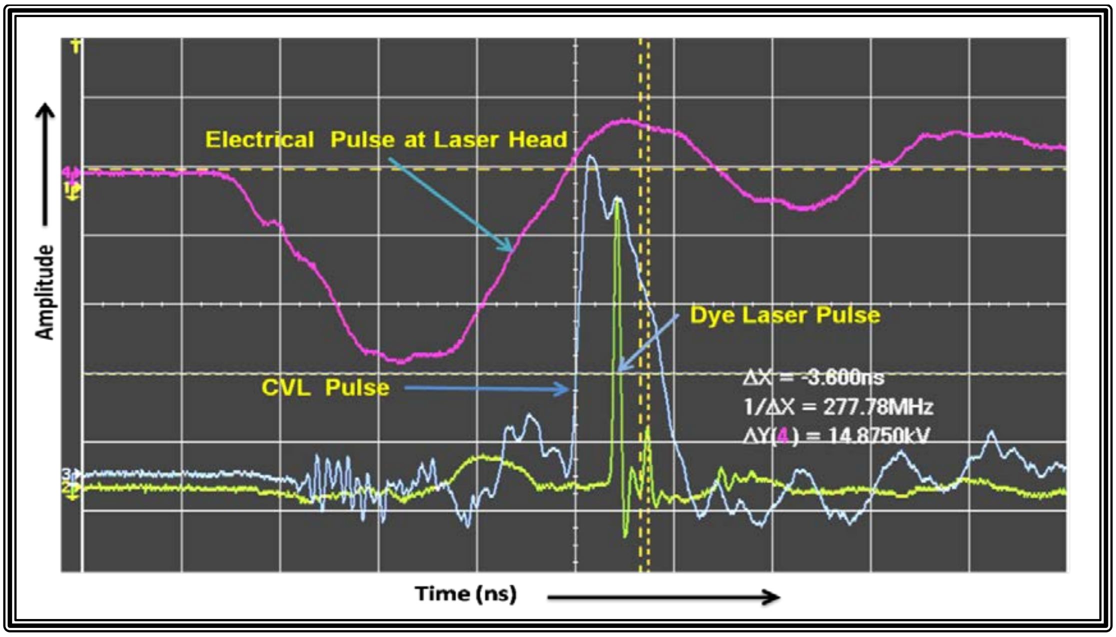

Fig 5.25: Electrical pulse, CVL laser pulse and SLM dye laser pulse {X- axis Amplitide, Y- axis time (ns)}

Figure 5.25 shows all the three pulses: a high voltage pulse of nearly 15 kV applied to the laser head, the optical pump pulse of CVL and SLM dye laser pulse recorded simultaneously by a four channel digital oscilloscope.

5.4.8 Measurement of Beam Divergence

The spatial profile of SLM laser beam was analyzed using OPHIR beam profiler. Figure 5.26 shows the intensity distribution obtained for SLM dye laser beam with the laser beam profiler, which shows the SLM dye laser beam is nearly (86%) Gaussian. The SLM beam profile needs to be near Gaussian to avoid the multimode oscillations. The SLM dye laser beam diameter was nearly 1.5 mm.

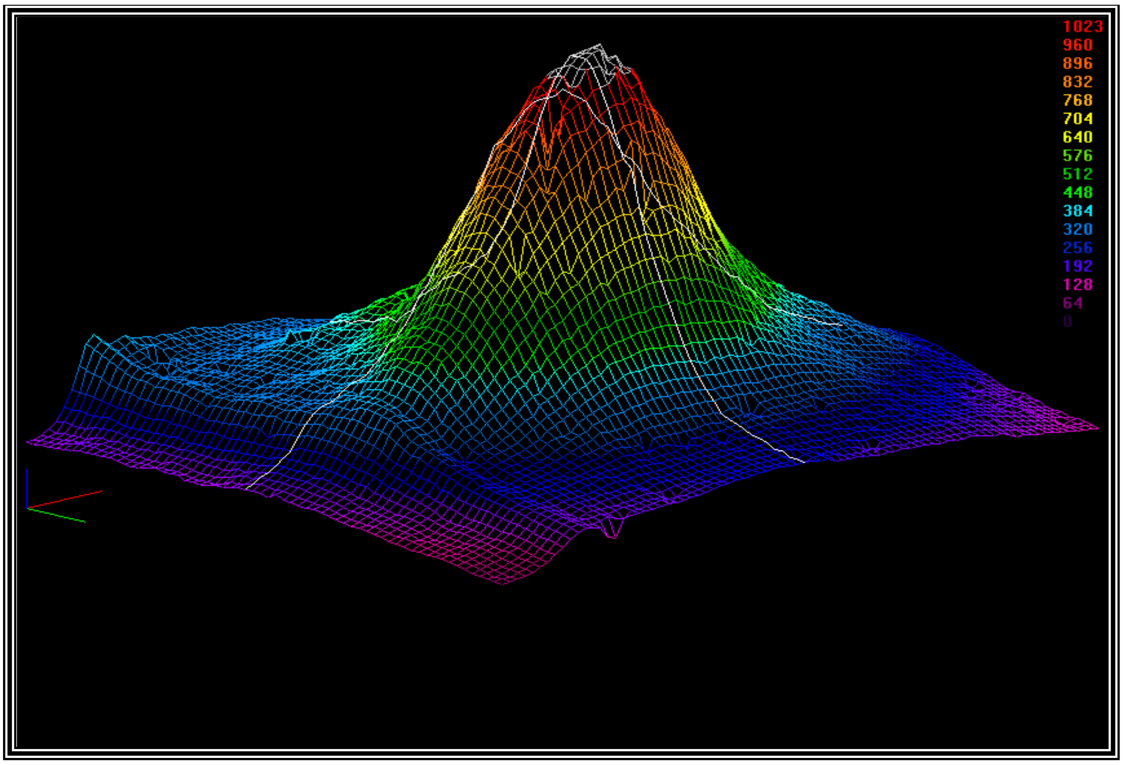

Fig: 5.26 Intensity distributions in the SLM dye laser Beam (~86% Gaussian)

The beam divergence of SLM dye laser as measured by the beam profiler was 0.512 mrad. The beam divergence of the SLM dye laser was also measured by propagating the SLM beam over 5.5 meters distance; it was measured to be 0.515 mrad.

5.5 SLM Operation with Higher Viscosity Solvent

In a set of experiments the SLM dye laser was operated with various viscosities of the solvent by use of binary solvent of ethanol and glycerol mixture and adjusting the composition to achieve different viscosities. In a typical experiment, where the ethanol and glycerol were mixed in the ratio of 50 : 50, the viscosity was 0.2 N s / m^2. The flow velocity was maintained at 0.9 m/s with the binary solvent. The bandwidth of the dye laser was measured to be 650 MHz and the output power of 25 mW was obtained with conversion efficiency of 1.66%. The tuning range was 12 nm with the peak wavelength at 564 nm. More of these studies have been reported elsewhere. Due to the difficulties of pumping highly viscous solvent, this was not the preferred option for high repletion rate lasers.

5.6 SLM Operation with Stretched Pump Pulse

To increase the SLM pulse duration a stretched pump pulse was used. The pump pulse was stretched using a beam splitter (30:70::R:T) and three mirrors. The schematic of a typical pump pulse stretcher is shown in figure 5.27 with two plane mirrors and beam splitter arranged in a triangular configuration. The delay in the path length was varied from ~ 171 cm to ~ 336 cm. The optical delay of 11.2 ns in the stretcher arm resulted in an increase in the pump pulse duration from 25 ns to 44 ns.

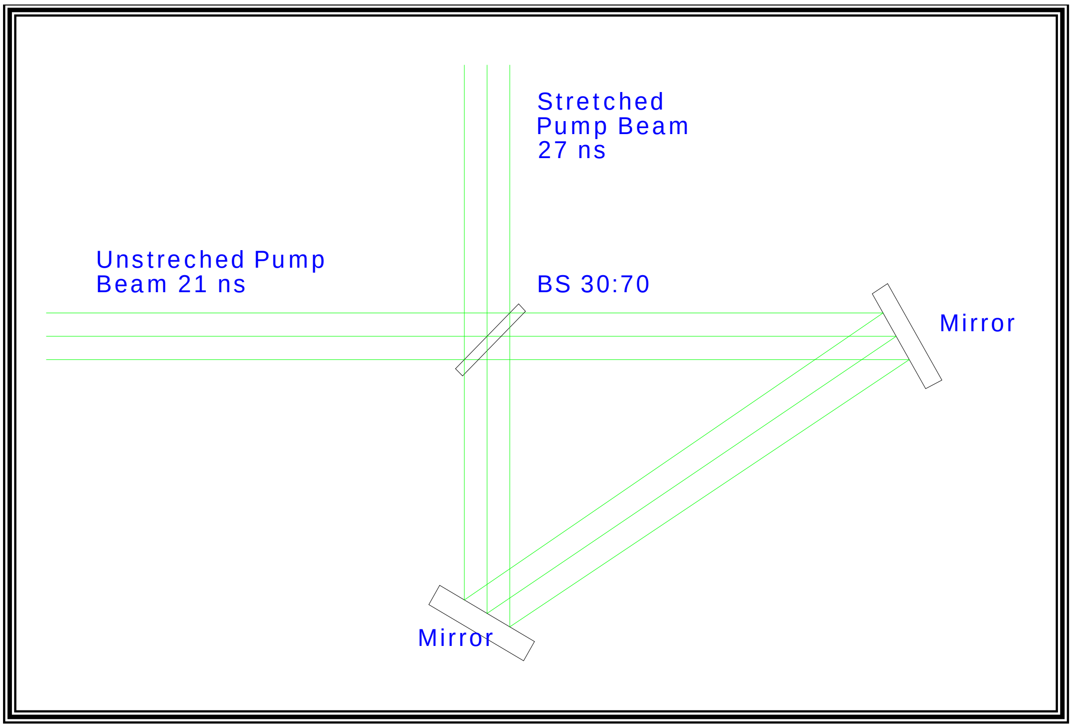

Fig 5.27: Schematic of the pump pulse stretcher for SLM dye laser

With this stretched pump pulse of 44 ns the SLM pulse increased to 21 ns as shown in figure 5.28.

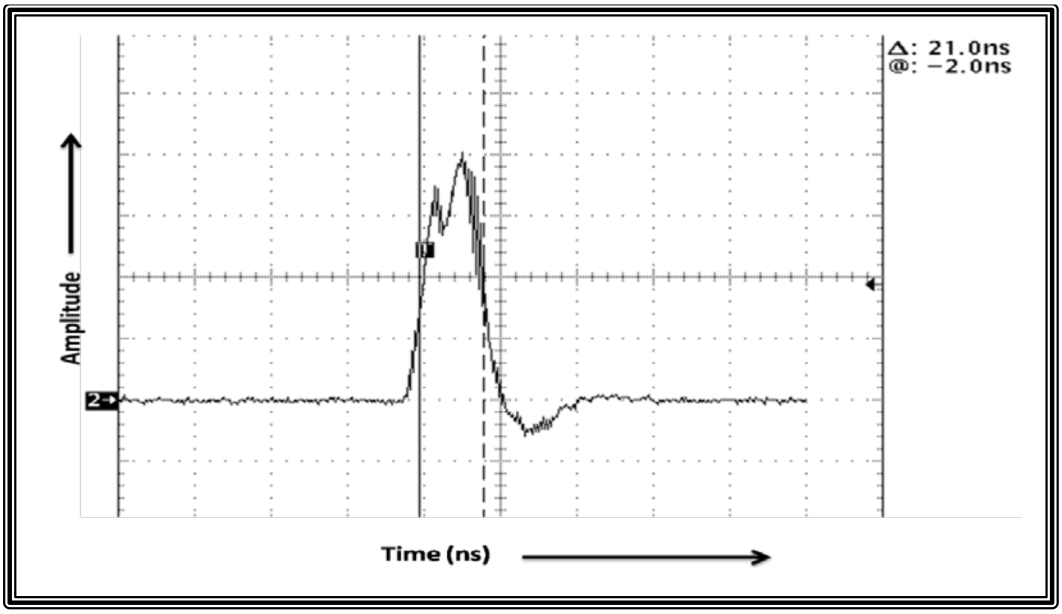

Fig 5.28: SLM pulse duration with Stretched pump Pulse of 40 ns (~ 2.15 Watts) {X-axis Amplitide, Y- axis time (ns)}

It was observed that the bandwidth of the SLM dye laser also increased by nearly 25 % with a stretched pump pulse. The pulse energy stability of SLM dye laser was measured to be ~ 4.45 %. The SLM dye laser parameters with a stretched pump pulse are tabulated in table 5.1.

S.No	Pump Parameters		SLM Dye Laser Parameters	
1.	Un-stretched Pulse Duration	21.5 ns	Un-stretched pulse duration	5.1 ns
2.	Stretched Pulse Duration	27.5 ns	Stretched Pulse Duration	18.1 ns
3.	Un-stretched pump power	0.7 W	Un-Stretched SLM power	10 – 15 mW
4.	Stretched pump power	0.7 – 1 W	Stretched SLM power	40 – 60 mW

Table 5.1: SLM Parameters with Stretched Pump Pulse: Un-stretched Bandwidth was 400 – 500 MHz, While Stretched Bandwidth was 550 – 650 MHz.

5.7 Long Term Operation of SLM Dye Laser

The SLM dye laser was operated in free running mode and the laser wavelength was monitored on wavelength meter continuously. The dye reservoir was cooled by a constant temperature bath, whose temperature was set to 290 ± 0.15 K. The stepper motor of the SLM dye laser was locked by holding torque. The wavelength was observed to decrease as the dye solvent temperature increased; the details of the temperature effect are described in the Chapter – VI of this thesis. A single mode to two mode transition was observed, which was periodic in nature. The periodic behavior of the SLM dye laser wavelength was due to periodic variations in the dye temperature.

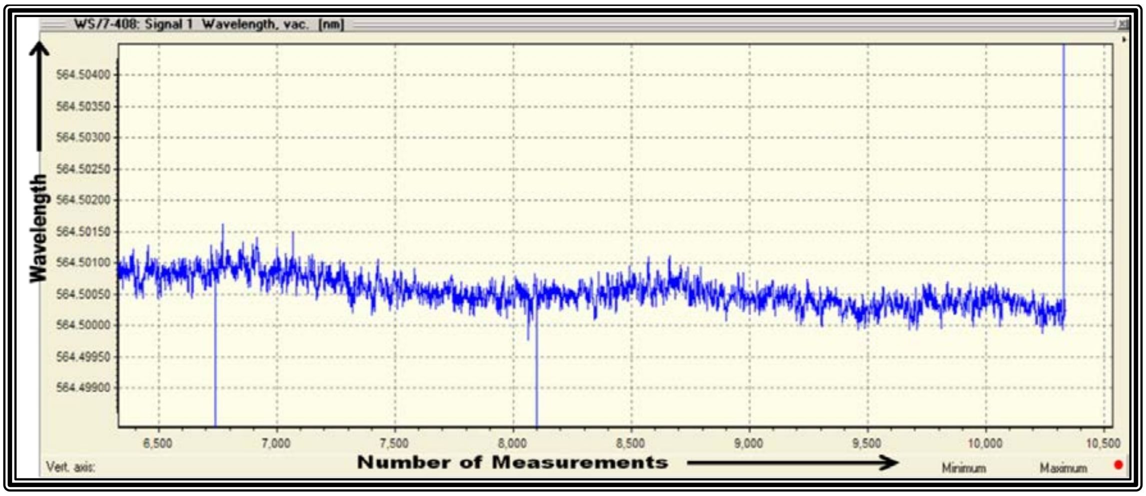

Fig 5.29: Record of wavelength drift for SLM dye laser {X- axis Wavelength (nm), Y- axis number of measurement}

Figure 5.29 shows the long term behavior of the SLM dye laser wavelength with time. The SLM dye laser was in free running mode without any feedback control. The change of SLM output from single mode to two modes is also shown in figure 5.30.

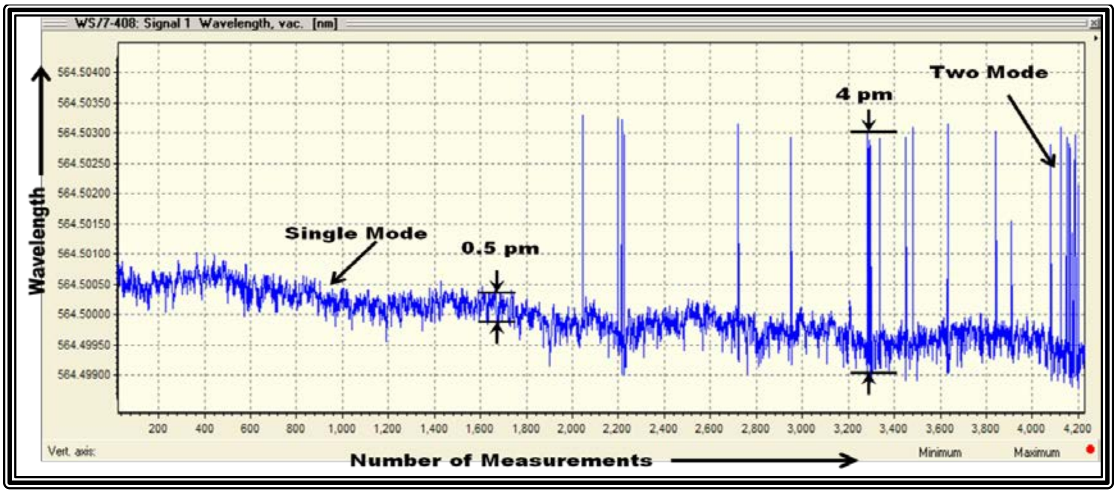

Fig 5.30: Single mode to two mode oscillation observed by laser wavelength meter {X- axis Wavelength (nm), Y- axis number of measurement}

The two mode oscillation was detected by the laser wavelength meter as well as by viewing FP etalon fringes. The wavelength fluctuation increased to ~ 3.5 GHz during the two mode oscillation and it continued in this manner till the two mode changed back to single mode. When there was a single mode operation the wavelength fluctuations were limited to 480 MHz. In order to correct the two mode oscillation the detector should be also to distinguish in between the single and two modes oscillations. This single mode to two mode oscillation of the SLM dye laser was correlated with the amplitude of fluctuation observed in the wavelength meter. The two mode oscillation in the SLM laser was corrected to single mode by applying nearly 2.28 volts to the end mirror PZT. Figure 5.31 shows the effect of correction by the end mirror displacement, which is discussed below.

The transitions were cyclic. The end mirror PZT was displaced by 304 nm for one cycle of single to two mode transition. The PZT at the end mirror had a full stroke length of 10 µm for the operating voltage of - 30 V to 150 volts. The input signal 0 – 10 V was generated using 16-bit digital to analog converter from a personal computer for controlling the PZT driver. The sensitivity of the end mirror was 8.5 MHz / nm for the cavity length of 60 x10^{-3} m. The wavelength tunability by end mirror displacement was limited to the grating pass band. While correcting the two mode behavior by moving end mirror PZT the laser wavelength also changed. The change in output wavelength was corrected simultaneously by using the tuning mirror PZT.

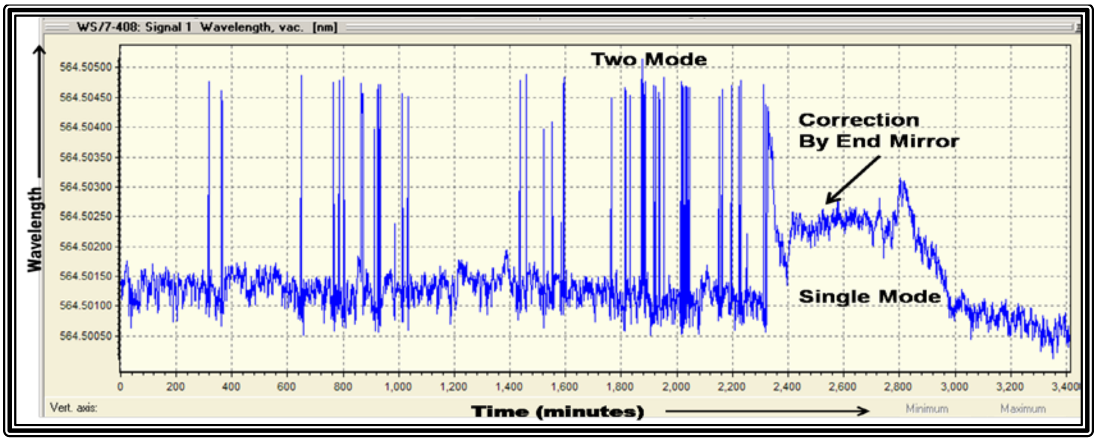

Fig 5.31: Two mode to single mode correction for SLM dye laser {X- axis Wavelength (nm), Y- axis number of measurement}

5.8 SLM Dye Laser Pumped with Yellow Beam

In yet another experiment, the yellow beam of CVL was used for pumping Rhodamine 640 laser dye in ethanol and the following laser parameters were measured. The SLM dye laser bandwidth was measured to be 450 MHz, the pulse duration 14 ns and build up time 5 – 6 ns. The single pulse bandwidth of this SLM dye laser was measured to be 300 MHz. The SLM dye laser pulse duration and build up time are shown in figures 5.32 and 5.33, respectively.

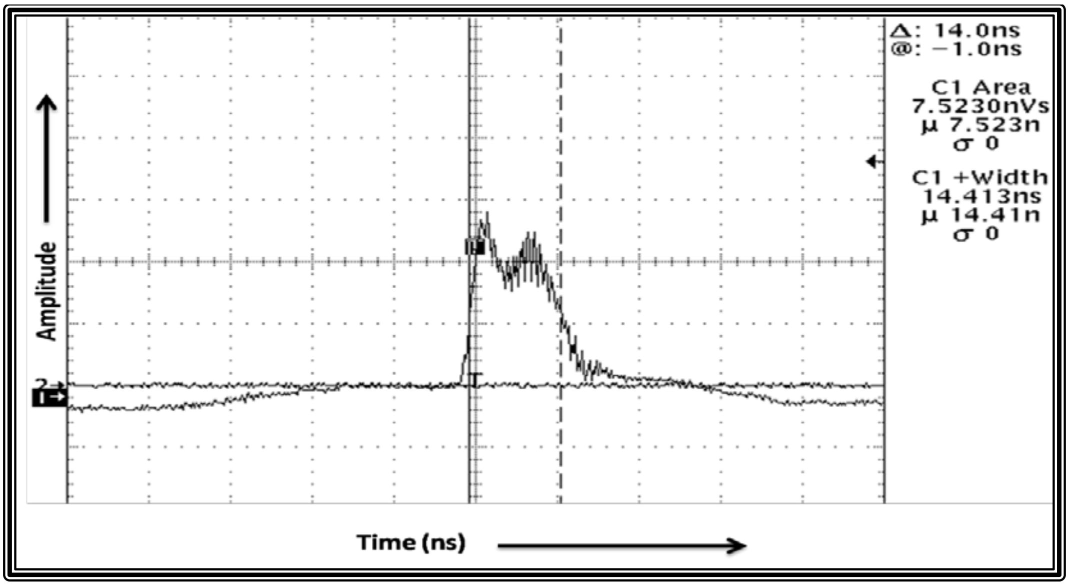

Fig 5.32: SLM dye laser pulse of Rhodamine 640, pumped by yellow beam of CVL. {X- axis Amplitide, Y- axis time (ns)}

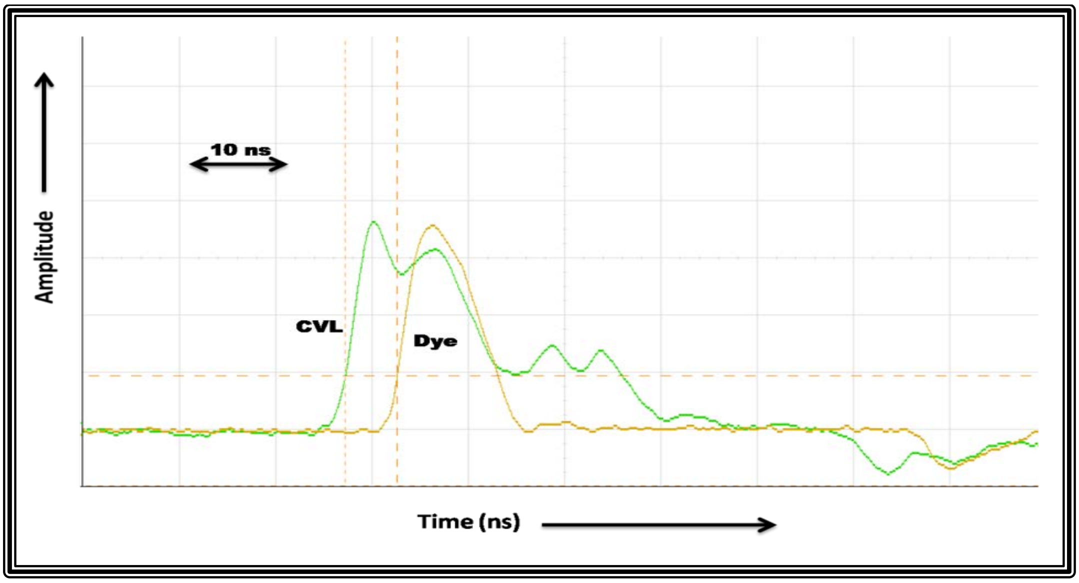

Fig 5.33: Build up time for Rhodamine 640 SLM dye laser, pumped by yellow part of the CVL beam. {X- axis Amplitide, Y- axis time (ns)}

The SLM dye laser pulse energy stability was measured to be ~ 30 %, while the pump pulse energy stability was 0.6 %. It was observed that the buildup time strongly depended on the pump power. The buildup time was ~ 9 ns for the pump power of ~ 245 mW, while it was reduced to 5 ns from 9 ns for the pump power of ~ 830 mW.

This SLM laser was operated for more than 8 hours in free running mode. It was observed that the stepper motor temperature stabilized in 110 minutes; a wavelength drift of around 25 GHz was observed during this period. The SLM was continuing to operate in free running mode after stabilization of temperature of the stepper motor. The wavelength changed from 564.646 nm to 564.664 nm in 2 hours 45 minutes. The SLM was also scanned for more than 130 pm from 563.11 nm to 563.24 nm with a scan speed of 130 MHz/sec as shown in figure 5.34.

Fig 5.34: Slow Wavelength Scanning of the SLM dye laser with scan rate ~ 130 MHz/sec {X- axis Wavelength (nm), Y- axis time in minutes}

This long term operation of the SLM dye laser had provided very crucial parameters for wavelength control loop. The details of the SLM wavelength stabilization technique are discussed in the Chapter – VII of this thesis.

5.9 SLM Dye Laser Pumped with Nd:YAG Laser

The second harmonic of Nd:YAG (532 nm @ 10 Hz) was used for pumping the SLM dye laser with the worm and wheel tuning mechanism on the tuning mirror. A 0.5 mM Rhodamine 6G dissolved in ethanol was circulated through the dye cell at an average flow velocity of 0.5 m/s. The bandwidth of the SLM dye laser measured by wavelength meter was 0.1 pm (~ 95 MHz), while the bandwidth measured by FP etalon was 170 MHz. Typical FP etalon fringes for the SLM dye laser are shown in figure 5.35. Single mode operation was confirmed by monitoring SLM dye laser output on the laser wavelength meter as shown in figure 5.36. The pulse duration of the Nd:YAG laser was ~ 18.5 ns, while the corresponding SLM dye laser pulse duration was ~ 9.7 ns. The pulse duration of the SLM dye laser and the Nd:YAG is shown in figures 5.37 and 5.38 respectively. This SLM dye laser was tuned through the central stepper motor from 559.931 to 571.190 nm (~ 11 nm). About 0.2 mJ pulse energy was obtained from the SLM dye laser with conversion efficiency of ~ 2 %. The SLM dye laser was also tuned from 562.8900 to 562.8985 nm (~ 85 pm) by moving the stepper motor attached to the worm and wheel tuning mechanism by 5000 steps. The resolution achieved was around 1.7 MHz/step.

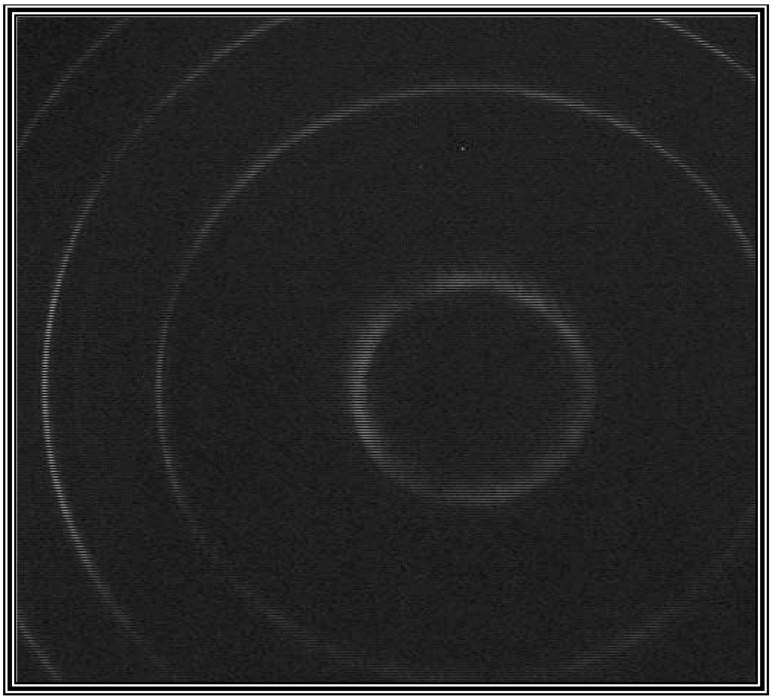

Fig 5.35: F P Etalon fringe of Nd: YAG pumped SLM Dye Laser

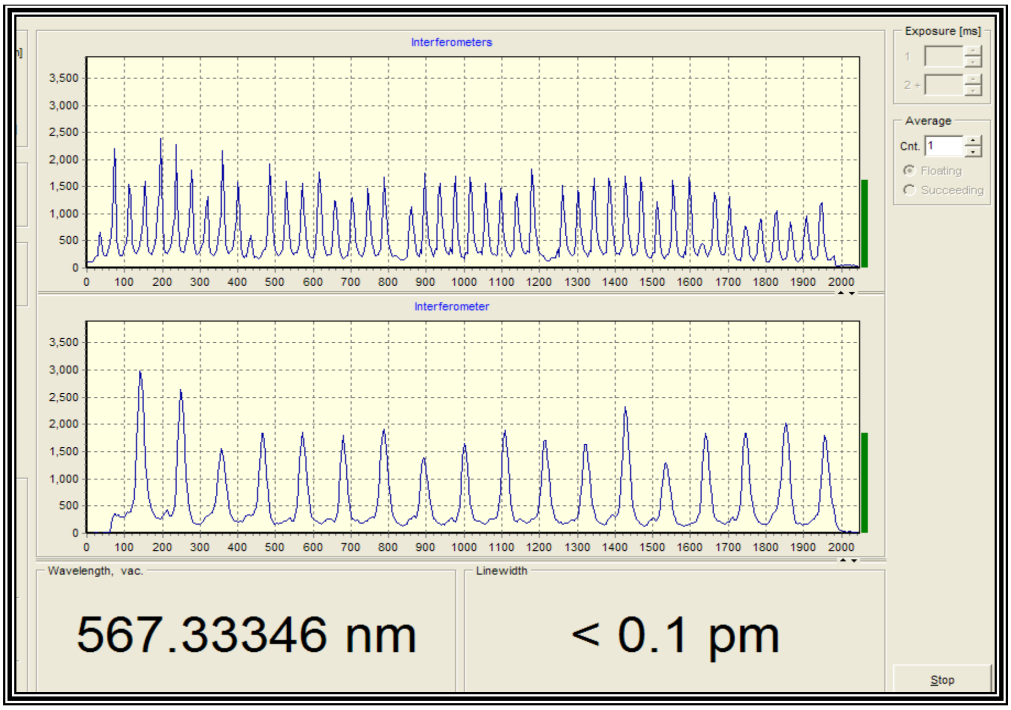

Fig 5.36: Wavelength meter output for Nd: YAG pumped SLM Dye Laser

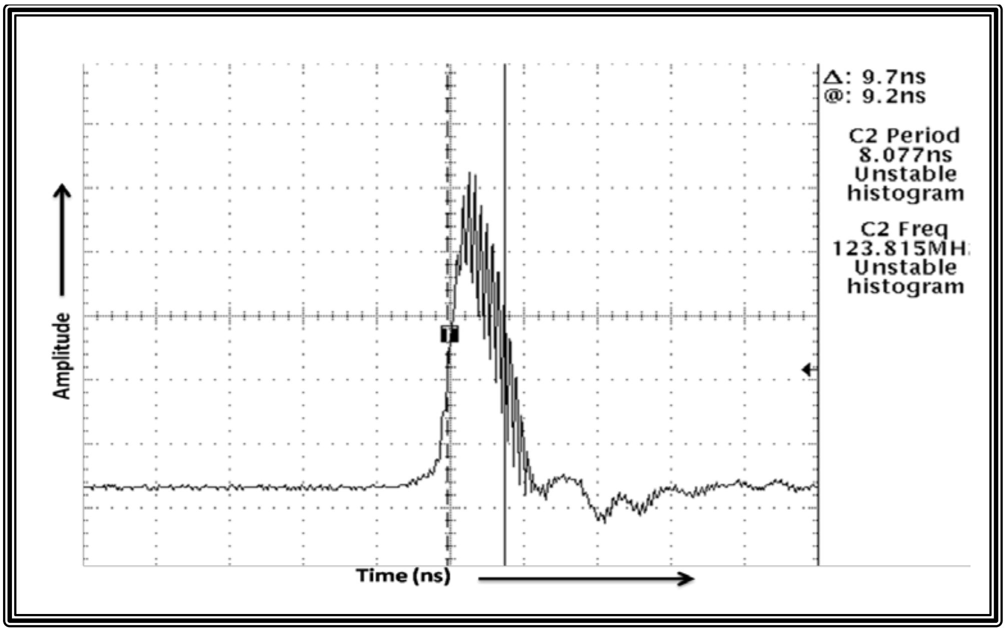

Fig 5.37: SLM dye laser pulse 9.7 nsec pumped by the second harmonic of Nd:YAG laser {X- axis Amplitide, Y- axis time (ns)}

About 15 GHz (565.1556 – 565. 170 nm) of mode hop free scanning could be achieved as shown in figure 5.39; the mode hop free scanning was confirmed by observing the wavelength meter output as well as F P Etalon fringes. The sudden jump of nearly 3 GHz (SLM cavity FSR) in the dye laser wavelength was not detected during scanning as shown in figure 5.39.

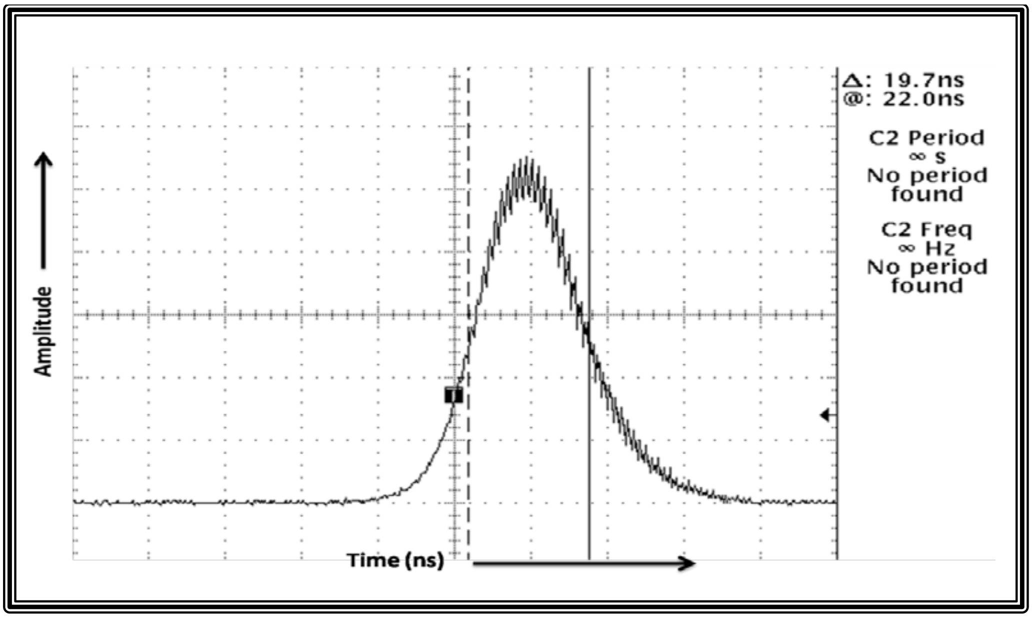

Fig 5.38: The pulse duration of Nd:YAG laser ~19.7 nanosecond {X- axis Amplitide, Y- axis time (ns)}

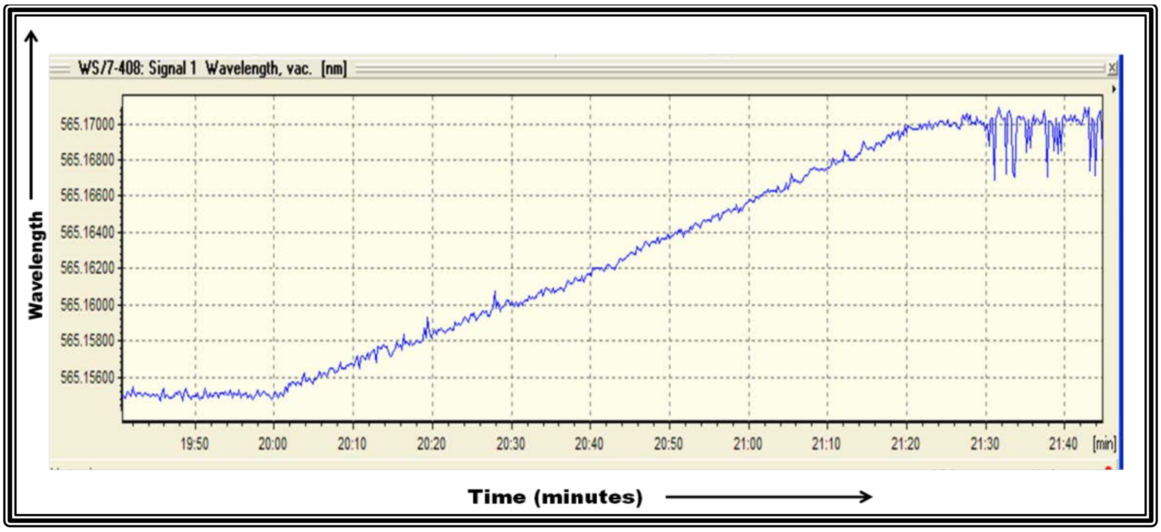

Fig 5.39: Mode hops free Scanning over ~ 15 GHz with Nd: YAG Pumped SLM dye Laser {X- axis Wavelength (nm), Y- axis time in minutes}

It was also observed that for the same flow velocity of 0.5 m/s, the bandwidth of the SLM dye laser decreased from 285 MHz to 175 MHz when the pump pulse energy of Nd: YAG was decreased from 0.75 mJ to 0.15 mJ. The change in the bandwidth of the SLM with the pump power is shown in figure 5.40

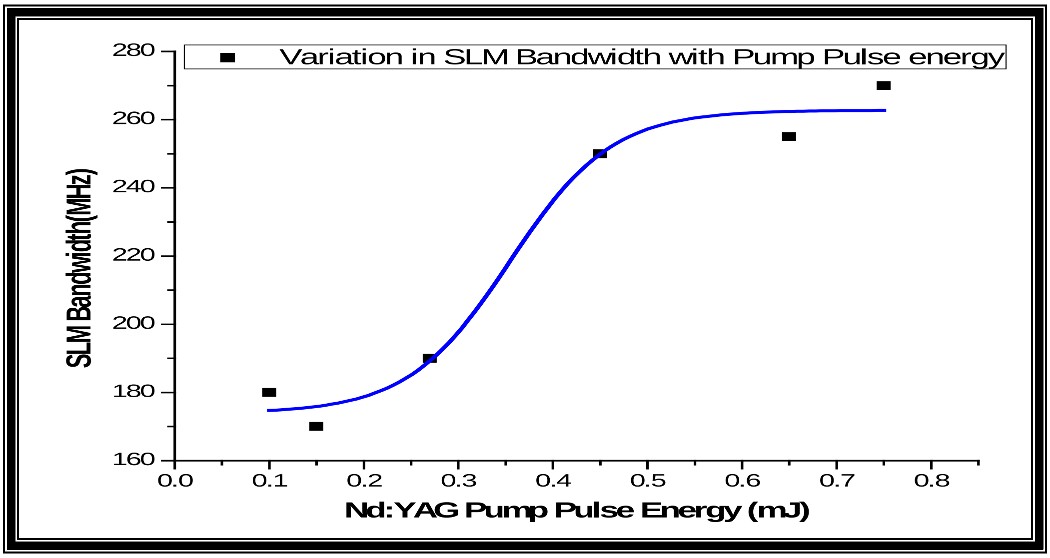

Fig 5.40: Effect of pump pulse energy on the SLM bandwidth for Nd:YAG pumped SLM Dye Laser.

5.10 Amplification of SLM Dye Laser Output

The small output power of a few mW from the SLM dye laser needs to be amplified in one or two amplification stages to a few watts. An experiment of amplification was conducted. A demountable metallic amplifier dye cell with flow channel cross section of 0.5 mm x 16 mm was used as an amplifying medium for the amplifier. This amplifier dye cell has converging, straight and diverging section similar to the design – XII, as described in Chapter – IV of this thesis. Before amplification, the SLM dye laser output was spatially filtered with 50 μm aperture to reduce ASE. The SLM dye laser signal was spatially and temporally matched with the gain of the amplifier, which was pumped transversely by the green beam of CVL at 9 kHz with a combination of spherical and cylindrical lens. Rhodamine 6G dissolved in ethanol was circulated through the amplifier dye cell at a flow rate of 7 – 8 lpm by a magnetically coupled gear pump. The amplifier was characterized with respect to pump power, input signal and wavelength of the SLM dye laser. The effect of dye concentration was studied by varying the dye concentration from 0.15 mM to 0.7 mM in the amplifier. It was observed that the variation in conversion efficiency of the dye amplifier with lower dye concentration was more for the peak wavelength of SLM dye laser at λ~ 560 nm; however, it was not linear as shown in figure 5.41. This was due to shift in the amplifier gain towards the higher wavelength side with increasing dye concentration and the amplifier gain available at peak wavelength of the SLM dye laser at 560 nm became less. A 12 mW signal of the SLM dye laser beam was amplified to 421 mW in the reflected beam geometry. The maximum conversion efficiency obtained was 4.45 % with pump power of 9 Watts to the amplifier dye cell having a gain length of 16 mm.

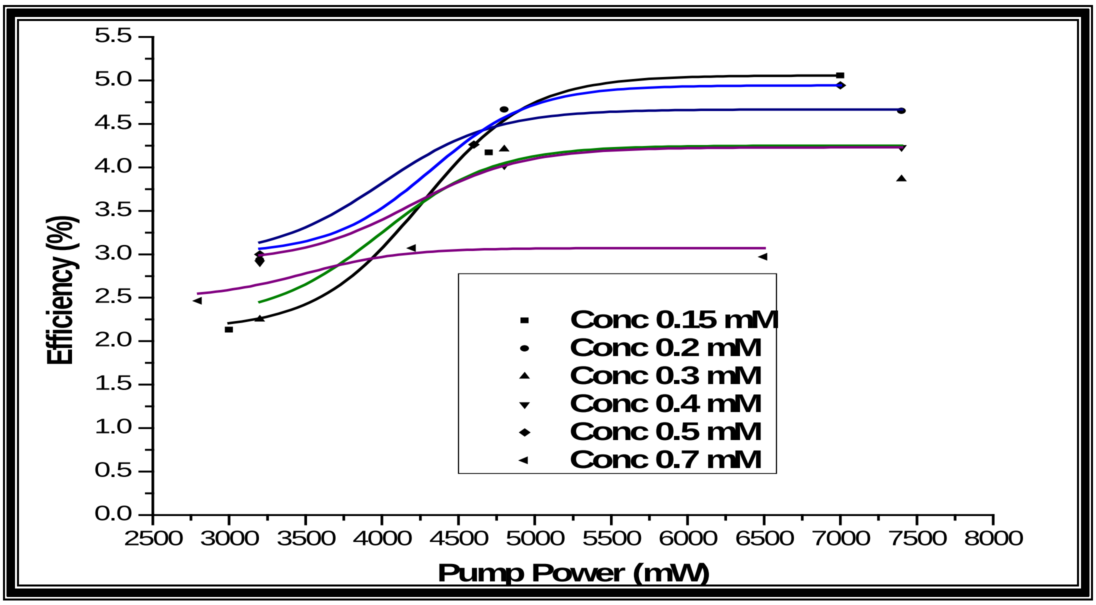

Fig 5.41: Effect of dye concentration on amplifier output for fixed SLM wavelength (560 nm)

It was observed that the conversion efficiency for the amplifier was higher at the red end of the tuning, while the input signal was highest at peak wavelength of 560 nm. Higher conversion efficiency towards higher wavelength has more contribution of ASE than that by amplification of the SLM laser signal beam. Figure 5.42 shows the wavelength versus conversion efficiency for the amplified signal. A 4 mW SLM signal operating at 564 nm was amplified with conversion efficiency of 9.5 % with 0.35 mM Rhodamine 6G in ethanol for pump power of 5.9 Watts to the amplifier cell.

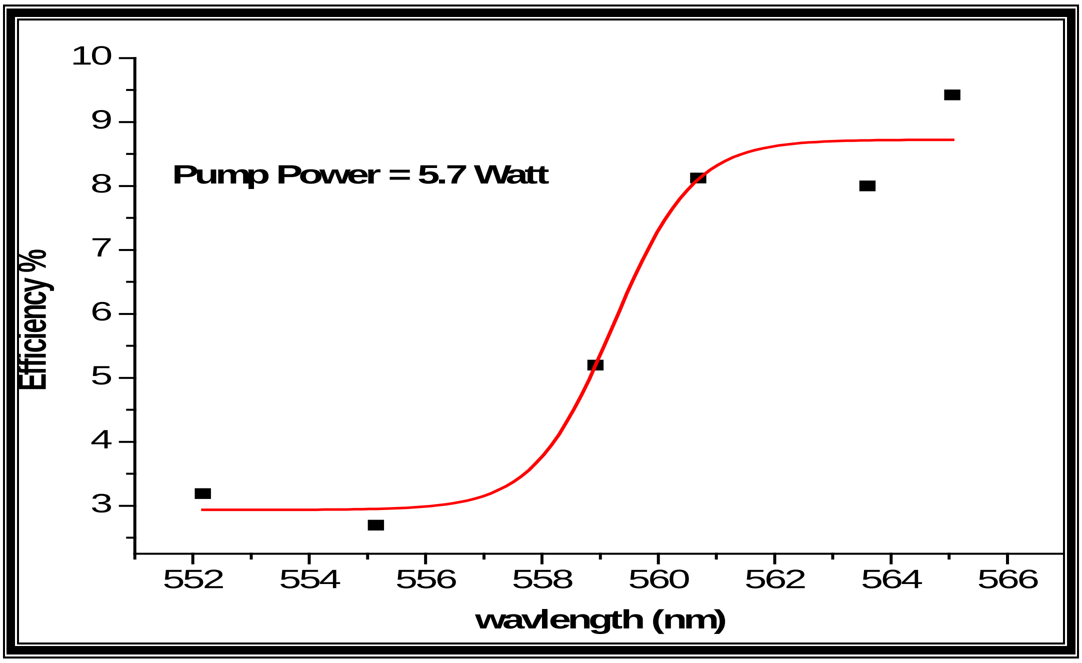

Fig 5.42: Conversion efficiency versus wavelength for SLM signal with fixed pump power

The ASE was spatially filtered using with a pair of 300 mm focal length lenses and 200 µm aperture placed in the focal plane of the lenses. The delay between the signal beam and the pump beam was adjusted for maximum amplification. It was observed that the amplifier conversion efficiency for the SLM dye laser depended on the wavelength. The 3 mW SLM signal was amplified to 480 mW in the amplifier with conversion efficiency of ~ 5.75 %. It was observed that the amplified power was higher for longer wavelength. The conversion efficiency for 560.906 nm was ~ 2.45 %, while the conversion efficiency was ~ 5.75 % for wavelength of 568.694 nm. This higher efficiency at longer wavelength was due to spectral gain mismatch in the oscillator and amplifier gain curves. The pulse duration of the amplified signal was increased to ~ 12 ns from 6 ns of the SLM signal pulse as shown in figure 5.43 and 5.44 due to a smaller gain in the wings of the pump pulse.

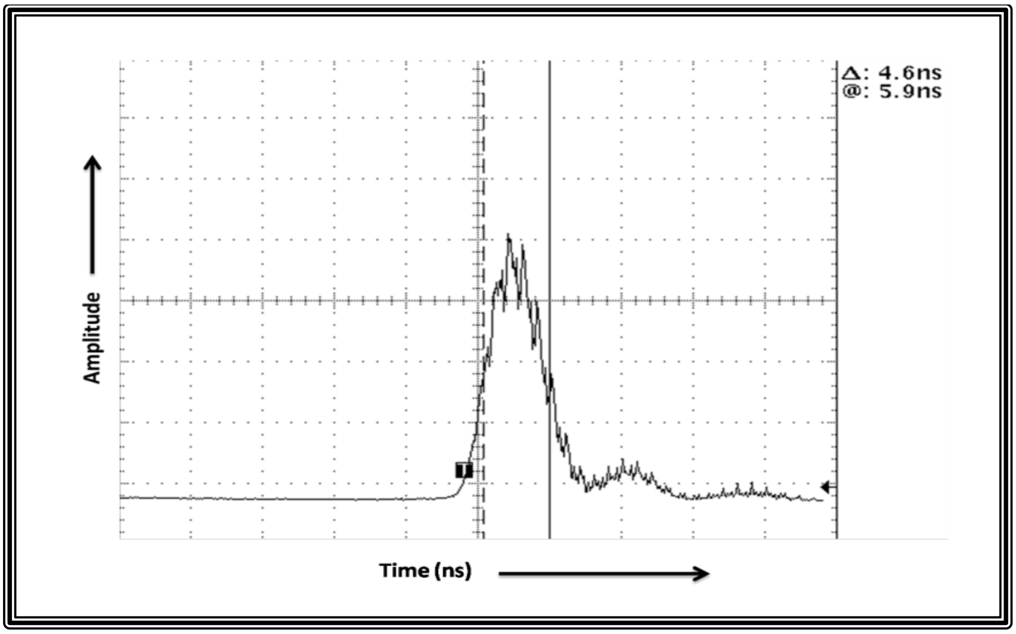

Fig 5.43: SLM dye laser pulse of Rhodamine 6G pumped by CVL {X- axis Amplitide, Y- axis time (ns)}

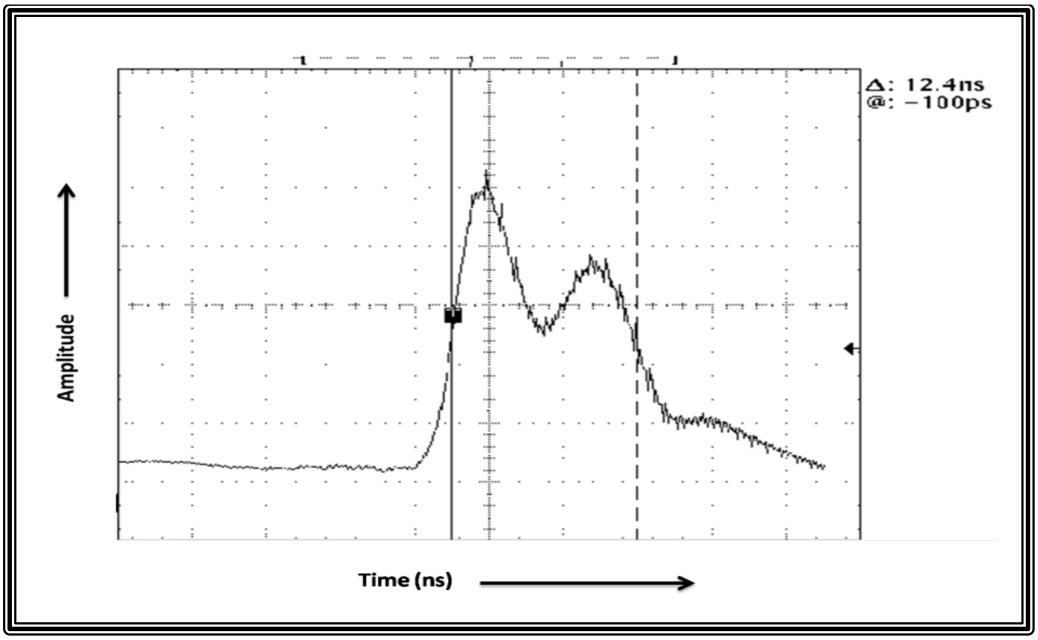

Fig 5.44: Amplified SLM dye laser pulse with Rhodamine 6G pumped by CVL {X- axis Amplitide, Y- axis time (ns)}

5.11 Measurement of ASE in the Amplified SLM Dye Laser Output

The ASE in the amplified output was measured using f/0.33 monochromator and photodiode. It was observed that the percentage of ASE was as high as 40 – 60% for lower wavelength (below 558 nm) and less than 1% at the 561 nm as shown in figure

5.45. In order to amplify the signal with less ASE, the delay between the signal beam and the pump beam was changed so that the dye signal pulse arrives 1 – 2 nanoseconds before the pump pulse. In general, the ASE was observed to be higher at lower wavelengths.

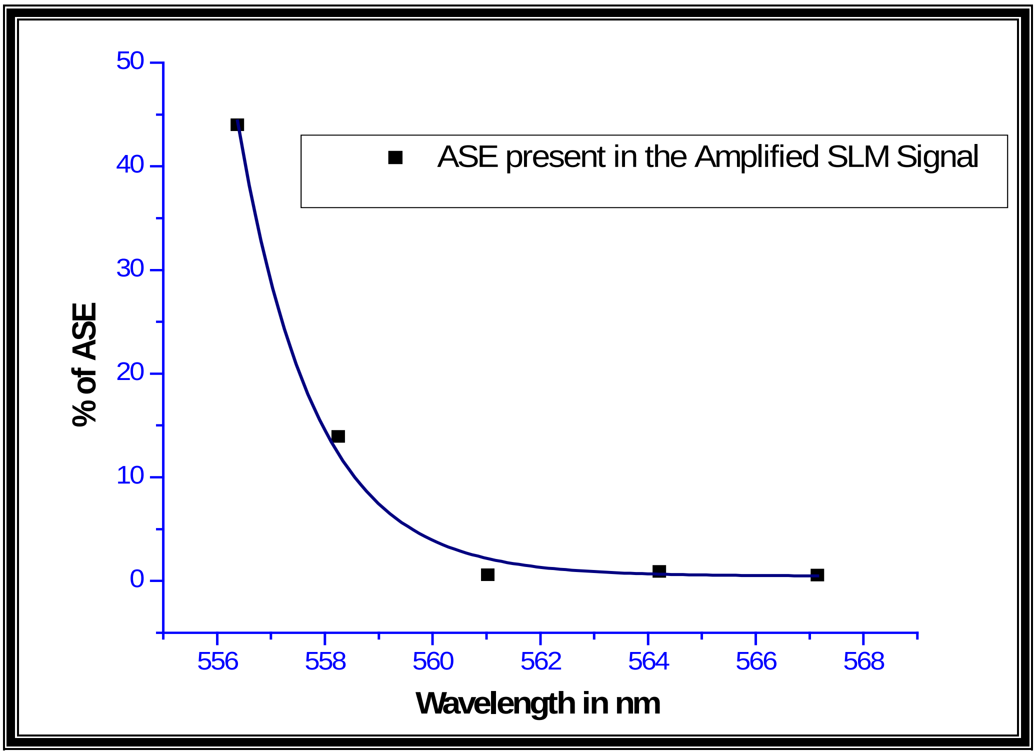

Fig 5.45: The percentage of ASE with amplified SLM dye laser wavelength

5.12 Gain Matching for SLM Amplifier

In order to match the gain of amplifier with the SLM dye laser wavelength, during the amplification process, a 0.6 mM Pyrromethene 567 (PM 567) dye solution with 100 mM antioxidant 1,4 –diazobicyclo [2,2,2] octane (DABCO) was used in the amplifier. The 0.2 mM Rhodamine 6G dissolved in ethanol was used as the gain medium for the SLM dye laser, while in the amplifier 0.6 mM PM 567 was used as the gain medium. This combination of different dyes for oscillator and amplifier resulted in the uniform conversion efficiency with smaller ASE over the entire tuning range of the SLM dye laser. Figure 5.46 shows the amplifier response over the tuning range of the SLM dye laser. It was observed that the amplified output follows the SLM dye laser wavelength tuning curve. With this combination (oscillator Rhodamine 6G + Amplifier PM 567) the gain mismatch in the oscillator and amplifier was virtually eliminated.

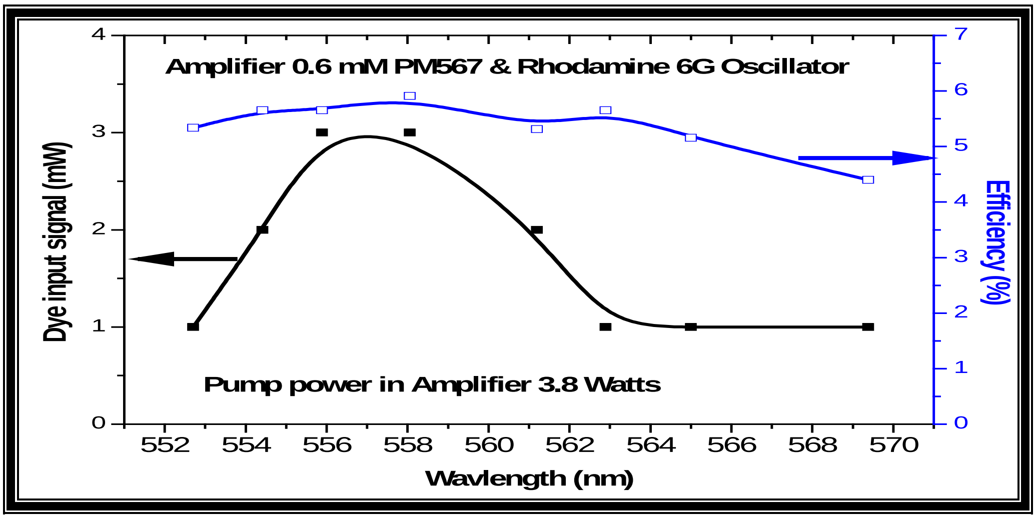

Figure 5.46: SLM Input Signal and Amplifier Efficiency versus Wavelength

5.13 Summary of the Characterization Experiments

1. A single longitudinal mode pulsed GIG dye laser pumped by 9 kHz repetition rate copper vapor laser has been indigenously developed and characterized.
2. The nominal laser single pulse bandwidth and time averaged linewidth were measured to be 315 MHz and 400 MHz respectively.
3. The SLM output wavelength was easily tunable over 12 nm. This tuning range was observed to be a function of the dye concentration and pump power.
4. A mode hop free tuning of 70 GHz was achieved.
5. The amplified spontaneous emission (ASE) was minimum at the peak of the tuning range and increased in both directions of the tuning curve. The ASE increased from 0.33 % to 2 %, the build up time reduced by 3 ns and the peak wavelength of the tuning curve was red shifted by 4 nm with an increase in dye concentration from 0.15 mM to 0.5 mM of Rhodamine 6G dissolved in ethanol.
6. The effects of pump power, grating efficiency and dye concentration on the buildup time was studied.
7. The buildup time decreased from 15 ns to 12 ns by increasing pump power from 1 Watt or 3 Watt; the pulse duration increased from 3.5 ns to 8.5 ns as the pump power was increased.
8. A single mode linewidth of ~ 180 MHz could be obtained from the SLM dye laser, when pumped by the second harmonic of Nd: YAG (10 Hz).

9. As the pump power increased in the Nd:YAG pump laser beam the bandwidth also increased for the same flow velocity.

5.14 Typical SLM Parameters

In summary, the typical / nominal SLM parameters found during the characterization experiment can be written as follows and summarized in table 5.2

S.No.	Parameters	Value
1.	Time average SLM bandwidth of 9 kHz	~ 400 MHz
2.	Single Pulse Bandwidth	~ 315 MHz
3.	Tuning Range	556 – 568 nm (~ 12 nm)
4.	Peak Wavelength for Rhodamine 6G	562 nm
5.	Mod Hop free Scanning	~ 70 GHz
6.	Output Power	~ 30 mW
7.	Amplified SLM Power	~ 450 mW
8.	Conversion Efficiency for SLM dye laser	~ 2 %
9.	Conversion efficiency for Amplifier	~ 9 %
10.	SLM Pulse Duration	~ 6 – 8 ns
11.	SLM pulse duration with stretched pump pulse	21 ns
12.	Bandwidth with stretched pump Pulse	600 – 650 MHz
13.	SLM buildup Time	~ 8 – 10 ns
14.	Beam Divergence	0.5 mrad
15.	Amplified Spontaneous Emission (ASE)	~ 0.3 % at peak wavelength
16.	Laser Dye	Rhodamine 6G in Ethanol
17.	Dye Concentration	0.2 mM
18.	Pulse Energy Stability of Dye laser	~ 4 – 10 %
19.	Free running wavelength variation	± 0.4 pm

Table 5.2: Summary of Experimentally Obtained SLM Parameters

References

[5.1] I S Grigoriev, A B Dyachkov, V P Labozin, S M Mironov, S A Nikulin, V A Firsov, “Tunable dye laser amplifier chain for Laser isotope separation”, Sov, Quantum Electronics 34, 447 – 450, 2004.

[5.2] G Z Zhang K Hakuta, “Scanning geometry for broadly tunable single mode pulsed dye lasers”, Opt. Lett. 17, 997 – 999, 1992.

Chapter – VI

TEMPERATURE EFFECT ON THE SLM DYE LASER

6.1 Introduction

The narrow band tunable dye laser oscillator shows an intrinsic sensitivity to certain physical phenomena. It is seen that increase in the temperature of active volume of transversely excited dye laser results in an increase in the beam divergence, decreases the laser output power and shifts the resonant laser frequency [1.8, 1.20, 1.26, 6.1–6.7]. Thus, thermal stability is an important requirement necessary to control the emission characteristics of dye lasers. In general, thermal effects can be classified into two categories: those that affect the molecular dye medium and those that alter the physical outline of the cavity. It is reported that the dye laser output is influenced by the temperature difference between the dye solvent and cooling water [1.6, 6.8]. It has also been reported that the optimum temperature difference may be bimodal and depends on the laser dye, the solvent and to a certain degree on the pump pulse energy. In addition, thermal gradients within the active medium in conjunction with turbulence are identified as the mechanisms causing bandwidth instabilities in the dye lasers [2.45, 6.9 - 6.12]. The decline in the output energy due to increase in temperature is ascribed to various effects, including conformational changes in the molecular structure of the excited dye molecules; this effect may be reduced by utilizing dyes with rigidized structures. It was reported that some of the laser dyes (Rhodamine 6G) exhibit good recovery characteristics when re-cooled. For the single mode laser even a small change of $\Delta T \sim 1\ ^{O}C$ can induce a serious frequency detuning [6.1]. Lalanne et al. had studied thermal relaxations in liquids by study of transient thermal blooming induced by a Nd:YAG microsecond pulse; the decay of the thermal lens was analyzed by a probe, namely non-absorbing CW He – Ne laser [6.13]. M V Muniz et al. had explained the various mechanisms of non radiative channel such as conversion of vibrorotational molecular energy into the kinetic energy of the solvent molecules, internal conversion processes non radiative deactivation of S_1 to S_O and S_n to S_1 and deactivation of the sublevels of the ground state [6.14]. The thermal characteristics of the solvent are directly responsible for temperature related changes in the optical parameters of the cavity.

Yaltkaya et al. had experimentally observed that with increasing dye solution temperature, refractive index decreases for commonly used dye solvents [6.5].

Burlamacchi et al. had reported, as the heat transfer proceeds, the thermal and refractive index gradient increases, which deflect the laser beam towards the higher refractive index region, this may change the incidence angle on the grating [6.7]

H W Schroder et al. had reported the temperature rise may be 3 – 5 K above ambient temperature in the dye cell close to dye cell windows [1.28]. Zhou had calculated temperature rise of 1.1 K for 1 mJ pulsed nitrogen laser with 25% conversion of pulse energy into heat in the dye solution [1.12].

Hercher and Pike had mentioned that at lower dye concentration the amount of absorption of the pump radiation in the dye cell reduces, while higher dye concentration increases the localized heating of the dye cell windows. This localized heating produced transient distortion in the dye cell windows, which could misalign the laser [2.2].

In this chapter the effect of dye solution temperature on the SLM dye laser is discussed and an estimation of the transient temperature rise in the dye cell due to absorbed pump pulse was carried out using general purpose CFD software.

6.2 Thermal Effect in Dye Laser

The energy deposited by the pump beam on the dye laser medium causes changes in the temperature and hence in its density. The density change, which is the main cause of change in the refractive index, occurs in a time scale of ~ 1μs. This time scale does not affect the optical homogeneity for the single pulse duration (30 – 40 ns) of the CVL. In the high repetition rate of (5 – 10 kHz) of CVL pumping the effect is cumulative and severe. Amit et al. had carried out a detailed study with CVL pumped Rhodamine 6G dye dissolved in methanol with 10 % ethylene glycol flowing through a dye cell of 0.5 mm width at velocities of 18.3 m/s [1.26]. They observed a strong perturbation of refractive index at all points downstream of the 0.2 mm x 10 mm pumped strip and also 1 – 2 mm in the upstream direction, when a 20 Watts CVL was used to provide one sided pumping to the dye cell. An experimental study carried out by Amit et al. with a He – Ne laser beam probing the dye cell parallel to pumped strip showed both angular broadening and steady deflection along the temperature gradient direction.

$$\theta_x = L_1 \frac{dn}{dx} = L_1 \frac{dn}{dT} \frac{dT}{dx} \tag{6.1}$$

where L_1 is the path travelled by He – Ne laser beam, which is equal to the length of the spot illuminated by the pump beam, $\frac{dn}{dT}$ is temperature dependent refractive index and $\frac{dT}{dx}$ is the temperature gradient along the pump beam (x – axis).

The broadening of the laser beam is termed as thermal blooming, which causes phase aberration to the laser beam. The thermal gradients can also cause thermal lensing effects.

The energy transfer from the excited dye molecule to the solvent is due to the non – radiative transitions in the vibrorotational states of the dye molecule. These transitions are singlet to singlet states inter system crossing and triplet to triplet states. The decay constants for these transitions are substantially different for each process; hence they contribute differently to the heating mechanism in the dye gain medium. The thermal effects observed during laser action, depends on the rise time and pulse duration of the pump pulse [6.7]. The rotational relaxation time for Rhodamine 6G in low viscosity solvents (alcohols) ranges from 100 – 400 psec to 2.3 nsec for soap solutions. The inter system crossing time is about ~ 40 ns and lifetime for the triplet state may vary from 10^{-7} to 10^{-3} sec depending on the amount of the triplet quencher present in the dye solvent. The triplet state transition is expected to give a negligible contribution for CVL pumped dye lasers as pump pulse duration is only 30 – 40 nsecs. The long term heating effects due to heat diffusion must be taken into account for repetitive pulsed operation of the dye laser. At the very beginning of the exciting pulse, the heat evolved is small, hence the thermal effects are minimal. As the heat transfer increases, the thermal and refractive index gradients increase, which results in deflection of the laser beam towards higher index region. The maximum bending of the laser beam occurs before it travels a distance equal to the absorption length in the propagation direction.

6.2.1 Thermal Blooming

The energy absorbed in the dye solution primarily determines the amount of heat available for perturbing the index of refraction in the dye medium. The flow velocity determines the time available for the heated medium, before it is swept out from the active region to affect beam propagation during the subsequent pulse. The pump power absorbed by the medium per unit volume is α_1 I, where α_1 is the absorption coefficient of dye medium and I is the intensity of the pump beam. The temperature change per unit time is defined by

$$\frac{dT}{dt} = \frac{\alpha_1 I}{\rho C_p} \tag{6.2}$$

where T is the temperature, ρ is the density of the medium and C_p is the specific heat at constant pressure. The temperature change per unit time in turn produces a change in the index of refraction per unit time

$$\frac{dn}{dt} = \left(\frac{\alpha_1 I}{\rho C_p}\right)\frac{dn}{dT} \tag{6.3}$$

where n is the refractive index.

Typically, in dye solvent ethanol the refractive index decreases with increasing dye temperature as $\frac{dn}{dt}$ is negative. The negative refractive index transforms the medium into a diverging lens, which leads to spreading of the laser beam, which is termed as thermal blooming. The thermal lens effect directly depends on the absorbance and the thermo optical properties of the dye solvent. Alcohol is more prone to thermal lensing effect due to its higher value of $\frac{dn}{dt}$ and lower value of thermal conductivity (k). Flow turbulences can exacerbate the effect of thermal blooming. In a turbulent flow, the laser beam develops irradiance variations on a smaller scale (due to eddies) transverse to the propagation direction, even as the heat deposited by the laser beam varies also in the same scale, producing a strong phase gradient (wave front distortion). This directly increases the angular deflection of the laser beam.

6.2.2 Thermal Diffusion

In the transient (unsteady state) heat transfer process, the temperature gradient caused by non-radiative relaxation of excited dye molecules induces thermal diffusion and also the migration of molecules in the thermal gradient. The thermal diffusivity, D_T, is given by

$$D_T = \frac{\boldsymbol{k}}{\boldsymbol{\rho C_p}} \tag{6.4}$$

where k is the thermal conductivity in W/m-K. The thermal diffusivities of various organic dye solvents and quartz are tabulated below.

S.No.	**Medium**	**Thermal diffusivity D_T (m^2s^{-1})**
1.	Methanol	1.08×10^{-7}
2.	Ethanol	9.33×10^{-8}
3.	Ethylene Glycol	9.71×10^{-8}
4.	Glycerol	1.00×10^{-7}
5.	Quartz	1.4×10^{-6}

Table 6.1: Thermal Diffusivity Values for Commonly Used Dye Solvents and Quartz Window of Dye Cell [6.15]

It is observed from table 6.1 that the thermal diffusivity of quartz is around 15 times more than the frequently used dye solvents. In the case of pulsed laser (CVL) excitation, the pulse width of the laser is very small (~30 ns) and the rate of the radiation less transition is very fast in comparison to the decay rate of the thermal lens effect. The decay time of thermal lens known as the characteristic time (t_c) is related to the thermal diffusivity (D_T) and the beam radius (ω_o) on the liquid through the relation [6.15]

$$t_c = \frac{\omega_o^2}{4D_T} \qquad (6.5)$$

6.3 Theoretical Simulations for Transient Temperature Rise

The transient temperature rise in the dye gain medium was simulated using a general purpose CFD code. The physics model used in the simulation is described below.

6.3.1 Physics Model

The pump energy absorbed by dye molecules in the dye cell follows the exponential absorption law i.e., Beer Lambert Law. It is reported that about 25% of absorbed pump power is converted into heat [1.26, 6.7, 6.9] for CVL pumped dye lasers and consequent temperature related optical in-homogeneities. Since, the CVL pulse duration (~30 ns) is long with respect to the radiative decay of the laser dye time (~ 4 – 5 ns), steady state absorption is assumed. For the calculations, only a linear absorption coefficient for the dye gain medium has been used. The effect of excited state absorption is not considered in these simulations. Relaxation from S_n to S_1 is very fast, hence to saturate S_n, transition pump intensities of 10^9 – 10^{10} W/cm^2 are required. At lower intensities the excited state absorption will represent the residual absorption [6.16, 6.17]. On absorption of the pump beam, the temperature gradient produces a refractive index gradient, which is maximum near the dye cell window from where the pump beam enters the dye cell. The temperature at any point varies according to the dye concentration and absorption coefficient. The rate at which, energy is absorbed at any point within the dye cell depends exponentially on the width of the dye cell through which the beam has travelled. If the dye cell width is l_d and pump intensity I_O (W/cm^2) is incident on the dye cell, the rate of heat absorbed per unit volume is given by

$$H_{abs} = \xi I_O\, e^{-\alpha_1 l_d(x)} \tag{6.6}$$

where ξ is the conversion factor for absorbed energy to heat; α_1 (= σ *N') is the linear absorption coefficient, which is a function of dye concentration (N' number of molecules per cc) and absorption cross section (σ) for pumping wavelength, $l_d(x)$ is the dye cell width. On absorption of the pump beam, the temperature of the liquid will become [6.18]

$$T(x) = T_O + T_m\, e^{-\alpha_1 l_d(x)} \tag{6.7}$$

where T_O is the initial temperature of dye solution, T_m is the temperature rise at the surface where the pump beam is focused. T_O temperature has contributions of ambient temperature, friction on the dye wall and heat added by the gear pump to the dye solution. This temperature is controlled by cooling the dye solution in a large reservoir in which a constant temperature is maintained. The second term in equation 6.7 is mainly due to pump pulse energy, which is controlled by removing the heated volume before the arrival of the next pump pulse.

It has been reported by Balucani and Tognetti [6.9] that of the two processes that contribute to the heat generation on the absorption of pump beam, one is due to the quantum yield (Φ) of the dye solution, where fraction (1 – Φ) of photons will directly convert into the heat. The second process is directly connected with the fluorescence process. The Stokes energy difference h$(\nu_{ab} - \nu_{em})$ is converted into heat energy and is commonly known as the quantum defect. They had also seen the maximum temperature rise at the cell wall is of the order of 1 K for 1 mM Rhodamine 6G dye dissolved in ethanol, and the magnitude of thermal lensing effect increases with dye concentration. Excess heating of dye solvent leads to undesirable changes in cavity length (thermal expansion), optical aberrations and also chemical changes in the active material [6.19, 6.20].

6.3.2 Computational Fluid Dynamics Model

The CFD software was used to numerically solve the fluid flow in the domain and estimate the temperature generated during the pulse and in steady state. The CFD code has been discussed in detail in Chapter – IV of the thesis. A user defined function (UDF) was written in the expression language of CFX for providing the exponentially decaying volumetric heat source in the flow domain of the active region of the SLM dye laser. For simulating the pulsed heat source, transient time (unsteady state) runs were conducted for 30 ns heat source. The 30 ns duration represents the ON state of heat source, while the OFF state of pump pulse was represented by transient time run for 111 µs without the volumetric heat source. This duty cycle corresponds to the 9 kHz pulse repetition rate of the pump pulse. The 30 ns time scale is very small for developing a velocity profile inside the flow channel of the dye cell. Hence the input file for the transient time run was generated with steady state velocity profile in the dye flow channel. The time for steady state was chosen to be three times the residence time for the SLM dye cell. For solving the partial differential equations, the solver requires boundary conditions to be imposed on the dye cell flow domain. The boundary conditions for the simulations were inlet flow velocity in meter/second at a constant inlet temperature of 300 K, outlet pressure of 1 atm and zero flow velocity (no slip) at the solid liquid interface. At the no slip condition boundary the fluid temperature is taken equal to the temperature of the surface. The heat source was represented by a cylinder of 200 µm diameter and 1 mm length, as the pump pulse energy is longitudinally focused on the dye cell by a plano convex lens of 200 mm focal length. This exponentially decaying volumetric heat source increases the dye solvent temperature locally along the pumping direction. The temperature distribution along the pump beam direction for the SLM dye laser was studied in detail.

6.3.3 Thermal Gradient Along Resonator Axis

As discussed, the part of the pump laser heats the dye solution in a time scale shorter than the thermal time constant of the system. The thermal time constants are governed by diffusion processes. The coefficient of mass diffusion is two to three orders of magnitude smaller than the coefficient of thermal diffusion. Hence the time required to create a thermal lens is much smaller than to create the concentration gradient. The temperature rise is evidently more near the wall of dye cell where the fraction of absorbed pump power is the highest.

The computational results show the highest temperature rise of ~ 3 K near the dye cell window for the dye concentration of 0.2 mM in ethanol and pump pulse energy of 166 µJ per pulse. Figure 6.1 shows the thermal gradient generated by the absorption of the pump pulse along the pump beam propagation direction and the angular deflection of the laser beam due to the thermal gradient as calculated using equation 6.1. It is clear from figure 6.1 the angular deflection is more near the dye cell window from where the pump beam enters into the dye medium.

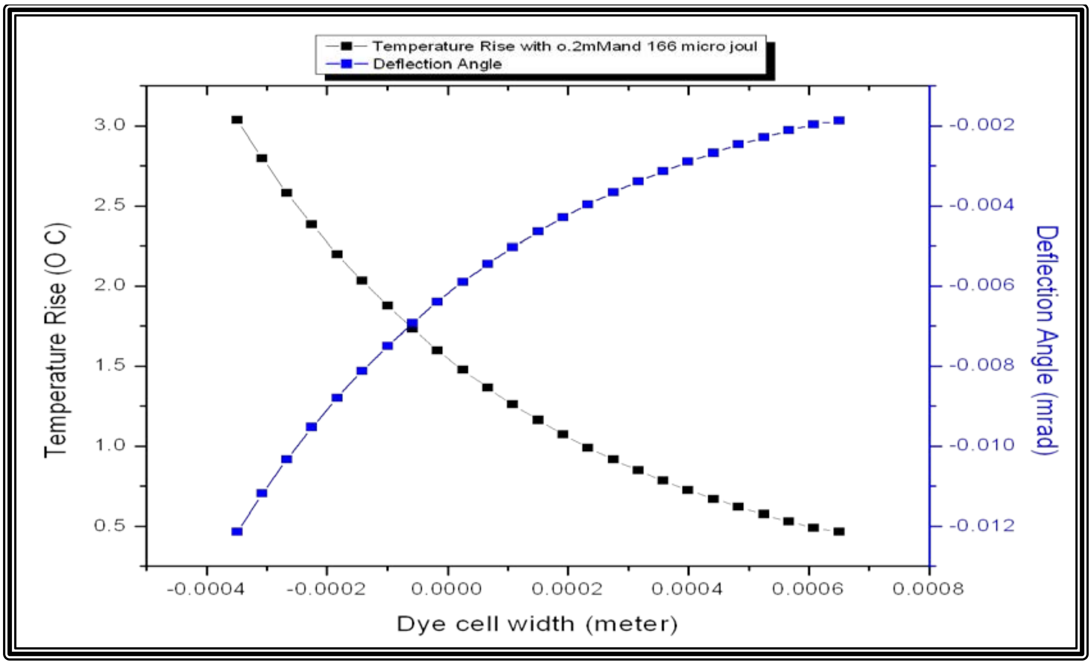

Fig 6.1: Temperature gradient generated along the pump beam direction by 166 µJ energy per pulse with 0.2 mM dye concentration and deflection angle in mrad.

6.3.4 Effect of Pump Pulse Energy

The temperature rise for three different pulse energies 166 µJ, 332 µJ and 489 µJ was simulated and the temperature rise along the pumping direction is plotted as shown in the figure 6.2 for the same dye concentration of 0.2 mM. It is observed that if a pulse energy is increased for constant dye concentration of 0.2 mM (absorption coefficient~ 1927 m^{-1}) the temperature rise was observed on the front face as well as the exit face of dye cell, that is, the temperature rise was observed over the full gain length of the dye cell. The change in the cavity length due to temperature change detunes the laser from the set wavelength. The maximum temperature rise was 9 K at the entrance face and nearly 1.5 K at the exit face of the dye cell for 498 µJ pump pulse energy. The temperature rise was only 3 K at the entrance face of the dye cell when the pump pulse energy is reduced by three times.

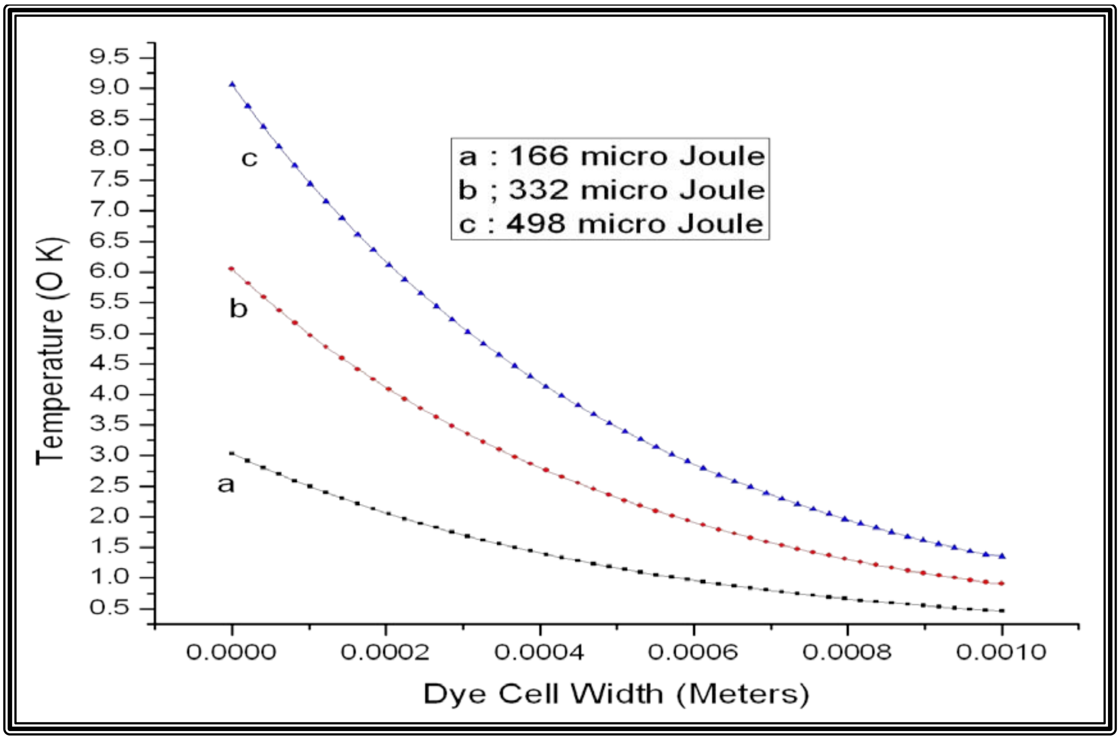

Fig 6.2: Temperature rise in the dye cell for different pump pulse energy with 0.2 mM Rhodamine 6G) in ethanol

6.3.5 Effect of Flow Velocity

The transient temperature rise for each pulse of 9 kHz pulse repetition rate CVL was computed. The code was run for different durations (total time) to simulate a number of pulses of the pumping laser, with 30 ns ON period and 111 µs OFF period. The results obtained from one simulation were taken as input to the transient solution of the next pulse. It was observed that the heated volume due to the first pulse is displaced by ~ 720 µm before the arrival of the next pulse as shown in figure 6.3. If the flow velocity is reduced, there is an overlap of both pulses resulting in higher temperature. Figure 6.4 shows the temperature contour for successive pulses where the heated volume by one pulse is not removed before the arrival of the next pulse.

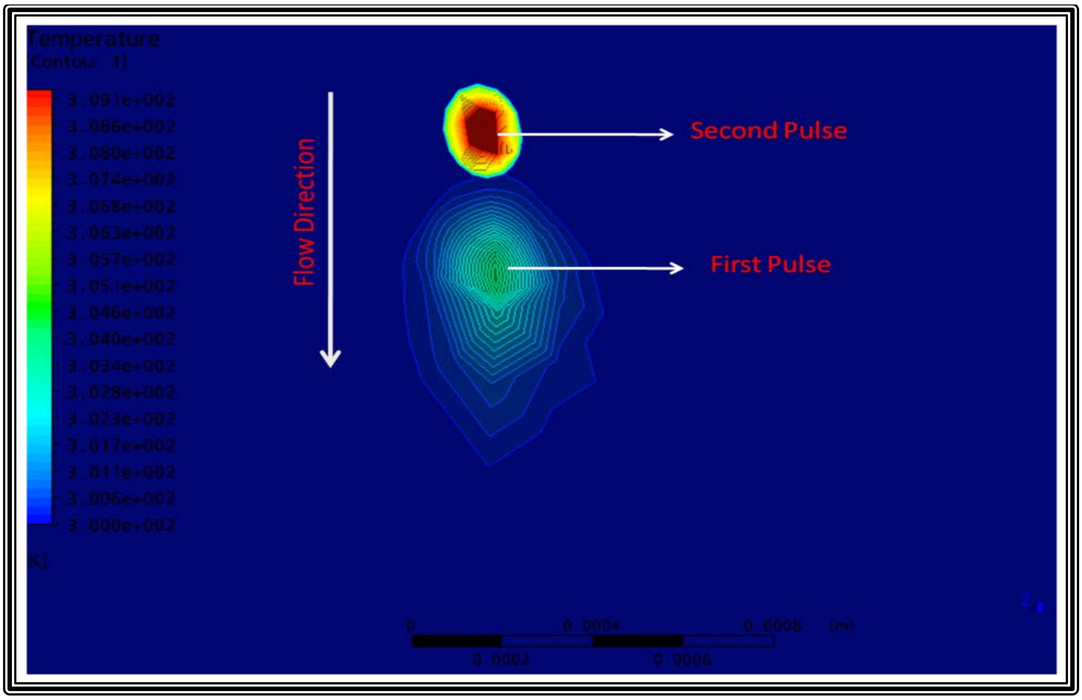

Fig 6.3: Temperature countours of two consucutive pulses, the heated volume is displaced before the arrival of the second pulse.

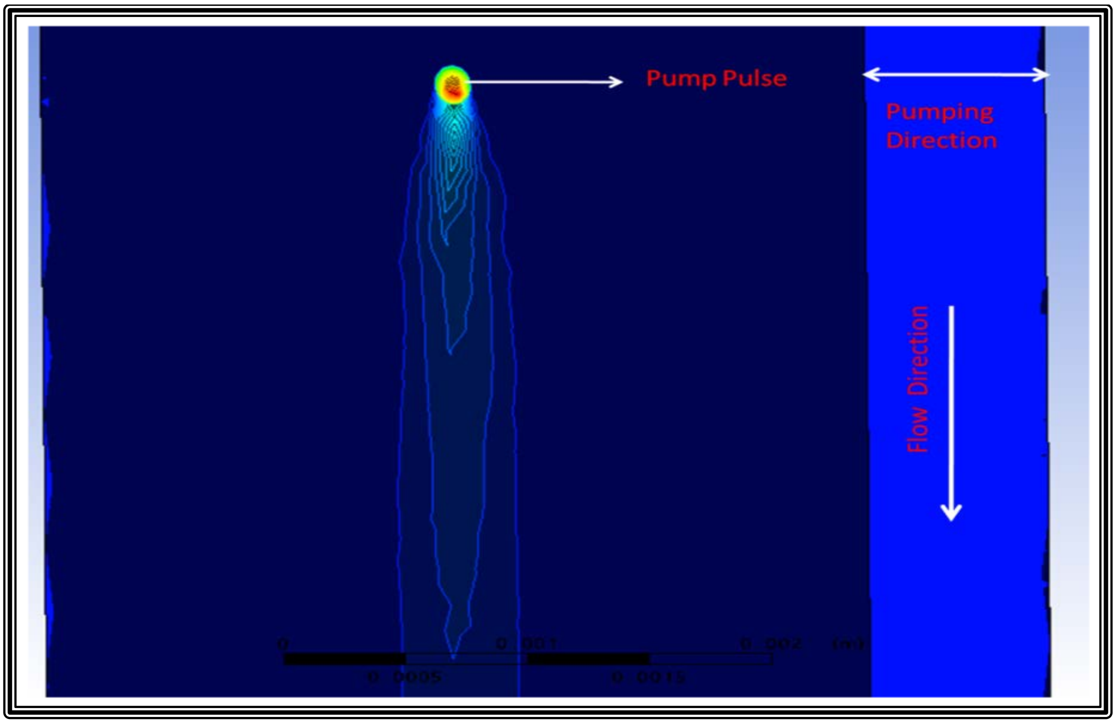

Fig 6.4: The temperature profile for pump in which the heated volume is not displaced completely before the arrival of the second pump pulse

In this case, the temperature rise is cumulative because both the pulses contribute to the temperature at the pumping location. The temperature contour in the dye cell shows the downward movement of the heated volume and for longer duration of simulation with more number of pulses, the heated volume was present downstream all the way to the outlet of the dye cell. A light ray which is parallel to the optic axis of the resonator will bend towards the higher refractive index in the dye cell. This bending of light will change the incidence angle on the grating and ultimately alter the spectral resolution of the grating, which is a function of incidence angle. This leads to higher bandwidth and large wavelength drift of the SLM dye laser. The thermal effects are more severe for higher temperature rise, which is obviously more with higher dye concentration and higher pump pulse energies.

6.3.6 Effect of Dye Concentration

For the computational experiment with different dye concentrations the value of absorption coefficient is changed in the UDF according to the dye concentration. With increase in dye concentration, the absorption coefficient increases as the number of dye molecules per unit volume of solvent increases. The CFD code was run with a transient time of 30 ns for each dye concentration. As expected, it is observed from the results (figure 6.5) that for higher dye concentration, the temperature gradients are higher near the entrance window of the dye cell.

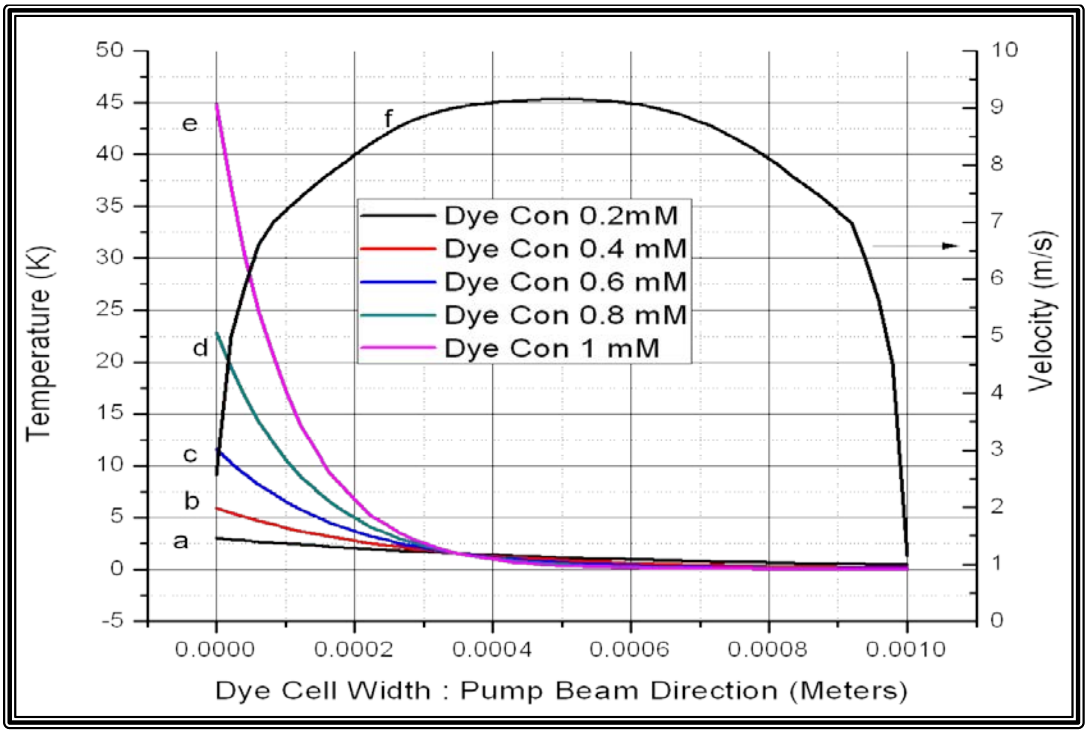

Fig 6.5: Temperature rise in the dye cell for different dye concentrations a: 0.2 mM, b: 0.4mM, c; 0.6 mM, d: 0.8 mM, e: 1.0 mM and f: velocity profile within the dye cell.

It was found that the temperature gradient remains only up to ~ 350 µm along the pump beam direction in the dye cell for each dye concentration. The temperature rise at the entrance window of the dye cell is as high as 45 K for the dye concentration of 1 mM. This high temperature gradient near the dye cell window seriously detunes the dye laser and also the operation of single mode is hindered. The figure 6.5 also includes the velocity profile inside the dye cell along the pump beam direction. The figure 6.6 shows the variation in the refractive index along the dye cell width for the dye concentration of 0.2 mM and pulse energy of 498 µJ. The higher dye concentration shows high thermal gradient that results in a high refractive index gradient, which creates a more diverging power of the thermal lens. It is observed from the figure 6.5 that the temperature rise near the dye cell window is almost 15 times higher for 1 mM dye solution in comparison to 0.2 mM dye concentration for the same pump pulse energy.

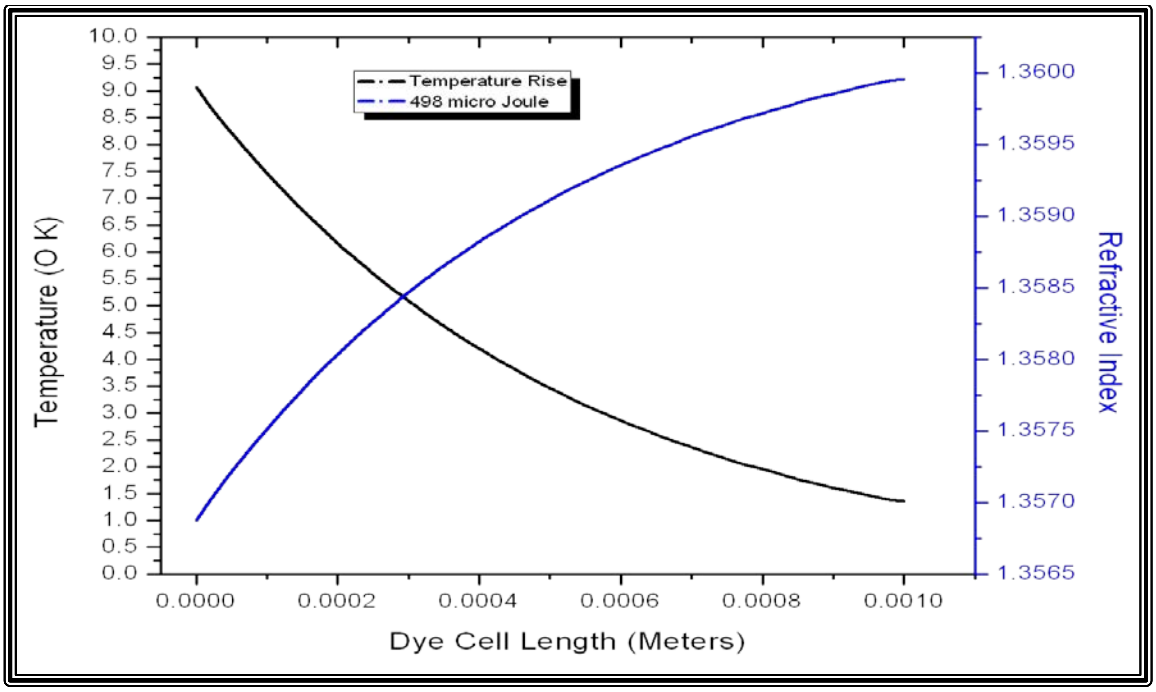

Fig 6.6: Temperature rise and refractive index variation of ethanol along the dye cell width

6.3.7 Frictional Temperature Rise

Fluid friction transforms the kinetic energy of (macroscopic) motion into the heat energy. The frictional temperature rise due to viscous dissipation in the dye cell was computed for three commonly used dye solvents using the CFD model. These solvents were ethanol (1.02 cP), ethylene glycol (30 cP) and glycerol (1400 cP). The temperature rise due to friction along the dye cell width was plotted as shown in figure 6.7 for these three solvents with inlet flow velocity of 1 m/s. It is observed that the frictional temperature is highest near the dye cell walls, where the flow velocity is minimum. The highest frictional temperature rise is about 1.1 K for glycerol; the lowest frictional temperature rise is for ethanol, about 29 mK. The frictional temperature rise for ethylene glycol was nearly 36 mK for inlet flow velocity of 1 m/s. The frictional temperature rise depends on the flow velocity inside the dye cell; it was ~ 29 mK for higher flow velocities (1 m/s) and lower (~ 9 mK) for smaller flow velocities (0.5 m/s) for ethanol. The steady state results of the simulation of the frictional temperature rise inside the dye cell are presented here.

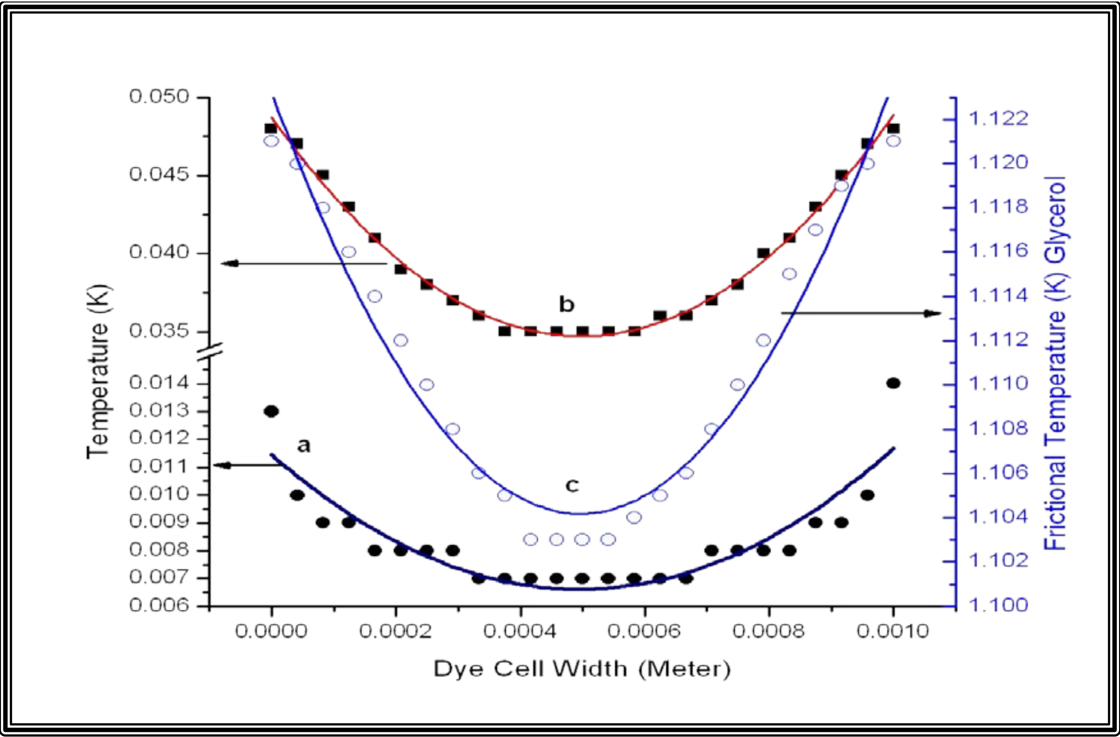

Fig 6.7: Temperature rise in the dye cell due to friction for three different solvents a: Ethanol with 0.5 m/s inlet flow velocity b: Ethylene Glycol and c: Glycerol for inlet flow velocity of 1 m/s in SLM dye cell.

The pressure drop across the dye cell for glycerol, ethylene glycol and ethanol for the above boundary conditions were 6.77 x 10^6 Pa, 3.3 x 10^6 Pa and 1.17 x 10^6 Pa respectively, as a direct consequence of their viscosity.

6.4 Validation of CFD Model

The validation of the model is done by comparing the computational results with the experimental results obtained from a similar system. First, the CFD model was validated with the published experimental results by Amit [1.26] et al. They had studied thermal conduction in a flowing dye cell and its effect on the temperature profile. In their experimental setup, they had used 10 mm x 0.5 mm dye cell with flow rates ranging from 0.3 to 5 lpm, resulting in average flow velocities ranging from 1.5 and 23 m/s respectively. The dye solution used was 1 mM Rhodamine 6G in a mixture of methanol with 10% ethylene glycol. A 20 Watts CVL pump beam having 30 ns pulse duration and 4 kHz pulse repetition rate was line focused on to the dye cell over 10 mm x 0.2 mm area normal to flow direction. A 0.5 mW He – Ne laser beam was used to study the temperature profile generated by the pump beam in the dye cell. When a pulsed CVL light was directed onto the dye cell, they observed broadening as well as steady deflection in the He- Ne laser beam, which is due to a steady gradient of refractive index caused by the non-uniform heating of the CVL light absorbed in the dye cell. The deflection angle is related to the refractive index gradient by the equation 6.1.

6.4.1 CFD Analysis for Temperature Rise

This dye cell domain was uniformly meshed by ANSYS ICEM CFD mesh generator. The decaying volumetric heat source was applied to the focused pump beam area of 10 x 0.2 mm^2. A1.25 mJ pulse energy was used for this simulation, as 25% of pump energy was converted into heat energy. The simulation results show a temperature rise of 0.503 K due to one pulse. The frictional temperature contribution for 1.5 m/s inlet flow velocity was 0.001 K, this frictional contribution was computed by running the simulation without any heat source for steady state time scales. The temperature rise for higher inlet flow velocity of 15 m/s was slightly higher (0.042 K) than the lower flow velocity of 1.5 m/s. The temperature rise due to absorbed pump pulse beam was the same for all inlet flow velocities ranging from 0.5 m/s to 15 m/s as shown in figure 6.8. This result confirms that the contribution of frictional temperature for higher flow velocity is more, which but slightly increases the temperature of active volume at higher flow velocity for the same pump pulse energy. As the pump pulse duration is only 30 ns the generated heat cannot diffuse within that time, hence the temperature rise for pulses remains the same for all the inlet flow velocities. The heated volume could be removed by the volumetric flow rate over the OFF period 250 µs (~ 4 kHz) of the pump pulse. It is clearly shown in the figure 6.9 that the heated volume is swept out of the pumping zone.

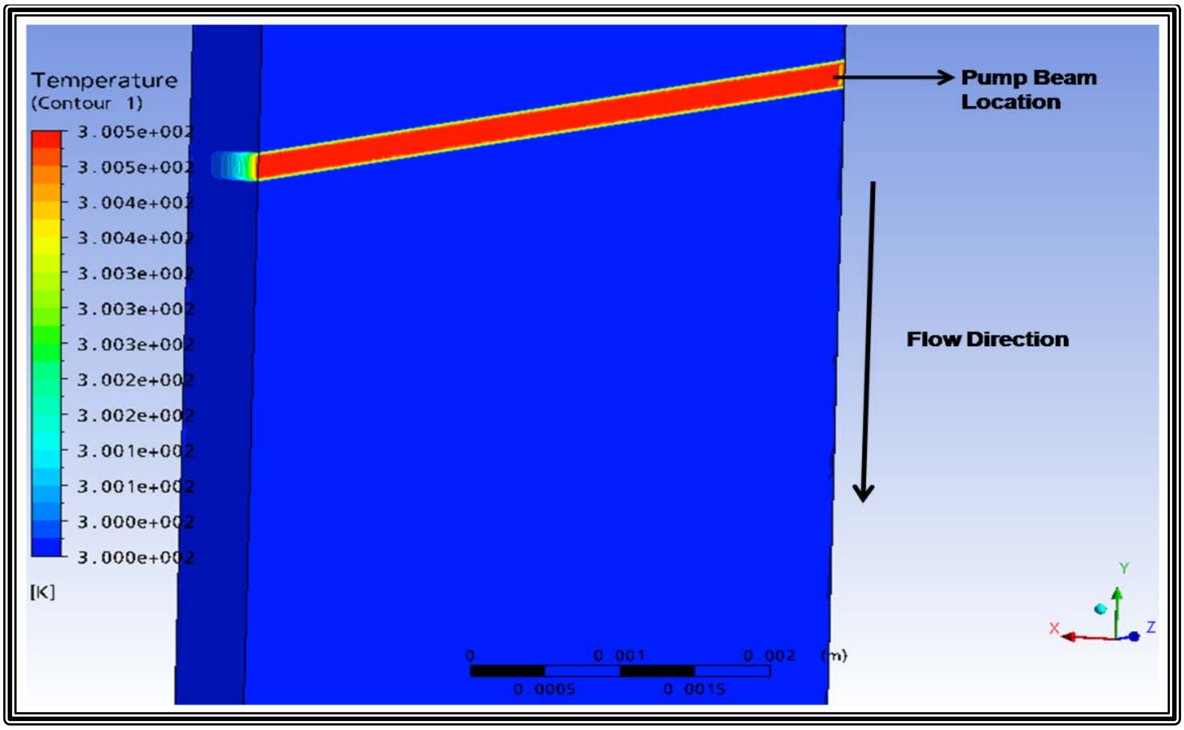

Fig 6.8: Temperature rise in the active volume of the dye cell after 1st Pulse

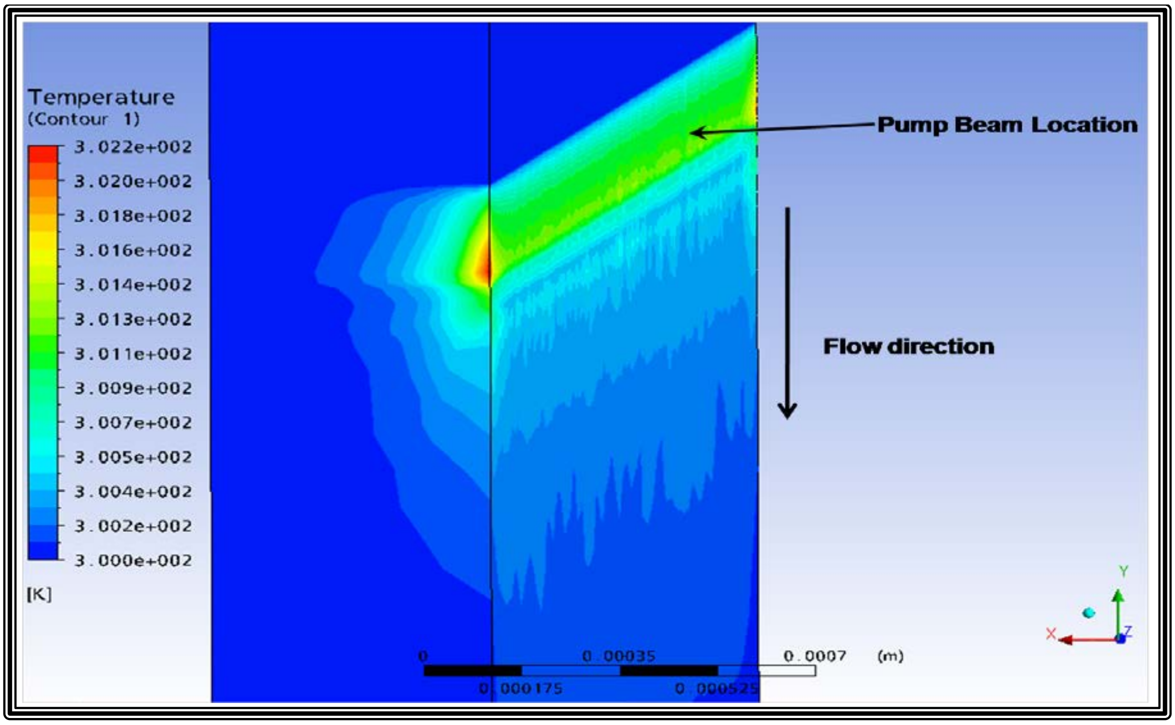

Fig 6.9: Displacement of heated Volume after 7th Pulse off for 1.5 m/s inlet flow velocity

There was no significant upward heat diffusion from the pumping location contrary to the conclusion made by Amit et al. It was observed that at lower flow rates of 1.5 m/s the temperature rises to 2.158 K from 0.503 K after 5th pump pulse reaches the heated volume as shown in figure 6.10, while at higher flow rate the heated volume was removed before the arrival of the next pulse; hence the temperature rise was limited to 0.543 K for successive pulses with inlet flow velocity of 15 m/s.

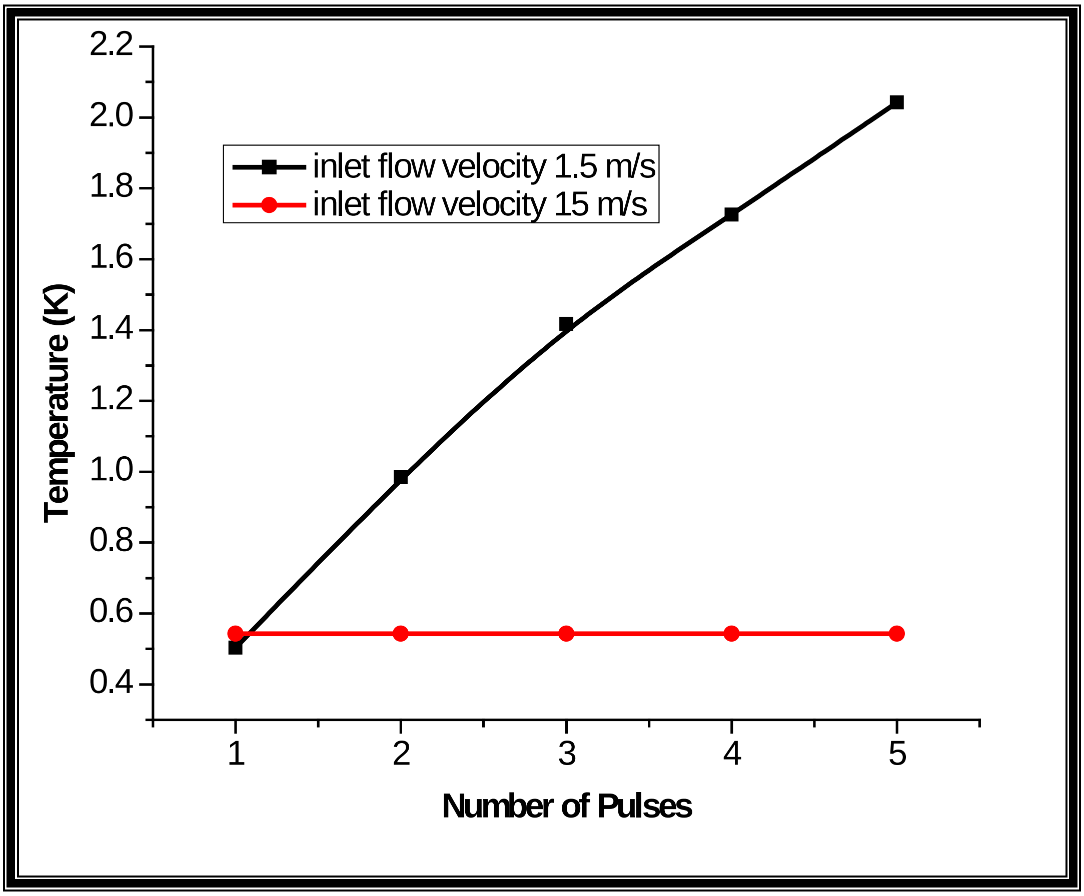

Fig 6.10: Temperature rise in the dye cell after 5 successive pulses with 1.5 m/s and 15 m/s inlet flow velocities.

6.4.2 Thermal Diffusion in Dye Cell

The diffusion length L_D over 250 μs during the off period of the pump pulse was calculated to be 5.196 μm as the diffusion length is related to thermal diffusivity by a relation

$$L_D = \sqrt{D_T T_1} \tag{6.9}$$

$$L_D = \sqrt{(1.08 \times 10^{-7}) m^2 s^{-1} (250 \times 10^{-6}) s} = 5.196 \times 10^{-6}\, m$$

This diffusion length is very small. While the experimental results of Amit et al. showed nearly 2 mm upward diffusion of heat. In the simulation results even for 7 successive pulses, no upward heat diffusion was observed while the heated volume was present for the full length in the downward direction. The absorbed pump energy causes a direct temperature increase with a very small diffusion of heat over the time of the transit period across the spot size of 200 µm at the flow velocity of interest. To observe the effect of flow velocity on the thermal diffusivity the inlet flow velocity was reduced to 1 mm/s from 1.5 m/s for simulation purpose and the CFD code was run for steady state time scales. Thermal diffusion over 275 µm in the upward direction was observed for 1 mm/s inlet flow velocity in the steady state analysis. Figure 6.11 shows the variation in thermal diffusivity length with inlet flow velocity. With higher inlet velocities, the upward thermal diffusion length was less as expected. In summary, the computational results showed no upward diffusion of heat in the dye cell at the flow velocity of interest, while the temperature rise was observed for the full length in the downward direction from the point where the pump pulse was focused.

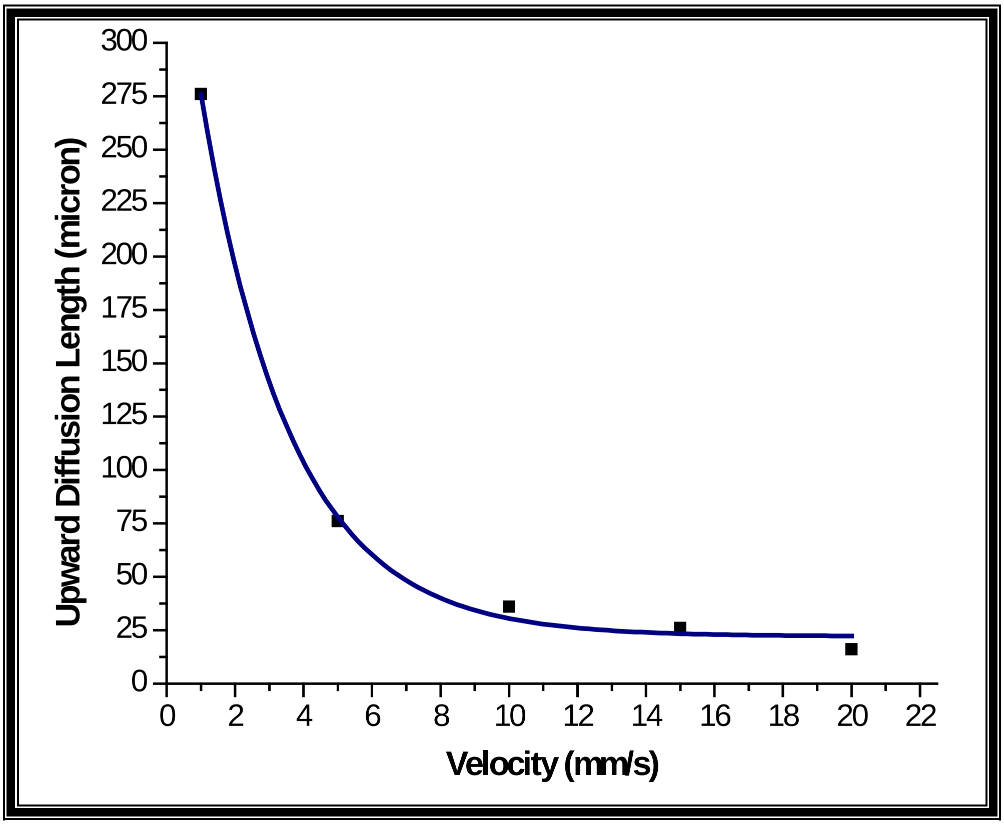

Fig 6.11: Thermal diffusivity for methanol with different inlet flow velocities

When a 0.5 mm thick quartz window was attached to the dye cell and the flow velocity of 1.5 m/s the results showed upward heat diffusion in the dye cell. The absorption coefficient for quartz used for simulation 0.0001 cm^{-1} and 1 mM Rhodamine 6G dye dissolved in methanol was used with 20 W CVL beam, pulse repetition rate of 4 kHz and 30 ns pulse duration. In these simulation pump beam was again focused from the quartz window to the flowing dye. The quartz window was treated as a solid domain, while the dye solvent was in the liquid domain. Figure 6.12 shows the temperature contour for quartz and in the dye cell flow domain, in which the heat diffused in both directions through the quartz as well as into the flowing dye.

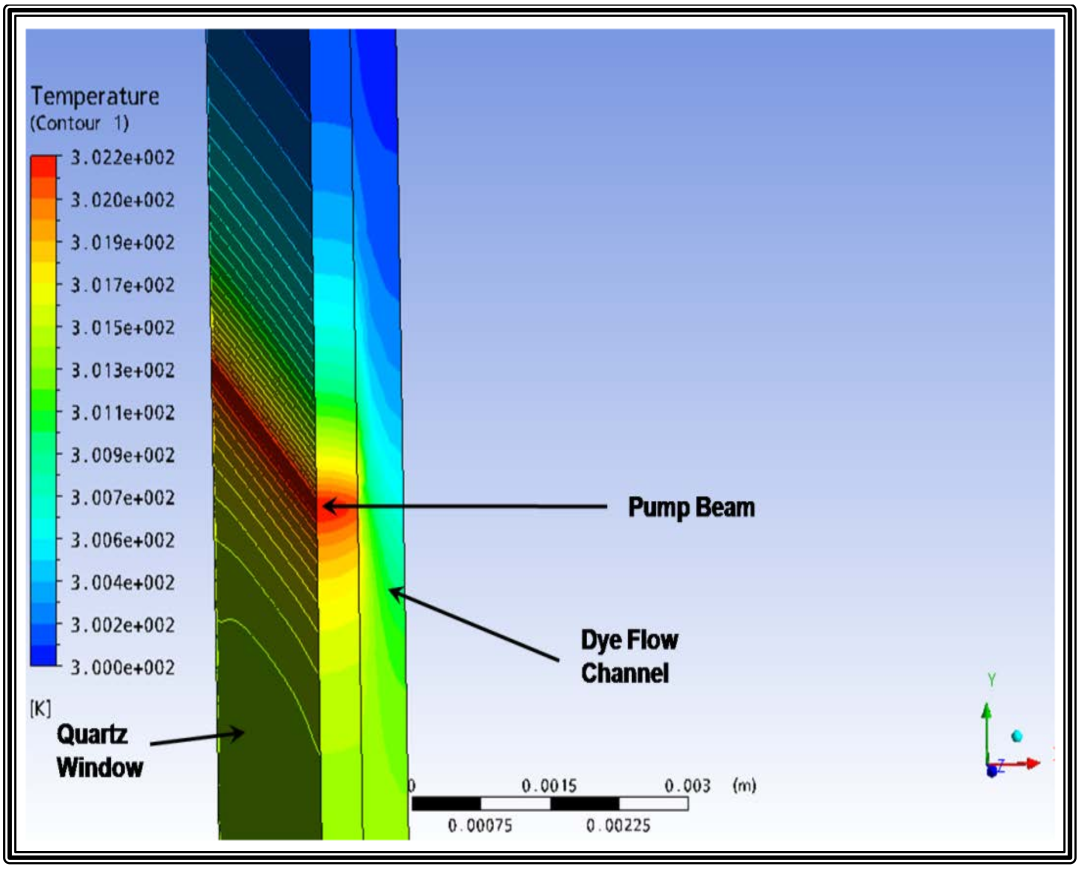

Fig 6.12: Temperature contour in the quartz as well as in the flow domain

The heat diffusion in the upward direction was up to 3 mm from the position of the focused pump beam and over the full cell length in the downward direction. Figure 6.13 shows the temperature rise in the quartz as well as in the dye flow, 4 mm above and 4 mm below from the focused pump beam on the dye cell. It was also observed that at higher flow velocities of 15 m/s, the upward diffusion was less than 0.5 mm for Rhodamine 6G dye in methanol. One can summarize that the disturbance in the heat balance between the heating and cooling cycles of the active volume is primarily responsible for temperature fluctuations in the dye lasers.

It is known that the dye laser power decreases and the beam divergence increases with increasing dye temperature. Increase in dye solvent temperature also causes the wavelength shift due to temperature dependent refractive index. These investigations show that the formation of non uniform refractive index gradients due to non uniform heating in the dye gain medium will be a major limitation in achieving high average power, single mode (spectrally narrow) and spatially coherent (low divergence) laser.

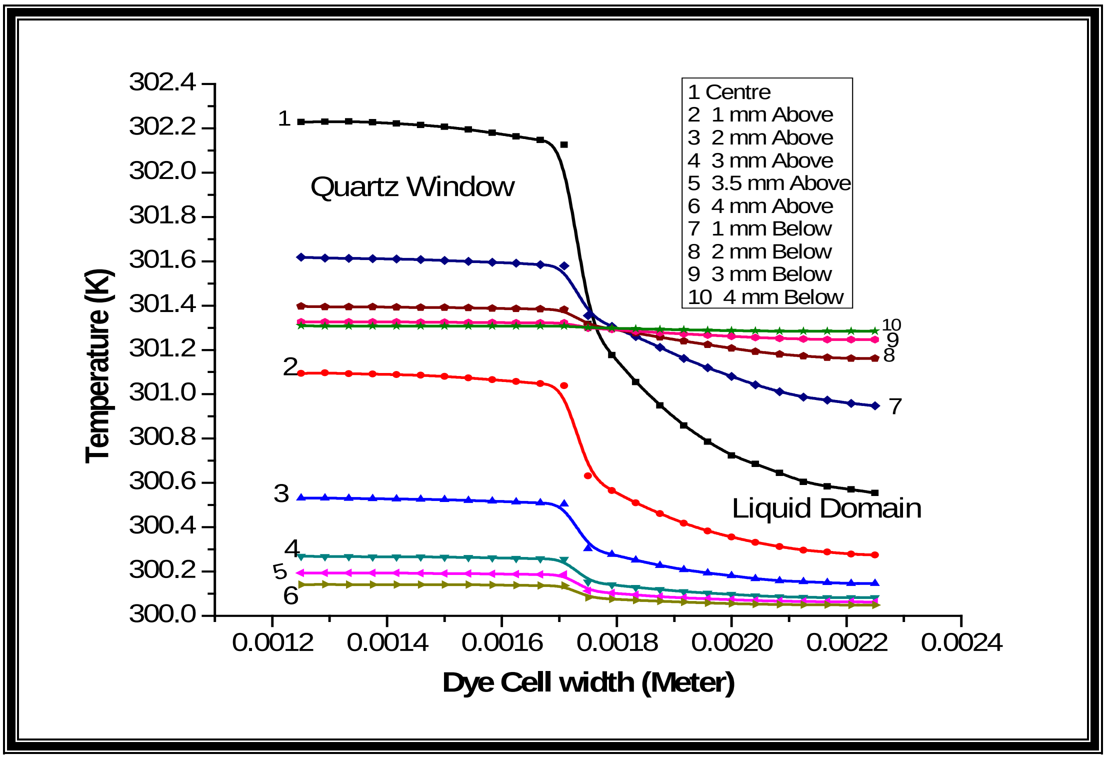

Fig 6.13: Temperature profile in the dye cell 4 mm above and 4 mm below from the focused pump beam.

6.5 Experimental Investigations

An experimental study of the wavelength drift in the SLM high repetition rate (~9 kHz) pulsed dye laser pumped by a CVL has been carried out. The variation in the SLM dye laser wavelength was studied over long hours for a free running operation. The SLM dye laser wavelength was monitored over 2 hours 40 minutes, while the cooling water temperature was kept reasonably constant for the entire period. The SLM dye laser wavelength was measured using a wavelength meter (Angstrom WS – 7L) with an absolute resolution of 60 MHz and accuracy of 10^{-8} [6.21].

6.5.1 Effect of Cooling Water Temperature on SLM

During this experiment, the dye solution temperature decreased from an ambient temperature of 25 ^{O}C to the set value temperature of 20 ^{O}C. As the temperature decreases the dye laser wavelength increases, which can be explained by the fact that the negative value of $\frac{dn_d}{dT}$ for ethanol results in increase of the optical path length of

SLM resonator cavity. The temperature of the dye solution stabilized within a temperature band of ± 0.15 ^{O}C, over 2 – 3 hours. If the dye solution temperature is controlled, then the switching time period, that is, going from the single mode to two mode operations of the SLM and back to single mode is longer. This was confirmed by operating SLM dye laser for a long duration of 2 hours 40 minutes as shown in figure 6.14. It can be observed from the figure 6.14 that the wavelength drift in the SLM dye laser from 564.648 nm (point A) to 564.662 nm (point C) was ~ 26 pm. As per our computational results this wavelength drift is due to the contribution from window heating as well as dye solution cooling. The large wavelength drift is also due to change in the grating incidence angle by laser beam deflection due to thermal gradient occurring in the dye cell windows.

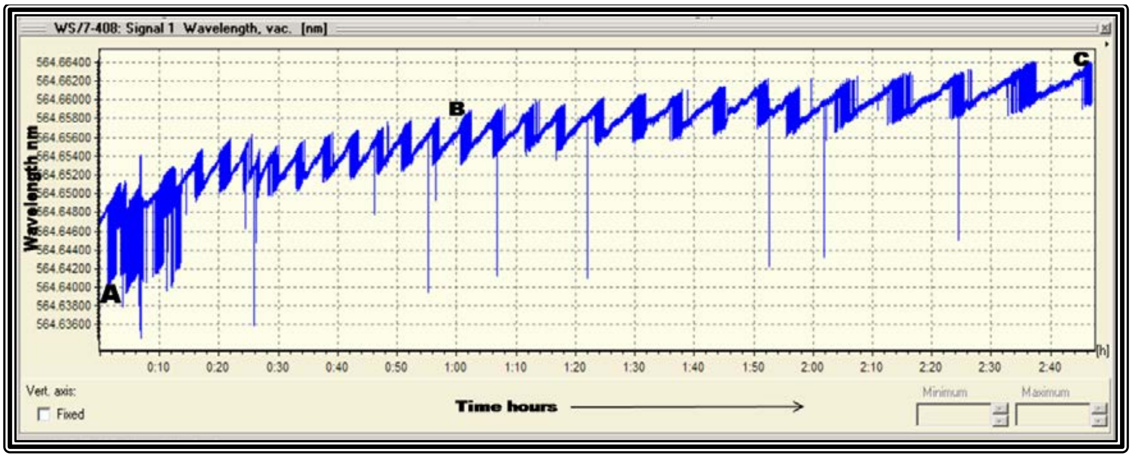

Figure 6.14: Wavelength versus time for a free running SLM operation over 2 hours 40 minutes {X- axis Wavelength (nm), Y- axis time in hours}

It is experimentally determined that the grating pass band at the grazing incidence angle of 89^{O} is nearly 2.5 GHz. Therefore, the cavity mode scanning will be limited to grating pass band (2.5 GHz) by the cavity length tuning procedure. When the cavity mode falls within the peak of the grating pass band, single mode operation is established. As the cavity mode detunes away from the peak of grating pass band peak, nearby modes start oscillating along with the principal mode leading to two mode oscillation.

6.5.2 Settling Time for Dye Solution Temperature

In another set of experiments, the SLM dye laser wavelength was recorded after 1 hour 30 minutes of operation, so that the initial wavelength drift could be avoided. Duration of the wavelength fluctuations measured by wavelength meter either in smaller band or in a larger band depends on the rate of cooling or heating of dye solution as shown in figure 6.15. It is seen that the time period for transition from a single mode to two modes oscillation was nearly 8 minutes from point B to point C and the corresponding wavelength change from 561.4055 nm to 561.4015 nm (~ 4 pm). The time period for single mode oscillation increases to 13 minutes from point F to point G. The increased time period for the single mode operation from point F to point G was due to smaller rate of change of dye solution temperature as it tried to settle to the steady state value of 20^{O}C. Although, the frequent transitions of single and two mode operations were observed, the overall drift in the mean SLM wavelength was limited to 1 pm (561.4055 nm to 561.4045 nm) over a period of 1 hour. The cyclic behavior of single mode to two modes was attributed to the grating, which does not allow the laser wavelength decrease or increase beyond the grating pass band. Thus, the SLM wavelength oscillates always within the grating pass band.

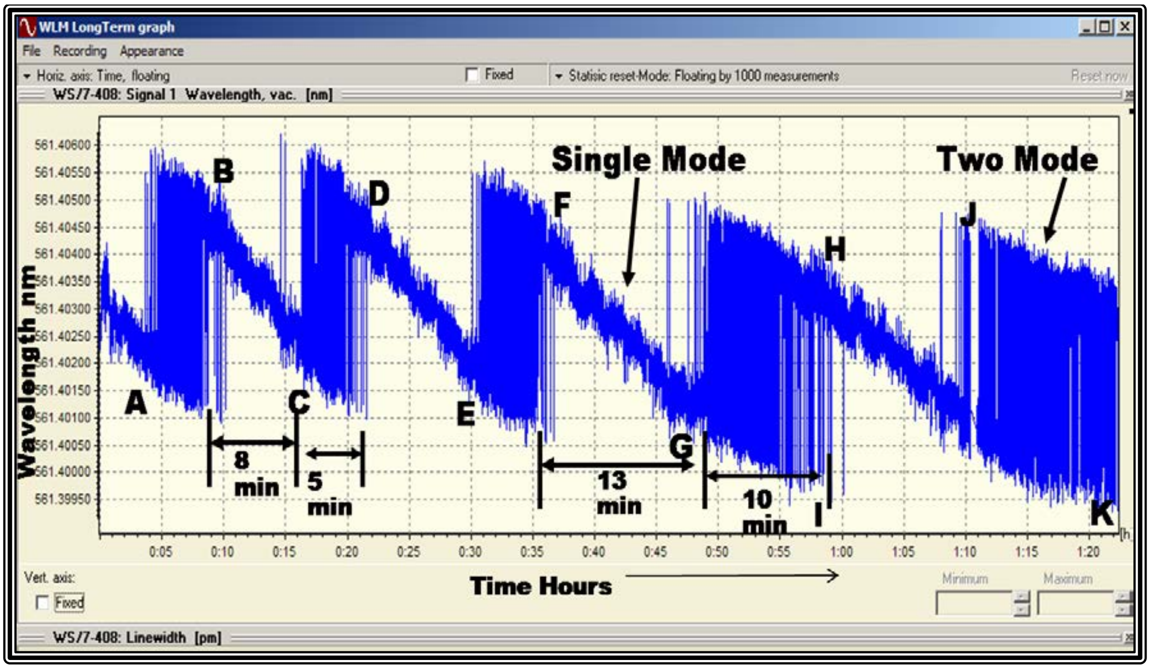

Figure 6.15: Wavelength versus time recorded after 1 hour 30 minutes of initial wavelength drift {X- axis Wavelength (nm), Y- axis time in hours}

The wavelength alteration rate varies from 0.3 GHz/min to 0.08 GHz/min corresponding to temperature change of 0.05^{O}C/min to 0.013^{O}C/min respectively. The wavelength meter (WS – 7L) is specifically designed only for single mode laser, which shows a smaller wavelength jitter band with a single mode laser, while for two mode oscillation the band of wavelength jitter is observed to be larger. In summary, the variation in dye temperature is directly reflected in the cyclic nature of single to two mode shifts for this short cavity SLM GIG dye laser.

6.5.3 Control of Mode Switching in the SLM Dye Laser

It was experimentally observed that the laser remains in single mode or two mode operation for a longer time if the dye solvent temperature reaches its set value as shown in figure 6.16. It shows the single mode oscillation of the SLM dye laser with stabilized temperature of the constant temperature bath. The free running laser operated in single mode for more than 35 minutes. A small variation of wavelength nearly 1.4 pm was observed, which may be due to a small variation in the environmental temperature caused by heating of the central stepper motor, when it was operated with holding torque for the entire duration of the experiment.

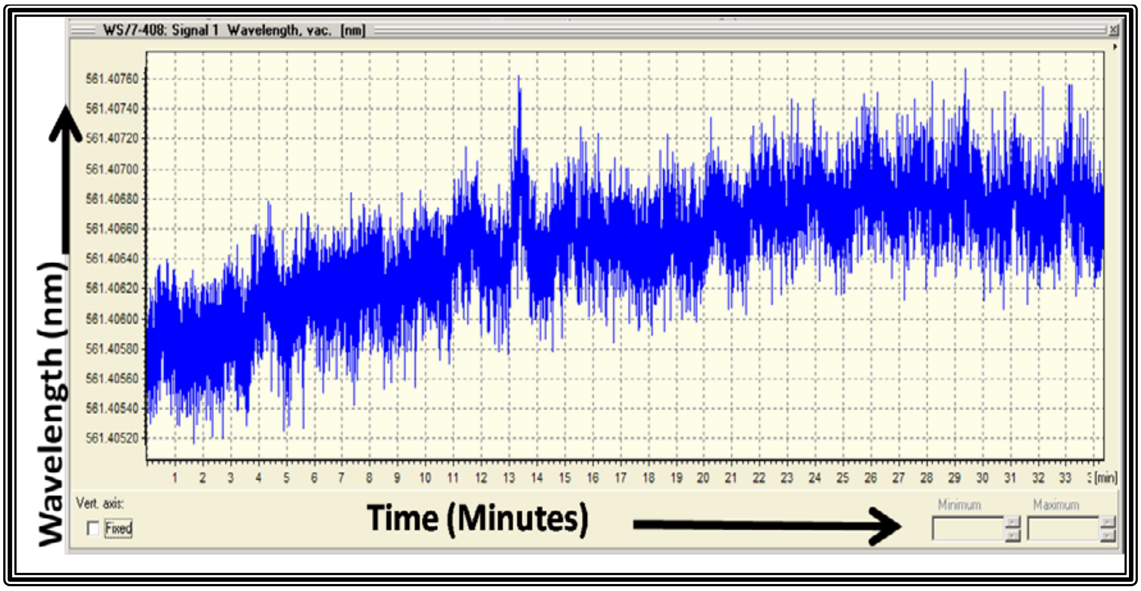

Figure 6.16: Wavelength versus time - Free running SLM dye laser after temperature is stabilized to 20^{O}C {X- axis Wavelength (nm), Y- axis time in minutes}

For stable single mode operation, the dye solution temperature needs to be maintained within the error band of less than ± 0.15 ^{0}C, which corresponds to frequency change of 375 MHz, which is approximately 10 times lesser than the cavity FSR and almost equal to the bandwidth of the SLM dye laser. From these observations it is concluded that if the dye solution temperature is controlled within the required temperature band of ± 0.15 ^{O}C there will be no cyclic behavior of single to two mode transitions for the SLM dye laser. In other words, if the heat balance between the heating and cooling cycles is well matched this cyclic behavior will not be present in the SLM dye laser.

6.5.4 Quantitative Correlation of Wavelength Drift with Temperature of the Dye Laser

The single or two mode oscillation of the SLM dye laser was confirmed by simultaneously viewing FP etalon fringes and laser wavelength meter. Here the set point temperature of the constant temperature bath was increased by $1^{O}C$ deliberately. As the temperature of dye solution gradually increased, the laser wavelength decreased from 561.40675 nm (point B) to 561.40425 nm (point C) (~ 2.5 pm or 2.39 GHz) as shown in figure 6.17. It leads to two mode oscillations at the end (point C to point D) and then laser settles to a higher wavelength at D in single mode.

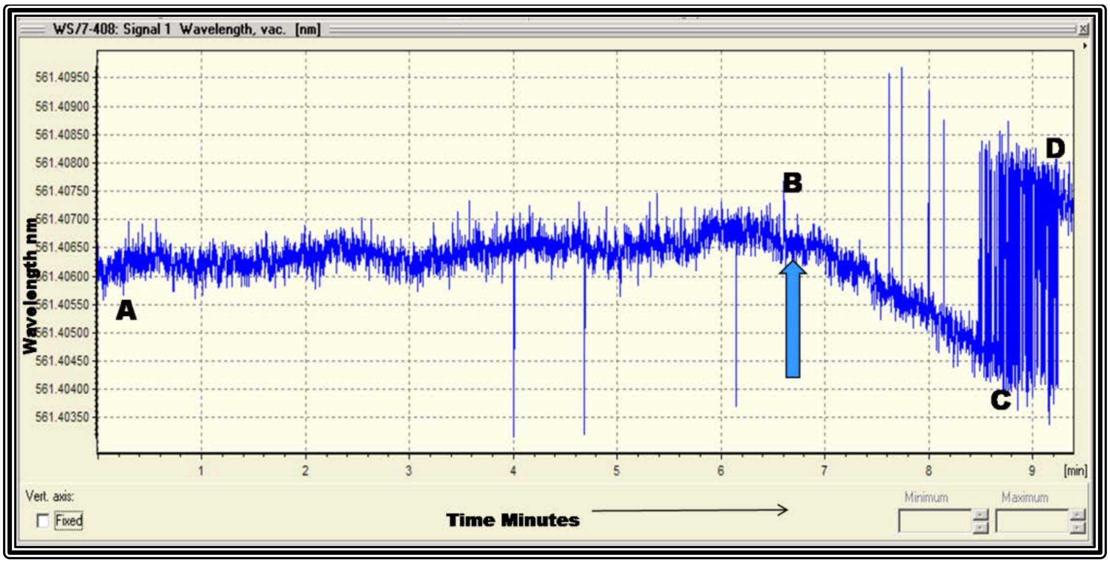

Figure 6.17: Wavelength versus time - Effect of increase of dye solution temperature from $20^{O}C$ to $21\ ^{O}C$. {X- axis Wavelength (nm), Y- axis time in minutes}

The change in the wavelength of the SLM dye laser due to any perturbation in the SLM dye laser cavity length is governed by the equation

$$\frac{\nabla\lambda}{\lambda} = \frac{\nabla L}{L} = \frac{\Delta \mathrm{n}}{\mathrm{n}} \qquad (6.10)$$

where λ is the wavelength, n is the refractive index and L is the cavity length. From the cavity path length equation 3.46 and 6.10

$$\frac{1}{\lambda}\left(\frac{d\lambda}{dT}\right) = \frac{1}{n}\left(\frac{dn}{dT}\right) = \frac{1}{L}\left[l_g\left(\frac{dn_g}{dT}\right) + l_a\left(\frac{dn_a}{dT}\right) + l_d\left(\frac{dn_d}{dT}\right)\right] \qquad (6.11)$$

$\frac{dn_g}{dT} = 9.8 \times 10^{-6}\ /^{O}K$, $\frac{dn_a}{dT} = 1 \times 10^{-6}\ /\ ^{O}K$ and $\frac{dn_d}{dT} = -3.9 \times 10^{-4}\ /^{O}K$, From these values of $\frac{dn}{dT}$ it is clear that the dye solvent (ethanol) is the most sensitive to temperature changes. Hence, temperature control for the solvent is one of the key issues for SLM dye laser.

The $\frac{dn_d}{dT}$ value of ethanol can also be estimated from the experimental results. From equation 6.10

The wavelength change is $\nabla\lambda$ = - 2.5 pm for 1^{O}C change in dye solvent temperature and λ = 561.406 nm and cavity length (L) of 60 mm and ∇L = - 4.3531 x 10^{-6}, the ∇n = - 2.672x10^{-4}. The reported value of $\frac{dn_d}{dT}$ is – 2.27x10^{-4} [6.5]

The temperature of dye solution changes due to heat coupled to the dye solution from the dye circulation pump and by pump pulse energy as discussed above. The change in the ambient temperature could change the cavity length in the air as well as in the glass windows of the resonator cavity. Since the optical path depends on the refractive index of the material in the cavity and the geometric length of the cavity, it can lead to variation of the laser wavelength. The SLM dye laser wavelength is proportional to the path length of the cavity. The cavity path length comprises of the width of dye medium, thickness of the glass window of the dye cell and the travel in air.

By considering temperature dependent refractive index for air and glass for the cavity length of 65 mm, laser wavelength 550 nm, 2 mm thick glass windows and dye cell width of 1 mm, the change in the wavelength is estimated to be 0.5 pm per ^{O}C change in ambient temperature. The change in wavelength due to dye solvent temperature is estimated as ~ 4 pm per ^{O}C. The SLM cavity is fixed on the stainless steel (SS) structure; hence the geometric cavity length change is determined by the thermal expansion coefficient of the metal. From thermal expansion coefficient

$$\frac{1}{L}\frac{dL}{dT} = \alpha \tag{6.12}$$

where α is the thermal expansion coefficient of metallic support structure.

Change in frequency of the SLM dye laser at 560 nm for increase of dye solution temperature by 1^{O}C, is estimated using equation 6.10 as 3.75 GHz/^{O}C. Experimentally, it is observed that a wavelength change of 2.4 GHz/^{0}C at 560 nm. The observed smaller value of frequency change is due to the grating pass band, which limits the SLM to operate within the pass band even as the dye laser cavity length varied. The other disturbances such as mechanical vibrations, flow fluctuations, beam pointing stability and pump beam divergence could not be incorporated through equations. But their effects on wavelength stability have been observed experimentally and discussed in Chapter – VII of this thesis.

6.6.5 Effect of Heating of Pump Pulse

To demonstrate the effect of pump pulse power the following experiment was carried out. At first with stabilized dye solution temperature single mode operation was established for a period of 45 minutes (point A to point B in figure 6.18). Control for cooling water of the dye solution was then switched off and pump power increased by a factor of two (~ 3 W from 1.5 W). The arrow marked on the figure 6.18 shows the time when the control for dye solution temperature was switched off. At first the wavelength starts to decrease from point B to point C by 1 pm due to increase in dye solution temperature and decrease in the cavity length. Then onwards the wavelength increased from point C to point E due to heating of the quartz window. This quartz window temperature leads to change in angle of incidence on the grating, leading to increase in the wavelength. At D the change in wavelength becomes greater than the grating pass band leading to a mode hop.

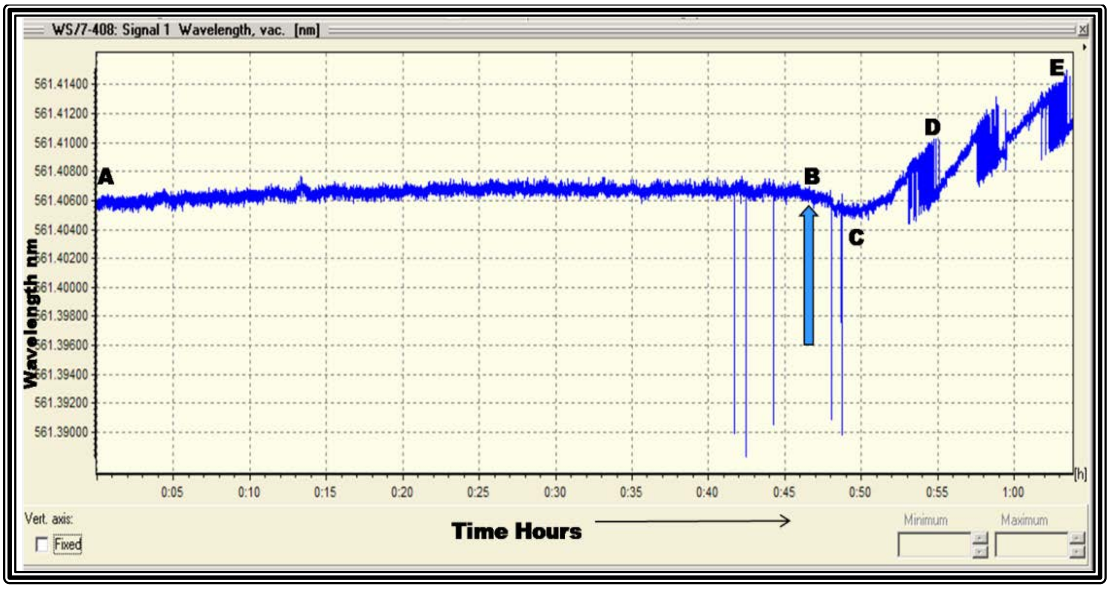

Fig 6.18: The cumulative effect of dye solution temperature and quartz window heating on the SLM dye laser wavelength. Pump power is increased by a factor of 2 and the dye solution temperature control is switched off. {X- axis Wavelength (nm), Y- axis time in hours}

6.7 Conclusions

A computational fluid dynamic (CFD) model for dye cell using a commercial CFD code was developed. This model is able to compute the transient temperature rise in the gain medium in the dye cell for each pump pulse. The transient temperature rise of ~3 K was found to occur with 166 µJ pump pulse of 9 kHz pulse repetition rate CVL pumping a dye laser containing 0.2 mM Rhodamine 6G dissolved in ethanol. The temperature rise is three times (9 K), when the pump pulse energy is increased by a factor of three. The temperature gradient near the dye cell wall was higher when the dye concentration was increased to 1 mM from 0.2 mM; this led to higher diverging power of the thermal lens formed by the temperature gradient. It was seen that the heated volume is displaced by 720 µm from pumped region before the arrival of the next pump pulse after 111 µs. The frictional temperature rise near the dye cell window was 29 mK for ethanol and 1.1 K for glycerol with the same inlet flow velocity of 1.5 m/s.

The computational model was validated with the experimental results published in the literature. It was found that in the time scale of 30 ns, the temperature rise was the same for each pump pulse irrespective of the inlet flow velocity for the same dye concentration as well as pump pulse energy. The contribution of thermal diffusion in the upward direction is effective only for very low flow velocities. In the dye cell, the quartz window contributes to the upward diffusion of heat to a length of nearly 3 mm, above the focal point at a flow velocity of 1.5 m/s, while it reduced to less than 0.5 mm for 15 m/s flow velocity. The change in the temperature of the dye solution directly affects single mode operation of the short cavity GIG SLM dye laser.

From the experimental study the following conclusions were made. It was determined that cavity length tuning of the SLM dye laser limited to grating band pass of 2.5 GHz. The settling time for the temperature of the dye solution was measured to be 2 – 3 hours, even while the temperature was actively controlled in the band of ± 0.15^{O}C. Increase in dye solution temperature, decreases the SLM dye laser wavelength, while the increase in temperature of the dye cell window due to heating by absorbed laser radiation increases the wavelength beyond the grating pass band. The magnitude of the laser wavelength jitter could distinguish the single mode and two mode output of the laser. The wavelength jitter was ~ 4 pm for two mode oscillation and 0.5 pm for single mode oscillation. The cyclic behavior of single mode and two mode operation was attributed to the temperature variation of the dye solution, which was prevented by controlling the dye solvent temperature.

References

[6.1] F. J Duarte, “Thermal effects in double prism dye laser cavities”, IEEE J Quantum Electronics Q E – 19, 1345 – 1347, 1983.

[6.2] D W Peter, C W Mathews, “Temperature dependence of the peak power of a Hansch type dye laser”, App. Opt., 19, 4131 – 4132, 1980.

[6.3] M A Ali, J Moghaddasi, S A Ahmed, “Examination of temperature effects on the lasing characteristics of rhodamine cw dye lasers”, App., Opt., 29, 3945 – 3949, 1990.

[6.4] O Teschke, J R Whinnery, A Dienes, “ Thermal effects in jet stream dye lasers”, IEEE J Quantum Electronics QE – 12, 513 – 515, 1976.

[6.5] S Yaltkaya, R Aydin, “Experimental investigation of temperature effect on the refractive index of dye laser liquids”, Turk J Phys, 26, 41 – 47, 2002.

[6.6] I A MeIntyre, M H Dunn, “Measurement of the temperature dependence of refractive index of dye laser solvents”’, J Phys. E: Sci., Instrum., 18, 19 – 20, 1985.

[6.7] P Burlamacchi, R Pratesi, U Vanni, “Refractive index gradients in a supperradiant slab dye laser”, Opt., Comm., 9, 31 – 34, 1973.

[6.8] A N Fletcher, R H Knipe, M E Pietrak, “Laser Dye Stability” Part7, Effects of temperature, UV filter and solvent purity”, Appl. Phys. B27, 93 – 97, 1982.

[6.9] U Balucani, V Tognetti, “Thermal effects in flash lamp pumped dye solutions”, Optica Acta, 23, 923 – 932, 1976.

[6.10] N Singh, “Analysis of the spectral variation of a dye laser by gain medium inhomogeneity”, Opt., Laser Tech., 42, 225 – 229, 2010.

[6.11] J R F Patrick, E H Piepmeier, “Thermal effects upon spatial mode structure of linear flashlamp pumped dye laser”, Ann., Chem., 50 1936 – 1937, 1976.

[6.12] F J Duarte, R W Conrad, “Diffraction limited single longitudinal mode multiple prism flashlamp pumped dye laser oscillator: linewidth analysis and injection of amplifier system”, Appl., Opt., 26, 2567 – 2571,1987.

[6.13] J R Lalanne, E Sein, J Buchert, S Kielich, "Measurement of heat transfer in microemulsions by laser induced thermal blooming", Appl. Phys., Lett., 36, 973 – 975, 1980.

[6.14] M V Muniz, CG Segundo, H F R Sandoval, C Gogorza, G M Bilmes, "Photoacoustic analysis of stimulated emission in pulsed dye laser", App., Phys. B 61, 361 – 366, 1995.

[6.15] C V Bindu, S S Harilal, V P N Nampoori, C P G Vallabhan, "Thermal diffusivity measurement in organic liquids using transient thermal lens calorimetry", Opt. Eng. 37, 2791 – 2794, 1998.

[6.16] R S Taylor, S Mihailov, "Excited singlet state absorption in Laser dyes at the XeCl wavelength" Appl. Phys. B 38, 131 – 137, 1985.

[6.17] P Venkateswarlu, M C George, Y V Rao, H Jagannath, G Chakrapani, A Miahnahri, " Transient excited state absorption in Rhodamine 6G" Pramana Journal of Physics Vol. 28, 59 – 71, 1987.

[6.18] N Arnaud, J Georges, "Investigation of thermal lens effect in water – ethanol mixtures: composition dependence of refractive index gradient, the enhancement factor and the Soret effect", Spectrochimica Acta Part A57, 1295 – 1301, 2001.

[6.19] D Comeau, A Hache, N Melikechi "Reflective thermal lensing and optical measurement of thermal diffusivity in liquids", App. Phys. Let., 83, (2003) 246 – 248.

[6.20] C E Mungan "Thermodynamics of radiation balanced lasing" Opt. Soc. Am. B 5, 1075 – 1082, 2003.

[6.21] Kobtsev S, Kandrushin S, Potekhin A, "A long term frequency stabilization of a continuous wave tunable laser with the help of a precision wavelength meter" Appl. Opt 46, 5840 – 5843, 2001.

Chapter – VII

WAVELENGTH LOCKING OF SLM DYE LASER

7.1 Introduction

A common characteristicddddd of narrow band tunable lasers which are used for high resolution laser spectroscopy and frequency standards is that they have high frequency stability. The wavelength stabilization or locking is used to minimize the wavelength drift in the dye laser output. A drift in a dye laser wavelength can occur due to several factors: thermal expansion/contraction of dye laser components, variations in the index of refraction of dye solution with temperature. These drifts can be in both direction and periodic in nature. There are other disturbances which cause fluctuations in the optical path length resulting in fluctuations in the wavelength such as turbulence, mechanical vibration, cavitation in flow, pump beam power fluctuations. They have been enumerated in the earlier chapters. The resultant change in the optical path due to each is in the nanometer to micrometer scale.

These fluctuations in the SLM dye laser output exhibit a broad frequency spectrum. In order to keep the laser wavelength stable, these fluctuations must be compensated by corresponding changes in the resonator length by adopting an electronic feedback control or eliminated by design. The short time constant disturbances due to vibrations are eliminated by design. The effects of turbulences and cavitation too are suppressed by CFD design. They have been addressed in Chapter – IV. The pump beam with the required stability is assumed to be present in this analysis. The wavelength locking of SLM dye laser can stabilize the wavelength by suppressing drifts over longer time scales of a second or more.

In general, an active feedback scheme presupposes a linear and stable error signal for controlling the laser wavelength. It is important to generate an error signal, which is a measure of deviation from the reference frequency of the laser. The reference can be a spectral line of a molecule or an atom, or a transmission curve of Fabry – Perot interferometer (FPI). This error signal is fed back to the controller after some signal conditioning. The feedback signal is used to generate a corrective signal to push the laser wavelength towards the set point wavelength. Lamour et al. had used closed loop wavelength stabilization using a position sensitive detector and PZT to modify the cavity length for optical parametric oscillator [7.1]. Drever et al. have described a highly effective optical discriminator and laser wavelength stabilization system based on reflected signals from a stable FPI. The high sensitivity is achieved by optical heterodyne detection with sidebands produced by rf phase modulation [7.2]. Manohar et al. have used temperature stabilized FPI for generating the error signal to quantify the dye laser wavelength fluctuations [7.3]. Ketskemety et al. described a method for the wavelength stabilization and line narrowing of distributed feedback (DFB) dye laser, using a dispersive pumping arrangement. In this method, the pump wavelength shift is compensated by a change in the incident beam angle [7.4]. There are two basic determining factors in the final performance of the wavelength lock: the initial noise spectrum of the laser and the electronic bandwidth achievable in the feedback system [7.5]. The long term (hours) stabilization of laser frequencies to a fixed reference requires smaller bandwidths, while short term stability (seconds) and line width control requires large feedback bandwidth (MHz).

7.2 Disturbances in SLM dye Laser Wavelength

The disturbances arising due to intensity fluctuations, beam divergence, beam pointing stability, mechanical vibrations and flow induced fluctuations are difficult to quantify individually for feedback corrective action. The combined effect of the contributions of all these disturbances was studied using a simple interferometric method. The block diagram of the experimental setup is shown in figure 7.1.

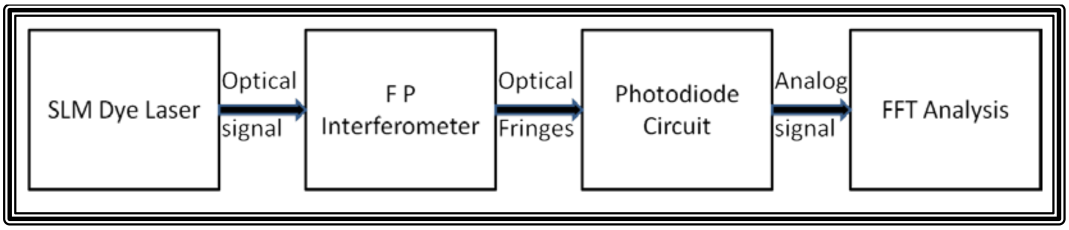

Fig 7.1: Block diagram of the experimental setup for FFT analysis

In this experimental setup SLM dye laser was fed to the FPI having FSR of 7.5 GHz. A plano convex lens of 750 mm focal length is placed after the FPI to form concentric circular fringes in its image plane. A split photodiode is placed in the image plane of the plano convex lens, which can be translated along the diameter of the fringe, so that the first fringe should lie on both the photodiodes. The signals from both the photodiodes are processed using trans-impedance amplifiers and differential amplifiers. The signal conditioning, electronic circuit is shown in figure 7.2.

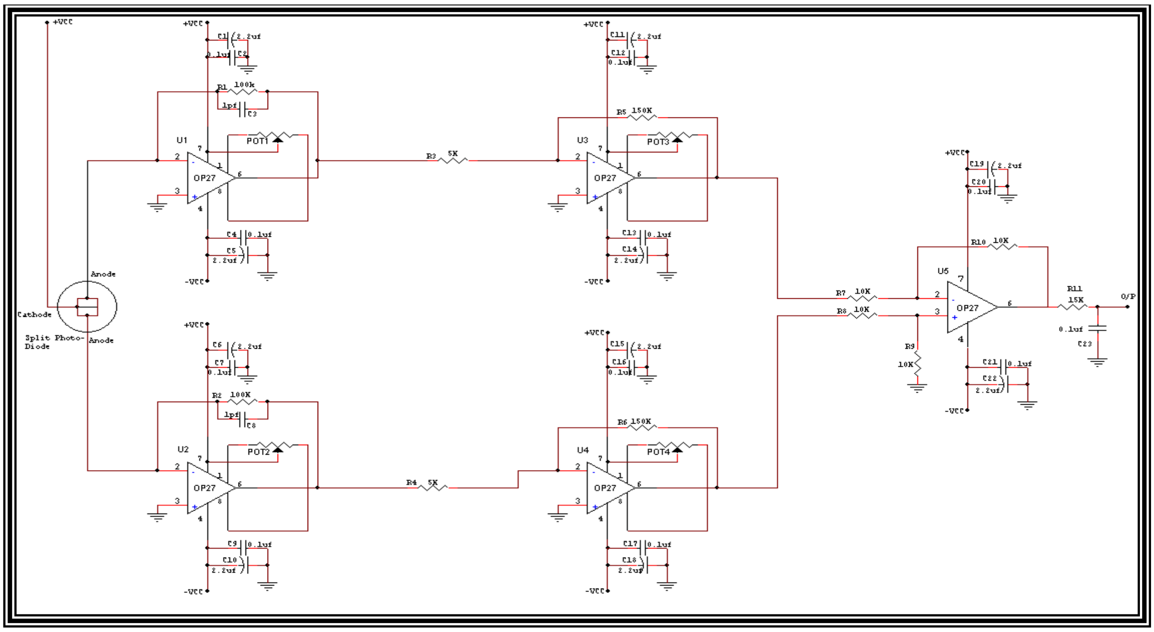

Fig 7.2: Circuit diagram of the processing signal from the Split Photodiode

Any disturbance in the SLM oscillator wavelength causes a change in the diameter of the fringe of FPI. Consequently, the fringe position on the split photodiode is altered. The extent of fringe displacement is proportional to change in the SLM wavelength. The positional change of the fringe is sensed by the split photodiode causing a change in the output of the differential amplifier. The signal obtained from the differential amplifier is fed to a low pass filter to average over several pump pulses at 9 kHz repetition rate. This output signal is fed to the four channel oscilloscope (Tektronix TDS 724D, 500 MHz). The fast Fourier transformation (FFT) signal is generated using **ORIGIN** software; FFT takes the discrete signal in the time domain and transfers it into its discrete frequency domain representation.

The working principle, methodology and the circuit were validated with a frequency stabilized He-Ne laser (SIOS Messtechnik GmbH make, Serial No. SL02 – 1). The frequency stabilized He- Ne laser was fed to the FPC and FFT signal was obtained as shown in figure 7.3. The FFT signal obtained with the frequency stabilized He-Ne laser has shown only one frequency component at 0.1 Hz. This 0.1 Hz is the default value of FFT signal for CW laser where no frequency component is present. There were no other frequency components observed in the FFT signal of stabilized He – Ne laser. The FFT signal obtained from the SLM pulsed dye laser pumped by 9 kHz pulse repetition rate of CVL is shown in figure 7.4. The prominent frequency components present in the FFT signal are 0.1 Hz and 107 Hz and relatively smaller magnitude frequencies are 162 Hz and 190 Hz as shown in figure 7.4.

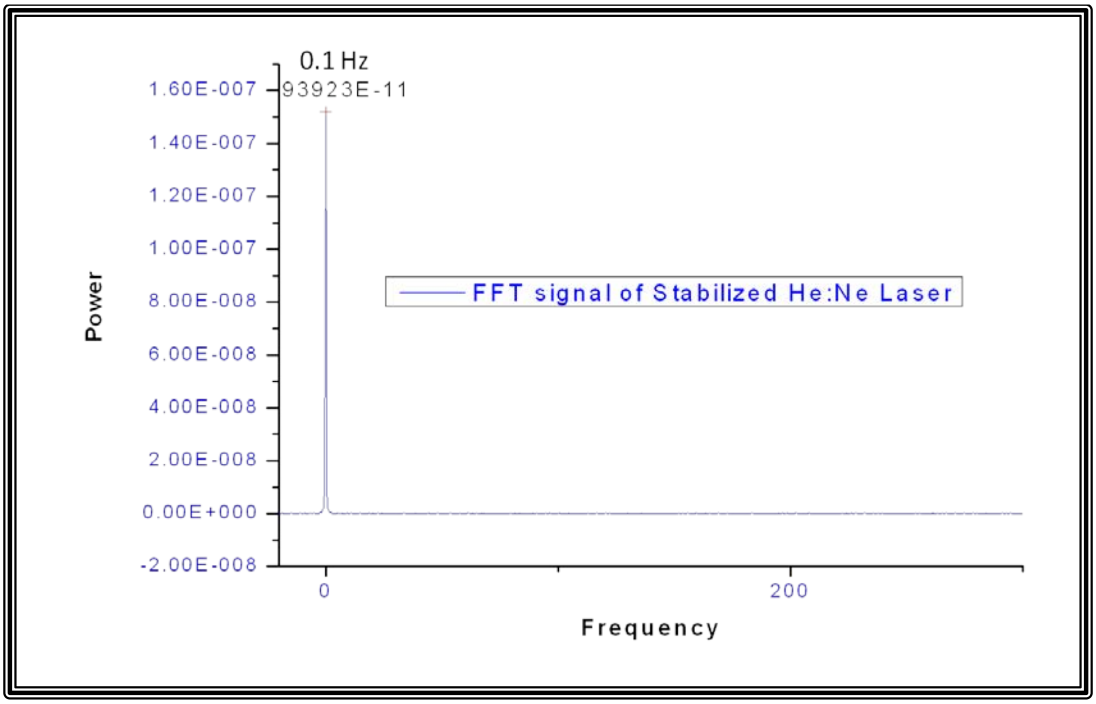

Fig 7.3: FFT signal obtained for frequency stabilized He – Ne Laser

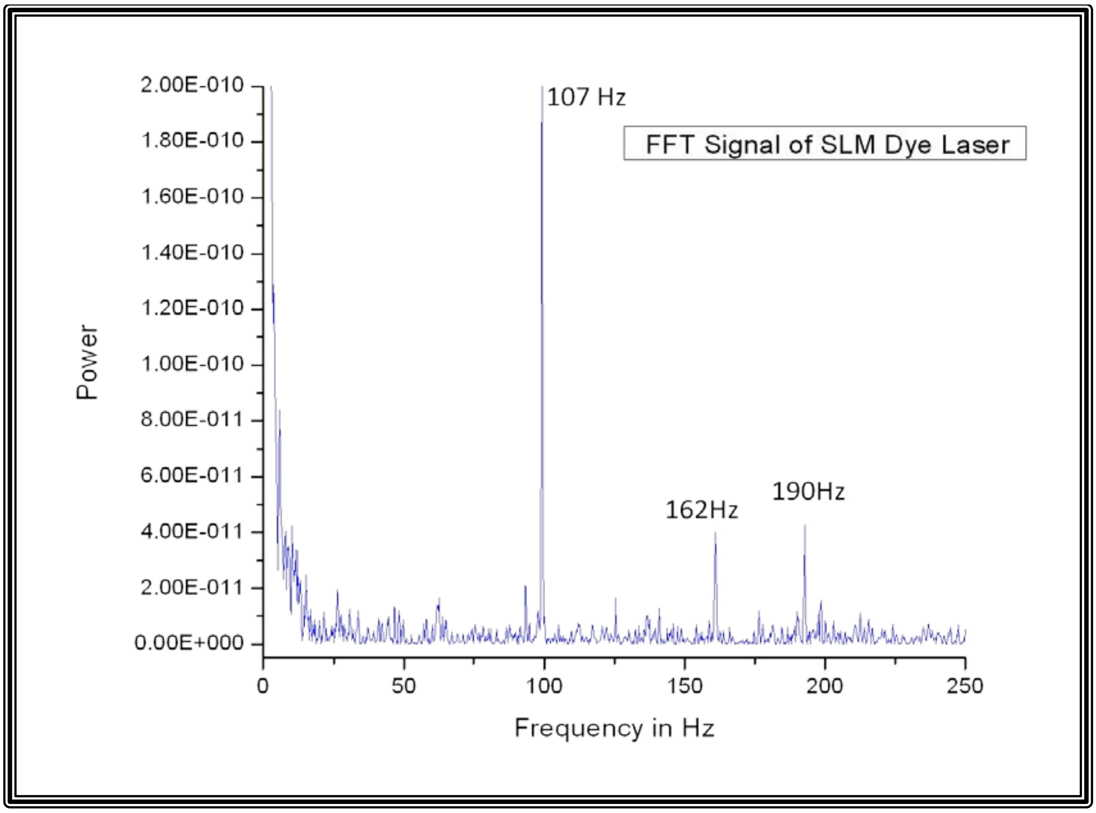

Fig 7.4: FFT signal obtained with pulsed SLM dye laser pumped by CVL.

7.3 Effect of Gear Pump in SLM

In a dye laser, the dye solution needs to flow rapidly, so that the heated volume is removed before the arrival of the next pump pulse. Magnetically coupled gear pumps are commonly used for this purpose. The main advantages of these pumps are lack of dynamic seals, smooth flow, self-priming and a direct relation between pump speed and flow. These pumps can be driven by different motors. The flow fluctuations are caused by the turbulence present in the flow and by the pulsation in the flow introduced by gear pump itself.

A simple optical technique has been used to investigate the flow induced fluctuation in the SLM dye laser. A frequency stabilized He-Ne laser (SIOS Mebtechnik GmbH make, Serial No. SL02-1) is passed through a metallic dye cell; in which a dye solution of 0.5mM Rhodamine 6G in ethanol was circulated by a gear pump (Iwaki MDG R-15). A He-Ne laser beam was fed to position sensitive quadrant photodiode after passing through the dye cell. Any disturbance in the dye flow velocity leads to change in the optical homogeneity of the dye flow, which could shift the laser beam from its mean position. The signal conditioning circuit for quadrant photodiode is shown in figure 7.5. The signal from the photo diode was amplified using trans-impedance amplifier and the difference signal from two diagonally opposite photodiode is generated to sense the X as well Y position of the laser beam on the quadrant photodiode.

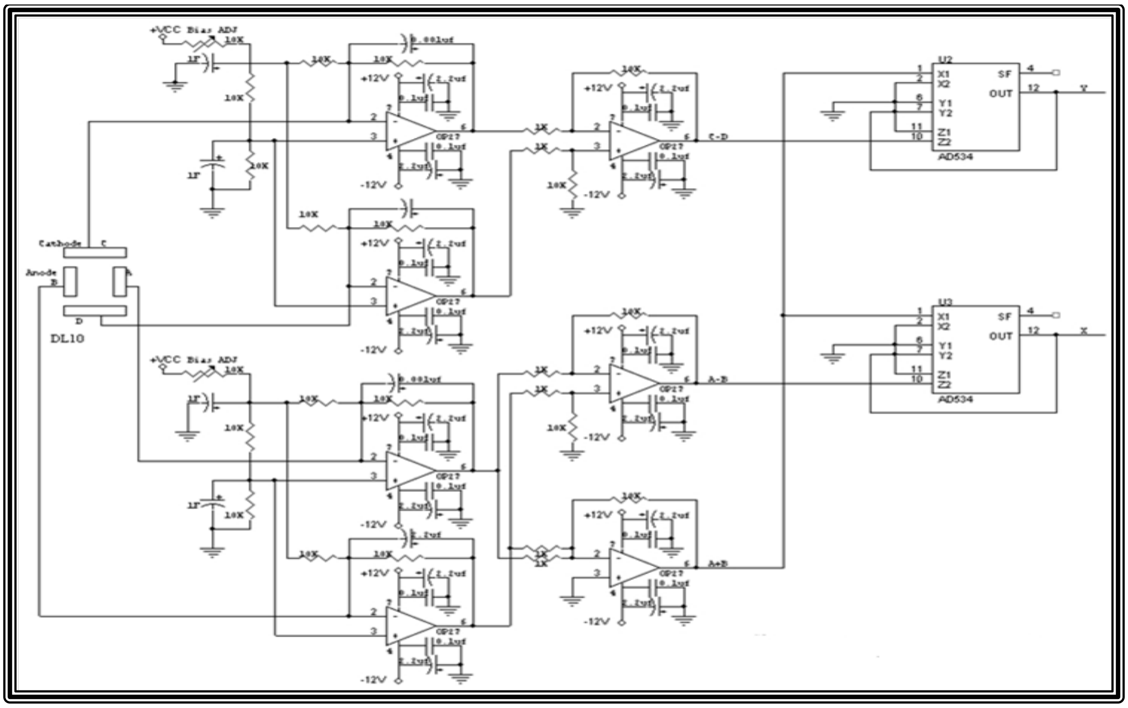

Fig 7.5: Electronic circuit for processing the position sensitive detector output

The amplified output was recorded on the oscilloscope (Tektronix TDS 724D, 500 MHz) and FFT analysis of this signal was carried out using **ORIGIN** software. The experimental setup is shown in figure 7.6.

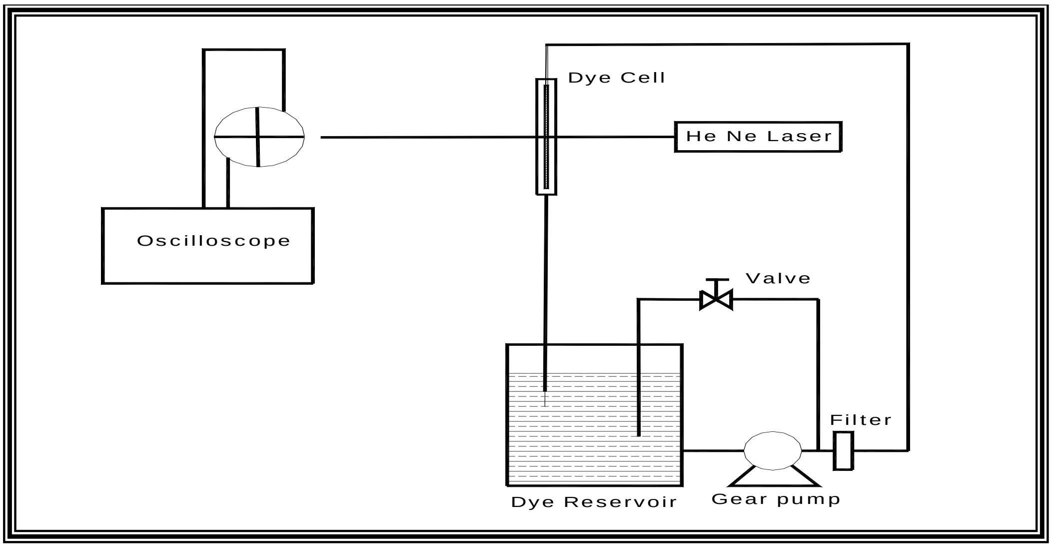

Fig 7.6: Experimental setup for measurement of flow induced fluctuations.

When a frequency stabilized He – Ne laser is passed through the center of the dye cell without flow, no frequency component appeared on the FFT signal as shown in figure 7.7a. The flow velocity inside the dye cell was changed from 1 m/s to 4.5 m/s by controlling the bypass valve in the dye flow system.

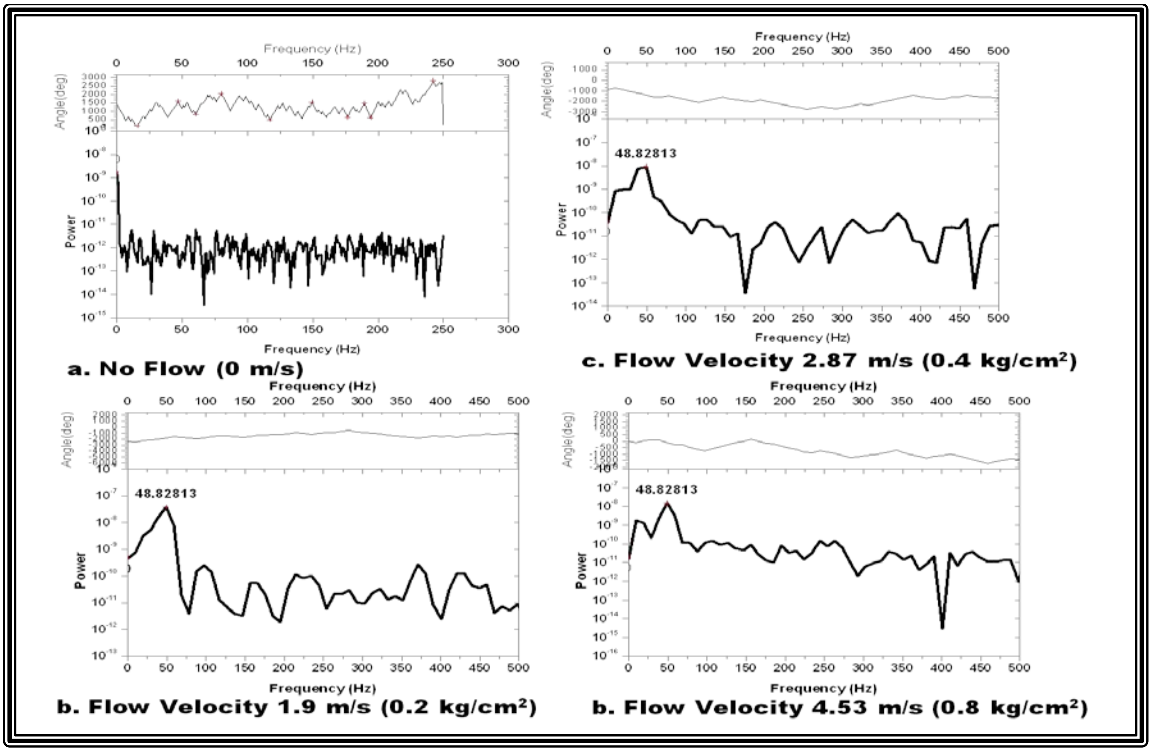

Fig 7.7: The FFT signal obtained from the position sensitive detector for Stabilized He-Ne Laser

It was observed as soon as the flow in the dye cell is present irrespective of the dye flow velocity there is a frequency component present on the FFT signal. The FFT signals for three different flow velocities are shown in the figure 7.7, in which a frequency component of 48.82813 Hz is present for all flow velocities.

In another set of experiments, the SLM dye laser was pumped by a frequency doubled Nd:YAG laser (~ 532 nm) with 10 Hz pulse repetition rate. The experimental set-up is shown in figure 7.8.

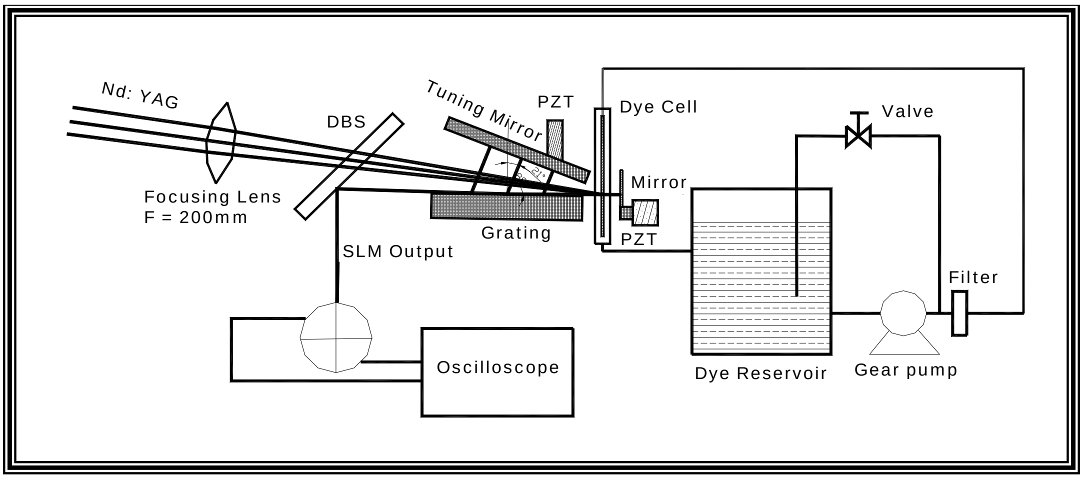

Fig 7.8: Experimental setup for Nd: YAG pumped dye laser.

The second harmonic of Nd:YAG laser was focused into the dye cell with plano convex lens of focal length 200 mm. The size of the focal spot in the gain medium was ~ 200 µm. The plano convex lens was mounted on a translation stage for precise positioning of the focal spot. The dye solution was cooled with a constant temperature bath, whose temperature was controlled by a PID controller in the temperature band of ± 0.15 ^{O}C. The SLM dye laser output is fed to the position sensitive detector, whose out signal was recorded on the oscilloscope. The flow velocity in the dye cell was controlled with bypass valve, which would keep the gear pump related noise constant. The line pressure was varied from 0.2 kg/cm^2 to 0.8 kg/cm^2. The FFT signal obtained by origin software shows two dominant frequency components such as 10.74219 and 48.82813 Hz as shown in figure 7.9.

The frequency component 48.82813 Hz is common in both experiments, which is related to the revolution per minutes (RPM) of the two pole induction motor attached to the gear pump, rotating at 50 Hz. The second frequency component 10.74219 Hz present in the figure 7.9 is related to the pulse repetition rate of the Nd:YAG laser as it was operating at the nominal pulse repetition frequency of 10 Hz. This has provided information regarding the frequency components present in the output of SLM dye laser, which has helped to find out the control loop parameters for wavelength stabilization.

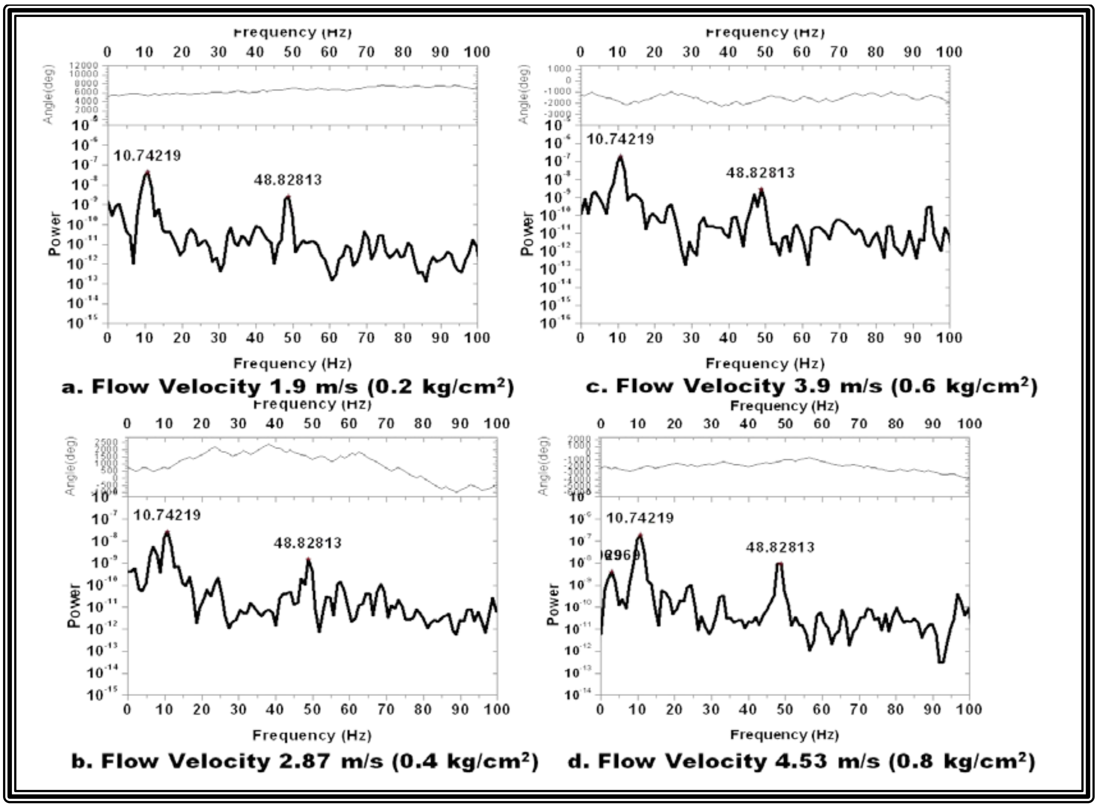

Fig 7.9: The FFT signal obtained from the position sensitive detector for Nd: YAG pumped SLM Dye Laser.

7.4 Disturbance Ranges and Behavior

The major disturbances considered for analysis are dye temperature variations and ambient temperature variations. The dye solution is heated by pump pulse; each pump pulse dumps 20 – 25 % of its energy into the dye solution. The fluctuation in the pulse energy causes fluctuation in the local dye temperature in the vicinity of active volume which in turn affects the SLM dye laser wavelength. Due to pump pulse energy instability the energy fluctuates pulse to pulse. It is difficult to control the wavelength from pulse to pulse when it changes at the pulse repetition rate of 9 kHz. If the instability is truly random, it is not difficult, but is impossible to control. The pulse energy instability shows a pattern with overall repetition rate ~ 100 Hz. The magnitude of wavelength fluctuation evidently depends on the amplitude of the pulse energy itself. Considering all the long term and short term frequency disturbances the end mirror PZT displacement range of ± 4 µm is sufficient which can correct the wavelength disturbances up to ± 40 pm. The tuning mechanism has been designed to achieve the wavelength tuning range of

100 nm with a resolution of 7.14 fm, that is, precision better than 10^7. It is difficult to achieve precision of 10^7 over the entire tuning range with a single actuator. Hence in this experiment 10^3 precision is achieved with coarse tuning mechanism and a precision of 10^4 is achieved using fine tuning mechanism. The fine tuning mechanism is implemented using PZT actuator with a resolution of 7.14 fm. The range of PZT actuator is selected to avoid the use of a stepper motor for fine tuning as it has more settling time, backlash error, dead - zone and also it can generate vibrations. The stroke length of the PZT actuator on tuning mirror is 100 micron; this range provides ± 4 times the resolution of the coarse tuning stepper motor. Identification of the dynamic frequency response of the SLM dye laser is important for selecting the time constant of active feedback control loop for the SLM dye laser wavelength. This time constant is useful for designing the electronic control loop circuit.

Various disturbances and their dynamic frequency response of the SLM dye laser have been tabulated in table 7.1.

Nature of disturbances	**Sensitivity**	**Range**	**Dynamic behavior**
Ambient temperature (RI changes)	0.5 pm / ^{0}c	± 3^0C	< 0.01 Hz
Ambient temperature (thermal expansion)	0.25 pm/ ^{0}c	± 3^0C	< 0.01 Hz
Dye Temperature (circulation pump)	4 pm / ^{0}c	± 2^0C	< 0.01 Hz
Dye Temperature (pump beam energy fluctuations)	4 pm / ^{0}c	-	107 Hz, 160 Hz, 190 Hz

Table 7.1: The Summary of Frequency Component Present in the SLM Dye Laser

7.5 The Error Signal

The first step in the locking process by a feedback loop is to generate an electronic error signal that tells if the laser frequency is in forward or backward position compared to the set point or locking frequency. After signal conditioning the error signal is fed back to the control circuit which generates appropriate gain and phase to actuate the tuning element of the cavity to push the laser frequency towards the locking point.

7.6 Frequency Reference

Absolute frequency references are provided by optical resonances in an atomic or molecular system, but there are some practical limitations [7.6]. The number density of atoms participating in the transition being small limits the signal to noise ratio. The stability of the laser is also limited to broadening of a transition line due to both power broadening as well as Doppler broadening. Furthermore, atomic interaction with electric and magnetic fields and collisions with neighboring atoms shifts the internal reference atomic energy levels [7.7]. Again the reference spectra of the atomic or molecular transitions are not available in all the regions of interest and cannot be recorded simultaneously.

The discriminator signal (error) produced by FPC is nearly a linear function of power and can have a high signal to noise ratio [7.3, 7.8]. The thermal distortion in the mirror coating caused by absorption of laser light and photochemical processes at the surface of the coating results in a frequency shift and fluctuations in the reference signal generated by the FPI. However, the signal to noise ratio obtained from the reference cavity is by many orders of magnitude larger than that obtained from atomic reference.

Another way to obtain a reference frequency is by direct measurement of the wavelength or frequency by a laser wavelength meter. It has been observed that it is possible to do so with an absolute precision of better than 1 MHz [7.9].

7.7 Fabry – Perot Cavity Sensor

To achieve laser frequency stability a common approach is to tune the laser output frequency to a resonance of an optical frequency of the reference cavity. The reference cavity does not have a gain medium, hence it can be made more stable than the laser cavity. The FPC provides a narrow line width reference frequency which can be kept very stable for locking the dye laser. The FPC consists of two semi transparent mirrors, which are separated by a distance d_m.

The interference condition in FPC can be defined by the equation

$$d_m = q\frac{\lambda}{2} \quad (7.1)$$

where d_m is the separation between the mirrors, q is the mode index number and λ is the wavelength of the incident light. The cavity length d_m includes the effects of optical field penetration into the mirror coatings, which typically requires a correction, of the order of the optical wavelength, to the physical length. The transmission from the FPC is maximized when the round trip phase is a multiple of 2π. When this condition is satisfied, the cavity is on resonance. The resonance condition for a standing wave is given by

$$\nu_q = q\frac{c}{2d_m} \quad (7.2)$$

The absolute accuracy can be quite high if it is possible to keep the optical spacing of the mirror constant. This is typically done by using a low thermal expansion spacer line Zerodur ceramic and high quality temperature control. In addition, the cavity has to be evacuated to avoid any drift of transmission fringes due to change in the refractive index of the cavity components caused by ambient pressure changes [7.9]. On solving superposition of the multiple transmitted beams from FPC, the transmitted intensity I_T is given in terms of the incident wave intensity I_O by

$$I_T = \frac{I_O}{1+F' \operatorname{Sin}^2\frac{\delta}{2}} \quad (7.3)$$

$$F' = \frac{4R}{(1-R)^2}$$

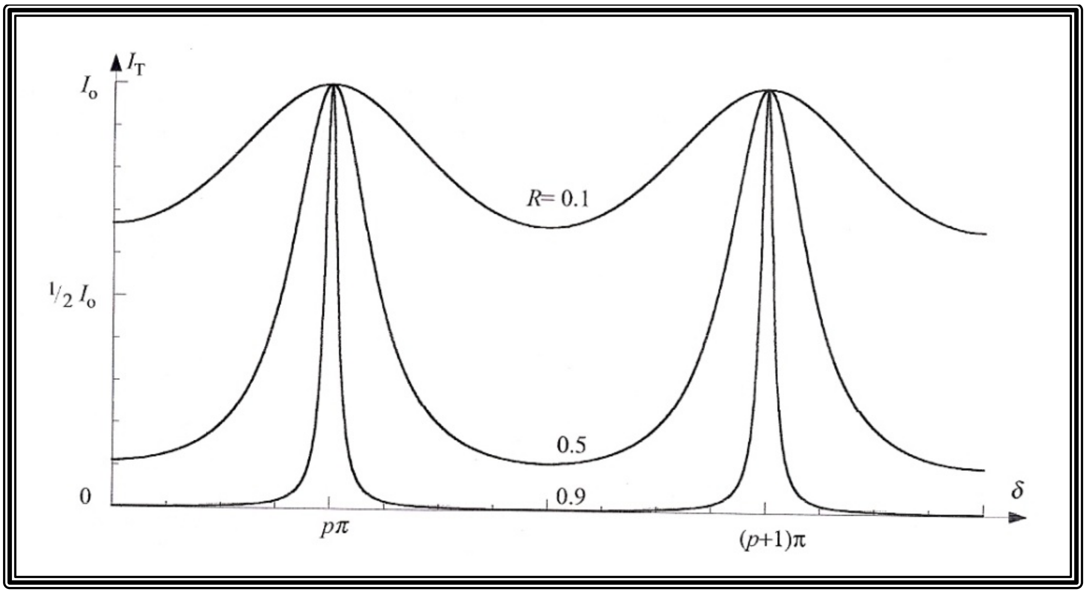

Fig 7.10: Fabry – Perot transmission as function of δ

And the phase δ given by

$$\delta = \frac{2\pi n d_m \cos\theta}{\lambda}$$

where F′ is the coefficient of finesse and R is reflectance. The transmitted intensities from FPC have concentric circular fringes known as an Airy's pattern.

From equation 7.3 it is seen that the transmitted intensity is a periodic function of δ that varies between a maximum and minimum as δ changes.

Figure 7.10 shows the transmitted intensity I_T as a function of δ. Note that the peaks get narrower as the mirror reflectivity increases. When peaks are very narrow, light can be transmitted only if the mirror separation d_m, refractive index n, and the wavelength λ satisfy the following relation precisely; otherwise no light is transmitted.

$$\delta = \frac{2\pi n d_m \cos\theta}{\lambda} = \text{integer } \times \pi = p\pi \tag{7.4}$$

It is this property that permits the FPC act as a very narrow band pass filter for a fixed d_m. If the incident light contains many wavelengths of varying intensities one can analyze its spectrum by scanning the length d_m of the FPC because for a given separation d_m, the FPC transmits only the wavelength that satisfies equation 7.4.

7.7.1 Finesse of Fabry Perot Cavity

Finesse is a numerical value which represents the sharpness of the interference fringes. The value of δ for FWHM, the transmitted intensity is reduced to half of its peak value and is derived from equation 7.3 as follows

$$\frac{1}{2} I_0 = \frac{I_0}{1+F' \sin^2\left(\frac{1}{2}\delta\right)} \tag{7.5}$$

This equation can be solved to give

$$\sin\left(\frac{1}{2}\delta\right) = \frac{1}{\sqrt{F'}} = \frac{1-R}{2\sqrt{R}} \tag{7.6}$$

In most cases of practical interest, the width of the peak is small compared to the free spectral range $\delta \ll \pi$. This is the case when F' is large. One can use the approximation $\sin\left(\frac{1}{2}\delta\right) \approx \frac{1}{2}\delta$ to obtain

$$\delta = \frac{2}{\sqrt{F'}} = \frac{(1-R)}{\sqrt{R}} \tag{7.7}$$

From the definition of finesse (the ratio of the separation between peaks to the FWHM)

$$F = \frac{\pi}{\delta} = \frac{\pi\sqrt{R}}{(1-R)} = \frac{\pi\sqrt{F'}}{2} \quad (7.8)$$

As only the influence of the reflectivity on the width is considered here, often this is known as reflectivity finesse. If the finesse is very high ~ 100,000 and corresponding power enhancement inside the cavity is as high as 30,000, then 100 μW of input power coupled to Fabry – Perot cavity translates into nearly 3 Watts of circulating power when the laser is resonant with the cavity.

7.7.2 Resolution of Fabry – Perot Cavity

The distance between the transmission peaks expressed in frequency is known as the free spectral range (FSR) of the resonator cavity. The FSR of the cavity is inversely proportional to the distance between the two mirrors and is given by the equation below.

$$FSR = \frac{c}{2n\, d_m} \quad (7.9)$$

where c is the velocity of light in the medium.

The resolution of the FPC, the minimum difference that can be distinguished two wavelengths, defines the instrumental line width. For normal incidence angle at the maxima, the phase difference δ is defined by

$$\delta = \frac{4\pi}{\lambda}\, d_m n = 2p\pi \quad (7.10)$$

The instrumental linewidth can be expressed as the ratio of FSR to finesse

$$\Delta\delta = \frac{2\pi}{F} \quad (7.11)$$

and equated with a spectral linewidth

$$\Delta\delta = \frac{2\pi}{F} = \frac{4\pi}{\lambda}\, d_m\, n - \frac{4\pi}{\lambda+\Delta\lambda}\, d_m n \quad (7.12)$$

The resolving power of the instrument is defined by the product of the finesse F and the interference order p. [7.15]

$$\frac{\lambda}{\Delta\lambda} = \frac{2F}{\lambda}\, d_m\, n = F\, .\, p \quad (7.13)$$

From equation 7.13 the resolution of a FPI can be improved by increasing n d_m, the optical path difference between the two reflecting surfaces; however, increasing the optical path length the order of interference is also increased, which leads to overlapping of the orders. By equating the phase shift for a certain wavelength λ, order p +1 with that for λ + FSR, order p, we get

$$\frac{2d_m n}{\lambda} = \frac{2d_m n}{\lambda + FSR} + 1 \tag{7.14}$$

$$FSR = \Delta\lambda_{FSR} = \frac{\lambda^2}{2d_m n} \tag{7.15}$$

FSR of FPI gives the change in the wavelength necessary to shift the fringe system by one fringe. Thus, for the cavity length of 30 cm the FSR of the cavity is ~ 500 MHz.

7.7.3 Coupling Light into the Fabry – Perot Cavity

The maximum coupling of light to a cavity requires consideration of two distinct concepts, mode matching and optical impedance matching. Mode matching refers to the adjustment of the input beam size, shape and wave front curvature to match the cavity mode. Impedance matching refers to adjustment of the cavity parameters (~finesse) to maximize coupling into the cavity. This occurs when the transmission through the input mirror equals all the other losses of the resonator such as transmission from the other mirror plus scattering losses plus absorption losses present in the mirror coatings and anything else in the cavity is referred as optical impedance matching. If the cavity is perfectly impedance matched the reflection of a perfectly spatially matched input beam will destructively interfere with cavity wave transmitted back through the input coupler. Thus, no net power will be reflected off the input mirror on resonance in steady state. Usually it is very difficult to match the impedance; hence all the power is not coupled into the cavity. The coupling efficiency of nearly 80 % can be achieved with a little more care. The mode matching is to shape and focus the laser beam such that it is exactly like a beam emanating from the waist in the cavity, except that it is moving towards the cavity. The perturbation in the length of the optical cavity ultimately limits the frequency stability that can be achieved.

7.7.4: Effect of Temperature on Reference Cavity

The temperature influences an open cavity in two ways. On the one hand an increase in temperature decreases the density of air inside the FPC and thereby reduces the optical path length of the cavity; on the other hand, the increase in physical spacing of the mirrors due to thermal expansion of the spacer increases the optical length. At a constant pressure, the change in frequency of the cavity mode due to ΔT and change in the density also is given by

$$\Delta\nu \approx (n-1)\frac{\Delta T}{T_0}\,\nu \qquad (7.16)$$

where n is the refractive index at a temperature T_O. For comparison, the He – Ne laser at atmospheric pressure exhibits a change in frequency of 455 MHz/K [7.9]. Since at ambient pressure a small change in temperature can drift the cavity frequency significantly, an evacuated chamber virtually eliminates the dependence of the mode frequency on the temperature.

The more common disturbing effect of temperature is due to coefficient of thermal expansion of the spacer material of the FPC. The effect of thermal expansion on frequency is given by [7.9]

$$\nu + \Delta\nu = \frac{qc}{4nd(1+\alpha\Delta T)} \approx \frac{q\,c}{4nd_m}(1-\alpha\Delta T) \qquad (7.17)$$

Or $$\Delta\nu \approx -\,\alpha\Delta T\nu \qquad (7.18)$$

where α is the thermal expansion coefficient of the spacer material, c is the velocity of light in vacuum and q the mode index number. For example, Zerodur ceramic $\alpha = -0.3 \times 10^{-7}$ / K and $\frac{\partial\nu}{\partial T} = 14$ MHz/K, while for fused silica $\alpha = 5.5 \times 10^{-7}$/K and $\frac{\partial\nu}{\partial T} = 260$ MHz/K [7.9]. This indicates that even for materials with extremely low thermal expansion coefficient such as Zerodur used as a spacer temperature of FPC needs to be controlled better than 0.1 K to ensure frequency stability of 1 MHz. The effect of deformation of mirrors becomes significant at high stability.

7.7.5 Effect of Pressure on Reference Cavity

The pressure change in the air between the mirrors of FPC produces density variation, which in turn changes its refractive index; it results in a change of the optical path length. At room temperature the index of refraction of dry air is related to its pressure P_d by [7.7]

$$n - 1 \approx 3 \times 10^{-9} P_d \tag{7.19}$$

where P_d is in Pascal. Thus, even if the cavity is evacuated up to 10^{-5} Pa, the absolute shift in the cavity resonance for optical frequencies near λ = 500 nm is about 15 Hz. A change ΔP in pressure at constant temperature, the change in frequency ν + Δν of a desired mode is given by [7.9]

$$\nu + \Delta\nu = \frac{qc}{4\left[n+(n-1)\left(\frac{\Delta P}{P_d}\right)\right]d_m} \approx \frac{q\,c}{4nd_m}\left(1 - \frac{n-1}{n}\frac{\Delta P}{P_d}\right) \tag{7.20}$$

For confocal FPC the longitudinal mode frequency ν is given by

$$\nu = \frac{q\,c}{4nd_m} \tag{7.21}$$

From equation 7.20 and equation 7.21 it can be shown that

$$\Delta\nu \approx -\frac{n-1}{n}\frac{\Delta P}{P_d}\nu \approx -(n-1)\frac{\Delta P}{P_d}\nu \tag{7.22}$$

For comparison, the sensitivity of He-Ne laser frequency at near ambient pressures amounts to – 172 MHz / Torr. Hence, the air pressure between the mirrors needs to be controlled better than 0.01 Torr for realizing stability of better than 1 MHz of FPC frequency. Hence, placing the FPC inside an evacuated chamber reduces the absolute pressure, which automatically reduces the perturbations in absolute pressure terms.

7.8 Disturbance Due to Vibration

The mechanical effects can be divided into two categories: those caused by vibration (acceleration) that structurally deforms the cavity and those that couple through the temperature due to coefficient of thermal expansion of the cavity materials. The disturbances are minimized by rigidly fixing to a vibration isolated structure and making the structure from a material having the same thermal expansion coefficient. Generally, there are two distinct factors: high frequency vibrations which may excite fundamental mechanical and low frequency vibrations that tend to produce non-resonant distortions. The first effect typically occurs at frequencies in the range of 100 – 1000 Hz and can be eliminated by mounting the system on vibration isolated platforms. The low frequency vibrations 0.1 Hz to 10 Hz that are typically driven by the ground noise and building are much harder to eliminate. Thus, mechanical vibration generated disturbances pose the problem of maintaining frequency stability for times longer than a few milliseconds. The fractional length change due to mechanical vibration can be estimated from

$$\frac{\Delta\nu}{\nu} = \frac{\Delta L}{L} = \frac{0.5\rho L\gamma}{E} \tag{7.23}$$

where $\frac{\Delta L}{L}$ the fractional change of the cavity length, ρ is the density of cavity material, E is the Young's Modulus and γ is the perturbing acceleration. As shown in the equation 7.23 above, a shorter cavity length would make the fractional change of length smaller and thus lead to a more stable cavity. Longer cavities are more sensitive to the amplitude of the mechanical vibrations. Sensitivities smaller than 2×10^{-11} /ms^{-2} have been realized for stabilized cavities of 10 cm length [7.10 – 7.14].

7.9 Limitation of Fast Detector and Actuator

The fluctuations in the rapid time scale are associated with flow velocity in the dye cell for SLM dye laser; hence to improve frequency stabilization performance at these time scales one needs fast transducers and electronic system. The miniaturization of the PZT transducer and laser mirror can provide ~ 200 kHz servo bandwidth and ~ 40 kHz residual laser frequency noise [7.2]. The fundamental limit on an optical frequency control system is governed by the photoelectron shot noise. The photocurrent from noise and from signal is not distinguishable from that caused by a real vibration frequency. When the servo gain and bandwidths are high, they suppress the laser's intrinsic noise. This noise is imposed onto the laser frequency to produce the appropriate servo null. The frequency variations associated with this unavoidable shot noise limit can be also calculated. For measurements with an averaging time of τ, the frequency fluctuation δν(τ), due to measurement shot noise is given by

$$\delta\nu(\tau) \geq \delta\nu_c \left(\frac{h\nu}{P_o T_e \eta}\right)^{\frac{1}{2}} \left(\frac{1}{\tau}\right)^{\frac{1}{2}} \tag{7.24}$$

where $\delta\nu_c$ is the reference cavity full width at half maximum, P_o the laser input power, T_e transmission efficiency on resonance, η quantum efficiency of photo detector, the measurement bandwidth B is 1/2πτ. For typical values of $\delta\nu_c$ ~2 MHz, P_O ~ 1/3 mW, $T_e = 0.2$, $\eta = 0.9$ and $\nu \sim 5 \times 10^{14}$ Hz, one can obtain a theoretical limit of frequency stability of ~ 150 Hz in a 1 MHz bandwidth. The fast frequency fluctuations of the laser are not detected in the transmission from the cavity due to a higher photon lifetime of the FPC. The final limitation is the narrow locking range. A small deviation from the locking point can cause the laser to unlock if the frequency momentarily shifts across the cavity transmission peak. High finesse cavities are desirable for providing a narrow line width for laser wavelength stabilization, but they simultaneously limit the bandwidth of the feedback loop and the reliability of locking.

7.10 Wavelength Control System of SLM Dye Laser

A control system is required to establish remote operation through closed loop control. An automated control system requires to be built with embedded intelligence with all the necessary functions and interlocks by considering the system constraints and that guarantees safe and reliable operation of the SLM dye laser. The functional requirements of the SLM dye laser are remote tuning of wavelength, wavelength stabilization / locking and mode correction. The ease of operation requirement is to provide functionality from a soft panel, which requires user interactive GUI and rugged control system.

The disturbance of any type detunes the SLM dye laser wavelength. Due to random nature of the disturbances, the wavelength fluctuations around the mean value increases. When the SLM dye laser is operated in free running mode drifts in the mean wavelength as well as a cyclic behavior between single mode to two mode occurs. The closed loop control output measure the wavelength through accurate sensors such as laser wavelength meter and temperature stabilized FPC and take the corrective action through actuators. The corrective action should take place according to the magnitude and nature of the error. This requires a rugged control mechanism with deterministic time response which can maintain the wavelength and single mode operation for longer duration. The system was built in-house based on the inputs generated in this research work. The details are given below.

7.10.1 Control System Architecture for SLM Dye Laser

The control system is designed with two level control strategy, i.e., embedded control and supervisory control. The supervisory control is implemented using a SCADA package and is useful for remote operation with a HMI. The embedded control is designed to operate the laser in manual mode as well as auto mode [7.16].

All the functionalities of laser operation with real time control features are implemented at the embedded level. The supervisory level has set point control, alarm monitor, data logging, trend display and status display of the various subsystems. The controller is connected to the operator console using Ethernet. The block diagram of control architecture for SLM dye is shown in figure 7.11. The SCADA specifications are driven by the application to which the SLM laser is put to.

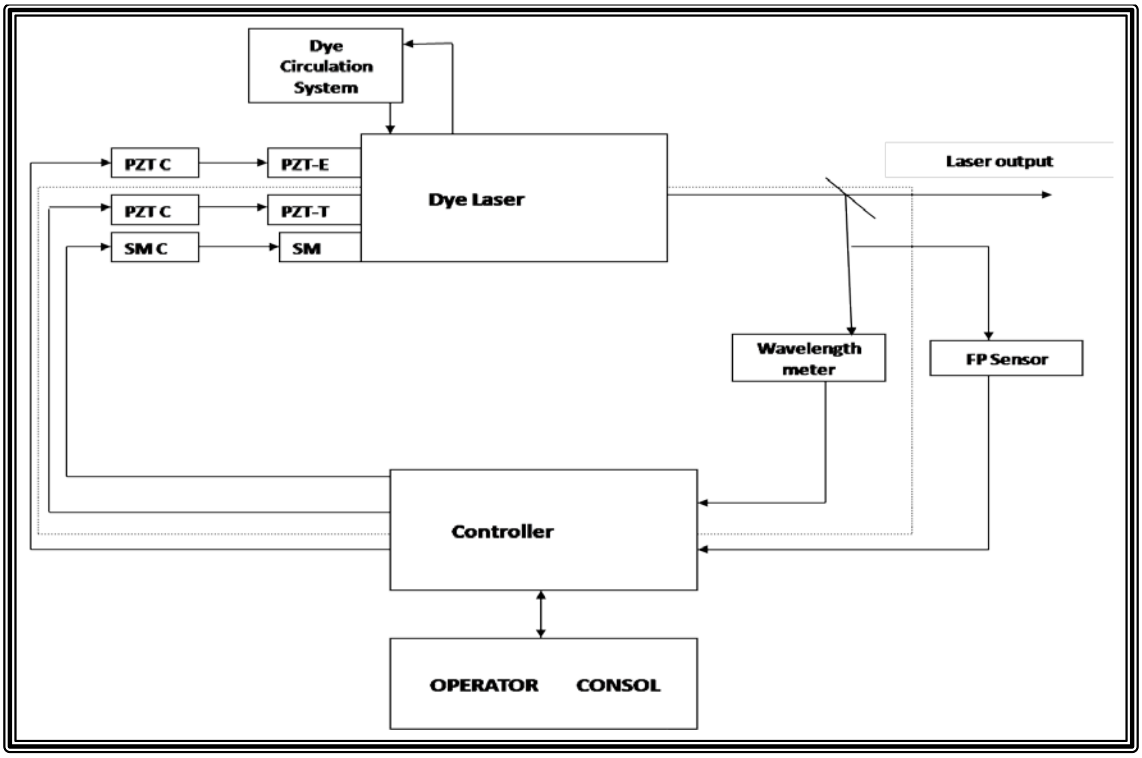

Fig 7.11: Block diagram for SLM Dye laser wavelength control architecture

A part of the SLM laser output is fed to the wavelength meter using fiber optic link. It measures the absolute wavelength with an accuracy of 100 MHz. The tuning loop is activated to tune the laser to set point value. Once, the laser reaches its set-point wavelength within an error band of ±100 MHz, the stabilization loop gets activated. The laser output is simultaneously sampled and fed to the FP sensor by a fiber optic link; it measures the relative change in wavelength. The resolution of the FP sensor in detecting changes in wavelength is 17 MHz which has been estimated based on the pixel size on the line CCD array.

7.10.2 Mathematical Model

The probable mathematical model of the control system is formulated by considering absolute wavelength control and relative wavelength control separately. The block diagram of closed loop wavelength control is shown in figure 7.12.

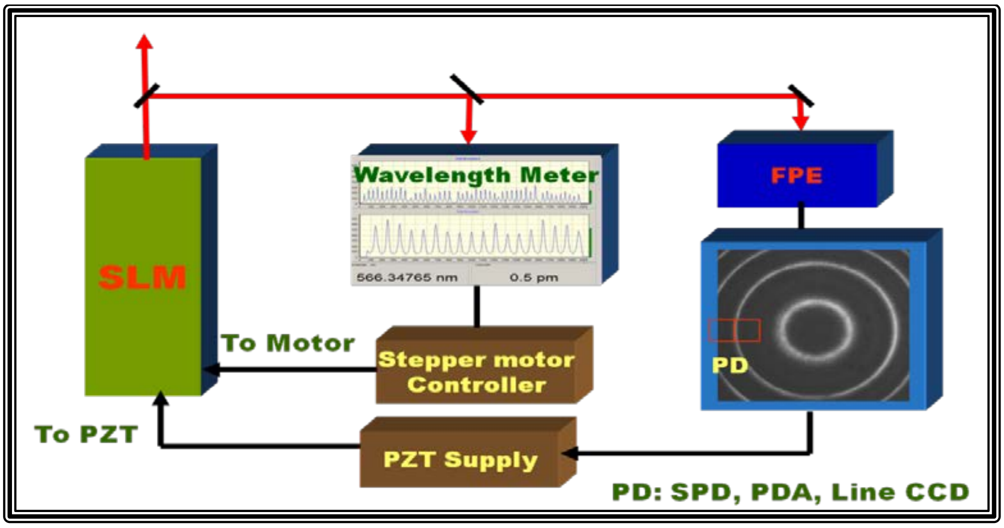

Fig 7.12: Block diagram of Wavelength Stabilization loop for SLM Dye Laser (FPE, Fabry – Perot Etalon, SLM: Single Longitudinal Mode, PD: Photo Detector, SPD: Split Photodiode, PDA: Photodiode Array, Line CCD Array)

There are two layers of wavelength control possible with this SLM dye laser. In the primary loop laser wavelength meter was integrated which corrects the wavelength error larger than cavity FSR. This loop takes corrective action by the central stepper motor attached to the tuning mirror or PZT attached to the tuning arm depending upon the magnitude of the error in the SLM wavelength. The secondary loop with split photodiode takes the corrective measures for smaller wavelength errors generated by temperature stabilized FPC. The temperature of the FPC is stabilized within a band of ± 0.01 ^{O}C at temperature of 45^{O}C. The SLM dye laser output is coupled simultaneously to both laser wavelength meter and temperature stabilized FPC by a multi mode optical fiber of core diameter 50 μm. The SLM laser illuminates evacuated solid 7 Fizeau interferometers of different FSR inside the laser wavelength meter. The interference fringes generated by SLM dye laser wavelength are compared with the frequency stabilized He-Ne laser fringes for determining the wavelength with an absolute accuracy of 60 MHz [6.21].

7.10.2.1 Model for Wavelength Tuning Loop

The absolute wavelength control or wavelength tuning block diagram of the closed loop control system implemented for SLM dye laser is shown in figure 7.13. For mathematical modeling the laser can be classified as a zero order system. A proportional control is implemented for controlling the SLM dye laser wavelength. The proportional control produces a 0 – 10 V signal finally at the output of digital to analog converter (DAC). The PZT controller is a DC amplifier with gain set to 15; it is a zero order system. The PZT actuator is modeled as a capacitive element with response time typically of a few hundreds of microseconds. It can be considered as a first order system. The wavelength meter gives out the wavelength in definite sampling intervals. It can also be represented using zero order hold. The block diagram shows the mathematical representation of the wavelength tuning loop.

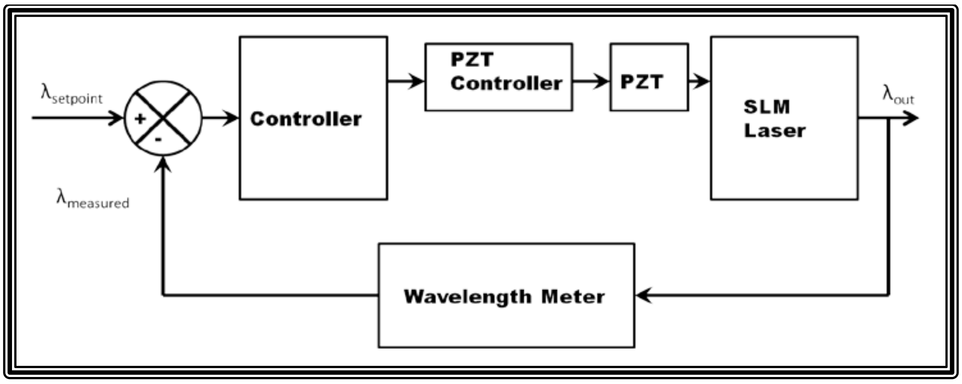

Fig 7.13 Block Diagram for control loop of wavelength tuning

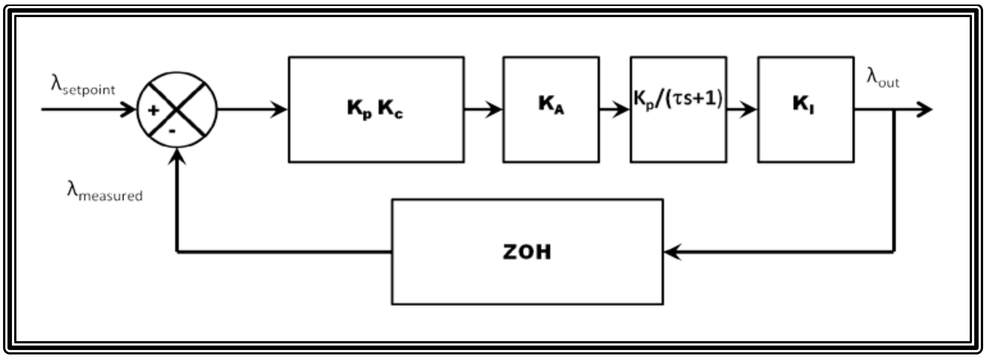

Fig 7.14 Mathematical Model for the Tuning Loop with PZT Block

where K_p – Proportionality constant

K_c – Conversion factor (Wavelength to voltage change)

K_A – Amplifier gain

K_D – PZT conversion factor

$\frac{1}{(1+\tau s)}$ - PZT transfer function

τ - The PZT response time

T – Sampling period

K_I – Laser transfer function $(\frac{\Delta\lambda}{\Delta d})$

ZOH – Zero order hold

The transfer function for closed loop

$$\frac{G}{1+GH} \tag{7.25}$$

where $G = K_p K_c K_A K_I \frac{K_D}{1+\tau s}$ (2.76)

and

$$H = \frac{1-e^{-Ts}}{s} \tag{7.27}$$

The transfer function presented here can be solved using Z – Transform. A suitable value of K_p can be calculated using the characteristic equation (1 + GH) and stability criteria. The parameters obtained are tabulated in table 7.2

S.No.	Parameter	Value	Unit
1.	K_I	10^{-5}	µm/µm
2.	K_A	15	V/V
3.	K_D	0.533	µm/V
4.	K_c	35	mV/pm
5.	K_p	< 1	
6.	T	40 – 100	msec
7.	τ	< 100	µ Sec

Table 7.2: Various Control Parameters Suitable to SLM Dye Laser Wavelength Tuning Loop

7.10.2.2 Model for Wavelength Stabilization Loop

It is assumed that the inherent stability of the laser is sufficiently good, so that the wavelength changes more than one FSR of FPC do not occur at a rate faster than the overall time response of the feedback stabilization system. Figure 7.15 shows the block diagram for the wavelength stabilization loop implemented here.

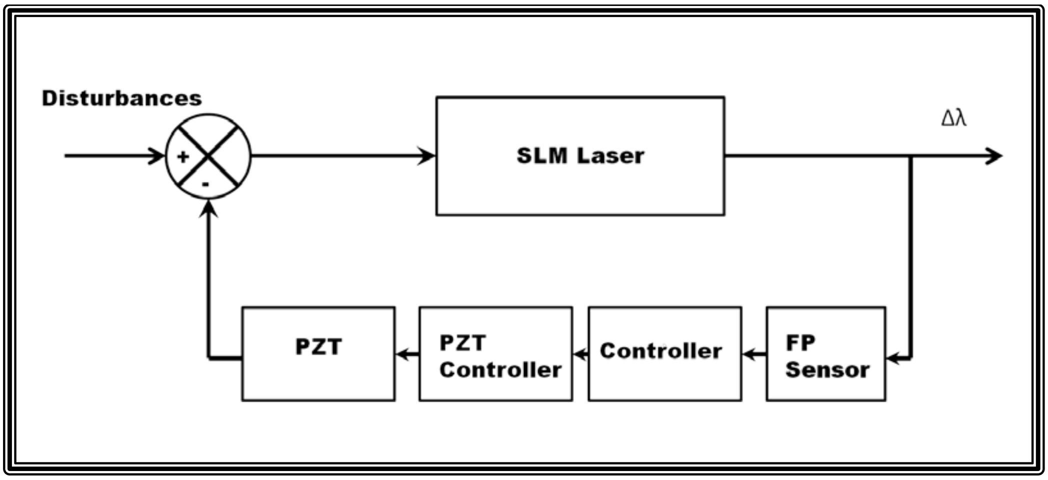

Fig 7.15 Block Diagram for the Wavelength Stabilization Loop

The wavelength stabilization control loop applies a proportional control to the SLM dye laser. The mathematical model for the wavelength stabilization control loop is shown in figure 7.16. The zero order hold was applied to the sampling point of the FP sensor. The transfer function and circuit parameter can be estimated by solving the mathematical model.

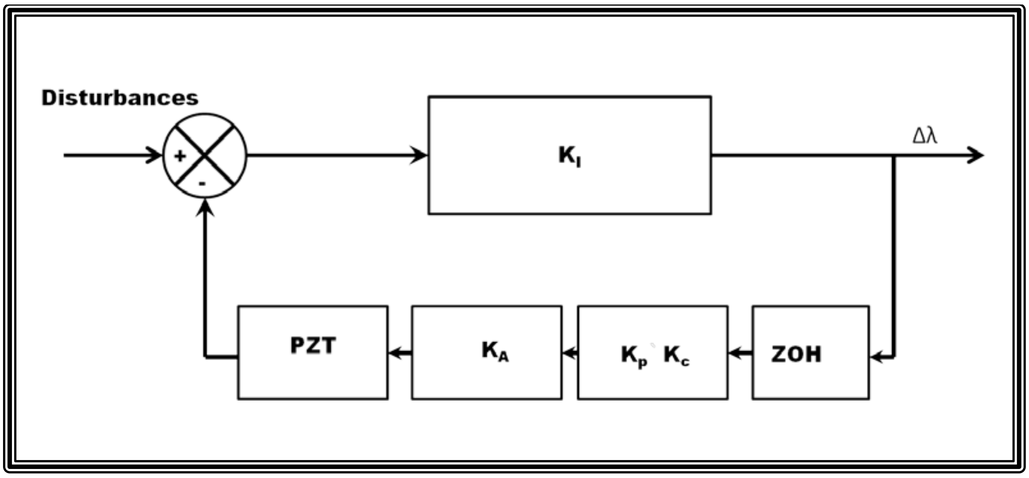

Fig 7.16 Mathematical model for the wavelength stabilization loop

The transfer function for closed loop is given by

$$\frac{G}{1+GH} \quad (7.28)$$

where H = K_I and

$$H = \frac{K_D}{\tau s+1} K_A . K_p . K_c . \frac{1-e^{-\tau s}}{s} \quad (7.29)$$

The characteristic equation is solved by using Z – transform to obtain the value of K_p for stable control loop.

The minimum time constant is determined by the response time of an actuator and controller while the maximum value is determined by the frequency of disturbances and the allowable band for wavelength control.

The sampling time is the response time of the control loop. The control parameter obtained are tabulated in table 7.3

S.No.	Parameter	Value	Unit
1.	K_I	10^{-5}	µm/µm
2.	K_A	15	V/V
3.	K_D	0.533	µm/V
4.	K_c	125	mV/pm
5.	K_p	< 1	
6.	T	5 – 20	msec
7.	τ	< 100	µ Sec

Table 7.3: Various Control Parameter Suitable to SLM Dye Laser Wavelength Stabilization Loop

7.11 Sensitivity of End Mirror

The cavity length of the SLM dye laser was tuned using PZT actuator on end mirror for stabilized dye solution temperature of 20 ^{O}C. The cyclic behavior of single mode to two modes due to the cavity length tuning was validated by applying a voltage to the end mirror PZT. The PZT at the end mirror has a full stroke length of 10 µm for the operating voltage of - 30 V to 150 volts. The PZT output voltage is controllable using 0 – 10 V input signal. The input signal was generated using 16-bit digital to analog converter from a personal computer. The sensitivity of the end mirror is 8.5 MHz / nm for cavity length of 60 mm. The PZT voltage was changed from 25 volts to 5 volts and SLM dye laser wavelength was monitored with a laser wavelength meter. Figure 7.17 shows the effect of cavity length tuning of the SLM dye laser by applying voltage to the end mirror PZT.

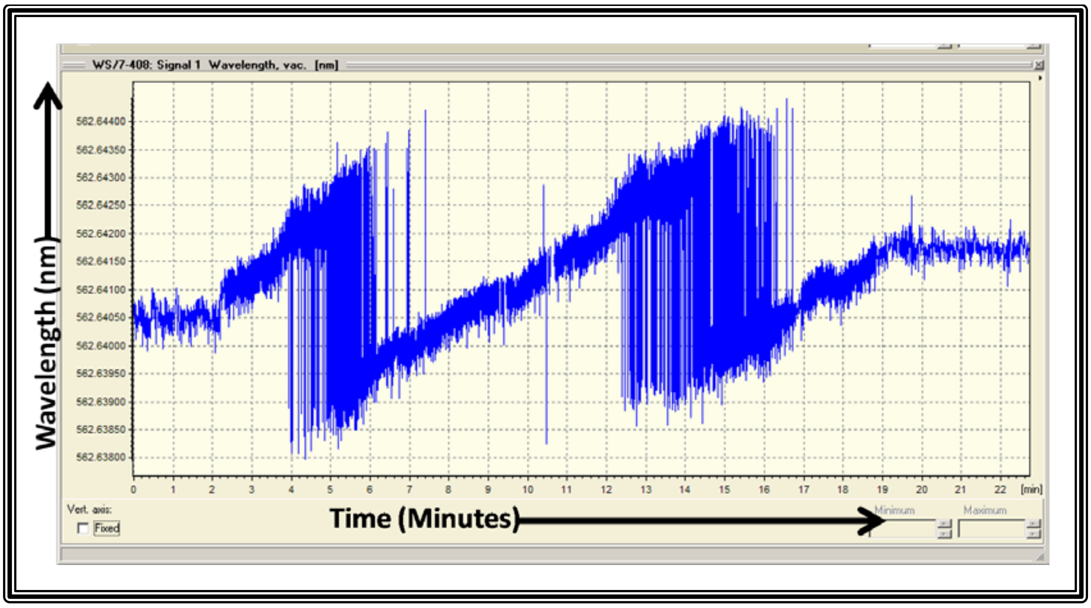

Fig 7.17: Wavelength versus time - The effect of cavity length tuning of SLM dye laser by applying ramp voltage to the end mirror PZT. {X- axis Wavelength (nm), Y-axis time in Minutes}

The change of PZT voltage by 20 volts should change the wavelength by nearly 27 GHz but the wavelength change is limited to only 2.5 GHz which corresponds to the grating pass band. Whenever, the wavelength change was more than grating pass band, a mode hop takes place and the set wavelength is restored.

7.12 Locking the SLM Dye Laser to the Fabry – Perot Cavity

The cavity length is effectively a set point, as this determines the frequency at which an inputted laser will resonate between the mirrors. The important quality of this cavity is its response, defined as the amount of transmitted light that resembles a Gaussian curve when the laser is near one of the resonant peaks. A lens of 750 mm focal length is placed after etalon to from the concentric fringes in its focal plane. The FPC was housed in a thermally insulated temperature stabilized oven whose temperature is controlled using Euro Therm PID controller, kept at 45^{O}C, almost 15^{O}

C above the ambient temperature. The temperature of the oven is stabilized within a temperature band of ± 0.1^{O}C. A split photodiode is placed in the image plane of the lens in such a way that both the photodiodes receive equal intensity from the one fringe so that the difference between the two-photodiode signals is zero. The split photodiode is fixed on a translation stage, so it can be placed precisely on one fringe of the FPC. The FPC fringe is centered on the photodiode to produce a null error signal. Any drift in the dye laser wavelength causes the change in the fringe diameter; hence the difference signal from the photodiodes is non-zero. The photodiode signals are subtracted in a differential amplifier to produce a signed error signal which is processed by a PID controller and amplified by an amplifier for controlling the cavity length of the SLM dye laser by PZT attached to the end mirror.

7.12.1 Electronic Locking Circuit

The locking circuit consists of three major parts, a proportional (P), an integrator (I) and a differentiator (D). The PID circuit for electronic wavelength locking of SLM dye laser is shown in figure 7.18. The design of this PID circuit is rather simple because it makes use of an operational amplifier, resistors and capacitors.

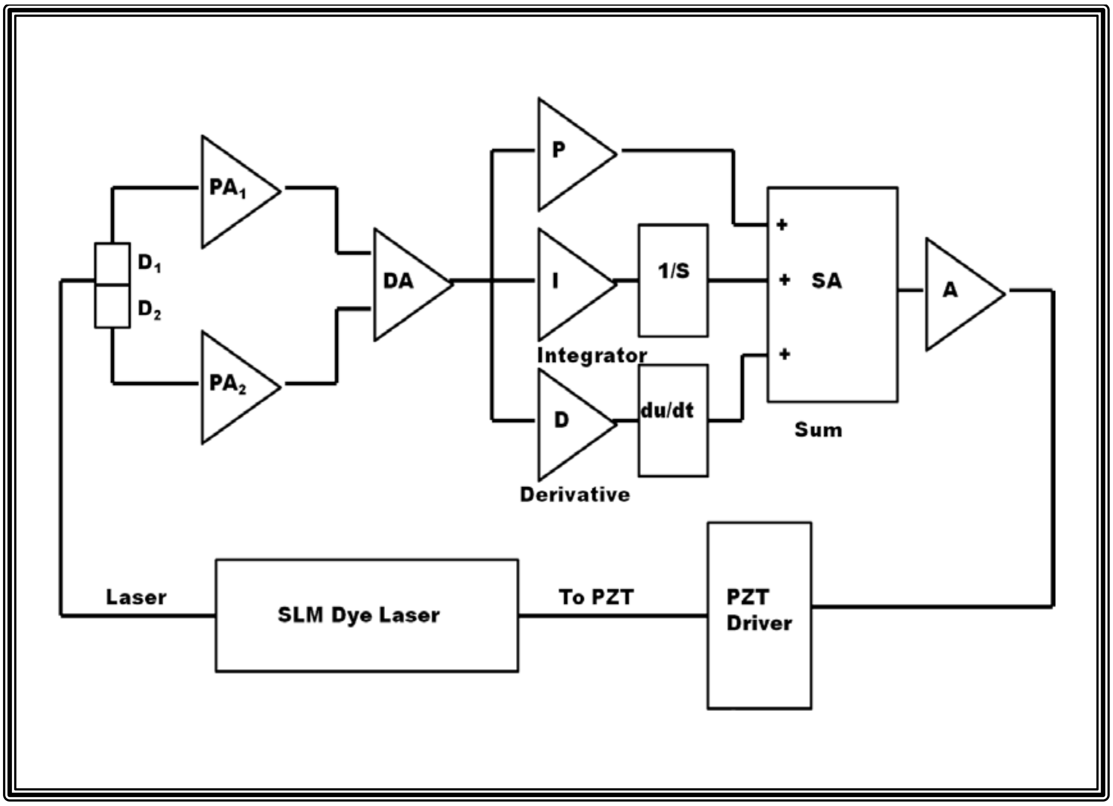

Fig 7.18: PID controller used for hardware lock of SLM dye laser

The OP07 operational amplifiers are used for this PID circuit. This operational amplifier was chosen due to its low noise, high stability of offset and gain. The typical operational bandwidth of this operational amplifier is ~ 600 kHz. The error signal provided by the temperature stabilized FPC and split photodiode was sent to a PZT controller using an ordinary proportional gain. The proportional part adds the appropriate offset and gain to the feedback signal. Although, higher gain locks faster, it induces oscillations or settles at a value far from the set point value, resulting in a large steady state offset. Using only proportional gain it is difficult to achieve active frequency stabilization. A proportional-integrating (PI) controller used to overcome the problems of offset. The main disadvantage of this approach of error accumulation is that it can result in unstable behavior or poor dynamic response if the parameters are not chosen carefully. The optimization of the closed loop circuit is carried out by adjusting the pot registers of the PI amplifier. The gain of the feedback loop is defined as the change in the error signal in response to the change in voltage applied to the PZT. To improve upon the dynamic response of the circuit, a differentiator is added to PI controller. The PZT voltage $u(t)$ varies with the error signal 'e' according to

$$u(t) = P\left[e(t) + \frac{1}{T_i}\int_0^t e(\tau)\,d\tau + T_d\,\frac{de(t)}{dt}\right] \qquad (7.30)$$

where P is the proportional gain constant, e (t) is the error signal, T_i is the integration time, and T_d is the derivative time; accordingly the first term of the equation is the proportional gain, second term the integral gain and the last term the derivative gain of the PID controller. The proportional gain acts for the error signal at the present time, while the integral gain acts for past values of the error signal and the derivative gain takes into account the rate of change in error at the present time.

The error signal e (t) is derived from the difference between the desired set point S and feedback signal F obtained from the temperature stabilized FPC

$$e(t) = S(t) - F(t) \qquad (7.32)$$

This error signal becomes zero as soon as the split photodiode provides the same value as some predefined set – point. The SLM dye laser output was monitored by a commercial wavelength meter (WS – 7L) which shows the reduced wavelength fluctuations of ± 0.4 pm around the mean wavelength of 564.3414 nm. It was observed from figure 7.19 as soon as the lock is removed, the SLM wavelength starts drifting from the mean wavelength. It was observed that the wavelength control loop logged the drift in the SLM dye laser wavelength from its mean value.

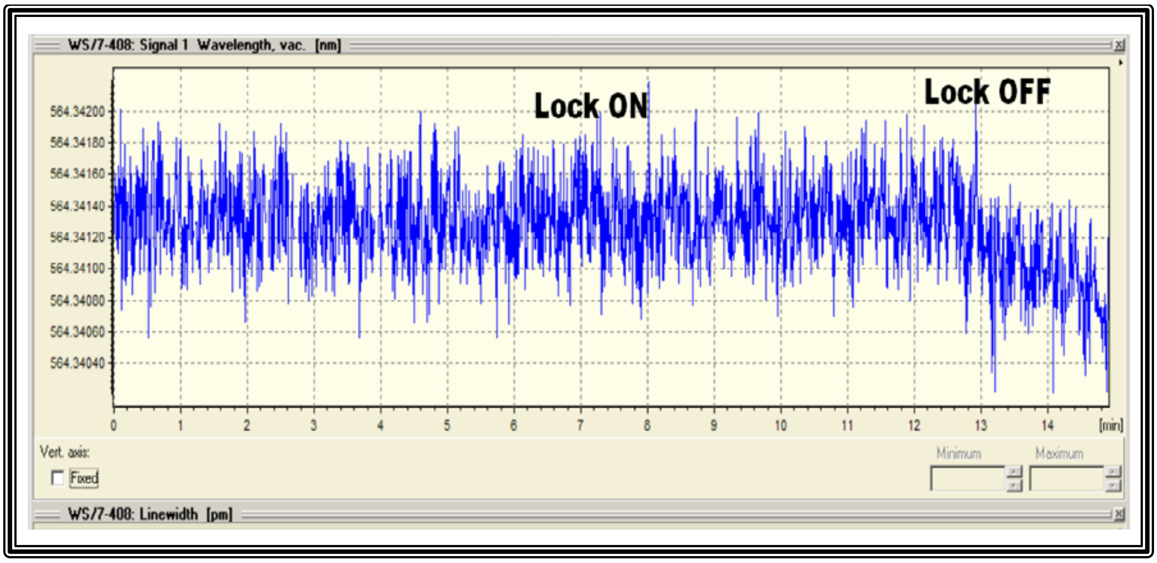

Fig 7.19 Wavelength output of frequency stabilized SLM dye laser {X- axis Wavelength (nm), Y- axis time in minutes}

7.12.2 VME Based control system for SLM Dye Laser

Advanced VME based wavelength control and stabilization was implemented with the SLM dye laser. The split photo diode was replaced by line CCD array. The use of line CCD array instead of split photodiode obviates the necessity of accurate alignment and provides mechanical stability of various optical assemblies. The optical alignment is simpler with line CCD array as all the fringes are intercepted by the array; this avoids the linear translation of split photo diode along the FP fringes. The supervisory control as before was implemented using CITECT SCADA on Window XP platform. The embedded control was implemented using VME and the real time operating system was QNX (6.3). The embedded control system was interfaced to a supervisory control system through an Ethernet link. The embedded control had two independent feedback control loops for wavelength tuning and wavelength stabilization (locking).

7.12.2.1 Wavelength Tuning and Control Loop

For wavelength tuning the wavelength meter described in para 7.10.2 was used. The wavelength meter was interfaced to an industrial computer operating with Windows XP. The wavelength information is then passed to the VME Single Board Computer (SBC) through RS232 link. QNX based software on VME SBC, which computes the required wavelength correction. Based on the magnitude of error, a corrective action was taken by either stepper motor or the PZT. VME based stepper motor control cards were used for driving the micro stepping drive which in turn drives the stepper motor with a resolution of 50,000 microsteps per revolution.

The PZT drives are driven by VME analog output cards. Both the control loops are schematically shown in figure 7.20.

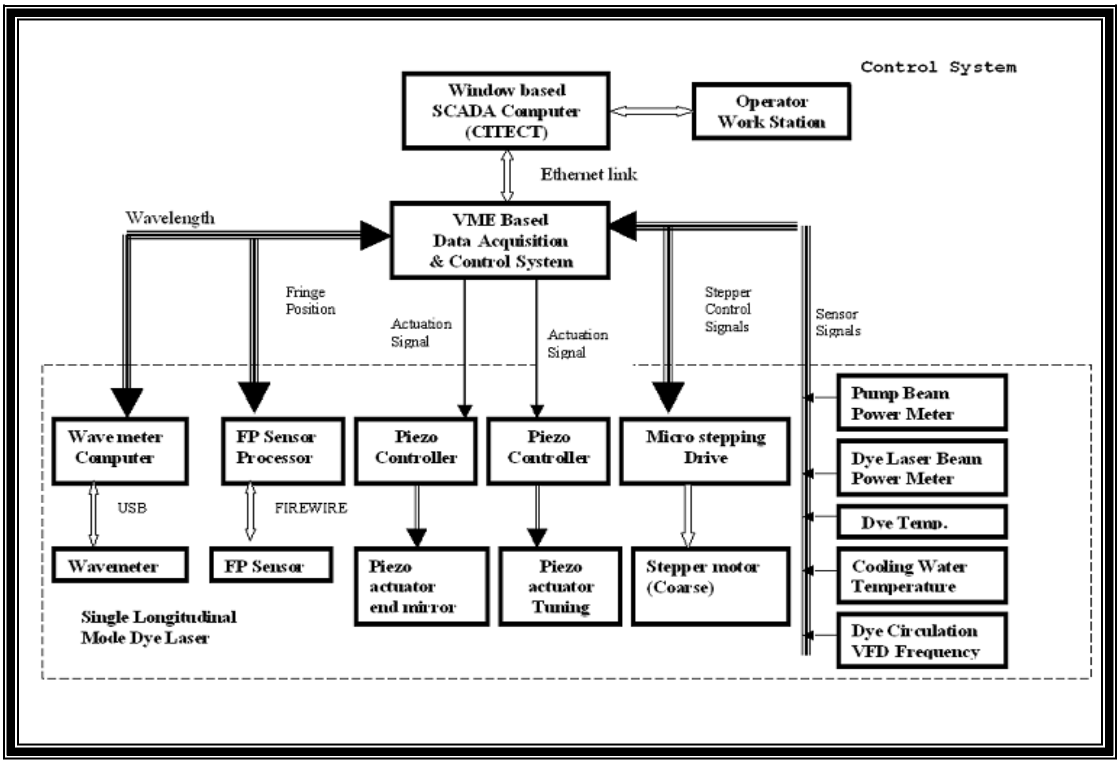

Fig 7.20: Schematic of the control System for SLM Dye Laser

7.12.2.2Wavelength Stabilization Loop

The FPC was used as the sensor that gave the wavelength in terms of locking fringe position and other parameters like line width from the captured fringe pattern. The wavelength information was then passed to VME SBC through RS232 link. In the event of a change in the SLM laser wavelength, QNX based software evaluates the correction required and the PZT drive actuated the PZT at the end mirror. From a series of experiments on two mode behavior of SLM dye laser, a control logic evolved for correction of two mode operations back to single mode. The control logic was implemented in the control loop and tested experimentally with the remotely tunable SLM dye laser system.

7.13 Reference Cavity Fringe for SLM Dye Laser

The Fabry – Perot fringes for the line CCD camera were generated by using a cylindrical lens before temperature stabilized FPC. With cylindrical lens the circular fringes are compressed into line fringes as shown in figure 7.21. The cylindrical lens was used as a mode matching lens for FPC having focal length 400 mm. It was observed that after applying the wavelength lock, the SLM dye laser stayed in single longitudinal mode for a longer time period.

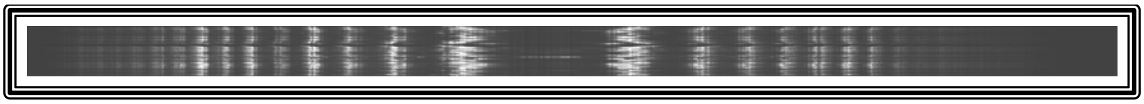

Fig 7.21: Fabry – Perot fringes for Line CCD camera of SLM dye laser

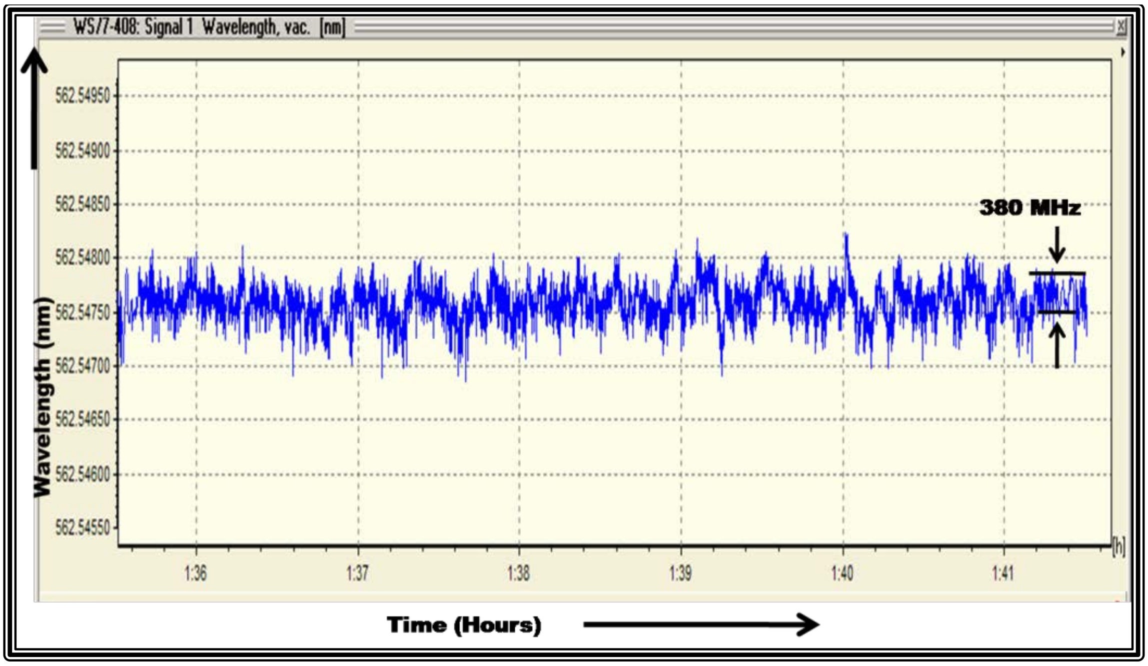

Fig 7.22: Frequency stabilized output wavelength of SLM dye laser {X- axis Wavelength (nm), Y- axis time in hours}

Figure 7.22 shows that the frequency stabilized wavelength output of the SLM dye laser recorded by laser wavelength meter for more than one hour; it showed a wavelength error band of ±190 MHz. The time constant for the locking loop was 20 ms.

7.14 Conclusions

The mode stability of free running GIG SLM dye laser pumped by 9 kHz CVL was studied in detail. The frequency spectrum of the disturbances present in the SLM dye lasers has been identified and quantified. The time constant of the feedback control loop was found out from the spectrum of the disturbances. The controllability of the laser to offset the disturbances of millisecond time constant was studied. A temperature stabilized FP sensor was built for generating an error signal of wavelength stabilization. The line CCD camera with 2048 pixels was used for detecting the frequency change in the range of 17 MHz. A two level VME based wavelength control loop was implemented for correcting the short term as well as long term wavelength drifts. The SLM dye laser wavelength was successfully stabilized in the frequency band of ± 190 MHz for nearly 2 hours of operation.

References

[7.1] T P Lamour, J Sun, D T Reid, "Wavelength stabilization of synchronously pumped optical parametric oscillator: Optimizing proportional – integral control", Rev. Sci., Instru., 81, 053101 – 1, 2010.

[7.2] R W P Drever, J L Hall, F V Kowalski, J Hough, G M Ford, A J Munley, H Ward, "Laser phase and frequency stabilization using and optical resonator", Appl., Phys., B31, 97 – 105, 1983.

[7.3] K G Manohar, K Dasgupta, B M Suri, D D Bhawalkar, "Dye laser wavelength stabilization: An active control by interfrometric fringe detection", Rev. Sci., Instrum., 58, 920 – 922, 1987.

[7.4] I Ketskemety, Zs Bor, B Racz, L Kozma, A N Rubinov, " Improved line narrowing and wavelength stabilization technique of distributed feedback dye laser", Opt., Comm., 22, 275 – 277, 1977.

[7.5] R W Fox, C W Oates, L W Hollberg, " Stabililizing diode lasers to high finesse cavities", Experimental methods in the Physical Sciences, 40, 1 – 46, 2003.

[7.6] R Kapoor, B M Suri, G D Saxsena, "Wavelength control for a pulsed dye laser using the optogalvanic effect", J Phys., E: Sci., Instrum., 18, 930, 1985.

[7.7] J C Bergquist, W M Itano, D J Wineland, "Laser Stabilization to a single Ion", report NIST, Boulder 359 – 375.

[7.8] M Zhu, J L Hall, "Stabilization of optical phase / frequency of a laser system: application to a commercial dye laser with an external stabilizer", J Opt. Soc., Am., B10, 802 – 816, 1983.

[7.9] E Riedle, S H Ashworth, J T Farrell Jr., D J Nesbitt, "Stablization and precise calibration of a continuous – wave difference frequency spectrometer by use of a simple transfer cavity", Rev. Sci. Insrum., 65, 42 – 48, 1994.

[7.10] T Legero, T Kessler, U Sterr, "Tuning the thermal expansion properties of optical refrence cavities with fused silica mirrors", J Opt. Soc. Am. B27, 914 – 919, 2010.

[7.11] M Notcutt, L S Ma, J Ye, J L Hall, "Simple and compact 1 – Hz laser system via an improved mounting configuration of a reference cavity". Opt. Lett. 30, 1815 – 1817, 2005.

[7.12] T Nazarova, F Riehle, U Sterr, "Vibration Sensitive reference cavity for an ultra narrow linewidth laser", Appl. Phys.,B: Lasers and Opt. 83, 531 – 536, 2006.

[7.13] S A Webster, M Oxborrow, P Gill, "Vibration insensitive optical cavity", Phys, Rev A75, 011801(R), 2007.

[7.14] J Millo, D V Magalhaes, C Mandache, Y L Coq, E M L English, P G Westergaard, J Lodewyck, S Bize, P lemonade, G Santarelli, "Ultrastable lasers based on vibration insensitive cavities", Phys Rev. A79, 053829, 2009.

[7.15] www.fen.bilkent.edu.tr/~aykutlu/msn513/fibersensor/fabryperot

[7.16] N O Kawade, V S Rawat, G Sridhar, S Singh, L M Gantayet, "VME baser automated wavelength control system for Single Longitudinal Mode dye laser", NLS – 8, LASTEC, New Delhi 2009.

Chapter – VIII

SUMMARY AND CONCLUSIONS

8.1 Description of the Research Work

Various short cavity SLM dye lasers were studied extensively and the Littman type configuration was chosen for detailed investigation as it has the following main advantages.

a. Littman cavity consists of only three optical components the laser alignment becomes simple.
b. The mode hop free scanning for the entire tuning range is possible.
c. This cavity design eliminates the magnifying components resulting in less losses due to fewer optical surfaces.
d. This cavity can be made extremely compact, so the shorter duration gain can be utilized efficiently.
e. The longitudinal pumping provides excellent beam quality close to diffraction limited beam divergence.

The Littman cavity utilized a nominal cavity of length of $60x10^{-3}$ m. The laser cavity consisted of an end mirror (R > 99 %), a strip-tuning mirror (R > 99%), a holographic grating (typically 2400 lines/mm) placed in grazing incidence configuration. Rhodamine 6G dye dissolved in ethanol was circulated through an indigenously designed metallic dye cell.

8.2 Computational Fluid Dynamics (CFD) Model for Dye Cell

Several configurations of flow channels with plane – plane and converging, straight and diverging geometries have been investigated for the SLM laser dye cell. As an alternative to time consuming experimental investigation, in the first step, detailed CFD analysis were undertaken for several rectangular flow channel dye cell configurations of cross sectional area ranging from 5 x 1 mm^2 to 20 x 1 mm^2 and cell lengths from 30 mm to 80 mm and entrance geometries being either rectangular or tubular. The entrance of the flow channel was rounded to avoid an initial disturbance to the entering flow stream. A finite volume method (FVM) with ANSYS CFX solver of general purpose CFD software was used to visualize the flow velocity vectors in the flow domain. The ANSYS CFX solved the Navier – Stokes equation for the flow domain, which was uniformly, meshed using ICEM CFD mesh. The shear stress transport (SST) model was used to solve the k-ω model at the wall and solve k-ϵ model in the bulk flow, where k is the turbulent kinetic energy, ϵ turbulent eddy dissipation and ω turbulent frequency. A blending function ensured a smooth transition between the two models. The grid independent results were obtained by refining the mesh element of flow domain so that with further refinement of grid the computational result did not change significantly. The boundary conditions used for this simulation study were inlet flow velocity in meter/second, outlet pressure in atm and no slip condition at the solid liquid interface. The velocity vectors for different flow cells were studied. The configurations which showed no flow circulation and low pressure drop were short listed.

The use of solvents with higher viscosity such as binary solvent (50:50 ethanol and glycerol) and pure glycerol eliminated the flow circulation that was observed in certain cell configuration. The vortex (flow circulation) creates undesirable local velocity and temperature gradients in the dye active medium, that contribute towards non-uniform refractive index in the volume thereby increasing the line width and frequency fluctuations of the SLM dye laser. The simulation results show boundary layer thickness was maximum at ~370 µm for an inlet flow velocity of 0.2 m/s, while it was minimum at ~327 µm for an inlet flow velocity of 2.5 m/s. Following these computational studies, two flow cells with the above geometries which were easier to fabricate were made. These flow cells were made with flow channel dimensions of 10 mm x 1 mm x 70 mm and 5 mm x 1 mm x 70 mm.

8.3 Design and Construction of the SLM Dye Laser

The metallic dye cell was made of stainless steel; it had two demountable optical quality quartz windows of 2 mm thickness. The active physical dimension of the dye cell was arrived at, that is, a 5 mm wide 1 mm thick dye flow channel. All the components of the SLM dye laser were mounted on a two stage differential rotary table. The first stage provided the coarse movement with a minimum resolution of 25.92 arc-sec (~46 picometer) with a stepper motor of 50,000 micro-steps per revolution. The second stage was used for the fine motion which provided a minimum resolution of 0.0014 arc-sec (~ 4 femtometer) with 100 mm arm length and utilized a

80 μm PZT with drive voltage of 150V. The end mirror was fixed to a piezoelectric transducer (PZT) stack, which provided a maximum displacement of 8 μm at a drive voltage of 150V. The three optical components (grating, tuning mirror and end mirror) were positioned precisely with the help of linear motion tables. This precise positioning is necessary to match the cavity pivot point for mode hop free tuning over a wide range of wavelengths. The dye cell, of internal dimensions 5x1x70 mm, was mounted in the center of the rotation table and was tilted with respect to the vertical axis by nearly 5^{O} to prevent the unwanted parasitic oscillations from the windows. The dye cell windows were anti reflection coated to avoid the sub cavity resonances inside the dye cell. The short cavity length (~ 60×10^{-3} m) of resonator provided wide axial mode separation (~ 2.5 GHz), which was larger than the single pass width (~ 2 GHz) of the dye laser. This made it possible to obtain lasing of the dye laser in single longitudinal mode. The angle of incidence on the grating was kept larger than 89^{O} for single mode oscillation. Longitudinal pumping and tight focusing of the pump laser provide control over the transverse modes. Longitudinal pumping is favorable for the single longitudinal mode selection because a virtual aperture is created by the pump beam within the gain medium.

The laser operating wavelength λ_0 is governed by the diffraction grating master equation. For mode hop free tuning the wavelength selected by grating equation (say λ_G) and wavelength supported by cavity length (say λ_L) were always kept the same ($\lambda_0 = \lambda_G = \lambda_L$) at all positions of the tuning mirror and the 100 % reflecting end mirror. When the cavity is tuned the comb of cavity modes (λ_L) shifts proportional to the change in resonator length in the direction of tuning. The grating wavelength (λ_G) also shifts in the direction of tuning, according to the angle of the tuning mirror. Single mode tuning without mode hop was achieved when the cavity modes and the wavelength selected by grating shifted together in such a manner that the same mode lases at all wavelengths throughout the tuning range.

8.4 Characterization of SLM Dye Laser

The green beam (510.6 nm) of the copper vapor laser (CVL) was focused into the dye cell with a plano convex lens of focal length 200 mm. The focusing lens was mounted on a linear translation stage for precise control over the focal spot. 0.2 mM Rhodamine 6G solution in ethanol was circulated in the dye cell with a gear pump and the flow velocity was controlled by a variable frequency drive (VFD). The mean flow velocity was measured to be 3.6 m/sec, which provided a clearance ratio of two for 9 kHz pulse repetition rate with a gain volume diameter of nearly 200 µm. The exact focal spot was located before the dye cell, which avoided both the damage to the dye cell windows and thermal distortion in the dye active medium. The diameter of the pump beam spot in the gain medium was ~ 200 micrometer. The pump beam diameter must be approximately matched with the mode diameter of the dye laser for maximum utilization of pump power in the single mode dye lasers.

The spectral bandwidth of the laser was measured by a Fabry Perot (FP) etalon of 7.5 GHz free spectral range in conjunction with a wavelength meter (Angstrom WS-7L). The laser was found to oscillate at a single frequency with a time averaged bandwidth of ~ 400 MHz for a pump power of 1.5 watts. The single pulse bandwidth was measured 315 MHz. At higher pump power (3.5 watts) the SLM pulse duration was 17 ns while at lower pump power of 1 watt it was 5 ns. When the pump power was increased beyond 3.5 Watts, the laser began to oscillate in two modes. The SLM was tuned from 554 nm to 566 nm (~ 12 nm) by rotating the tuning mirror and mode hop free tuning of 70 GHz was obtained with 20µm PZT attached to the tuning arm. It has been experimentally observed that the laser buildup time is 11.7 ns for pump power of 3 watts, while the buildup time is 15 ns for pump power of 1 watt. At the line centre, the buildup time was small (~ 12 ns) and as the lasing mode was tuned on either side of the line centre the buildup time increases. The buildup time of SLM dye laser reduced to 8 ns from 12 ns for holographic grating of 5% diffraction efficiency in comparison to a conventional grating with diffraction efficiency of 2% at the same incidence angle. The contribution of ASE in the SLM signal also has been found to increase with increasing dye concentration from 0.1 mM to 0.5 mM.

8.5 Temperature Effects on the SLM Dye Laser

The change in the temperature of the dye solution directly affects single mode operation of the short cavity GIG dye laser. It has been observed that the cavity length tuning of the SLM dye laser was limited to grating band pass of 2.5 GHz. There was a settling time for the dye solution, whose temperature was actively controlled in the band of $\pm$ 0.15^{O}C. It has been confirmed that with increasing dye solution temperature, SLM dye laser wavelength decreases, while the simultaneous increase in temperature of the dye cell window increases the wavelength beyond grating pass band. The wavelength jitter band was ~4 pm for two mode oscillations and 0.5 pm for single mode oscillation. The cyclic behavior of single mode and two mode operations has been attributed to the temperature variation of the dye solution. The cyclic behavior has been prevented by controlling the dye solvent temperature. The CFD model has been able to compute the transient temperature rise in the dye cell for each pump pulse. The temperature rise due to frictional heating in the dye cell window for commonly used dye solvents has been computed. Temperature gradient near the dye cell wall was slightly higher when the dye concentration was increased leading to thermal lensing.

8.6 Wavelength Stabilization of SLM Dye Laser

The studies have been carried out to test the wavelength controllability and mode stability of the SLM dye laser. For this, both the end and tuning mirrors mounted on the PZTs were manipulated by the controller output (0 – 150 V). The input (0 - 10 V) signal was generated from 16 bit digital to analog converter (DAC) by computer. The sensitivity of the PZT at end mirror was 8.5 MHz / nm for the cavity length of 62 x10^{-3}mm. The SLM dye laser output was fed to a homemade FP sensor housed in a temperature controlled (± 0.01^{O}) bath by an optical fiber of core diameter 200 μm. The fringe formed by the FP sensor was focused into a line CCD array sensor. Change in the fringe diameter of FP sensor corresponded to the change in wavelength of the SLM. The shift in the position of the fringe generated the error signal that was fed to the cavity end mirror PZT. It has been observed the laser wavelength could be locked within the band of ± 200 MHz for nearly 2 hours.

8.7 Summary and Conclusions of the Work Done

In the research work, the following have been completed.

8.7.1 Design Architectures

1. The remotely tunable SLM dye laser, which is pumped by the Copper Vapor Laser (CVL) operating at 9 kHz pulse repetition rate, has been designed and developed.

2. The tuning mirror, grating and end mirror, which form the cavity optics, are mounted on flexure base mounts specially designed for the SLM dye laser. These types of mounts have been successfully implemented for the first time with the SLM dye laser.
3. The SLM dye laser components were fixed on a two stage differential rotation table. With the above mentioned mounts the planes of grating, end mirror and tuning mirror could be precisely positioned, so that the common point of intersection passes through the center of the rotation axis of the differential table. This common point works like a pivot point for mode hop free tuning of the SLM dye laser.
4. Several methods have been implemented for rotating the tuning mirror such as PZT of different stroke lengths, motorized mike, cascaded PZT for increasing the stroke length without hampering the resolution, cascaded PZT and motorized mike and worm and wheel mechanism having an eccentricity of 1.5 mm and 1:120 gear reduction. The worm and wheel arrangement with stepper motor of 50,000 micro steps has been implemented successfully. This could provide angular resolution of 0.001146 arc sec, corresponding to 1.7 MHz per step.

9.7.2 Dye Cell Design and Construction

1. The dye cell is the heart of the SLM dye laser, which feeds gain to the passive cavity mode. The pressure and thermal variations in the vicinity of the active volume could be controlled by higher flow velocity allowing several active volume clearances in between the pump pulses. This could be done without the onset of cavitation. The flow circulations (vortices) in the dye cell flow channel have been eliminated by judicious design of the dye cell.
2. Commercial computational fluid dynamic (CFD) software has been used for visualizing the flow velocity vectors and pressure drop inside the dye cells. The dye cell models have been generated in the solid works – 2005 and ANSYS ICEM CFD was used to create the fine mesh for the dye flow domains.
3. Two dye cells of 10 x 1 x 70 mm were fabricated and integrated with SLM dye laser assembly. The stable SLM dye laser has been obtained with the dye cell internal dimensions of 10 x 1 x 70 mm with higher viscosity solvents such as binary solvents of ethanol and glycerol, in 50:50 volumetric ratios.

4. With computational studies an optimum dye cell of internal dimensions of 5 x 1 x 70 mm has been obtained, which could provide stable SLM dye laser operation with a lower viscosity solvent such as ethanol.
5. The flow circulation (vortices) in the SLM dye cell has been eliminated by reducing the flow channel width. The pressure drop across the dye cell could be reduced by 25% and the linewidth of SLM dye laser could be reduced by 40% with this new dye cell.

5.7.3 Parametric Studies

1. The SLM dye laser was pumped by copper vapor laser operating at 9 kHz and the second harmonic of Nd:YAG laser operating at 10 Hz. The time average and single pulse linewidth of SLM that have been achieved were 400 MHz and 315 MHz respectively for Rhodamine 6G dissolved in ethanol.
2. The stepper motor with 50,000 micro steps could provide coarse tuning to the SLM dye laser in steps of 45 GHz. The 80 µm PZT attached to the tuning arm could provide fine tuning to the SLM in steps of 28 MHz.
3. The minimum angular resolution has been achieved by the end mirror PZT, which is controlled by the input drive signal to the PZT drive. A 16 - bit analog to digital converter has been used for generating the 0 – 10 volt input signal for the PZT drive. This could provide a resolution of 7 MHz.
4. This SLM dye laser could be tuned over 12 nm and it has been observed that the tuning range is a function of dye concentration and pump power.
5. A mode hop free tuning over 70 GHz has been achieved for this SLM dye laser.
6. The ASE was minimum (~0.33%) at the peak of the tuning range, while it increased in both directions of the tuning curve.
7. The buildup time of SLM dye laser is a function of several parameters such as dye concentration, pump power, diffraction efficiency of the holographic grating and the position of the wavelength on the tuning curve. It has been observed that the buildup time reduces by 20% as the pump power to the SLM dye laser is increased three times. It has been found that the buildup time of the SLM dye laser was smaller when the Stoke shift in the emission and absorption wavelength was small.
8. The peak of the tuning curve has been seen to shift by 4 nm with an increase in dye concentration from 0.15 mM to 0.5 mM. The optimized dye

concentration for SLM dye laser has been found to be 0.2 mM in terms of the specific dye laser parameters.

9. It has been seen that the pulse duration of the SLM dye laser increased to 8.5 ns from 3.5 ns when pump pulse energy was increased by three times. This SLM dye laser was pumped with yellow (578 nm) beam of the CVL, in which Rhodamine 640 laser dye was used.
10. The SLM dye laser signal of 3 mW has been amplified to 480 mW with conversion efficiency of nearly 6 % in the first amplifier stage.
11. It has been observed that the percentage of ASE is higher for longer wavelength of the amplified SLM dye laser output due to gain mismatch in the oscillator and amplifier configuration. The gain mismatch could be eliminated by using two different laser dyes in the oscillator (Rhodamine 6G) and amplifier (PM 567) stages. This combination of laser dyes results in a lower percentage of ASE and similar conversion efficiency for the entire tuning range of the SLM dye laser.
12. The CVL pump pulse of 25 ns has been stretched to 44 ns in a triangular pulse stretcher unit. The SLM bandwidth has been found to increase to 550 MHz from 400 MHz with this stretched pump pulse.
13. The time average bandwidth for SLM dye laser pumped by the second harmonic of Nd:YAG has been measured to be 180 MHz. The time averaged bandwidth has been found to increase by 40 % with an increase in pump pulse energy from 0.1 mJ to 0.8 mJ for Nd:YAG pumping of SLM dye laser for the same flow velocity of 0.5 m/s.

5.7.4 Temperature Effects on SLM

1. The instantaneous temperature rise in the active volume has been simulated using ANSYS CFX and the maximum temperature rise has been found to occur near the dye cell window. The temperature rise dependence on the dye concentration could be modeled.
2. The frictional temperature rise could also be estimated 1.1 K, which becomes significant for high flow velocities. This restricts the choice of solvent to low viscosity solvent such as ethanol for high repetition rate dye lasers.
3. It has been seen that the higher thermal and refractive index gradients resulted in a deflection of the laser beam towards higher refractive index regions, thus

acting like a diverging lens. This computational model has been validated using the published experimental data for the dye cell.

4. It has been found that the temperature rise in the upward direction was due to thermal diffusion in the quartz window and not due to the thermal diffusion in the dye solvent as the time required for the thermal diffusion process in dye solvent is much larger than the transit time of the dye volume.
5. It has been experimentally observed that with increasing dye solvent temperature the SLM dye laser wavelength decreases as dn/dt for ethanol is negative. For single mode dye laser, even a small change of dye solvent temperature by ~ 1^{O}C induces a frequency detuning by a few GHz.
6. It has been observed that monotonous drift in dye solvent temperature results in the cyclic behavior of the modes in the SLM dye laser. As solvent temperature increases the SLM dye laser wavelength decreases and the laser mode switches between single mode and two mode oscillation. This cyclic behavior of the modes is due to the limited grating pass band, which provides feedback to resonator for very small bandwidth of wavelength. The cyclic behavior, that is, single mode to two mode transition of the SLM dye laser has been found to cease when the dye solvent temperature was controlled in the band of ± 0.15 ^{O}C.
7. The cyclic behavior due to changes in the optical length of the cavity has been further confirmed by changing the cavity length of the SLM dye laser with end mirror PZT, after the solvent temperature was stabilized within the band of ± 0.15^{O}C.

8.7.5 Wavelength Locking for SLM

1. It has been shown that the wavelength locking of SLM dye laser by the feedback control loop could eliminate the wavelength drift over long duration of operation time and help to reduce the bandwidth.
2. The frequency spectrum of the disturbance has been experimentally estimated using a very simple technique, in which the FFT analysis of the disturbance to the Fabry Perot fringes is carried out for determining the frequency spectrum of the disturbance present in the SLM laser output. The major prominent frequency components present in the SLM output have been identified and each assigned to a source, namely 0.1 Hz and 107 Hz. Two relatively weaker

components have been seen in the spectrum of the disturbance, closer to flow fluctuations of gear pump and mechanical vibration.

3. A temperature stabilized (± 0.1^{O}C) Fabry – Perot sensor has been built with cylindrical optics designed for the line CCD array. The temperature of the Fabry Perot cavity is stabilized at 45 ^{O}C within a band of ± 0.1^{O}C. The change in the fringe position could be detected using the CCD array with the in-house developed software. The FP sensor could detect the frequency change of 17 MHz. This SLM dye laser has been locked using a PID controller and a combination of software and hardware locks.
4. It has been shown that the cyclic behavior of the SLM dye laser can be eliminated by applying required corrective voltage through the feedback control loop, to the end mirror PZT. The wavelength has been stabilized in the band of ± 0.2 pm for Rhodamine 6G dye in ethanol.

The present work has contributed to a better understanding of the single mode dye lasers and its dependence on the temperature and its amplification process for the generation of higher pulse energies. The study of the amplification process of SLM dye laser shows that for uniform amplification and lower ASE in the amplified SLM dye laser, the gains of signal and amplifier needs to be just matched. The results of the study are useful in the design of the single longitudinal mode pulsed dye laser system.

8.8 Major Contributions

1. A CFD model of the dye cell for the SLM dye laser has been developed and validated.
2. The new dye cell has been developed for better performance of the laser at high repetition rate.
3. A CFD model has been used for estimating the transient temperature rise in the dye cell due to pump beam absorption; this has been useful in designing laser system with high repetition rate capability.
4. Temperature controlled F-P Etalon based wavelength locking unit has been developed.
5. Remotely tunable computer controlled SLM dye laser has been developed, integrated and characterized.

8.9 Future Work

Although many unattended areas have been investigated, the following suggestions may be made as an extension to the reported work.

1. Amplification of the SLM dye laser signal of a few mW to a few tens watt with two to three amplification stages, where they need higher pump power and larger gain area, needs to be systematically investigated.
2. Further computational studies with the CFD model may be extended to flow cell geometries with higher volumetric flow through a larger active area. The pressure drop across the flow cell needs to be minimized to reduce the demands on gear pumps used in large flow system.
3. The flow cell geometries for higher repetition rate (~ 18 kHz) should have innovative designs of the flow geometries, so that the permanent pressure loss as well as boundary layer effects can be minimized.
4. For calculation of transient temperature rise in the flow cell, the non – linear absorption coefficient may be included in the physics model to predict the temperature rise in the active volume; excited state absorption in the dye gain medium may also be accounted.
5. Deflection of the laser beam in the heated volume within the resonator cavity can be determined by ray tracing software and coupled to the CFD model.